January 2013

Synoptic to interannual variability in volumetric flushing in Tampa Bay, FL using observational data and a numerical model

Monica Wilson
University of South Florida, wilsonm@mail.usf.edu

Synoptic to Interannual Variability in Volumetric Flushing in Tampa Bay, FL using Observational Data and a Numerical Model

by

Monica Wilson

A dissertation submitted in partial fulfillment
of the requirement for the degree of
Doctor of Philosophy
Department of Marine Science
College of Marine Science
University of South Florida

Major Professor: Mark E. Luther, Ph. D.
Steven M. Meyers, Ph. D.
Gary Mitchum, Ph. D.
James Hagy, III, Ph. D.
Christopher D'Elia, Ph. D.

Date of Approval:
November 25, 2013

Keywords: Estuary, Climate, Wavelet analysis, Subtidal circulation, ENSO

Dedication

I would like to dedicate this dissertation to my husband, parents, brothers, and children. To my husband Kendrick, thank you for all of your encouragement and support. You have always provided a listening ear, helped me get through all of the tough times, read and edited my manuscripts, and were always willing to listen to all of my presentations and provide advice. Thank you to my parents, for your unconditional love and support and for teaching me how to strive for and reach my goals. Thank you to my brothers, who helped shape me into the strong woman that I am today. To Roman, thank you for always being there for me and knowing how to make me laugh. To Mike (1975-2013), who I miss dearly, he was always one of my biggest supporters. I know he would have been extremely proud of me, and would have uttered the words, "It's about time, punk." To my kids Kendrick Jr., Caleb, and Gabriella, you are the light of my life. Thank you for always making me smile, teaching me how to be patient, how to enjoy the smaller things in life, and how to love unconditionally.

Acknowledgments

Funding for this work is provided by the National Oceanographic and Atmospheric Administration, Greater Tampa Bay Marine Advisory Council-Physical Oceanographic Real Time System (GTBMAC-PORTS), Alliance for Coastal Technologies (ACT), Alfred P. Sloan Scholarship Foundation, and Florida Education Fund's McKnight Doctoral Fellowship. I would like to thank the members (past and present) of the Ocean Monitoring and Predication Laboratory at USF's College of Marine Science, Vembu Subramanian, Sherryl Gilbert, and Heather (Holmes) Havens for their friendship and support during my time here. Thank you to Mark Luther and Steve Meyers for their unwavering support, guidance, and leadership that has helped me tremendously through my journey at USF. Thank you to Linda Kelbaugh and Dean Dixon for also providing endless support, advice, and encouragement.

Table of Contents

List of Tables

List of Figures

Abstract

This research provides insight into changes in volumetric flushing of the Tampa Bay estuary caused by synoptic scale wind events. The two main studies of this dissertation involve 1) using wavelet analysis to investigate the link between the El Niño-Southern Oscillation (ENSO) and the frequency and strength of volumetric flushing driven by synoptic variability and 2) using a multi-decadal model simulation to examine how extratropical/winter storms and hurricanes affect the overall flushing rates for Tampa Bay, FL.

In the first study, two analyses are performed on 55 years of observational data to investigate the effect of multiple small wind events on estuarine flushing. First I use subtidal observed water level as a proxy for mean tidal height to estimate the rate of volumetric bay outflow. Second, I use wavelet analysis on sea level and wind data to isolate the synoptic sea level and surface wind variance. For both analyses the long-term monthly climatology is removed to focus on the volumetric and wavelet variance anomalies. The overall correlation between the Oceanic Niño index and volumetric anomalies is small (r^2=0.097) due to the seasonal dependence on the ENSO response. The mean monthly climatology between the synoptic wavelet variance of elevation and axial winds have similar seasonal behavior. During the winter, El Niño (La Niña) increases (decreases) the synoptic variability, but decreases (increases) it during the summer. The difference in winter El Niño/La Niña wavelet variances is about 20% of the climatological value. ENSO can swing the synoptic flushing of the bay by 0.22 bay

volumes per month. These changes in circulation associated with synoptic variability have the potential to impact mixing and transport within the bay.

In the second study, volumetric changes from large scale weather events are investigated using a numerical circulation model simulation (1975-2006) to find the cumulative impact of flushing on the bay by extreme events. The strong wind speeds, duration of high winds and wind direction during these events all affect the amount of water flushed in and out of the estuary. Normalized volume anomalies are largest when wind components blow up/down the estuary in the NE/SW direction. Wind induced normalized flushing rates for all 10 extratropical/winter storms range from 12% to 40% and from 14% to 40% for all 10 hurricanes. All storms discussed in this study caused winds greater than 15 m s^{-1} (~30 knots). The direction of the winds had an impact on the flushing rates during these extreme events. Storm9 (February 1998) and Hurricane Gabrielle (September 2001) experienced the smallest total volume changes (14% and 13%). Both storms experienced weak axial and co-axial winds causing volume changes to be small. The Storm of the Century (March 1993) and Hurricane Frances (September 2004) saw the largest total volume changes of 40%. They both had strong winds blowing in the NE direction. Hurricane Frances had two wind peaks and lingered in the area for approximately 48 hours, so both strength and duration of winds played a large role in the total volume change. Total inflow and outflow rates per year show that there is year to year variability of flushing in Tampa Bay.

Introduction

Estuaries are semi-enclosed coastal regions where ocean water mixes with significant amounts of freshwater from rivers (Dyer, 1973). They form a transition zone between river environments and marine environments that are biologically productive and economically important. They range from pristine bays to highly urbanized estuaries. About half of the largest cities in the world are built around estuaries (Shi and Singh, 2003). Tampa Bay is the largest open water estuary in Florida and is home to the 10th largest port system in the United States (Lewis et al., 1999). It is also one of the most biologically diverse subtropical estuarine areas in the United States (Harwell et al., 1995). The water quality and overall health of the bay is critical to the humans and wildlife that live near or in the estuary and is often related to its ability to remove pollutants through hydrodynamic flushing. Flushing rate is defined as the time required to replace the volume of a basin by the volume influx. Flushing can be affected by multiple mechanisms such as tidal currents, baroclinic exchange, and winds. These mechanisms can influence the mixing and transport within an estuary. The mixing or circulation of water can have an impact on transport and retention of organisms, nutrients, oxygen, sediments and waste. It is important to understand of how flushing is affected or altered by synoptic wind events to help aid in determining and improving water quality within an estuarine system.

With the use of 55 years of observational data and a 32-year model simulation the long-term cumulative impacts of wind driven volumetric changes in Tampa Bay will be

the main focus of this dissertation. Estuarine circulation is controlled by many factors that include density-driven circulation, tides, and wind driven currents that all contribute to the horizontal exchange processes in estuaries (Geyer and Signell, 1992). Specifically, winds can induce subtidal variability in an estuary through remote and local effects. Remote wind effects come predominantly from along-shelf winds, which produce coastal sea level fluctuations along the shelf at the mouth of an estuary. Local wind effects act directly over the surface of an estuary to produce subtidal variability within the system (Janzen and Wong, 2002). Remote and local wind effects can produce very different patterns of exchange between an estuary and the continental shelf (Wong and Valle-Levinson, 2002). Weisberg and Sturges (1976) found that wind fluctuations dominated the low frequency circulation in the Providence River and the west passage of Narragansett Bay. Changes in wind patterns due to extratropical/winter storms and hurricanes can also alter the wind-induced circulation. Throughout the Gulf of Mexico coastline winds caused by winter weather systems affect sea level at times of several days (Kennedy et al., 2007). Strong winds associated with winter storms can flush 30-50% of water volume out of shallow bays in the Atchafalaya/Veermilion Bay regions in Louisiana (Walker and Hammack, 2000). Hurricane induced winds can also produce massive disturbances in estuaries (Greening et al., 2006). Approximately one-third of the net outflow in Chesapeake Bay during Hurricane Floyd was caused by wind forcing (Valle-Levinson et al., 2002). Wilson et al. (2006) found that winds caused by Hurricane Frances displaced about 40% of Tampa Bay's volume in a single day. These studies discuss short term impacts of strong wind events on estuarine flushing. Long-term (multi-decadal) studies are rare.

This dissertation has two main objectives: 1) to investigate the link between the El Niño-Southern Oscillation (ENSO) and the frequency and strength of volumetric flushing driven by synoptic variability and 2) to use model output from a multi-decadal run to investigate how extratropical/winter storms and hurricanes affect the overall flushing rates for Tampa Bay, FL. In the first study, wavelet analysis, as described by Torrence and Compo (1998) and (Grinsted et al., 2004), is used to isolate the synoptic sea level and surface wind variance. In the second, study the findings of Schmidt and Luther (2002) and Burwell (2001) are combined to examine the changes in volumetric flushing caused by strong wind events and to possibly find a link between ENSO and yearly flushing rates of the bay.

The model used in this study is the Environmental Fluid Dynamics Code (EFDC). It is equivalent to the Blumberg-Mellor model and was developed at the Virginia institute of Marine Science (Hamrick, 1992). The main reason this model was chosen is that it can simulate wetting and drying allowing for improved simulation of water level changes during extreme events compared to models that do not simulate wetting and drying.

The first step of this study was to gather data from many different agencies around the bay area. This data are used to make input files to run a numerical estuarine circulation model and perform short tests to validate model output. The input files used to run the model consist of freshwater input, salinity, zonal and meridional wind components, and elevation. Once input files are created, they are added one at a time between test runs to make sure that input files are formatted correctly and do not cause any instabilities within the model. After all input files are included, short test runs of approximately 1 year are done and model output is evaluated. Evaluation of the model

entails comparing model output with observational data as well as calculating mean errors for model accuracy. Once evaluation of model output is complete, the multi-decal model run (1970-2006) is started.

This dissertation begins with a description of the bay, and operational data. This is followed by a description of observational data. The type of data gathered, the agencies that provide the data, and any formatting done to average or fill in gaps is discussed in detail. The next section describes the EFDC model. Specifics about the computational and numerical scheme, mass conservation, and model bathymetry are explained. The chapter then ends with an explanation of the multi-decadal model simulation and evaluation. Mean errors and correlation values are also calculated evaluate model accuracy.

The next chapter presents a wavelet analysis investigating a link between ENSO and the frequency and strength of volumetric flushing driven by synoptic variability, building on Wilson et al. (2013). Two types of analyses are performed on the 55 years of observational data. The first analysis uses the residual observed water level as a surrogate for mean tidal height to calculate total volume and get an estimate of the rate of volumetric outflow. The second analysis uses wavelet analysis to isolate and quantify the variance of elevation and winds in the synoptic frequency band. Details about the volumetric analysis and how wavelet variance is used to examine the time-frequency variations in the synoptic activity are described. The chapter ends by describing the results from applying these methods and discusses the impacts of ENSO on estuarine flushing.

The second study is described in the final chapter. This study uses the model output from the multi-decadal run. The objectives of this study are: 1) to use the model to examine how large-scale weather patterns such as winter storms and hurricanes alter the wind-induced circulation, and 2) to find the cumulative impact of flushing of the bay by these wind events. Model elevation is used to calculate normalized volume anomalies and flushing rates for the entire 32-year period. Volume anomalies and flushing rates for 10 extratropical/winter storms and 10 hurricanes that occurred during 1975-2006 are then estimated. The specifics of two of these extratropical/winter storms and hurricanes are discussed in detail. The chapter ends with results for each extreme event, describes the differences in the volume changes and flushing rates between extreme events, and evaluates how characteristics of individual events (e.g. wind speeds, directions, and duration) affect flushing rates to either increase or decrease.

Together, these studies will provide a better understanding of how the Tampa Bay estuary responds to synoptic scaled weather events. The influence of flushing, mixing and transport caused by synoptic events can affect the nutrient and pollutant distribution, sediment resuspension, and turbidity, potentially affecting the biological condition of the Bay.

Chapter 1: Tampa Bay, Data Collection, Model Simulation and Evaluation

Tampa Bay

Tampa Bay is located on the central part of the west coast of Florida., and is the largest estuary and port in Florida as well as the tenth largest U.S. commercial port in terms of tonnage handled (Lewis et al., 1999). It is also one of the most biologically diverse subtropical estuarine areas in the United States (Schmidt and Luther, 2002). The bay is a significant marine resource for the State of Florida and provides major ports of commerce, supports a variety of fisheries, offers important recreational opportunities for Florida's residents and visitors, and also accommodates the community needs of power generation, fresh water supply and wastewater reception (Weisberg and Williams, 1991; Weisberg and Zheng, 2006).

Tampa Bay begins at the Gulf of Mexico near 82.50° W and 27.60° N, and extends in a northeast direction approximately 53 km. The bay has natural channels that follow the main core of the Y-shaped estuary with depths up to 10 meters. The estuary has two branches and lower and middle stem segments that are referred to as Old Tampa Bay, Hillsborough Bay, Lower and Middle Tampa Bay (Figure 1), respectively (Lewis, 1982). Tampa Bay covers approximately one thousand square kilometers and has an average depth of approximately 4 meters (Goodwin, 1987). The width of the bay is about 15 km at its midsection. Dredged navigation channels lead to many of the main port facilities. The depths of the channels have increased to 15 meters to meet the requirements of

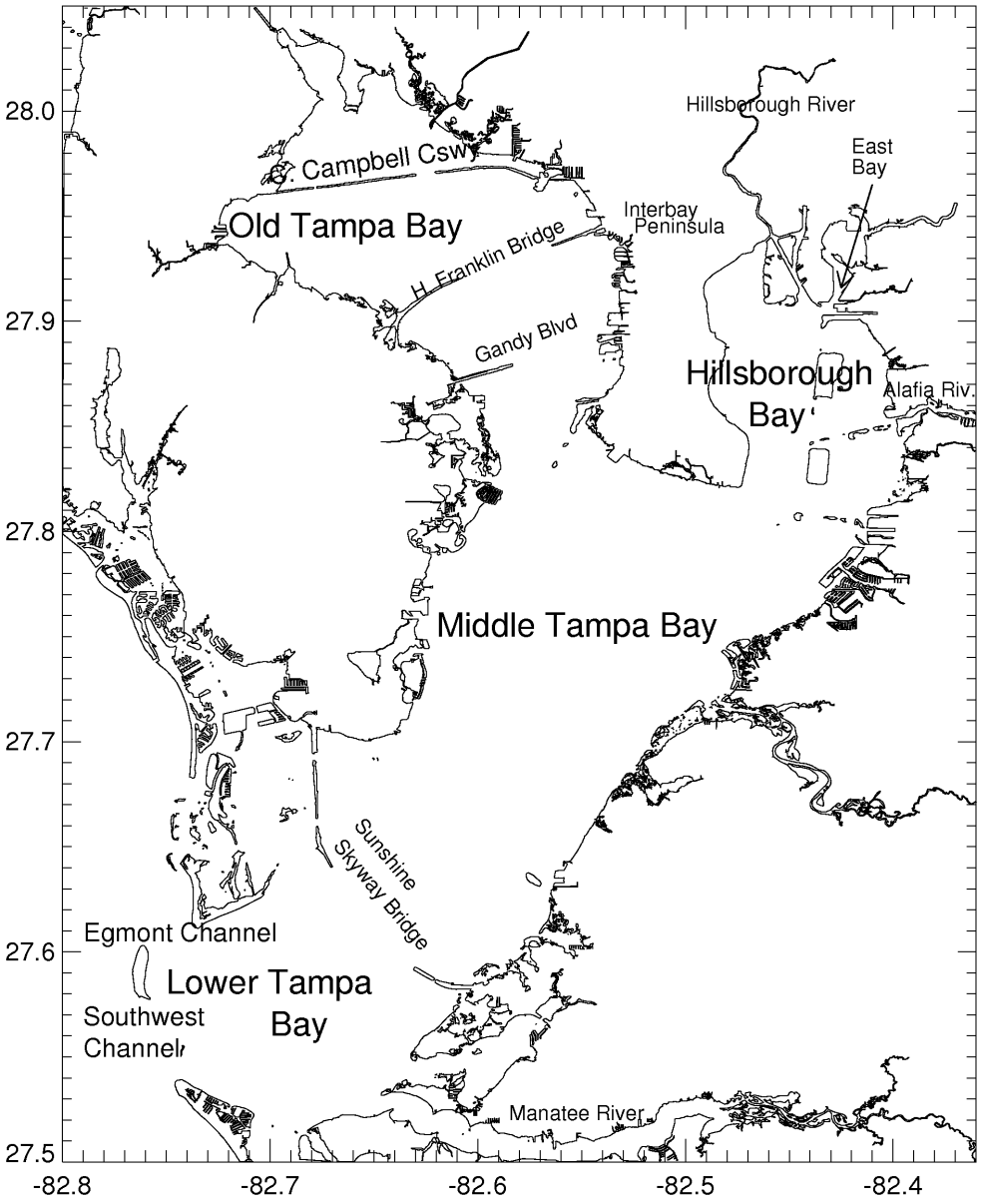

Figure 1. Map of Tampa Bay.

shipping to occur in the bay (Zervas, 1993). The maximum depth is about 27 meters in Egmont Channel near the mouth of the Bay.

Tampa Bay has a circulation that is 3-dimensional and time dependent. Tides, winds, and rivers all have a significant effect on the circulation (Galperin, 1991; Weisberg and Zheng, 2006). Tides are mixed semidiurnal and diurnal, with a range of less than a meter at the Bay mouth to over a meter at the Bay head. The tidal entering the Bay can be characterized as a progressive wave, that transitions into a standing wave in Hillsborough Bay. Tidal epochs indicate that the tide travels from the mouth of the Bay to the head of Old Tampa Bay and Hillsborough Bay in approximately 4.6 hours and 3.2 hours, respectively (Zervas, 1993). In the ship channel under the Sunshine Skyway Bridge, tidal currents are uniform with depth and have peak amplitudes ranging from 0.5 $m\ s^{-1}$ during a neap cycle and 1 $m\ s^{-1}$ during a spring cycle (Li, 1993). The tidal currents have also been observed to have maximum speeds on the order of 1.0 to 1.5 $m\ s^{-1}$ in the Egmont Channel and the channel leading to Old Tampa Bay (Vincent, 2001).

The Bay has major inputs of fresh water located on the east and south sides. The Alafia and Hillsborough Rivers drain into the bay from the northeast, near the head of the bay. The Little Manatee River enters on the eastern side and the Manatee River on the south near the mouth of the Bay. Using flow rates from table 4 in Meyers et al. (2007), these four rivers account for 27% of the average total freshwater input to the bay.

The salinity of the bay is regulated by the fresh water sources and the Gulf of Mexico water at the open boundary. Salinities in the bay vary from a high of approximately 35 at the entrance of the bay to a low of 20 ppt or less in the northern and eastern parts of Hillsborough Bay and the northwest part of Old Tampa Bay (Boler,

1992). Salinities in the bay are lowest in the summer and highest in the winter due to the pronounced influence of seasonal precipitation patterns, characterized by wet summers and dry winters.

With the amount of freshwater inflow into the bay, shallow average depth, and strong tidal mixing, salinity is well mixed vertically. Significant horizontal salinity gradients persist due to the distribution of fresh water inflow. These horizontal gradients and surface wind forcing maintain the fully three-dimensional circulation of the bay (Li, 1993). Lower salinity at the head of the Bay and higher salinity at the mouth cause an axial pressure gradient force to exist that drives the non-tidal (residual), gravitational convection mode of circulation (Weisberg and Zheng, 2006).

Burwell (2001) found the residual circulation in Tampa Bay appears to be a mix of classical two layer flow over the shipping channels with denser ocean water flowing in at depth and fresher water flowing out of the bay near the surface and along the relatively shallow sides of the bay. The residual circulation speed can vary by a factor of 3 and alter in direction (Meyers et al., 2007). Flushing of the bay occurs through the deep navigational channels running northeast/southwest from the mouth. Residence times in the channels are on the order of 15 days to one month and increase to over three months outside the channels near the edges of the bay and in persistent eddies (Burwell, 2001).

Data Collection

57 years of observational data are collected from various sources. Data includes precipitation, streamflow, waste water treatment plant discharge, water level, winds, and salinity. Precipitation data for 22 sites around the bay are used, with four of the sites

having data dating back to 1950 (Southwest Florida Water Management District; Figure 2). Daily averages are calculated for sites that had complete daily records for 1/1/1950–12/31/2006 (Figure 3). The least number of sites available to compute the daily averages is 3 and the most is 13 (Figure 4). These daily averages are used uniformly across the model grid and will contribute to the total fresh water input.

Streamflow data from the United States Geological Survey (USGS) for 22 sites are downloaded and compared with 3 (Little Manatee, Alafia, and Hillsborough) sites having data dating back to 1950 (Table 1). Correlations are done between all the sites that have 5 years of data (2002-2007). The average flow from 2002-2007 ($\overline{riv}$) from all sites are calculated and used to find scales (1) between sites that have correlations higher than 0.7, these scales are used to fill in the gaps of all the rivers with missing data from January 1, 1950 to December 31, 2006. Equation 2 is an example of how gaps are filled within the data.

$$if\ \ correlation\ of\ \ riv1\ and\ \ riv2 \geq 0.7\ then\ scale = \frac{\overline{riv1}}{\overline{riv2}} \tag{1}$$

$$to\ \ fill\ \ riv2, riv2 = riv1 \times scale \tag{2}$$

Each site is filled with the scaled data from another site with the highest correlation first, if there are still gaps in the data the scale of the site with the next highest correlation is used, and so on. At most, this process is done 4 times, but most of the sites are completely filled when this process is done twice. Each site is correlated with the Little Manatee, Alafia, or Hillsborough River, so every river is able to be filled to January 1, 1950.

Discharge are collected from each waste water treatment plant. Data from the Tampa Bypass Canal is collected from Tampa Bay Water. The Tampa Bypass Canal and

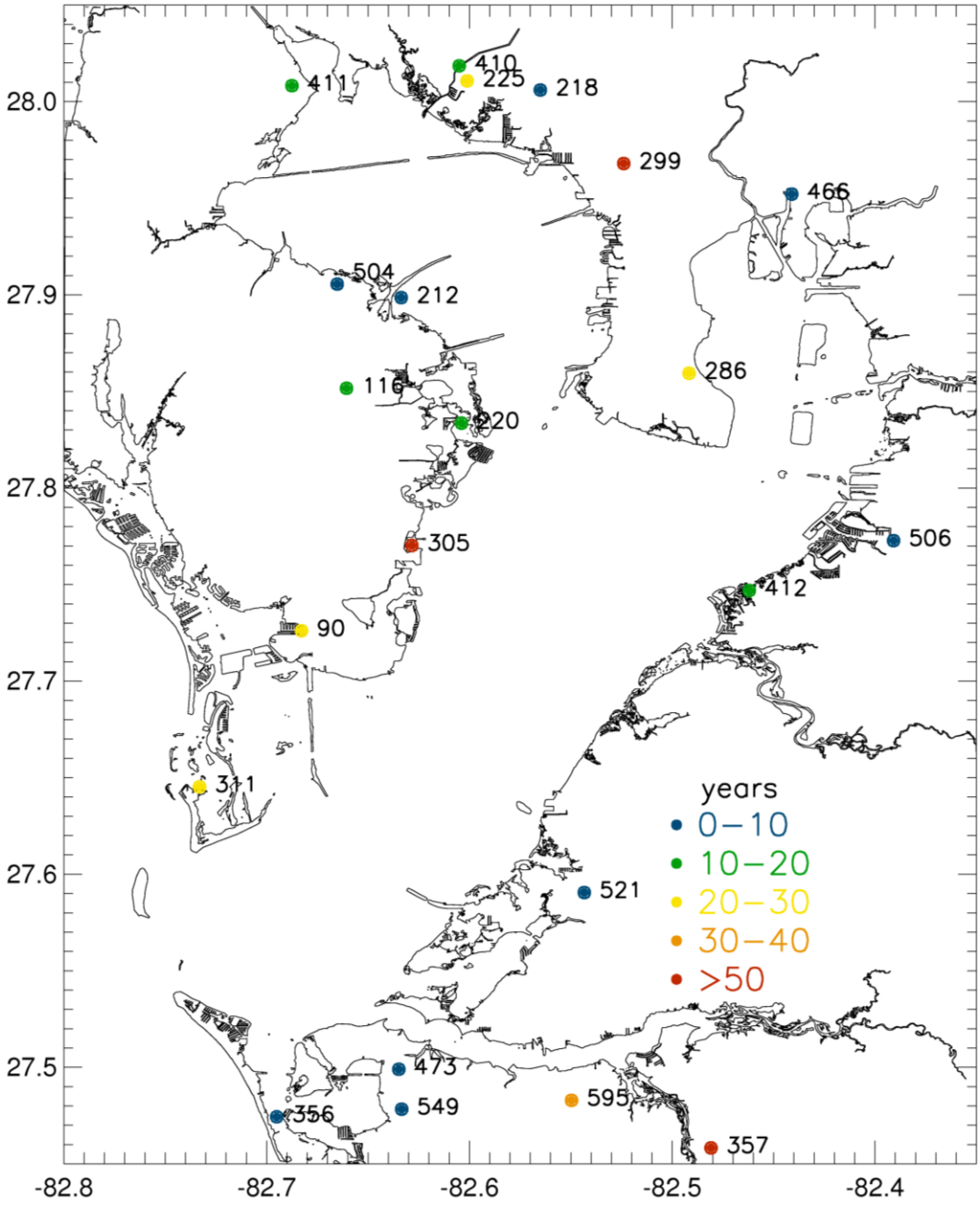

Figure 2. Location, site number, and approximate record length of each precipitation site from Southwest Florida Water Management District.

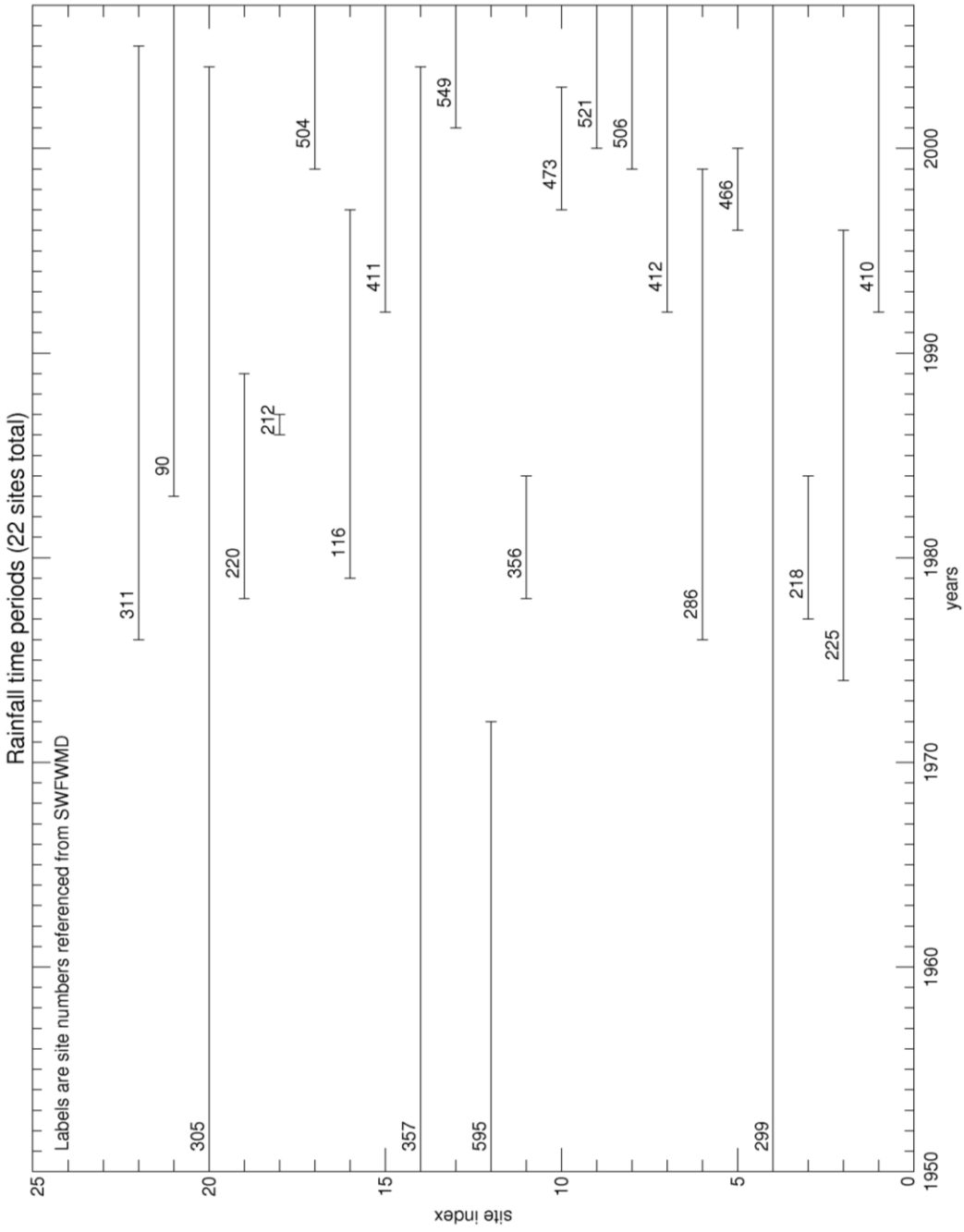

Figure 3. Date range for each precipitation site.

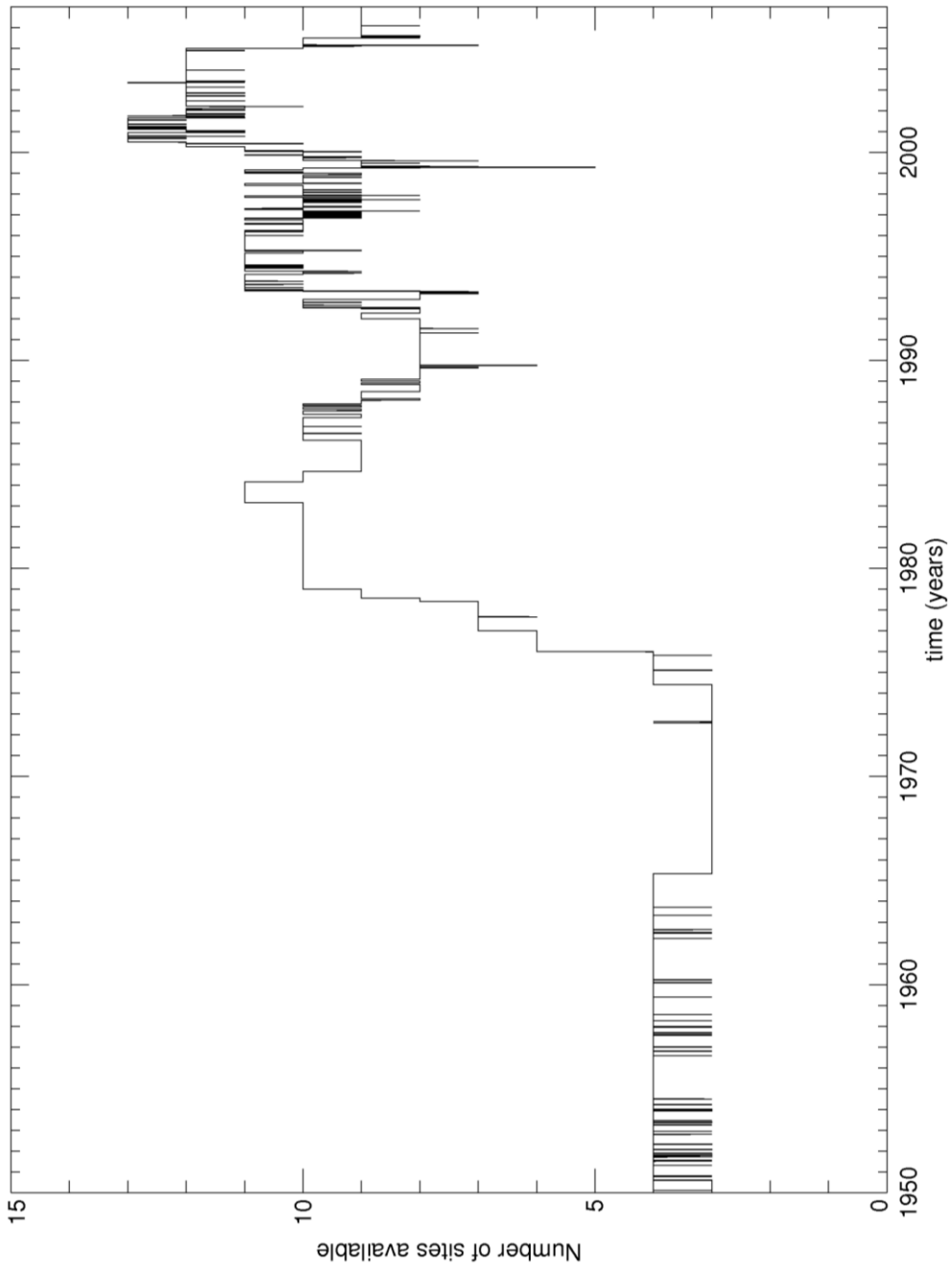

Figure 4. Total number of sites that have data for each day in the 57-year time period.

Table 1. Streamflow gauges, discharge start and end date used for fresh water input.

	Discharge	
Station Name	**Start**	**End**
Ward Lake near Bradenton, FL	4/1/1992	5/27/2007
Gamble Creek near Parrish, FL	10/1/2000	5/27/2007
Manatee River near Myakka Head, FL	4/20/1966	5/27/2007
Little Manatee River near Wimauma, FL	4/1/1939	5/27/2007
Bullfrog Creek near Wimauma, FL	10/1/1956	5/27/2007
Alafia River near Lithia, FL	10/1/1932	6/17/2007
Archie Creek at 78th Street near Tampa, FL	2/1/1999	5/27/2007
North Archie Creek at Progress Blvd. near Tampa, FL	2/1/1999	5/27/2007
Delaney Creek popoff canal near Tampa, FL	2/8/1999	5/27/2007
Delaney Creek near Tampa, FL	10/1/1984	5/27/2007
East Lake outfall at E. Chelsea St. near Tampa, FL	2/3/1999	5/27/2007
Sulphur Springs at Sulphur Springs, FL	7/1/1959	5/27/2007
	4/25/1974	9/30/2006
Hillsborough River near Tampa, FL	10/1/1938	5/27/2007
Sweetwater Creek near Tampa, FL	10/1/1985	5/27/2007
Henry Street Canal near Tampa, FL	10/1/1985	5/27/2007
Rocky Creek at St Hwy 587 at Citrus Park, FL	10/1/1985	5/27/2007
Brushy Creek near Citrus Park, FL	6/1/1993	5/27/2007
Brooker Creek near Tarpon Springs, FL	9/1/1950	5/24/2007
Curlew Creek at County Road 1 near Ozona, FL	8/9/1999	5/27/2007
Curlew Creek at Evans Road near Dunedin, FL	8/9/1999	5/27/2007
Pinebrook Canal at Bryan Dairy Road at Pinellas Park, FL	8/1/1999	5/27/2007
Saint Joe Creek at Pinellas Park, FL	6/29/2000	5/27/2007

the Howard Curren Waste Water Treament Plant discharge the largest amounts of water into the bay (Meyers et al., 2007), so these two sites are used. The Howard Curren treatment plant has monthly data available from 1951 to present and the Tampa Bypass Canal has daily data dating back to 1974.

Hourly water levels referenced to mean sea level (MSL) are available for are the St. Petersburg tide gauge (station 8726520) for the entire 57-year period (NOAA Tides and Currents). Two 1-2 year gaps in the data are omitted from the record; small gaps (< 1 week) are filled with predicted tide data from the NOAA Tides and Currents website.

The filled data is given a 2 hour lag (the approximate lag from the St. Petersburg tide station to Egmont Key) to represent the water level at the open boundary of the model located at the mouth of the bay (Figure 5).

Hourly wind speed and direction are from Albert Whitted Airport, MacDill Air Force Base, and Tampa International Airport (NOAA National Climatic Data Center). MacDill Air Force Base and Tampa International Airport each had data dating back to 1950 (Table 2). Zonal (east/west, u-component) and meridional (north/south, v-component) components are calculated using the wind speeds and directions from each site, then the hourly components from all three sites are averaged. After averaging, any small gaps are filled by interpolation.

Monthly salinity data is collected and provided from the Environmental Protection Commission of Hillsborough County (EPCHC) at approximately 100 sites in the bay (Figure 6). Salinity data is available from 1974-present. Salinity from site 93, just south of Egmont Key, is used at the open boundary of the model. Small gaps in the data are filled by interpolation (Figure 7).

Table 2. Start and end date of wind data downloaded from the NOAA National Climatic Data Center.

Station	Start Date	End Date	Type	Dir. Units	Spd. Units
Albert Whitted	1/1/1986	12/31/2006	Hourly	Angular Degrees	m/s
MacDill	1/1/1950	12/31/1999	Hourly	Angular Degrees	m/s
	1/1/2000	12/29/2006	Hourly	Angular Degrees	m/s
Tampa	1/1/1950	12/31/1972	Hourly	Angular Degrees	m/s
	1/1/1973	12/31/2006	Hourly	Angular Degrees	m/s

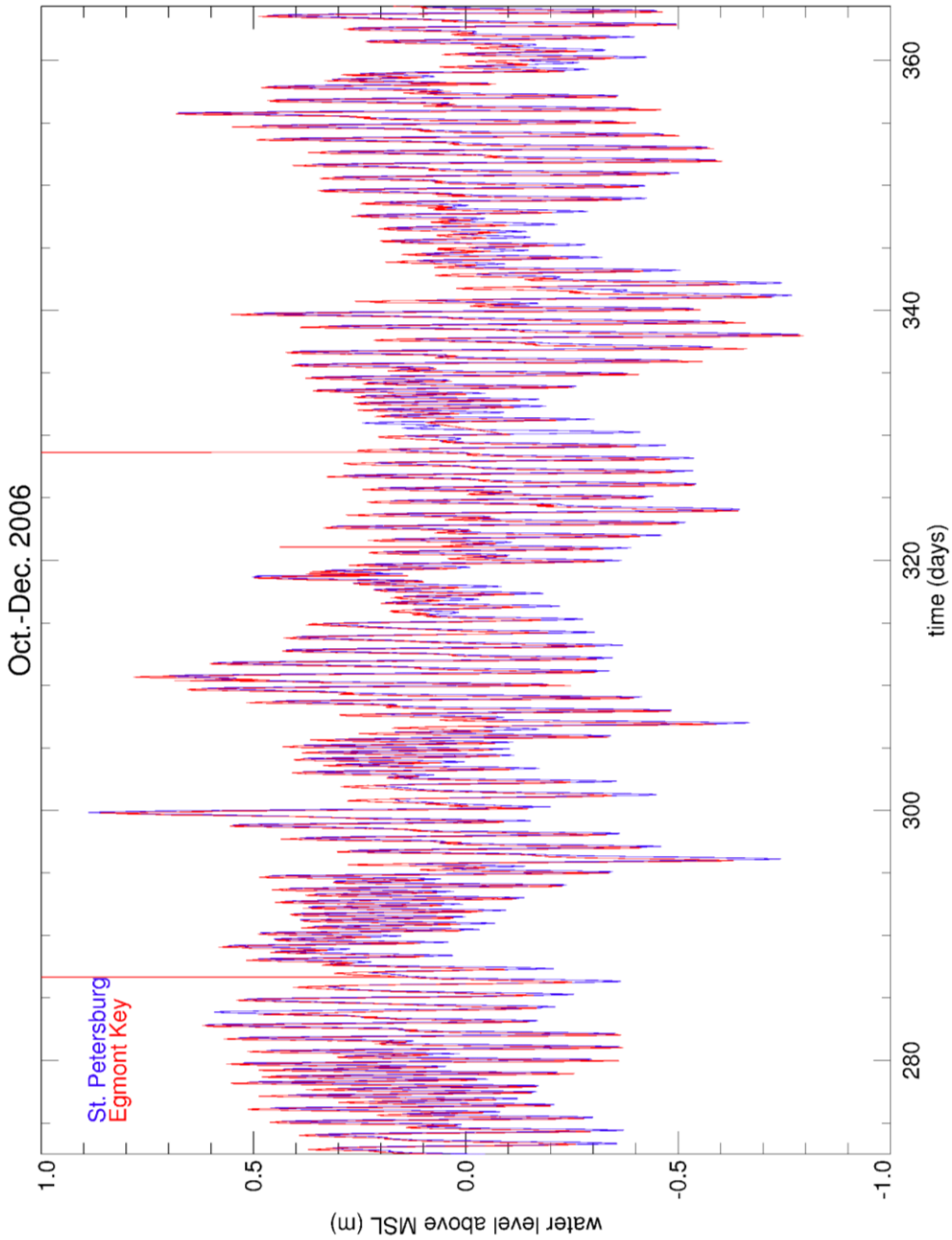

Figure 5. Comparison of water levels at St. Petersburg (red) and Egmont Key (blue)

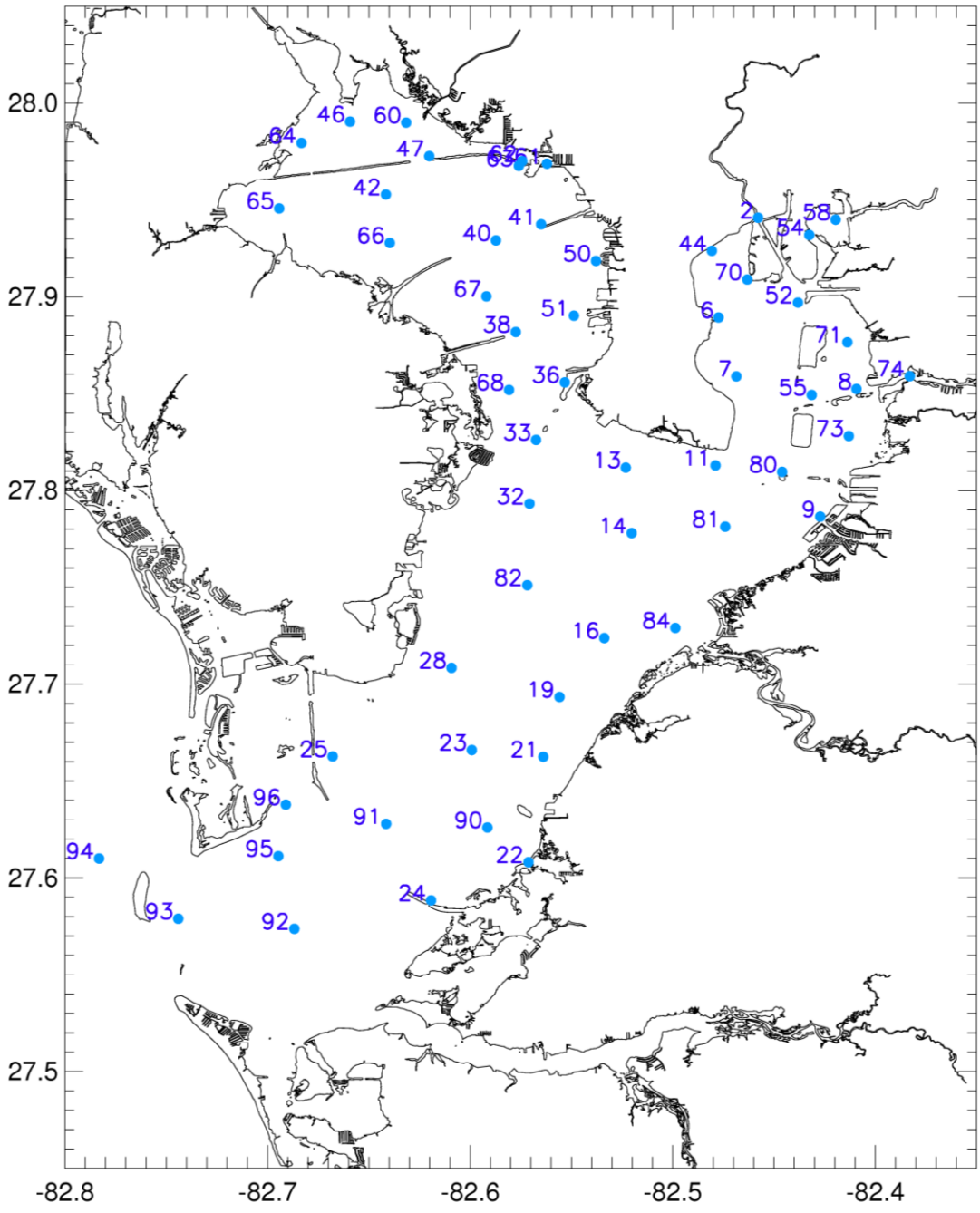

Figure 6. EPCHC salinity site locations within Tampa Bay.

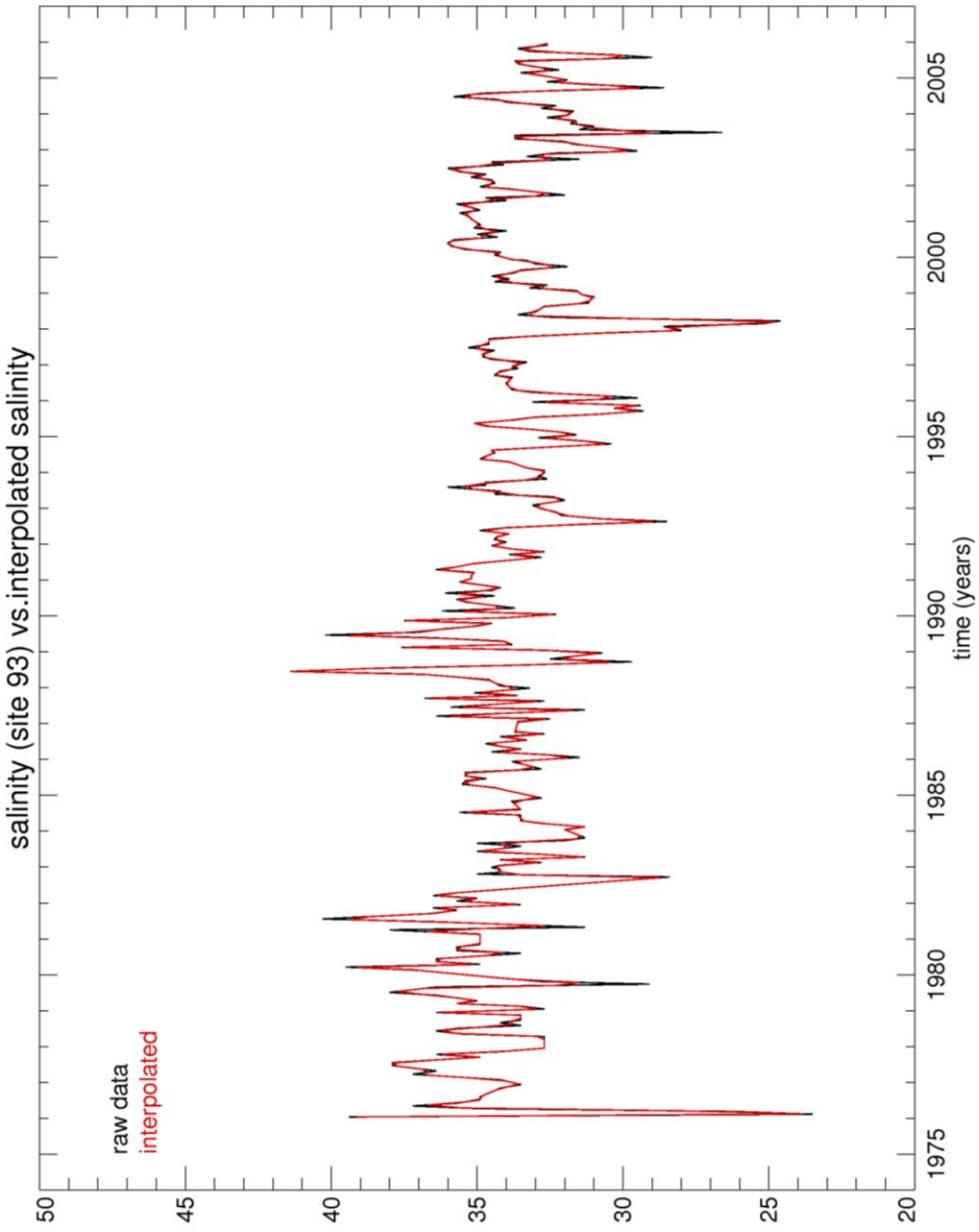

Figure 7. Raw salinity (black) versus interpolated salinity (red).

EFDC Model

The model used for this study is the Environmental Fluid Dynamics Code (EFDC) model that was developed at the Virginia Institute of Marine Science (Hamrick, 1992). The physics and many aspects of the computational scheme of the EFDC model are equivalent to the Blumberg-Mellor model. The model solves the three-dimensional, vertically hydrostatic, free surface, turbulent averaged equations of motion for a variable density fluid. EFDC uses a stretched or "sigma" vertical coordinate and Cartesian or curvilinear, orthogonal horizontal coordinates and solves the dynamically coupled transport equations for turbulent kinetic energy, turbulent length scale, salinity and temperature. The model allows for drying and wetting in shallow areas by a mass conservative scheme. This wetting and drying capability allows for model stability during extreme events. Without this stability the model bathymetry would have to be artificially deepened so that no grid cells go dry during an extreme event. With this capability a more accurate picture of how water levels change during extreme events can be produced.

The numerical scheme to solve the equations of motion uses second order accurate spatial finite difference on a staggered or C grid. The model's time integration employs a second order accurate three time level, finite difference scheme with an internal-external mode splitting proceducre to separate the internal shear or baroclinic mode from the external free surface gravity wave or barotropic mode. The internal momentum equation solution is implicit with respect to vertical diffusion and is in terms of the vertical profile of shear stress and velocity shear, which results in the simplest and

most accurate form of the baroclinic pressure gradients and eliminates the over determined character of the alternate internal mode formulations.

The EFDC model implements a second order accurate in space and time, mass conservation fractional step solution scheme for the Eulerian transport equations at the same time step or twice the time step of the momentum equation solution. The advective stop of the transport solution uses either the central difference scheme used in the Blumberg-Mellor model or a hierarchy of positive definite upwind difference schemes (Hamrick, 1996). The difference scheme of Blumberg-Mellor will be used in this study.

Bathymetry of the model is based on the previous ECOM-3D model of Tampa Bay. It uses a 70 by 100 grid in the horizontal and 11 sigma levels in the vertical and has a minimum depth of 1.3 MLLW (Figure 8). Model input consist of freshwater input, salinity, zonal and meridional wind components, and elevation. Open boundary conditions at the mouth are provided by measured salinity and sea surface elevation. The EFDC runs on a Dell Precision Workstation 470. A 60 second time step is used. This represents a compromise between the need to satisfy numerical stability and the need for the most rapid computation time. Even with this compromise, the total computation time for the 37 year run was approximately 2 months.

Model Simulation/Evaluation

The EFDC model is run from 1970-2006, with a model time step of 60 seconds. The input files needed to run the model are created from the observational data described previously. The model is initialized with uniform salinity of 35 and elevation throughout the model grid. Salinity from EPCHC site 93 and 2-hr lagged elevation data from the

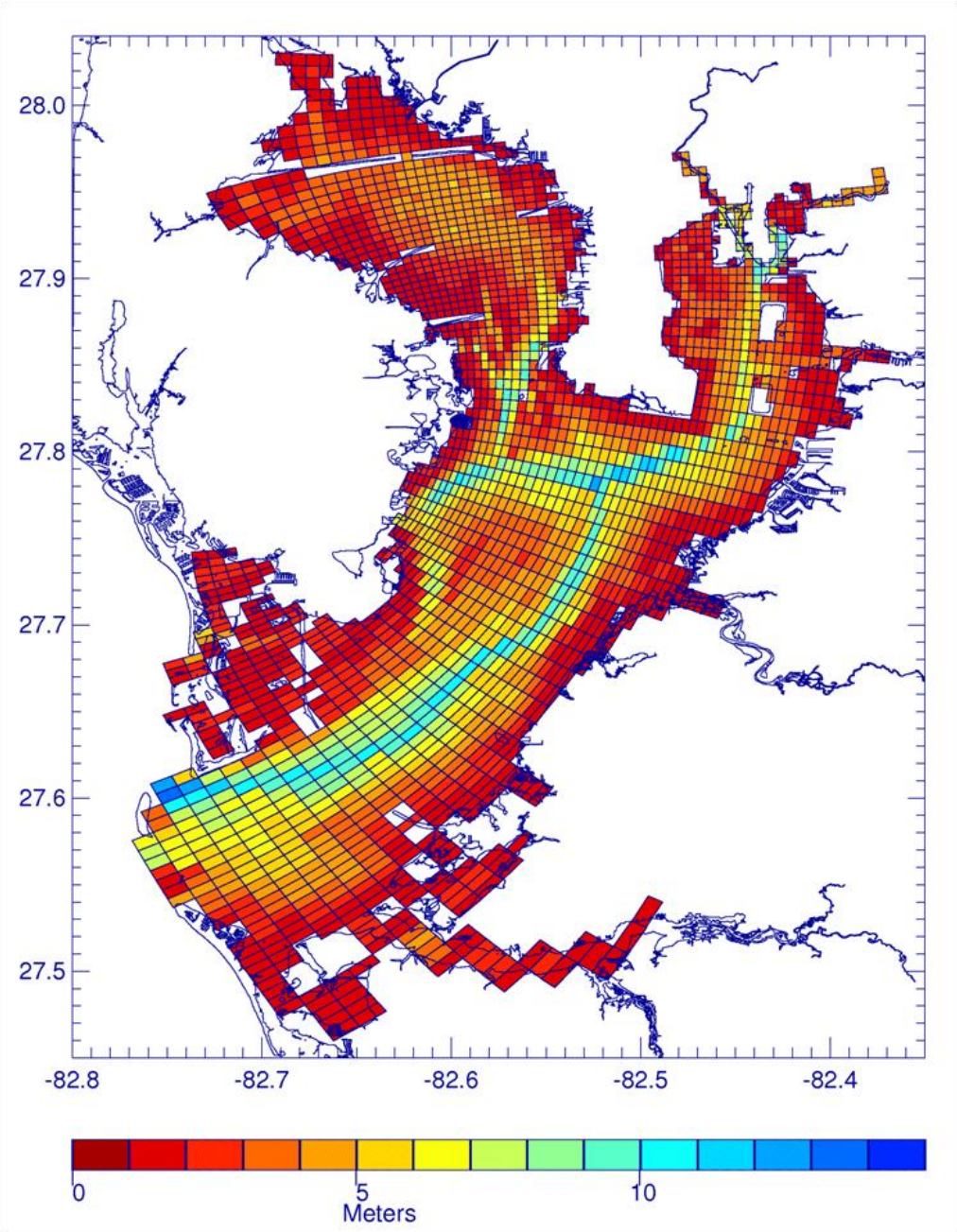

Figure 8. Model bathymetry**.**

St.Petersburg tide gauge are used at the open boundary of the model, near the mouth of the estuary. Spatially uniform winds were used throughout the model grid**.** Winds speed and directions from 5 airports around the bay and the CCUT tower located in the middle of the bay show that wind speeds and directions do not vary much across the bay (Figure 9). This justifies the use of spatially uniform winds. Freshwater was used at the point source locations mentioned previously. The model output was archived hourly for all 37 years.

The 37 year model simulation is divided into two separate model runs (run 100 and run 101). Run 100 archives model output from 1970 -1993 and run 101 archives years 1985 – 2006. Run 100 started in January of 1970 and crashed in April of 1993. This run took approximately two weeks to complete. Reasons as to why the model crashed are still unknown. Model output during the end of run 100 is looked over extensively and no known source for the crash is found. Speculation is that the total run time of 37 years is too long for the model to handle. To accomplish the second half of the 37 year run the model is restarted in 1985. A cold start is used with elevation and velocity initialized to 0. A new salinity initialization file is created using model salinity output for 1985 from run 100. Run 101 starts in January of 1985 and ends at the end of 2006. To get a continuous 37 years of model output, comparisons between the overlapping years of run 100 and run 101 are done. Mean differences of model output between runs 100 and 101 are calculated for the years of 1985 to 1993 for elevation, salinity, and the u, v, and w-components of velocity (Figures 10-14). These plots show that it takes ~5 years for the model to converge, so we allow 5 years for model spin up time and model output from 1970-1974 is omitted and a total record of 32 years is used.

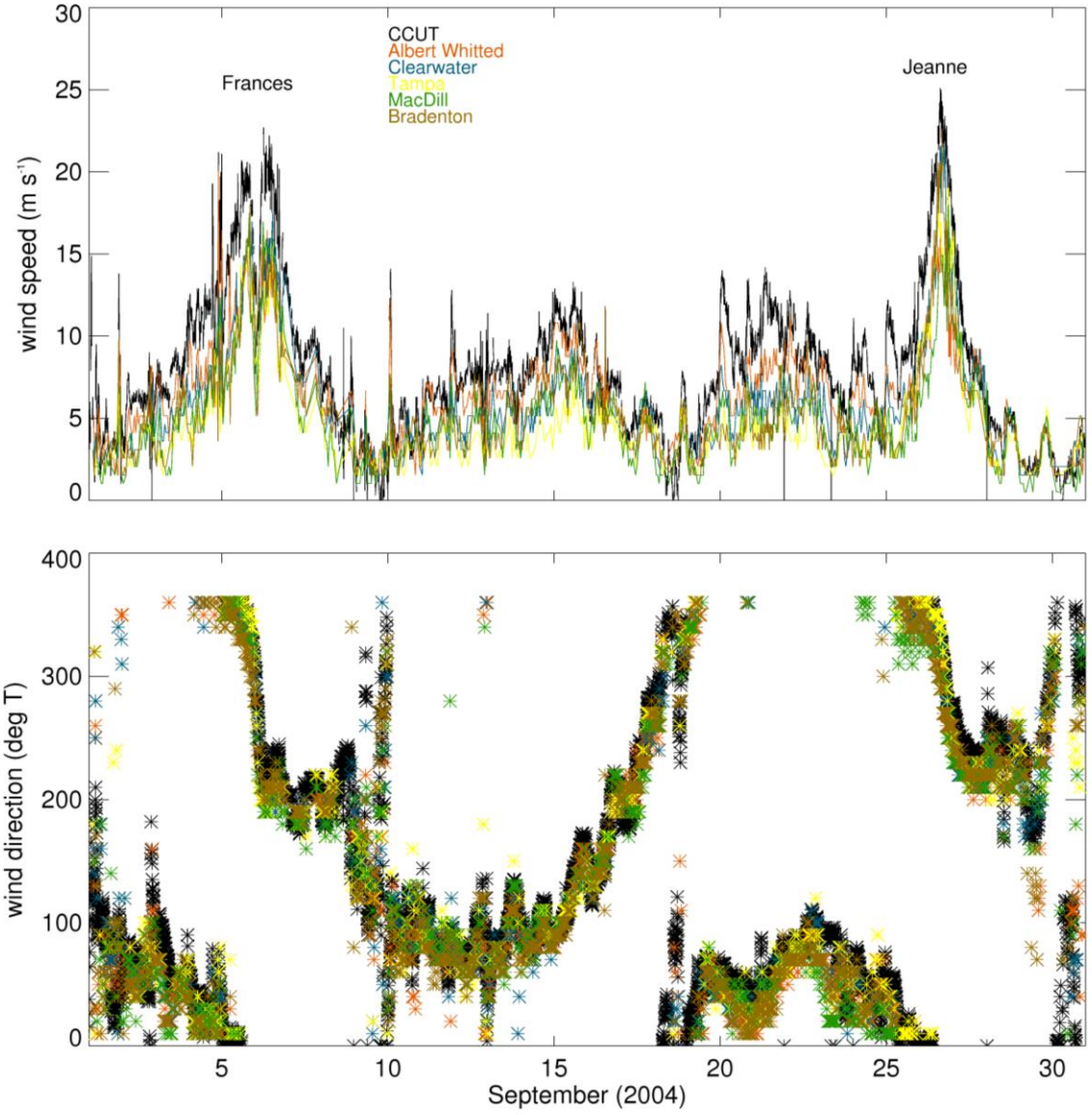

Figure 9. Comparison of wind speeds and directions from 5 airports surrounding the bay and the CCUT tower (black) located in the middle of the bay for September 2004.

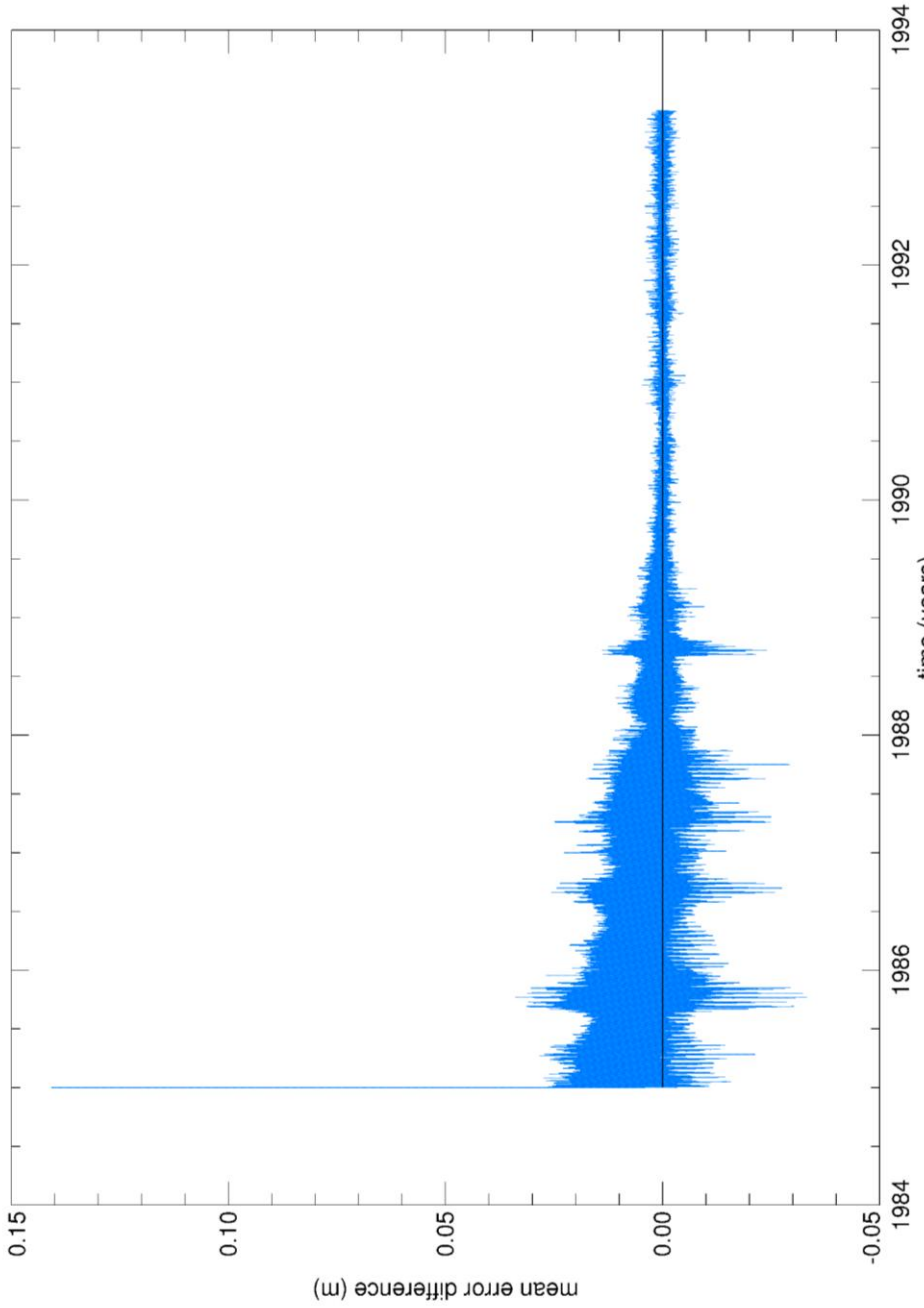

Figure 10. Mean elevation error for model runs 100 and 101.

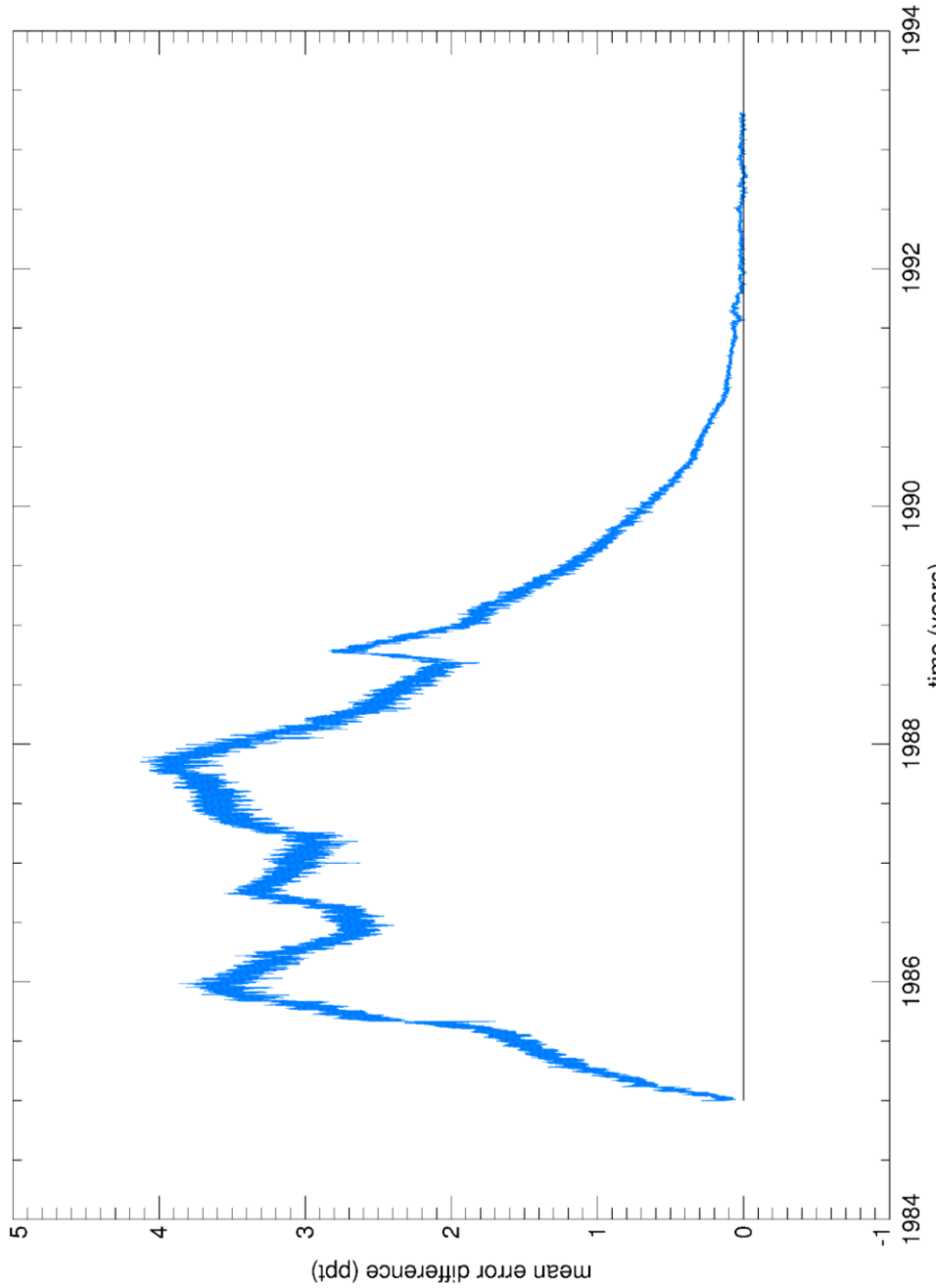

Figure 11. Mean salinity error for model runs 100 and 101.

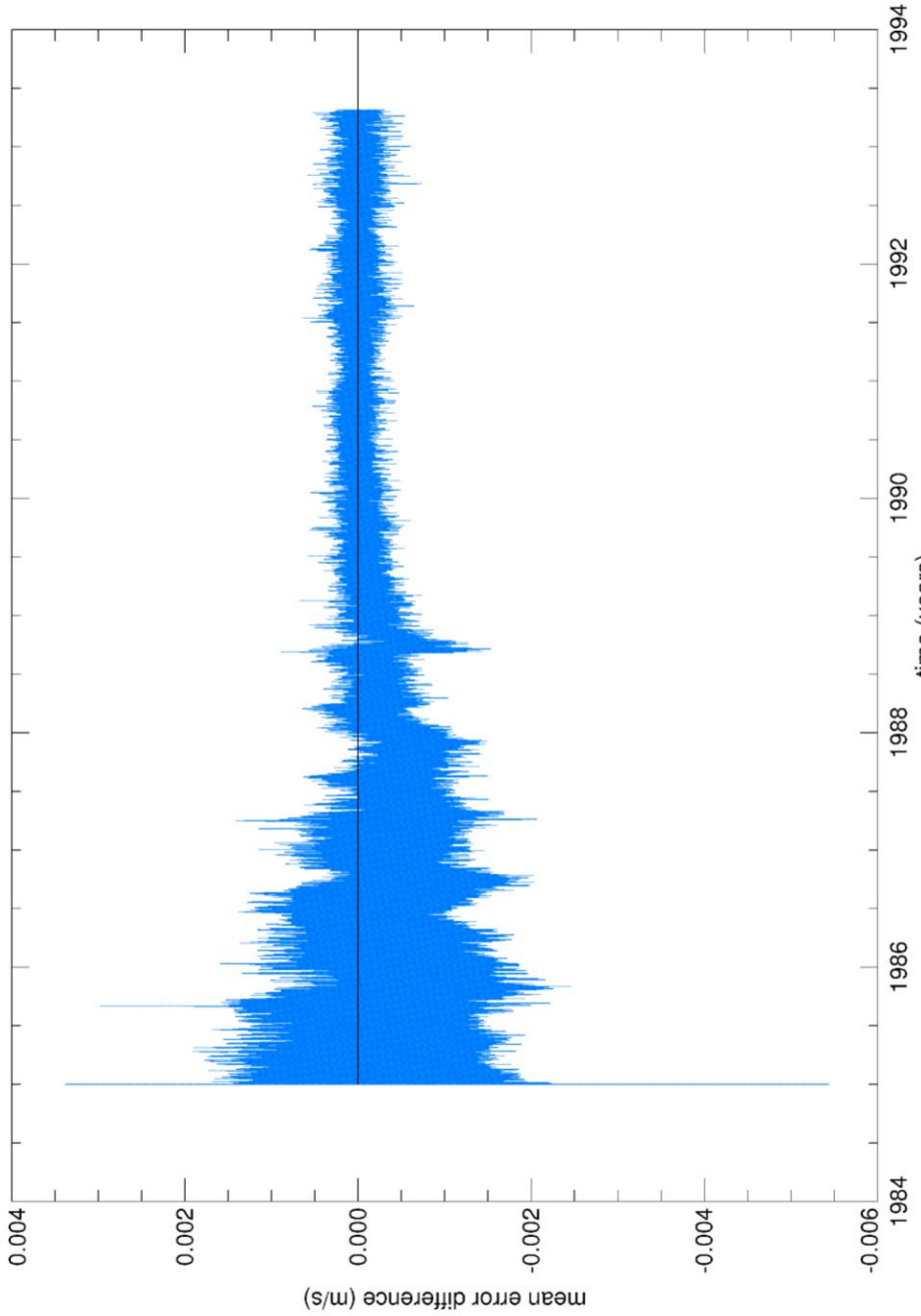

Figure 12. Mean velocity (u-component) error for model runs 100 and 101.

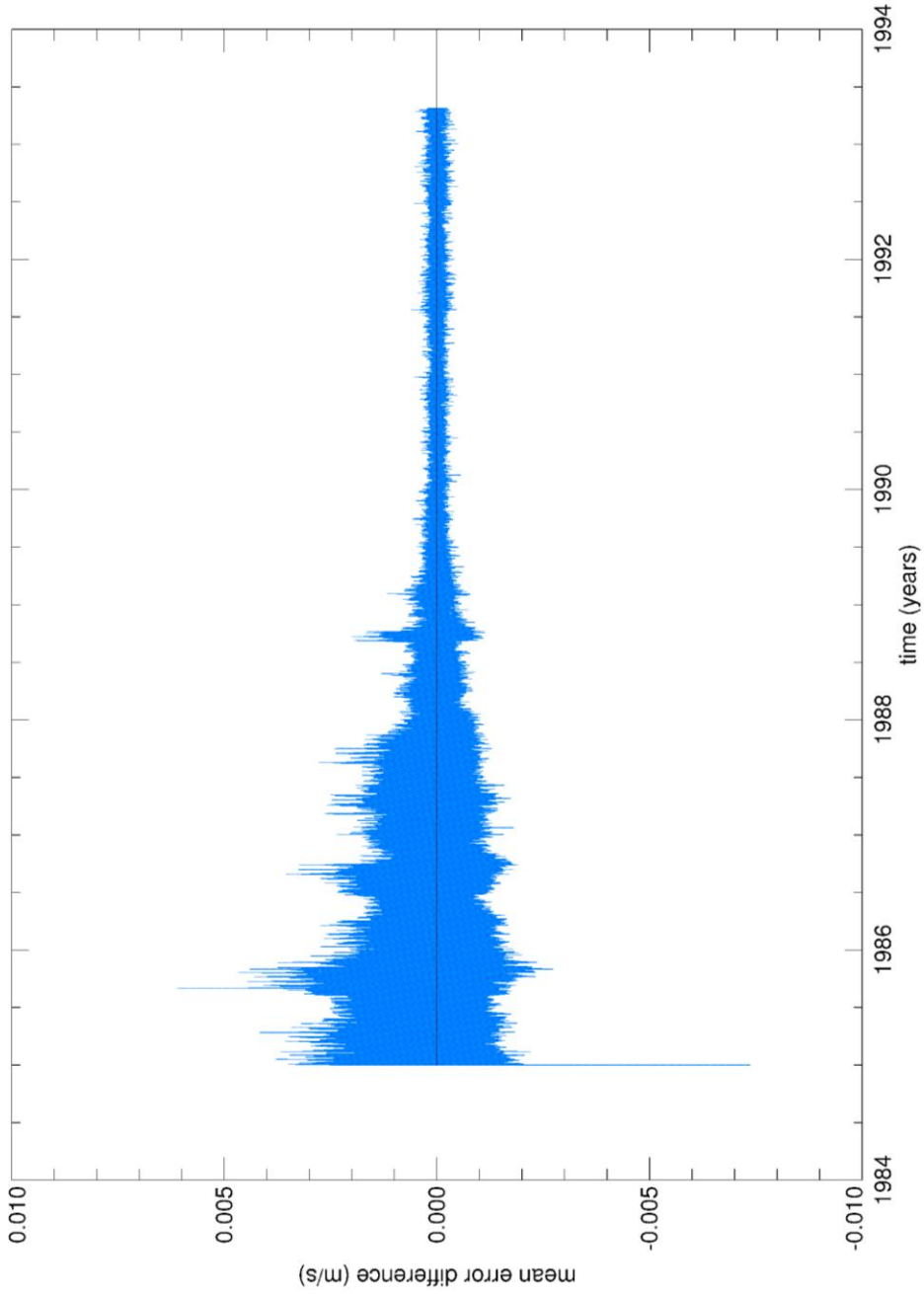

Figure 13. Mean velocity (v-component) error for model runs 100 and 101.

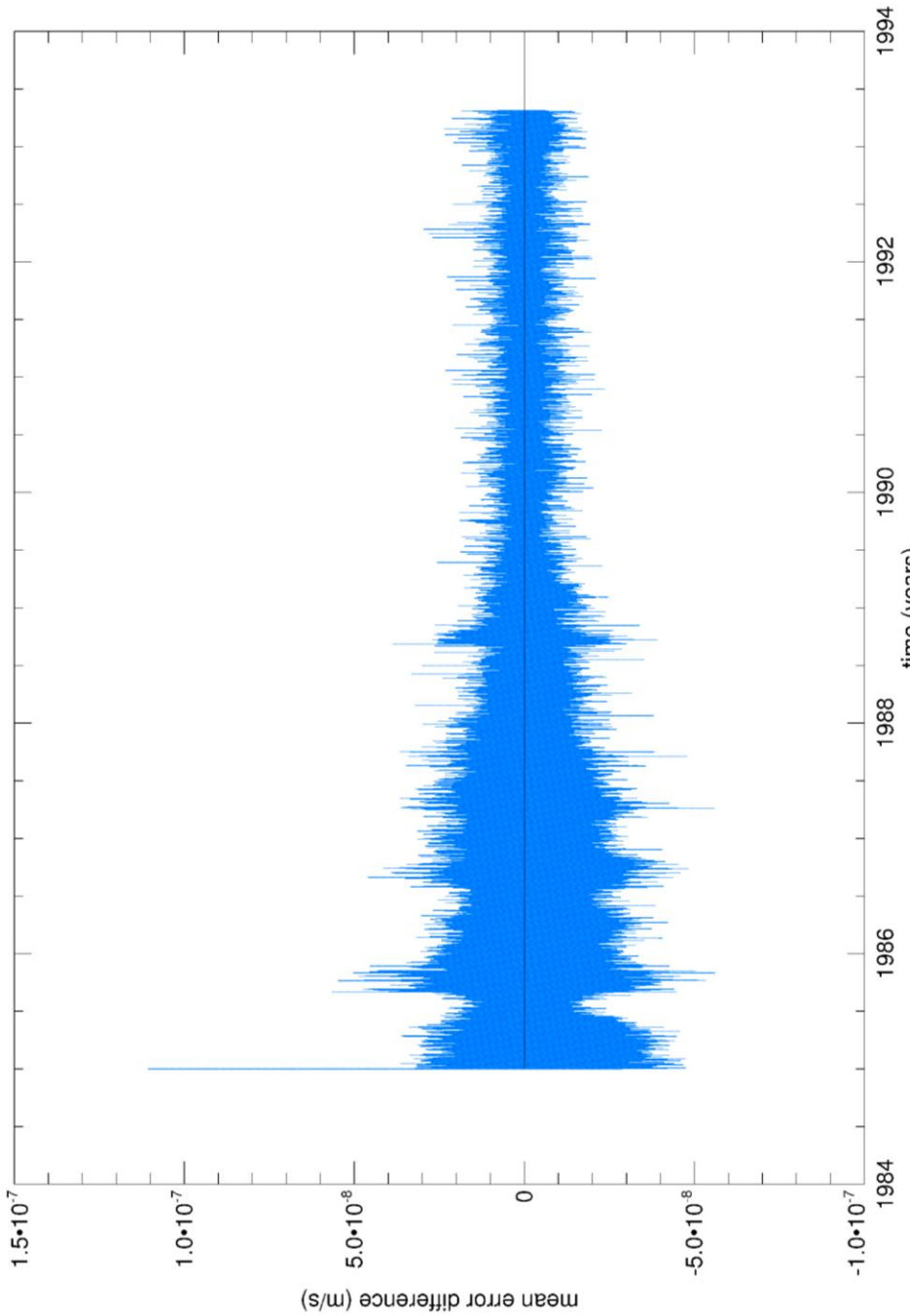

Figure 14. Mean velocity (w-component) error for model runs 100 and 101.

The plots also show that by the beginning of 1993 the mean differences are almost 0 for all variables. This allows the piecing together of model output from both runs without having to do any type of smoothing between years 1992 and 1993.

To evaluate model accuracy, model salinity and elevation output from 1975-2006 are compared to observational salinity and elevation data. I allowed for five years of model spin up time so model output from 1970-1974 is omitted and a total record of 32 years is used. Salinity data from the Bay are compared to the model salinity from the grid cell closest to the locations of each EPCHC site (Appendix A). Model salinity closest to the time of each salinity measurement are extracted from 1975-2006 for a total of 432 data points to calculate bias mean errors and normalized root mean square errors (RMSE) between model salinity output and observed monthly salinity. Normalized RMSE was calculated using the following equation

$$N_{RMSE} = \frac{\sqrt{\frac{\sum (X_M(t) - X_O(t))^2}{n}}}{\sigma_O}$$

where $X_M(t)$ is model ouput, $X_O(t)$ is observational data, n is the number of data points in the integration, and σ_O is the standard deviation of $X_O(t)$. Yearly bias bay mean errors and normalized RMSE for the near surface and bottom are shown in Appendix B. The average bay mean error and normalized RMSE for all 32 years at the near surface is -1.336 and 0.916, -1.455 and 0.993 at the bottom (Figures 15-18). The largest bias errors are seen in Hillsborough Bay and Old Tampa Bay. This is most likely due to the freshwater input flow not being represented accurately and the model resolution. Model elevation is compared to elevation data from the St. Petersburg, Old Port Tampa, Port Manatee, and McKay Bay tide gauges at the 4 grid cell locations closest to each tide

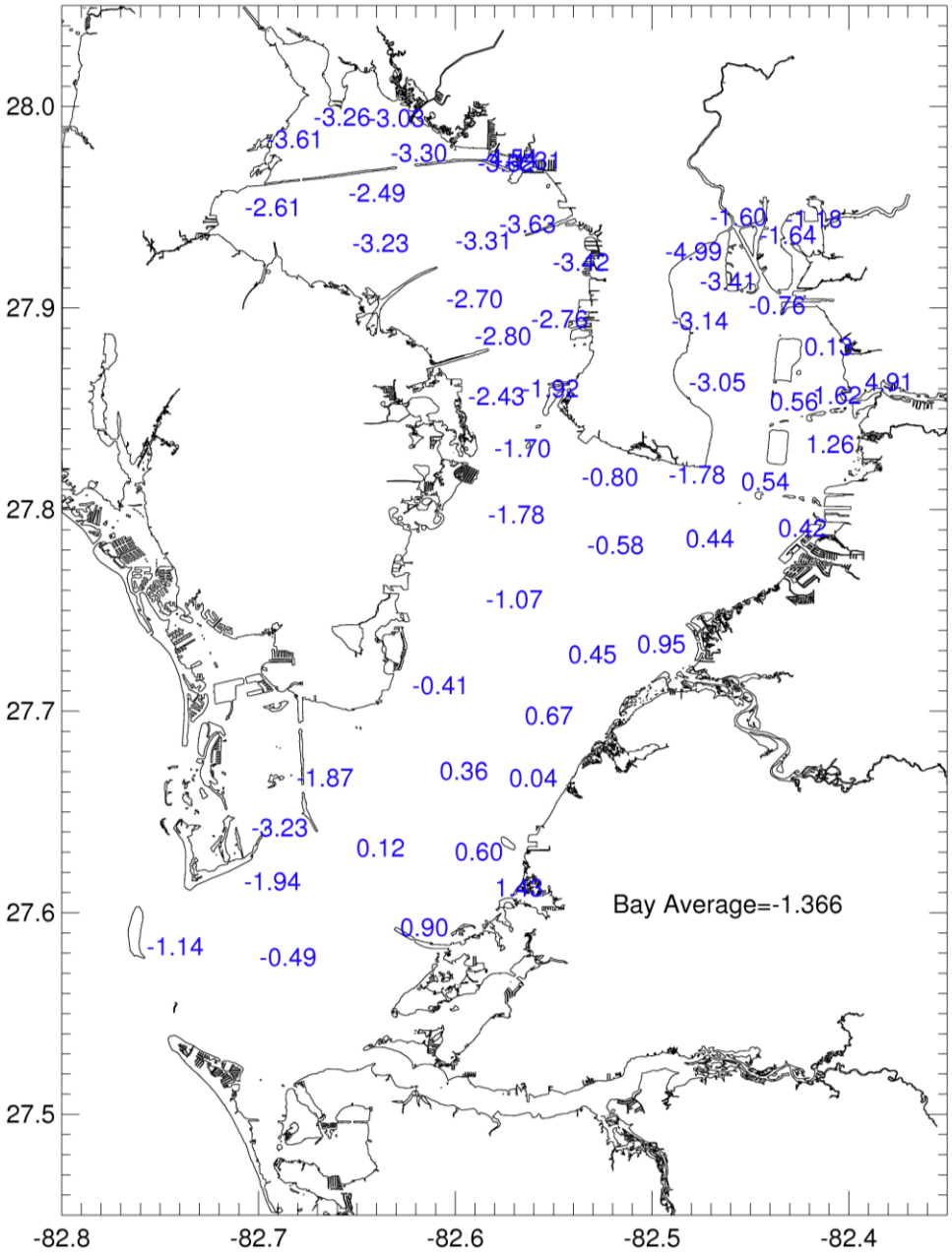

Figure 15. Near surface bias mean error between EFDC salinity output and EPCHC sites for 1975-2006.

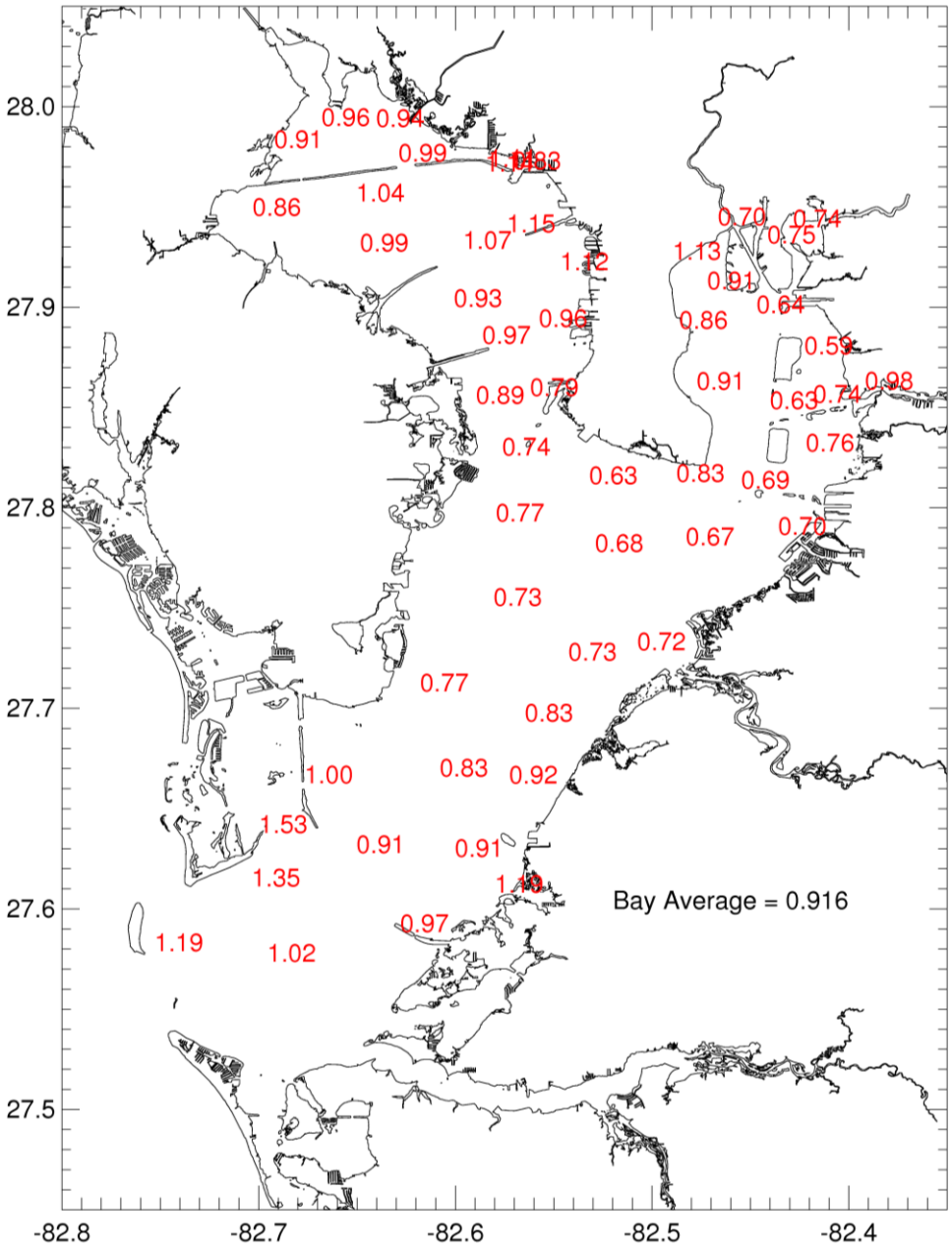

Figure 16. Near surface normalized RMSE between EFDC salinity output and EPCHC sites for 1975-2006.

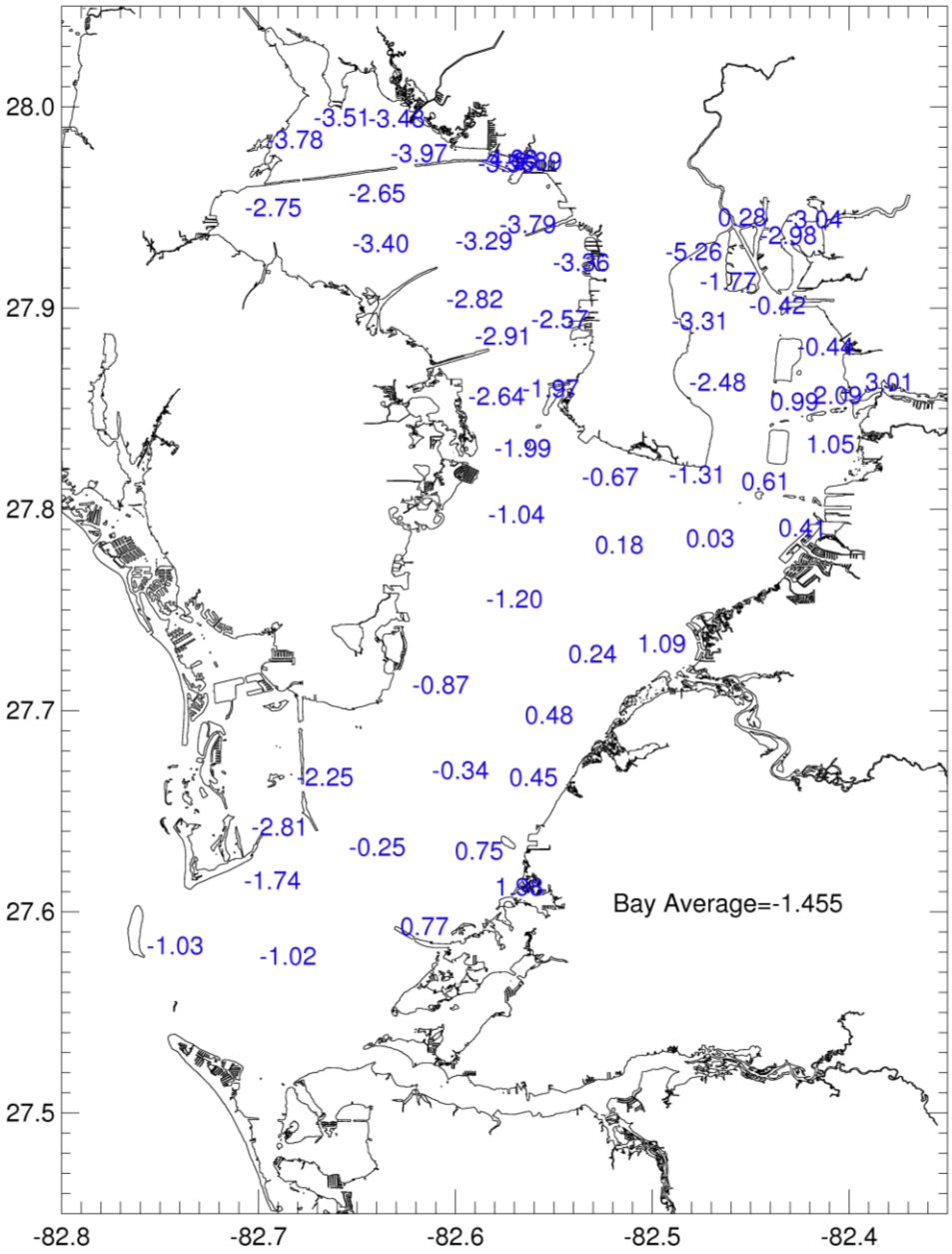

Figure 17. Same as 15 for near bottom.

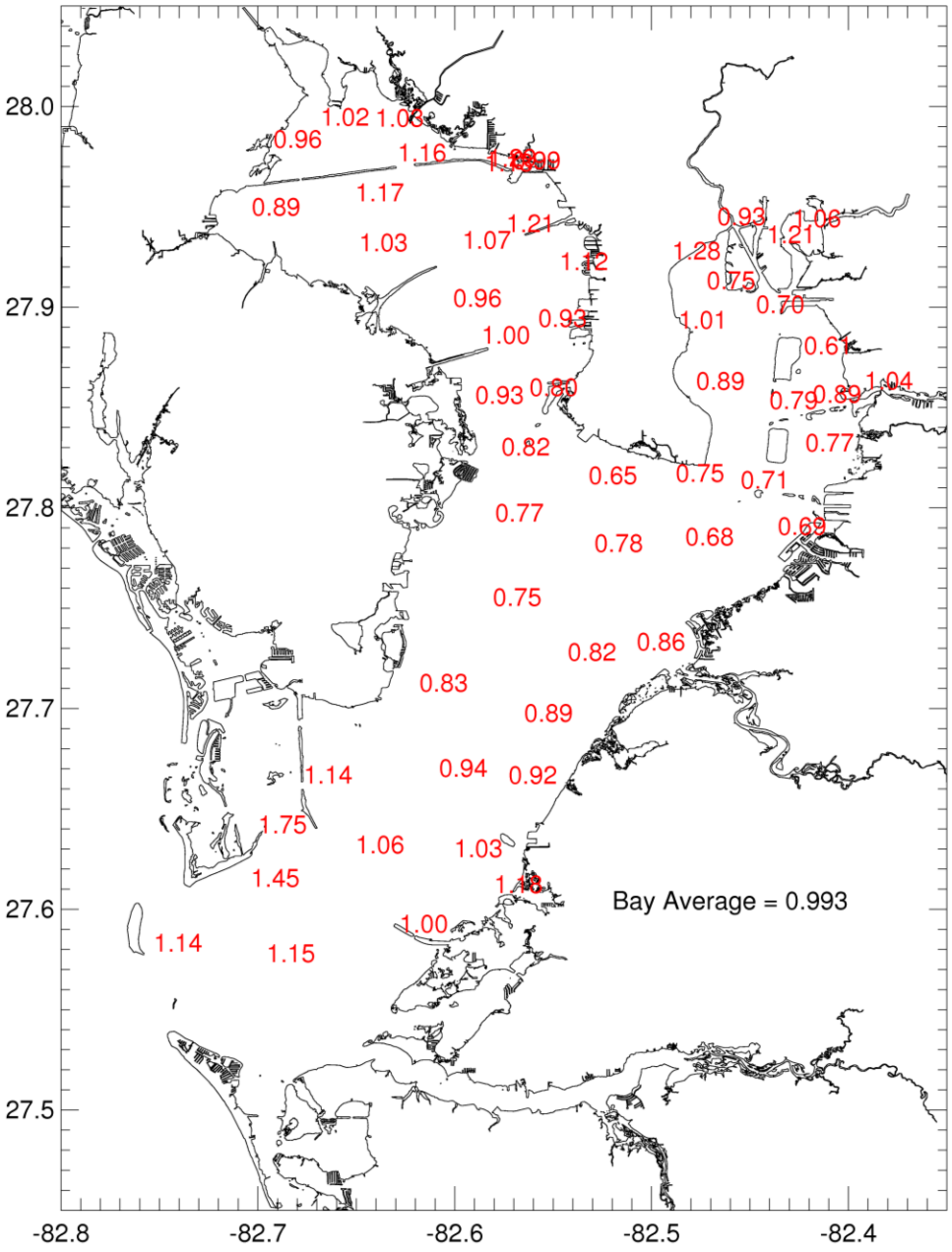

Figure 18. Same as 16 for near bottom.

gauge for the year 2005 (Figure 19). The bias mean errors for elevation at the four different locations are -0.024, -0.019, -0.006, and -0.022, respectively, and 0.21, 0.262, 0.192, and 0.284 for the normalized RMSE. The r^2 values are 0.965, 0.941, 0.965, and 0.925. Yearly comparisons of the model output and the St. Petersburg tide gauge for the entire 32 year period can be seen in Appendix C.

The axial (v) velocities of the model at grid cell (34, 24) and the bottom mounted ADCP located under the Sunshine Skyway Bridge are also compared for 2004 (Figure 20). The ADCP failed twice during 2004 splitting the data into three segments (first, second, and third in figure 20). The axial model velocities corresponding to the time frames of the three segments are compared to the ADCP data. The three segments for both the model and ADCP are averaged and compared as well. Positive values indicate inflow into the estuary and negative values indicate outflow. Both the model and ADCP velocities show an inflow at depth and outflow near the surface. The ADCP shows stronger inflows than the model, this is due to the model bathymetry. The ADCP is located in the middle of the shipping channel, and the model bathymetry is unable to exactly replicate the steep and narrow channel. The shipping channel in the model bathymetry is wider, causing velocities to be slower at depth. The width of the shipping channel under the Sunshine Skyway Bridge is ~213 m and the depth is ~14 m, making the cross-sectional area ~2982 m^2. The cross-sectional area of the channel represented by the model grid cell at the location of the ADCP is ~6064 m^2. The ratio of the cross-sectional areas is ~2 which would account for the velocity differences between the model and the ADCP. The good representation of salinity throughout the bay by the model shows that the transport is correct.

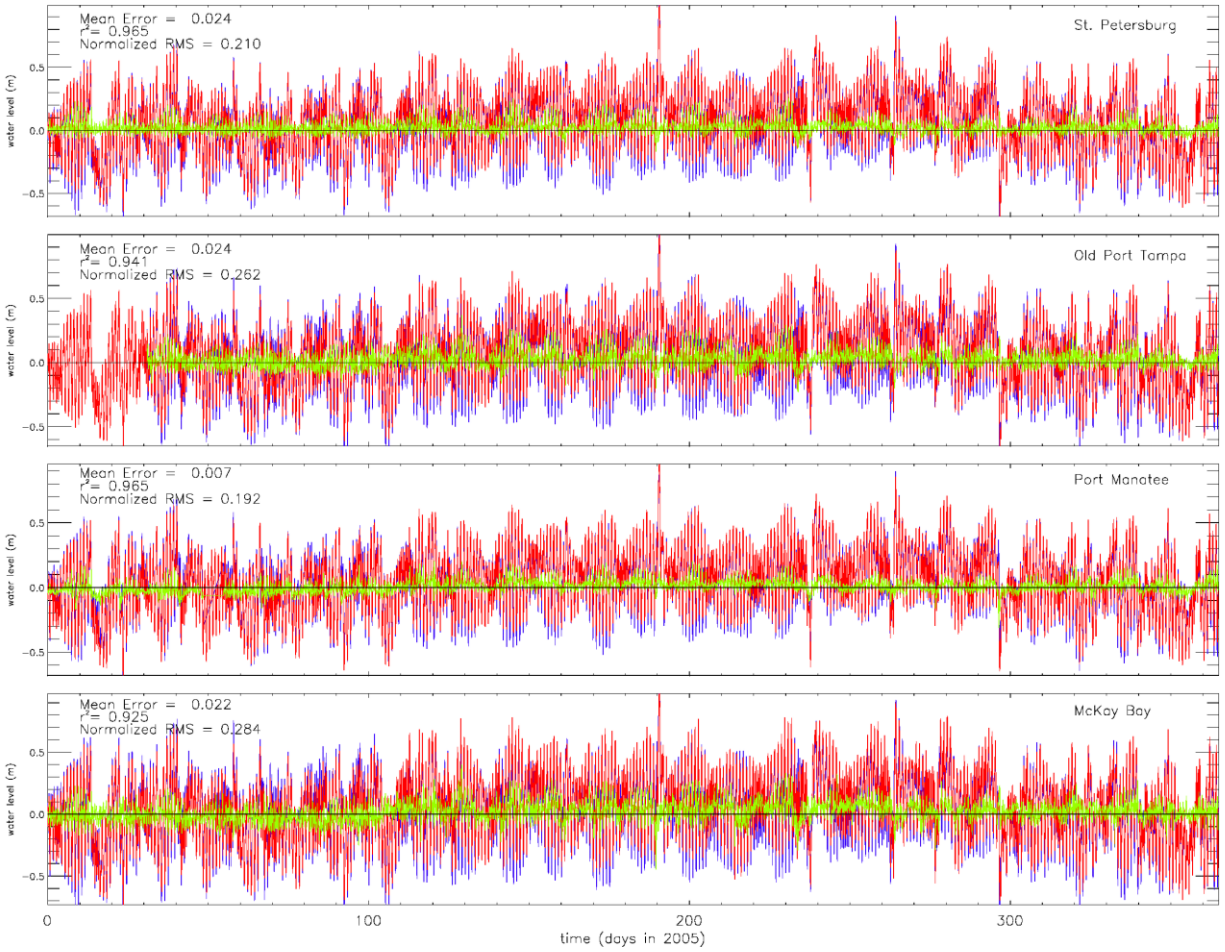

Figure 19. Elevation comparison between EFDC elevation (red) and tide gauges (blue) at (top to bottom): St. Petersburg, Old Port Tampa, Port Manatee, and McKay Bay. The difference is shown in green.

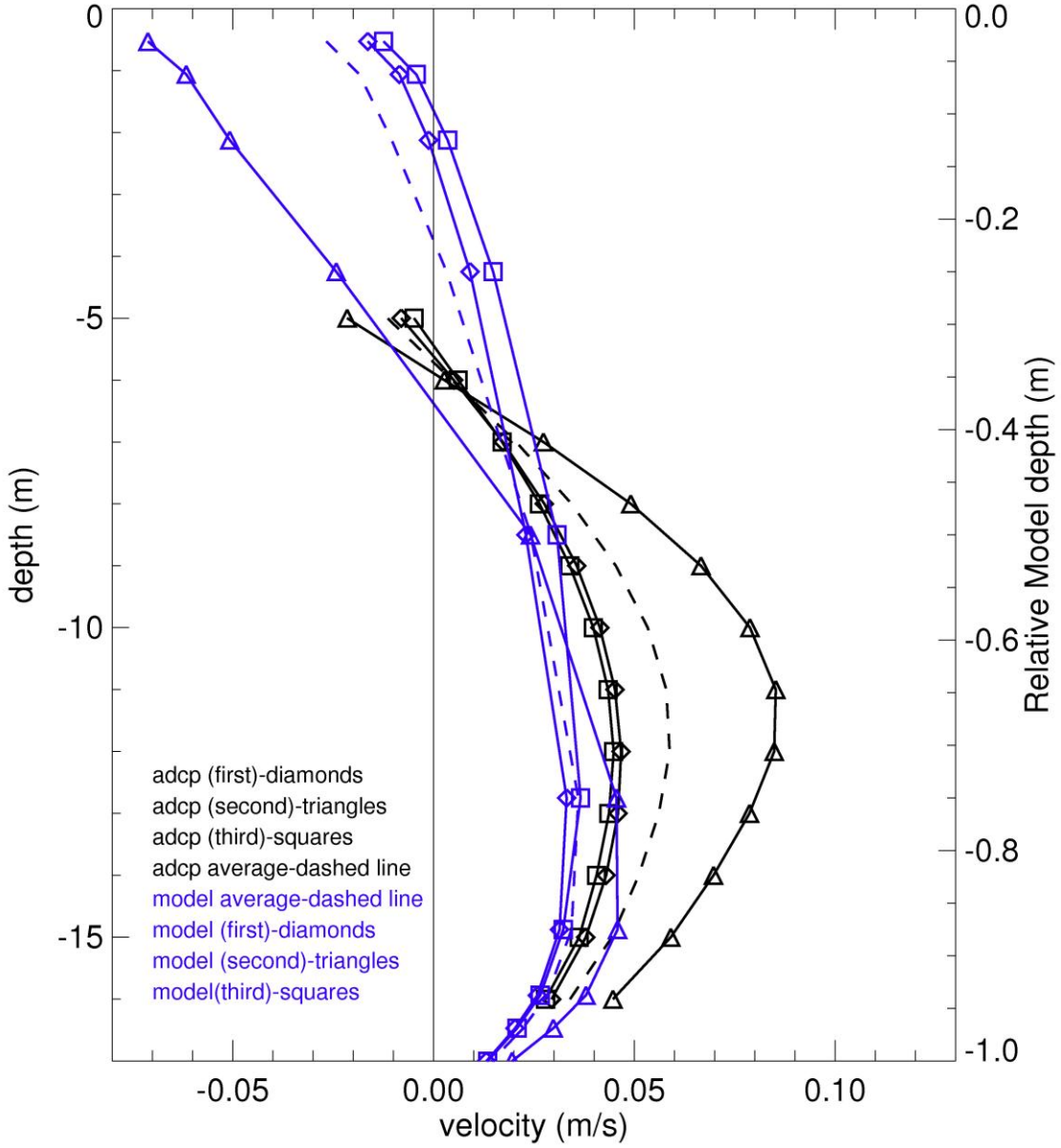

Figure 20. Axial (v-component) velocity depth comparison between the ADCP (black) under the Sunshine Skyway and the corresponding model grid cell (blue) for 2004.

Chapter 2: Synoptic Volumetric Variations and Flushing of the Tampa Bay Estuary

Note to Reader

Work, tables, and figures from this chapter has been previously published (Wilson et al., 2013) and is utilized with permission of the publisher (Springer).

Introduction

In the extratropics, day-to-day weather is controlled by synoptic-scale atmospheric circulation. The main features of this circulation dictate the type of air mass, radiation, temperature, moisture, and pressure over an area (Comrie and Yarnal, 1992). There are two dominant air masses over the southeastern United States, the maritime tropical and continental polar. During summer the maritime tropical air masses are driven into the Southeast by the clockwise flow of air around the Bermuda High. As these warm, the moist air moves inland and interacts with the relatively hot surface to produce frequent air mass thunderstorms (Critchfield, 1983). This convective storm activity, usually in the form of late afternoon thunderstorms, supplies most of the precipitation for the southeast during the summer. In winter, the southeastern states are an interaction zone between the warm, moist maritime tropical air from the Gulf of Mexico and the cold, dry polar air from Canada. The contrast in air masses creates baroclinic instability, which leads to cyclogenesis, and the development of middle latitude wave cyclones. The wave cyclone is associated with warm, cold, and occluded fronts that supply the bulk of wintertime

precipitation in the region. The polar front jet stream also tracks directly across the Southeast, which causes the region to experience frequent cyclonic activity in winter from storms that are spawned within the region (Soulé, 1998). In Florida, winter-frontal systems pass through bringing cold air from Canada and generating strong, sustained wind and increased precipitation (Schoellhamer, 1995).

The El Niño-Southern Oscillation (ENSO) is a dominant source of interannual climate variability around the world (Trenberth, 1997). Changes in atmospheric pressure across the equatorial Pacific during ENSO are accompanied by shifts in tropical rainfall, and affect wind patterns over most of the globe (Rasmusson and Carpenter, 1982), e.g.strengthening of jet streams and steering of extratropical storms and frontal systems along paths that are significantly different than normal. Climate changes associated with ENSO occur across the United States (Enloe et al., 2004). At time scales greater than a year, ENSO dominates the sea level signal in San Francisco Bay where it creates a 10-15 cm fluctuation (Ryan and Noble, 2007). During El Niño enhanced precipitation occurs over the Gulf Coast and Florida (Smith et al., 1998). Kennedy et al. (2007) analyzed the effects of ENSO on sea level anomalies along the Gulf of Mexico coast and showed that the maximum sea level variability occurred during the winter months of the ENSO warm phase. These changes are caused by deviations in wind speed and direction from extratropical cyclones and frontal boundaries, sea level pressure differences, and tropical cyclones near or in the Gulf of Mexico. Midlatitude synoptic winter weather patterns shift equatorward (poleward) across North America during El Niño (La Niña) events and lead to shifts in temperature and precipitation patterns (Rasmusson and Carpenter, 1982). In Florida, El Niño years tend to be cooler and wetter, and La Niña years tend to be

warmer and drier than normal from fall to spring, with the strongest effect in the winter (Sittel, 1994).

ENSO impacts can also be highly local. Schmidt and Luther (2002) showed that the connection between Tampa Bay (TB) salinity and ENSO is a complicated chain of impacts, from ENSO sea surface temperature anomalies, to global weather patterns, local precipitation effects, spatially variable discharge and runoff patterns within the TB drainage area, through to the salinity distribution. The residual circulation in Tampa Bay estuary is largely driven by the salinity (density) gradient between the bay head and mouth which has a strong annual and interannual signal (Meyers et al., 2007). Important supports of this gradient are freshwater sources near the head which in turn are fed by rainfall in the estuarine watershed. Over the TB watershed, winter wind and rainfall are dominated by synoptic weather events, and in the summer, hurricanes contain energy at the synoptic scale. Strong wind events can drive water across the mouth of the bay, producing a relatively rapid change in bay volume. This happened, for example, when Hurricane Frances displaced about 40% of the bay volume with new ocean water and enhanced the freshwater discharge for days in September of 2004 (Wilson et al., 2006). The effect of multiple smaller wind events on estuarine flushing is not yet well understood, and is what we focus on here.

Estuaries are semi-enclosed coastal regions where ocean water mixes with significant amounts of freshwater (Dyer, 1973; Pritchard, 1956). These freshwater/ocean/land interfaces are biologically productive and economically important. They range from nearly pristine bays to highly urbanized estuaries with extensive built infrastructure supporting large human populations. About half of the largest cities in the

world are built around estuaries (Shi and Singh, 2003). The health of estuaries is often related to their ability to remove pollutants through hydrodynamic flushing, which in turn is driven by multiple mechanisms (Geyer and Signell, 1992). These include tidal currents, baroclinic exchange, and surface wind stress along the main estuarine axis. The tidal and wind-driven flushing produces changes in the estuarine volume, whereas the exchange flow is associated with constant volume (Knudsen, 1900). The biology within an estuary can also be affected by estuarine flushing. For example, by relating phytoplankton species composition to estuary hydrology, Ketchum (1954) demonstrated how the rate of estuarine flushing can be a determining factor for the presence of phytoplankton populations. With phytoplankton playing a key role in the biological food chain, changes in flushing that affect phytoplankton populations could potentially harm the biology at higher trophic levels.

In spite of this complexity, the overall flushing of an estuary often simplifies to a simple mathematical form (Meyers et al., 2013). The linear response of sea level to winds at angular frequency $\omega=2\pi f$ in a narrow estuary of length L, constant depth h, and bottom stress $r(U/h)$, is given by (Wong and Moses-Hall, 1998)

$$\eta(x,\omega) = \left\{\frac{\cos\left[k(L-x)\right]}{\cos\left(kL\right)}\right\}\eta_0 + \frac{1}{ghk}\frac{\sin(kx)}{\cos(kL)}\tau(\omega) \quad (1)$$

where η_0 is the elevation at the mouth, x is the distance from the head (x=0) to the mouth (x=L) in the estuary, g is gravitational acceleration (10 m^2/s), and

$$k = \sqrt{\frac{\omega^2}{gh} - i\frac{r\omega}{gh^2}} \quad (2)$$

with $i = \sqrt{-1}$. The first term is the response to the total remote signal or coastal setup, generated by winds and currents outside the estuary. The second term is the response to

local wind forcing. At low frequencies $\|k\| \ll L^{-1}$ (1) becomes $\eta = \eta_0 + x\tau/gh$, indicating the estuarine response loses phase information and the water level response is "instantaneous." Synoptic winds satisfy this low frequency condition since their frequency is given by $f \ll \frac{\sqrt{gh}}{2\pi L} \sim 1.8 \times 10^{-5}$ s^{-1}.

Wavelet analysis has become a common tool for analyzing localized variations of power within a time series (Torrence and Compo, 1998). The analysis shows how the spectral amplitude and phase change in time-frequency space. Goring and Bell (1999) used wavelets to analyze interannual and decadal variability in sea-level data from two sites in Northern New Zealand along with the Southern Oscillations Index (SOI). Their results show that during El Niño, negative SOI is accompanied by negative mean sea level, however, the relationship is sometimes weak and non-stationary. Percival and Mofjeld (1997) demonstrated that subtidal sea level fluctuations are strongest during the winter and occur at the synoptic scales of 4-16 days, and that there were interannual variations in both the seasonal and intraseasonal fluctuations that coincided with major ENSO events in the Equatorial Pacific Ocean.

This study investigates the link between ENSO and the frequency and strength of volumetric flushing driven by synoptic variability in Tampa Bay. The next section details the data used in this study and explains the volumetric analysis performed and how wavelet variance is used to examine the time-frequency variations in the synoptic activity. The third section gives the results of applying these methods to the observational data. The final section discusses the results and implications of ENSO impacts on estuarine flushing.

Data and Methods

Data

Fifty-seven years of hourly elevation and wind data are obtained. Elevation, relative to Mean Sea Level (MSL), is provided by National Oceanic and Atmospheric Administration (NOAA) Tides and Currents for the St. Petersburg tide gauge (#8726520). Small gaps (< 1 week) in the record are filled with predicted tides. The years 1952 and 1964 are omitted due to large gaps (> few months) in the record.

Hourly wind data are obtained from the NOAA National Climatic Data Center at three locations: Albert Whited Airport, MacDill Air Force Base, and Tampa International Airport (Figure 21). Both the MacDill Air Force Base and Tampa International Airport had data dating back to 1950. The zonal (u) and meridional (v) components are calculated using the wind speeds and directions from each site, then the hourly components from all three sites are averaged. All three sites are used to fill gaps and reduce local effects. All remaining gaps in the data are small and filled by linear interpolation. The zonal and meridional wind components are rotated 40° clockwise from true north to yield the axial (along the main axis of the bay) and co-axial (perpendicular to the main axis of the bay) wind components.

Sea surface temperature monthly Oceanic Niño Index (ONI) is obtained from NOAA's Climate Prediction Center. The warm and cold episodes are identified using a threshold of +/- 0.5°C relative to the average of the 1971-2000 base period (http://www.cpc.ncep.noaa.gov/products/analysis_monitoring/ensostuff/ensoyears.shtml).

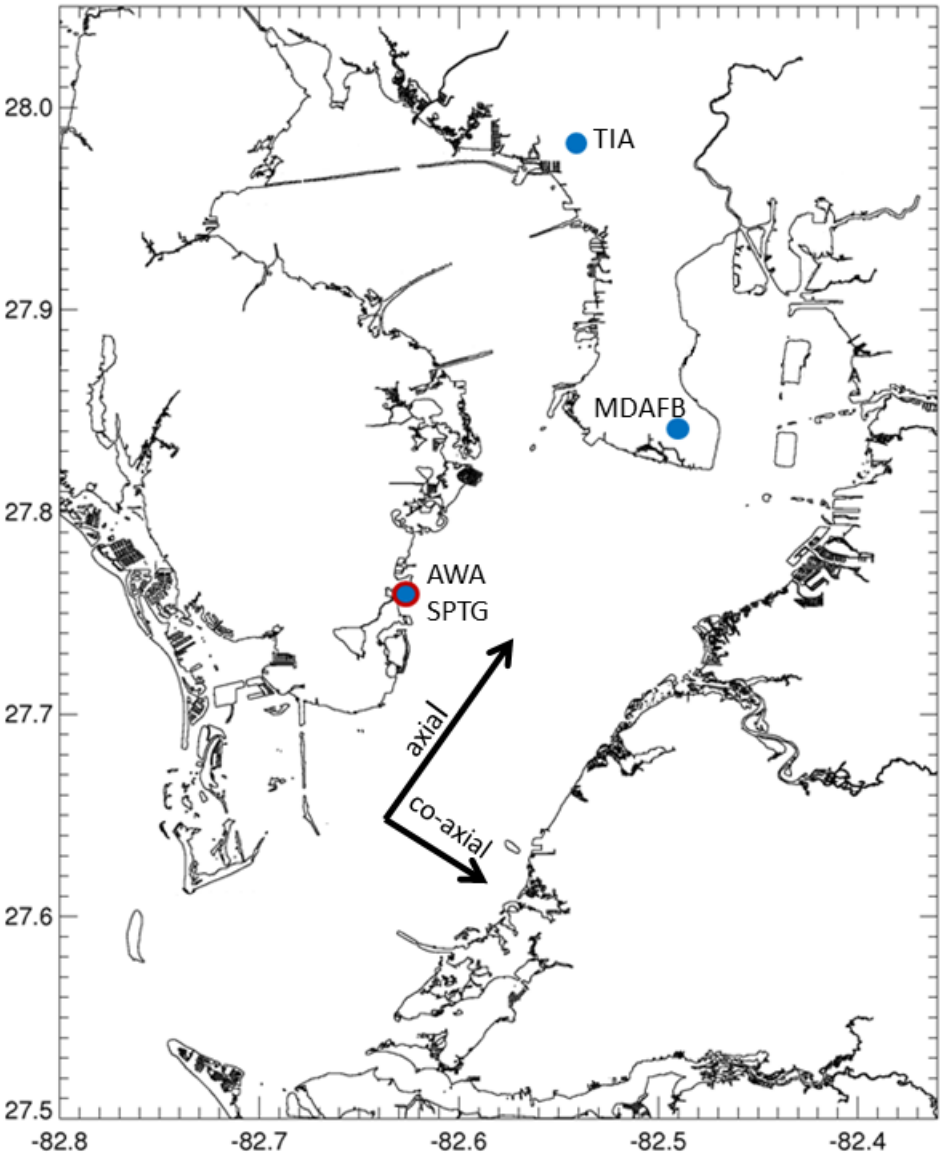

Figure 21. Map of Tampa Bay. Red circle indicates location of the St. Petersburg tide gauge (SPTG) and blue circles indicate airport locations (TIA Tampa International Airport, MDAFB MacDill Air Force Base, AWA Albert Whitted Airport). Arrows show direction of axial and co-axial winds.

Volumetric Analysis

Elevation data from the St. Petersburg tide gauge is used to calculate volumetric changes in the bay. Using a least squares method, the 10 largest tidal constituents in TB are removed from the elevation data. It is then smoothed with a 25-hr box-car filter to remove any residual signals outside the synoptic band. The observed and filtered time series are shown in figure 22. Equation 1 presumes that the synoptic elevation changes at any point are in phase across the estuary so the elevation at any point can be used to represent the mean elevation change and therefore the volumetric change. That is, the synoptic volume is given by

$$V(t) = \alpha \iint_A \eta_i(t) dx dy$$

where η_i is the filtered elevation at location *i*, the integration is over the surface area (*dxdy*) of the bay, and α is an unknown scaling factor to account for the spatial variations of the response in (1) to τ. This is not as simple as creating a linear function $\approx x\tau/gh$ as the η_0 term is also largely driven by the wind stress (Wong and Moses-Hall, 1998). For simplicity we assume $\alpha \equiv 1$.

Ignoring temporal changes to the coastline induced by the contrast between high and lower water levels, the total bay volume can be estimated as $V(t) = \alpha A \eta(t)$. All though this approximation is less accurate at tidal frequencies it still provides a useful value by which to assess the relative importance of the synoptic-scale flushing. The total volumetric flushing is estimated as

$$F(t) = \sum_j \left.\frac{\partial V}{\partial t}\right|_{<0} \quad (3)$$

with the summation limited to time periods *j* when the derivative is negative. $F(t)$ is then

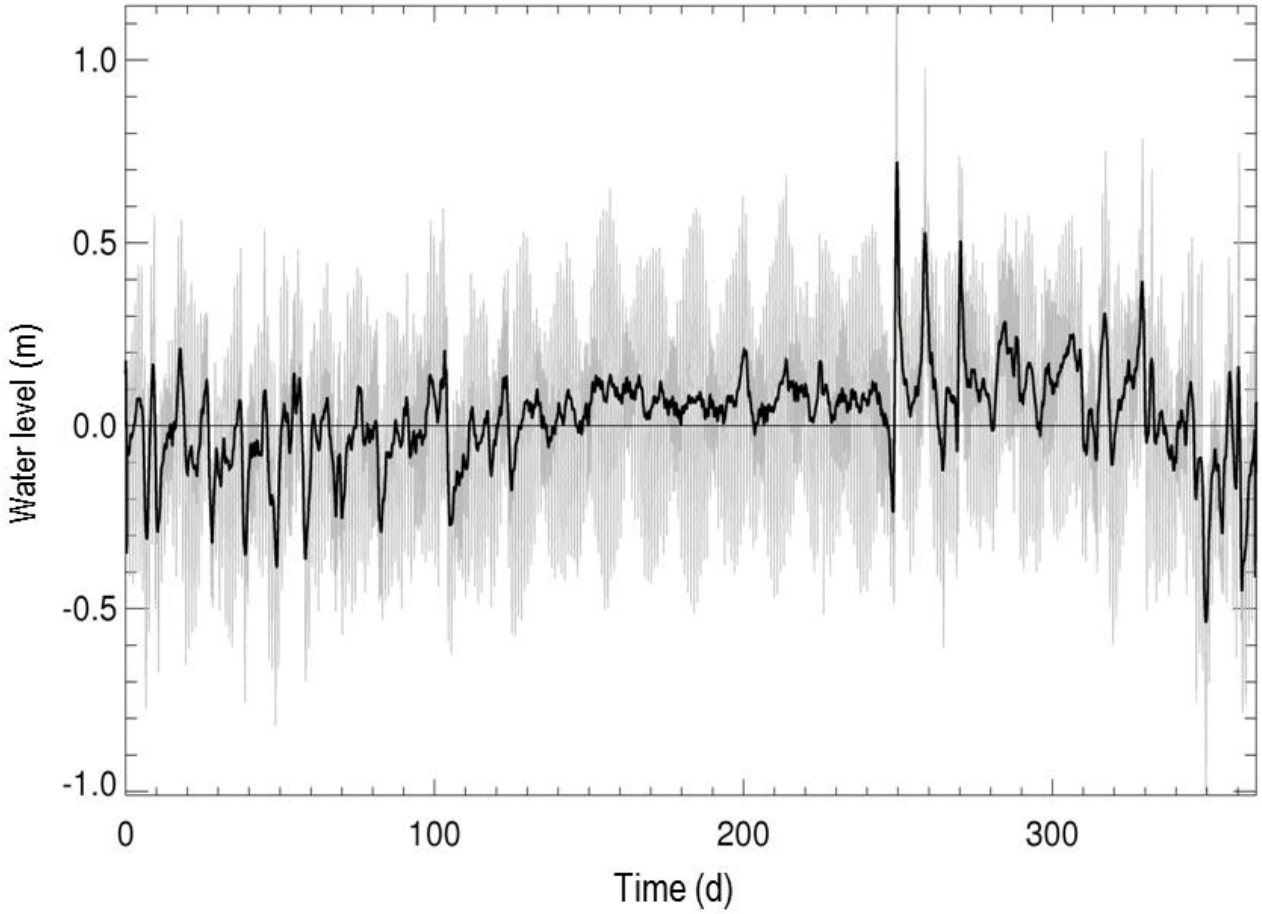

Figure 22. Instantaneous (grey) hourly elevation and elevation low-pass filtered with a 25-hr box car window (thick black) from the St. Petersburg tide gauge for 2004.

normalized by the mean bay volume ($3.8 \times 10^9\ m^3$). A monthly time series $F_m(t)$ is formed by calculating the total of (3) for each month *m* over all the years of data (Figure 23). These monthly values are then used to obtain the monthly climatology, $F_c(t)$, which is subtracted from the monthly values to produce monthly anomalies $F_a(t)$. $F_a(t)$ is then smoothed with a 5-month box-car filter, and the same is done with the monthly ONI sea surface temperatures also shown in figure 23.

Wavelet Analysis

Traditional Fourier spectral methods assume that the underlying (synoptic) processes are stationary in time. However, it is well established that there is a significant seasonal dependence on the impact of ENSO in Tampa Bay. The assumption of stationarity in these methods would "smooth out" this seasonal dependency in the data.

Continuous wavelet transforms expand a time series into time frequency space and as a result find the localized intermittent periodicities (Grinsted et al., 2004). Wavelet analysis provides a better method to filter the synoptic signal and allows for the synoptic scale variance to be calculated without losing the seasonal dependency.

In order to isolate and quantify the variance in the synoptic frequency band as a function of time a wavelet transform (4) is performed on normalized hourly elevation, and the axial and co-axial components of the wind for the entire 55 year record (Appendix D). The wavelet transform is a consecutive series of band-pass filters applied to the time series where the wavelet scale is linearly related to the period of the filter (Grinsted et al., 2004). The one-dimensional continuous wavelet transform is given by

$$T_g(t,a) = \frac{1}{a^{1/2}} \int g\left(\frac{t'-t}{a}\right) f(t')dt' \qquad (4)$$

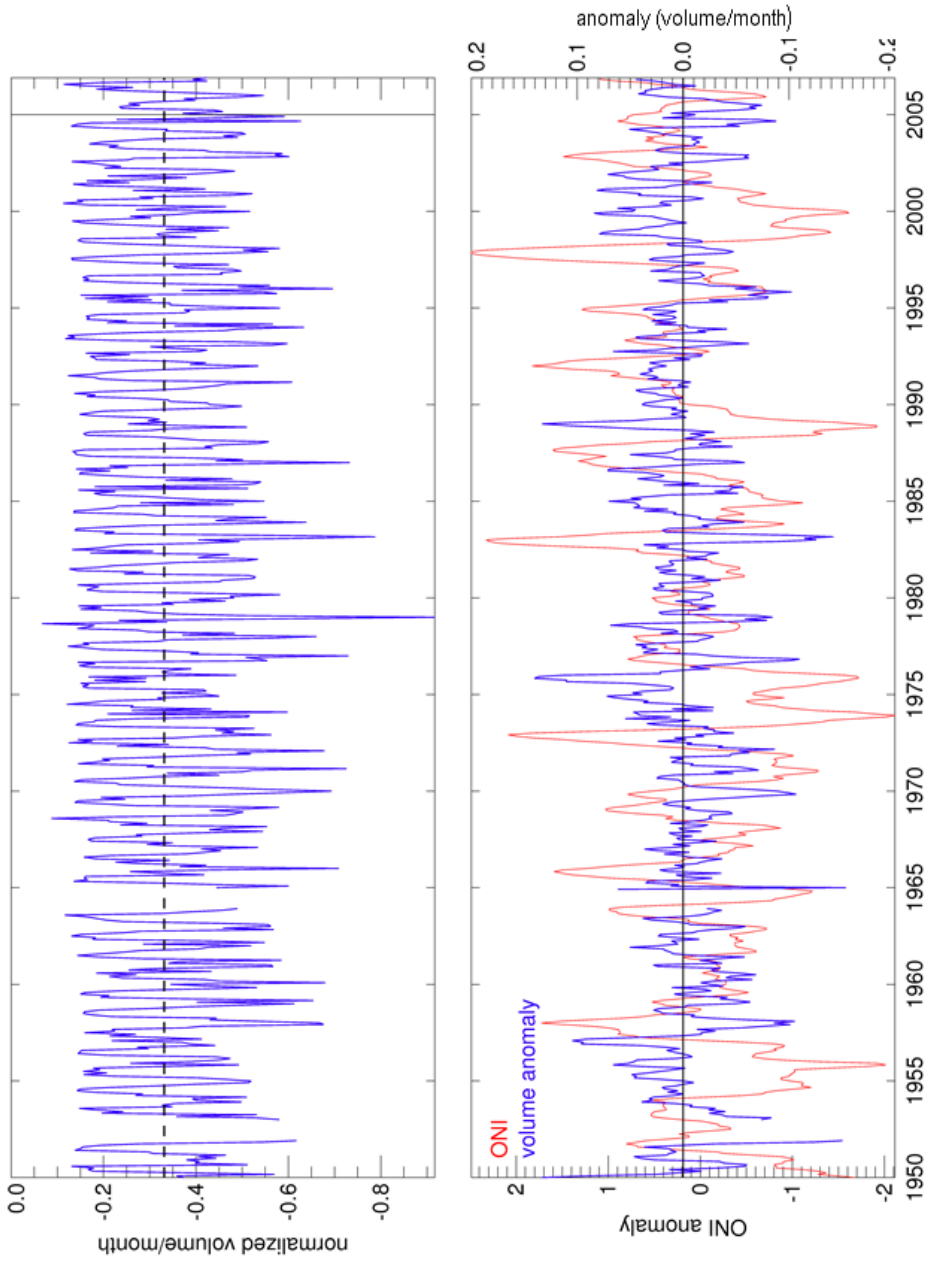

Figure 23. (Top) Total monthly volume outflow normalized by the mean bay volume, dashed line represents the mean (-0.331). (Bottom) Monthly ONI anomaly (red) and monthly normalized volume anomaly, $\boldsymbol{F_a(t)}$, after applying a 5-month box car filter (blue).

where $f(t)$ is the data time series, t corresponds to the time, and a is a scaling parameter (Farge, 1992). All time series examined here are normalized to unit variance before the transform is computed. The Morlet wavelet

$$g(t) = e^{ict}e^{-t^2/2} \tag{5}$$

is used, where $i = \sqrt{-1}$ and c is a scalar here chosen to be 5. The Morlet wavelet provides a good balance between time and frequency localization (Grinsted et al., 2004). The relation of Meyers et al. (1993) converts between the more commonly used and intuitive Fourier period λ and wavelet scale (for the Morlet wavelet) as

$$a = \frac{c+(2+c^2)^{1/2}}{4\pi}\lambda \tag{6}$$

Equation (4) yields a two-dimensional parameter space (t,a) from a one dimensional time series (Emery and Thomson, 2001). The total wavelet variance between periods of λ=2 to 20 days is:

$$E(t) = \sum_\lambda \left\| T_g(t,\lambda) \right\|^2 \tag{7}$$

Using the same methods described in the previous subsection a monthly time series $E_m(t)$ and monthly climatology $E_c(t)$ are calculated to produce monthly anomalies $E_a(t)$ as shown in figure 24. The anomalies are then averaged over seasons as defined by Schmidt and Luther (2002), binned according to the warm, cold, or neutral ENSO phases defined by ONI, and then averaged to produce seasonal anomalies (SA) (Figure 25).

A Kruskal-Wallis test is used to compare variations of ENSO phases during each season for each variable. The Kruskal-Wallis test is a non-parametric form of the ANOVA (a collection of statistical models used to analyze the differences between group means and their associated procedures) that is used to compare three or more groups of

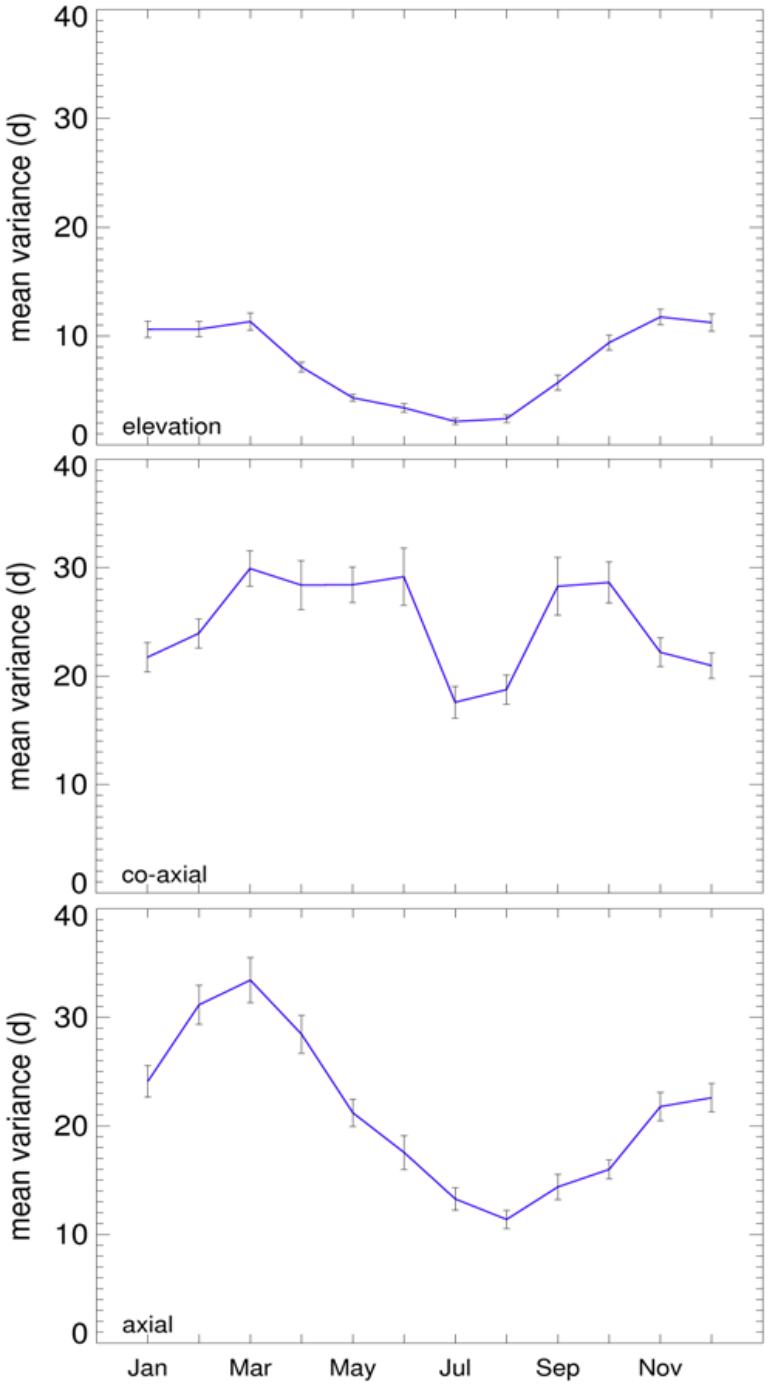

Figure 24. Monthly annual climatology, $E_a(t)$, of synoptic wavelet variance for normalized elevation, co-axial, and axial wind components as indicated. Error bars are the standard errors of each monthly bin. Normalization is 0.25 cm for elevation and about 4m/s for wind, respectively.

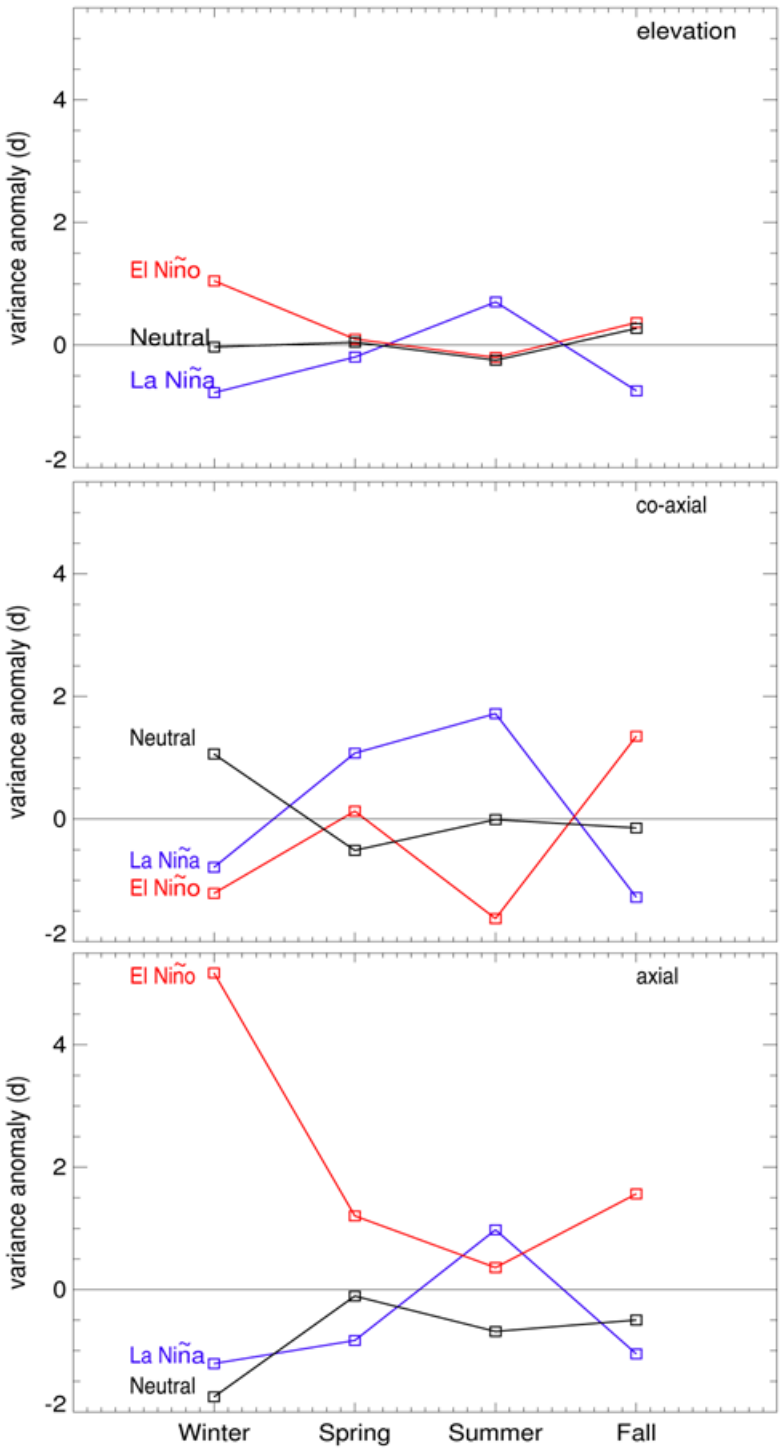

Figure 25. Seasonal anomalies of synoptic wavelet variance for normalized elevation, co-axial, and axial wind components. La Niña years are shown in blue, El Niño in red, and neutral years are in black (note the lines are drawn for presenting purposes but do not indicate a continuous function)

sample data. This method is used to determine if the mean anomalies are significantly distinct from each other within each season. The Kruskal-Wallis test returns the H-statistic and the probability of obtaining a value equal to or greater than H from a Chi-square distribution (Table 3) (Kruskal and Wallis, 1952).

Table 3. Results of Kruskal-Wallis test. Table provides the H-statistic and probabilities of the null hypothesis being true.

	Winter		Spring		Summer		Fall	
Variable	H-stat	Prob.	H-stat	Prob.	H-stat	Prob.	H-stat	Prob.
Elevation	4.825	0.096	0.7418	0.69	2.841	0.242	2.12	0.346
Co-axial	1.201	0.548	0.305	0.859	2.389	0.302	2.789	0.248
Axial	4.868	0.0878	0.145	0.93	2.452	0.294	2.029	0.363

Results

The volumetric flushing (3) has an annual cycle ranging from approximately -0.1 to -0.7 bay volumes per month (Figure 23). The mean total monthly outflow is -0.331 bay volumes. The minimal outflow occurs during the summer/early fall months and maximums in the winter. The summer/early fall outflows are typically -0.15. A large summer outflow, about -0.25 bay volumes/month, is found during 2005. This increase in volumetric outflow flushing can be attributed to an extremely active hurricane season in Florida with a total of 6 named hurricanes passing through the area that year. The winter volumetric outflow ranges from -0.4 to -0.9 bay volumes/month and varies much more than the summer.

The volumetric anomalies are nominally ± 0.1 bay volumes per month and weakly anti-correlated with ONI anomalies ($r^2 = 0.097$) (Figure 23). The low r^2 value

is partly due to the use of a stationary technique to analyze a non-stationary signal. Wavelet analysis allows for improved temporal-spectral analysis of the synoptic variance.

The climatological wavelet variance $E_a(t)$, as defined by (7), for elevation and the axial component of the wind have similar seasonal behavior (Figure 24). Both have an annual cycle with summer minimums and winter maximums. The maximum mean normalized variance for elevation is approximately 12 and the minimum is about 2, a factor of 6. For the axial wind component the maximum mean normalized variance is approximately 33.5 and the minimum is about 12. For both elevation and the axial wind the standard errors are much less than the seasonal variation. The co-axial variance is semi-annual and shows a double maximum, during the spring (~30) and early fall (29), and minimums during the summer and winter (17 and 21, respectively). All climatological values in figure 24 are above the 95% confidence level (not shown).

The SAs of elevation and the axial component show a similar pattern for all three ENSO phases (Figure 25). The SA of the axial component of the wind is positive during all seasons of El Niño years. SA is negative during winter, spring, and fall and positive during summer of La Niña years. Elevation shows a similar pattern to the axial component of the wind, during El Niño (La Niña) years, SA is positive (negative) during the winter, spring, and fall seasons and negative (positive) during the summer season. The highest SA for elevation (~1) and the axial component (~5) of the wind occur during El Niño winters and the lowest (-1.8 for elevation, -1.2 for the axial component) occur during La Niña winters. For the co-axial component during the spring and summer of La Niña years, SA is positive. During El Niño years, SA is almost 0 in the spring and negative in the summer. In the winter and fall of La Niña years, SA is negative. During

El Niño years, it is negative in the winter and positive in the fall. The elevation and axial wind component show greater synoptic variance during El Niño winters.

The Kruskal-Wallis test is carried out with the null hypothesis that all values of each ENSO phase in a season are the same. The test results are summarized in table 4. The lowest probabilities of the null hypothesis being true is found during the winter season for both elevation (0.096) and the axial wind component (0.088). The other values range from 0.242 to 0.859.

Summary and Discussion

Changes to the synoptic wind-driven flushing of the Tampa Bay estuary in response to the ENSO cycle is examined using tide gauge data at St. Petersburg, FL for a period of 55-years (Figure 22). Two types of analysis are performed. The first uses the subtidal observed water level as a proxy for mean tidal height (and therefore total volume) to estimate the rate of volumetric outflow. The second uses wavelet analysis to bandpass elevation and wind data in the time-frequency domain in order to isolate the synoptic variance of the elevation and winds.

At time scales longer than about one day, the synoptic scales dominate the variability of surface winds. The response of the water level to wind forcing along the axis of the estuary at these frequencies is in phase across the estuary, though the amplitude will vary, according to (1). This implies elevation at any point in the estuary (in this case St. Petersburg) is a good proxy for total bay volume, this is presumed throughout the analysis here. The strength of the axial synoptic wind varies seasonally, with a summer minimum and winter maximum. This drives a strong seasonal cycle of

volumetric flushing (3) in phase with the wind. The synoptic volume exchange $F(t)$ in winter is about 3.5 times the summer minimum (Figure 23). Mean annual total volumetric flushing is about 4 bay volumes. Winter anomalies of $F(t)$ also vary with the ENSO phase, with higher flushing in the warm phase and lower flushing in the cool phase. The difference between the El Niño and La Niña values is about 0.2 bay volumes/month. If this is maintained over one three-month season it would represent about 15% of the net annual volumetric flushing.

The overall correlation between the ONI and the anomalies of $F(t)$ is small due to the seasonal dependence of the ENSO response. This might suggest using a window technique over a few weeks, but standard Fourier techniques are insufficient for quantifying a 2-20 day signal over a time period of one month. Wavelet analysis provides a quantitative measure of variance and its temporal evolution. The wavelet variance of the elevation and wind components is filtered according to (7) and the monthly average climatology and anomalies are computed. The analysis here examines the average wavelet amplitude between 2-20 days. The quantitative results are weighted to the longer synoptic scales as the wavelet transform puts more energy into the longer scales relative to the shorter scales, both in terms of peak amplitude and scale-"width" of the transform. A partial solution for this is to rectify the amplitude by the wavelet scale $a^{-1/2}$ (Liu et al., 2007). This does not solve the issue associated with the spread (proportional to a) of the wavelet power over multiple scales. The true wavelet amplitude is used since an unbiased measure is not available.

There is close agreement in the mean monthly climatology between the synoptic wavelet variance of elevation and axial winds (Figure 24). The axial wind has a single

summer minimum and winter maximum, as does the elevation. In contrast, the co-axial wind component has both a summer and a winter minimum. The summer minimum in the variance of the axial wind component (Figure 24) is by a factor of three lower than the peak in late winter. The elevation also has a summer lull that is almost a factor of six lower than the winter peak. The increased seasonal change in elevation variance relative to that of the axial wind may be due to additional effects of the co-axial wind component which, though semi-annual, has a late winter/early spring maximum and a summer minimum. Other influences such as freshwater input are not sufficient to account for this variation.

El Niño increases the synoptic variability in elevation during the winter, but decreases it during the summer (Figure 25). The converse is true for La Niña. However, only in the winter season are the difference between all ENSO phases statistically significant (Table 3). This is consistent with previous studies that showed El Niño (La Niña) suppressing (enhancing) hurricane activity in the tropical Atlantic (Bove et al., 1998; Gray, 1984; Smith et al., 2007) and by extension, Florida.

The difference in winter El Niño-La Niña wavelet variances of the synoptic elevation signal is about 20% of the climatological value. Since the winter flushing is about 0.5 bay volumes per month, this means that ENSO can swing the synoptic flushing of the bay by 0.22 bay volumes per month. This contrasts with the volumetric changes of the bay generated by the tides, which is nominally 5.8 bay volumes per month. However, the tidal excursions are only O(1 km) because the frequency of the tidal signal is relatively large. This limits the exchange of water with the Gulf of Mexico to lower Tampa Bay. The tidal excursions associated with the synoptic winds might be longer than

those due to tides because of their relatively low frequency. This is difficult to assess analytically, though a simple model of the length of the tidal excursion is $l = uT/2$, where u is the velocity generated by the wind stress $\tau_w = C_D \rho w$ over the synoptic period T, with drag coefficient $C_D = 0.0012$ and density of air $\rho = 1.2$ kg/m^3. The axial velocity is proportional to $u = \tau_w H/A_z$, where H=4 m is the water depth and A_z is the vertical eddy viscosity. A recent estimate of $A_z = 0.0025$ m^2/s (Arnott et al., 2012) was obtained using observational data from an Acoustic Doppler Current Profiler and a Self Contained Autonomous Microstructure Profiler. If the sustained synoptic wind speed is nominally 1 m/s for 2 days then $l \simeq 86$ km, larger than the length of TB. Even though this calculation is simplistic it does demonstrate the capacity for slow sustained wind stress to have an important impact on mass exchange between the estuary and the ocean. A detailed study of the Lagrangian displacement associated with tides, winds, and exchange flow is beyond the scope of this paper.

The described changes in circulation associated with synoptic variability have the potential to impact mixing and transport within the bay, as well as flushing of the bay and the exchange of water with the Gulf of Mexico. This could in turn impact the retention of pollutants and nutrients, sediment re-suspension and turbidity. These impacts would not only affect the water quality of the bay, but the biological aspects as well. Future work can address these topics by examining time series of velocity, water quality and turbidity for synoptic variability and their links to larger scale climate patterns.

Chapter 3: Simulated Wind Driven Anomalies in Tampa Bay, FL 1975-2006

Introduction

Estuaries are regions of transition from rivers to the open ocean and are characterized by tidal motions from the ocean and gradients of salinity and density associated with the mixing of river water and sea water. These coastal regions are biologically productive and economically important, making the health of these estuaries very important. The health of estuaries is directly related to the ability for pollutants to be removed through hydrodynamic flushing. The rate of estuarine flushing can be a determining factor for the presence of phytoplankton populations (Ketchum, 1954). Flushing times in estuaries can range from hours to minutes for small streams entering directly into the sea, to weeks or months in bigger systems having a large volume (Statham, 2012). To help aid in determining and improving the water quality of an estuary, the effects of winds, tides, and freshwater inflow on these systems must be well understood. The effect of these physical processes, primarily winds, in Tampa Bay, Florida will be the focus of this study.

Circulation plays a key role in nutrient distribution, pollutant distribution and overall health of an estuary, it is important to understand how wind events can alter estuarine circulation and hydrodynamic flushing. Winds can induce subtidal variability in an estuary through remote and local effects. The remote wind effects come predominantly from along-shelf winds, which produce coastal sea level fluctuations along the shelf at the mouth of an estuary. The local wind effect acts directly over the

surface of an estuary and induces estuarine sea level and current fluctuations (Janzen and Wong, 2002). The remote and local wind effects can produce very different patterns of exchange between an estuary and the continental shelf (Wong and Valle-Levinson, 2002).

Weisberg and Sturges (1976) found that fluctuations caused by winds dominated the low-frequency circulation in the Providence River and the west passage of Narragansett Bay. Valle-Levinson et al. (2001) used water density and velocity data from two 75-day deployments across the entrance of Chesapeake Bay in conjunction with wind velocity and sea level records to identify three different scenarios of wind-induced exchange. Their results showed that 1) northeasterly winds tend to cause depth-independent volume inflow only over the northern half of the entrance to the estuary, 2) southwesterly winds caused opposite sea level gradients (relative to NE winds) which caused near surface outflows throughout the entrance and near bottom inflows restricted to the channels, and 3) northwesterly winds were the most efficient in flushing estuarine waters out at every depth. Wong (2002) used data from 2 surveys, lasting approximately 2 months, to show that coastal sea level fluctuations at the entrance to the Indian River Inlet are coherent with winds over periods of 2-10 days, with the highest response corresponding to winds aligned along two directional bands, one broadly centered around the large-scale alongshelf direction and the other centered around the local across-shore direction. In the first case, a positive alongshelf wind toward 40°T forces a drop in coast sea level by prompting a large-scale across-shelf Ekman transport over the continental shelf to the right of the wind. For the second case, winds blowing in the direction normal

to the coastline (90°T) cause a rise/drop in coastal sea level corresponding to an onshore/offshore wind.

Large-scale weather patterns such as winter storms and hurricanes have been known to also alter the wind-induced circulation causing an increase or decrease of water flow into or out of an estuary. Winter storms, extratropical storms, or extratropical cyclones are all large-scale weather systems that are related to strong cold fronts (Feng, 2009). Cold fronts are the boundary between air masses where colder, denser air is moving towards warmer, lighter air (Hsu, 1988). They are the dominate synoptic scale disturbance in the Gulf of Mexico and occur most frequently during the months of October through April, with storm frequency increasing from September to October, reaching a maximum in midwinter, and decreasing more gradually in the spring (Dagg, 1988). They propagate from the northwest to southeast with a recurrence interval of 4-7 days (Angelovic, 1976). Extratropical cyclones tend to form along these fronts due to the atmospheric instability produced by the strong horizontal temperature gradients. Associated with these extratropical cyclones are strong wind fields that can then generate waves and storm surges that may cause large sea level fluctuations along the coasts (Davis and Dolan, 1993). Throughout the Gulf of Mexico coastline these winter weather systems affect sea level at times of several days (Kennedy et al., 2007). The coastal responses, particularly volume exchange between the Gulf of Mexico and coastal bays, to cold fronts and winter storms in the northern Gulf of Mexico have been studied by many. Swenson and Chuang (1983) found that a frontal passage that occurred near Lake Pontchartrain, Louisiana on March 3, 1980 induced volume fluxes that were about six times greater than the normal tidal prism. Walker and Hammack (2000) showed that the

strong northwest winds associated with winter storms could flush 30-50% of water volume out of the shallow bays in the Atchafalaya/Vermilion Bay regions in Louisiana. In Tampa Bay, the high winds and fresh water inflow associated with these extreme events alter the circulation of the bay, producing a significant flushing by increasing water exchange with the Gulf of Mexico (Wilson et al., 2006). On time scales of days, persistent winds that occur during winter frontal passages have a strong impact on residence time in Tampa Bay (Burwell, 2001).

Hurricanes can produce sudden massive disturbances in estuaries and other coastal ecosystems around the world (Greening et al., 2006). Each hurricane has its own individual characteristics causing their effects on ecosystems to be unpredictable. Valle-Levinson et al. (2002) used the data mentioned in Valle-Levinson et al. (2001) to study the response of lower Chesapeake Bay to Hurricane Floyd. The northeasterly winds prior to the passage of the storm caused a net inflow over the shallow northern half of the bay entrance and outflow in the deep channel to the south of the entrance. After the passage the winds shifted to the northwest and coincided with a pulse of freshwater, which set up a seaward barotropic pressure gradient force that drove a net outflow everywhere across the entrance to the bay, allowing no inflow for almost 24 hours. Approximately one-third of the net outflow was caused by wind forcing and two-thirds by freshwater discharge. Walker (2001) studied changes in circulation, water level, salinity, suspended sediments and sediment flux in the Vermiliona-Atchafalaya Bay caused by winds from Tropical Storm Frances and Hurricane Georges in 1998. Both storms caused the highest salinity spikes in the 16-month record and turbidity levels increased by an order of magnitude in this shallow bay system. The winds associated with Tropical Storm Frances cause water

levels to reach the highest value of the year. Wilson et al. (2006) found that during Hurricane Frances there was a displacement of about 40% of the Tampa Bay's volume in a single day. Results indicated that Hurricane Frances dominated the residual circulation during its passage. The high winds associated with Hurricane Frances directly affected the circulation of the bay by increasing surface wind stress. These changes in circulation produced a significant flushing of Tampa Bay.

The previously mentioned studies discuss the short term impacts of extreme weather events on estuarine flushing, long-term (multi-decadal) studies are rare. With the use of a realistic numerical model of Tampa Bay called the Environmental Fluid Dynamics Code (EFDC) the long-term effects of these extreme weather events are examined. Observational data only provides us with point source information, the use of the model allows us to create a 37-year (1970-2007) simulation of salinity, currents, and elevation within the bay. The model output aids in accounting for water level spatial variations when examining the volumetric flushing and calculating flushing rates, allows the investigation of year to year flushing variability, and the examination of the long-term cumulative impacts of wind driven volumetric changes in Tampa Bay.

Flushing rates are a key variable for maintaining estuarine viability. Due to these large scale weather events volumetric changes are induced and so are the associated flushing rates of these estuaries. The objectives of this study are: 1) to use the model output to calculate the wind induced volumetric changes caused by winter extratropical storms and hurricanes, and 2) to find the cumulative impact of flushing of the bay by these wind events. The paper proceeds as follows: section 2 describes the study site, Tampa Bay, Florida, section 3 (model and methods) describes the EFDC model used, the

observational data used to construct the model boundary conditions, model simulation, and the evaluation of model output, section 4 will present our results, and the summary and discussion of this study will be discussed in section 5.

Study Site

Tampa Bay

Tampa Bay is located on the central part of the west coast of Florida, covering approximately one thousand square kilometers with an average depth of approximately 4 meters (Figure 1) (Goodwin, 1987). The width of the Bay is about 15 km at its midsection and roughly 53 km in length. Dredged navigation channels lead to the main port facilities. The depths of the channels have been increased to 15 meters to create the minimum depth required for large container ships to have access to the Bay (Zervas, 1993). The bay has a maximum depth of about 27 meters in Egmont Channel near the mouth of the Bay.

Tampa Bay has a circulation that is 3-dimensional and time dependent (Galperin et al., 1991; Weisberg and Zheng, 2006). Tampa Bay sea level and current variations are controlled by the tides, winds, and river discharge. Tides in the Bay consist of mixed semidiurnal and diurnal tides, with a tidal range of just less than a meter at the mouth to over a meter at the head (Wilson, 2007).

The major freshwater sources for the Bay are located on the east and south sides. The Alafia and Hillsborough rivers drain into the Bay from the northeast, the Little Manatee enters on the eastern side, and the Manatee on the south near the mouth.

Salinities in the bay vary from a high of approximately 35 at the entrance of the Bay to a low of 22 ppt or less in the northern and eastern portions of Hillsborough Bay and the northwest portion of Old Tampa Bay (Boler, 1992).

Ocean water from the Gulf of Mexico enters Tampa Bay through the mouth located on the southwest boundary. With the amount of freshwater inflow into the Bay, its shallow depths, and strong tidal mixing, the salinity is well mixed vertically, however, it does have significant horizontal salinity gradients due to the distribution of fresh water inflow. Freshwater from the north together with saltwater coming from the south produce a strong horizontal salinity gradient. These horizontal gradients and surface wind forcing maintain the fully three-dimensional circulation of the Bay (Li, 1993). Lower salinities at the head of the Bay and the higher salinities at the mouth cause an axial pressure gradient force to exist that drives the non-tidal, gravitational convection mode of circulation (Weisberg and Zheng, 2006).

Burwell (2001) found the residual circulation in Tampa Bay appears to be a mix of classical two layer flow over the shipping channels, denser ocean water flowing in at depth, and fresher water flowing out of the Bay near the surface and along the relatively shallow sides of the Bay. Flushing occurs through the deep navigational channels running northeast/southwest from the mouth. Residence times in the channel are 15 days to one month and increase to over 3 months in regions outside the channels.

Model and Methods

EFDC Model

The Environmental Fluid Dynamics Code (EFDC) model (developed at the Virginia Institute of Marine Science (Hamrick, 1992)) is used for this study. The physics and

computational scheme of the EFDC model are equivalent to the Blumberg-Princeton Ocean Model (Blumberg, 1990). The model solves the three-dimensional, vertically hydrostatic, free surface, turbulent averaged equations of motion for a variable density fluid. It uses a stretched or "sigma" vertical coordinate and Cartesian or curvilinear, orthogonal horizontal coordinates. The model allows for drying and wetting in shallow areas by a mass conservative scheme and a number of alternatives are in place in the model to simulate general discharge control structures.

The numerical scheme to solve the equations of motion uses second order accurate spatial finite difference on a staggered or C grid. The model's time integration employs a second order accurate three time level, finite difference scheme with an internal-external mode splitting procedure to separate the baroclinic mode or internal shear from the barotropic mode or external free surface gravity wave. The internal momentum equation solution is implicit with respect to vertical diffusion and is in terms of the vertical profile of shear stress and velocity shear. This results in the simplest and most accurate form of the baroclinic pressure gradients and eliminates the over determined character of the alternate internal mode formulations.

The model implements a second order accurate in space and time, mass conservation fractional step solution scheme for the Eulerian transport equations at the same time step or twice the time step of the momentum equation solution. The advective stop of the transport solution uses either the central difference scheme used in the Blumberg-Mellor model or a hierarchy of positive definite upwind difference schemes (Hamrick, 1996). The difference scheme of Blumberg-Mellor will be used in this study.

Bathymetry of the model is based on the previous ECOM-3D model of Tampa Bay. It uses a 70 by 100 grid in the horizontal and 11 sigma levels in the vertical and has a minimum depth of 1.3 m MLLW (Figure 8). Model inputs consist of freshwater input, salinity, zonal and meridional wind components, and elevation. Measured salinity and sea surface elevation provide the open boundary conditions at the mouth of the bay. The EFDC runs on a Dell Precision Workstation 470. To reach a compromise between the need to satisfy numerical stability and the need for the most rapid computation time, a 60 second time step is used. The total computation time for the entire run was approximately 2 months.

Data Collection

Observational data for a period of 57 years are collected from various sources. Data includes: precipitation, streamflow, waste water treatment plant discharge, water level, winds, and salinity. Precipitation data is provided by the Southwest Florida Water Management District for 22 sites around the bay. Four of the sites have data dating back to 1950. Daily averages are calculated using any available data from the 22 sites. From 1950-1976 there are only 3-4 sites available to compute daily averages. After 1976 that number increased and by 2000 13 sites are available to compute daily averages (Figure 4). These daily averages contribute to the total fresh water input.

Streamflow data from 22 sites is downloaded from the USGS real-time water data website. The Little Manatee, Alafia, and Hillsborough sites have data that dates back to 1950. Once all the data is gathered correlations are done between all the sites that have 10 years of data (1997-2007). The average flow from all sites is calculated and used to

find scaling factors (8) between sites that have correlations higher than 0.7. These scaling factors are then used to fill in the gaps of all the rivers that have missing data from January 1, 1950 to December 31, 2006. Equation 2 is an example of how gaps are filled within the data.

$$\textit{if correlation of } riv1 \textit{ and } riv2 \geq 0.7 \textit{ then scale} = \frac{\overline{riv1}}{riv2} \tag{8}$$

$$\textit{to fill } riv2, \; riv2 = riv1 \times \textit{scale} \tag{9}$$

Each site is filled with the scaled data from the site with the highest correlation first, if there are still gaps in the data the scale of the site with the next highest correlation is used, and so on. Each site is correlated to the Little Manatee, Alafia, or Hillsborough rivers, so gaps for every river are able to be filled to January 1, 1950.

Discharge from the Howard Curren Waste Water Treatment Plant and the Tampa Bypass Canal is collected from each individual treatment plant. These two sites are used because according to Meyers et al. (2007) they discharge the largest amounts of water into the bay. The Howard Curren treatment plant has monthly data available from 1951 to present and the Tampa Bypass Canal had daily data dating back to 1974. The data from these sites are combined with the precipitation and streamflow/river data to make a total freshwater inflow source file for the model.

Hourly water levels from the St. Petersburg tide gauge, station #8726520, are provided by NOAA Tides and Currents. Water level data is available for the entire 57-year period. The data is in hourly time intervals and is relative to MSL. There are two noticeable gaps in the data that are between 1-2 years long. These years (1954 and 1962) are omitted from the record and all small gaps (< 1 week) are filled with predicted tide data from the NOAA Tides and Currents website.

Hourly wind speeds and directions are provided from the NOAA National Climatic Data Center. Data from the Albert Whitted Airport, MacDill Air Force Base, and Tampa International Airport is downloaded. Both the MacDill Air Force Base and Tampa International Airport have data dating back to 1950. Zonal (u) and meridional (v) components are calculated using the wind speeds and directions from each site using equations 10 and 11:

$$u = wsp \times \cos\left(\pi \times \frac{wdir}{180}\right) \tag{10}$$

$$v = wsp \times \sin\left(\pi \times \frac{wdir}{180}\right) \tag{11}$$

where *wsp* is wind speed and *wdir* is wind direction in degrees T. Hourly components from all three sites are then averaged and small gaps are filled by interpolation.

Monthly salinity data is provided by the Environmental Protection Commission of Hillsborough County (EPCHC) at approximately 100 sites in the bay (Figure 6). Salinity data is available from 1974-present. Small gaps in the data are filled by interpolation.

Model Simulation/Evaluation

The EFDC model is run from 1970-2006. The input files needed to run the model are created from the observational data previously mentioned. The model is initialized with uniform elevation and salinity of 35 throughout the model grid. Salinity from EPCHC site 93 and elevation data from the St. Petersburg tide gauge are used at the open boundary of the model, near the mouth of the estuary. A 2-hour lag is added to the St. Petersburg tide gauge elevation data, this is the approximate lag time for tides to travel from the entrance of the estuary at Egmont Key to the location of the St. Petersburg tide

gauge. Spatially uniformed winds are used throughout the model grid**.** Freshwater is used at the point source locations mentioned previously. The model output is archived hourly for all 36 years.

To evaluate model accuracy, model salinity and elevation output from 1975-2007 are compared to salinity and elevation data. As stated earlier, I allow five years of model spin up time so model output from 1970-1974 is omitted. Salinity sites within the bay are compared to the model salinity from the grid cells closest to the locations of each site. Model salinity data closest to the time of the salinity measurements are extracted from 1975-2006. Mean errors between observed monthly salinity and model salinity are calculated for all sites. The bias bay mean error for all sites at the near surface is -1.336 and -1.455 at the bottom (Figures 15 and 17). The normalized RMSE for the near surface and bottom are 0.916 and 0.993 (Figures 16 and 18).

Model elevation at grid cell (17, 36) is compared to elevation data from the St. Petersburg tide gauge for 2004 (Figure 26). The year 2004 is chosen due to that year being an extremely active hurricane year and I wanted to test the response of the model and make sure it captured the large elevation changes observed during these extreme weather events. The mean error for elevation in 2004 is 0.022, with an absolute mean error of 0.036, and an r^2 value of 0.97.

The axial (v) velocities of the model at grid cell (24, 34) and the bottom mounted ADCP located under the Sunshine Skyway Bridge were also compared for 2004 (Figure 20). Inflow into the estuary is indicated by positive values and outflow by negative values. Both the model and ADCP velocities show an inflow at depth and outflow near the surface. The ADCP shows stronger inflows than the model, this is due to the model

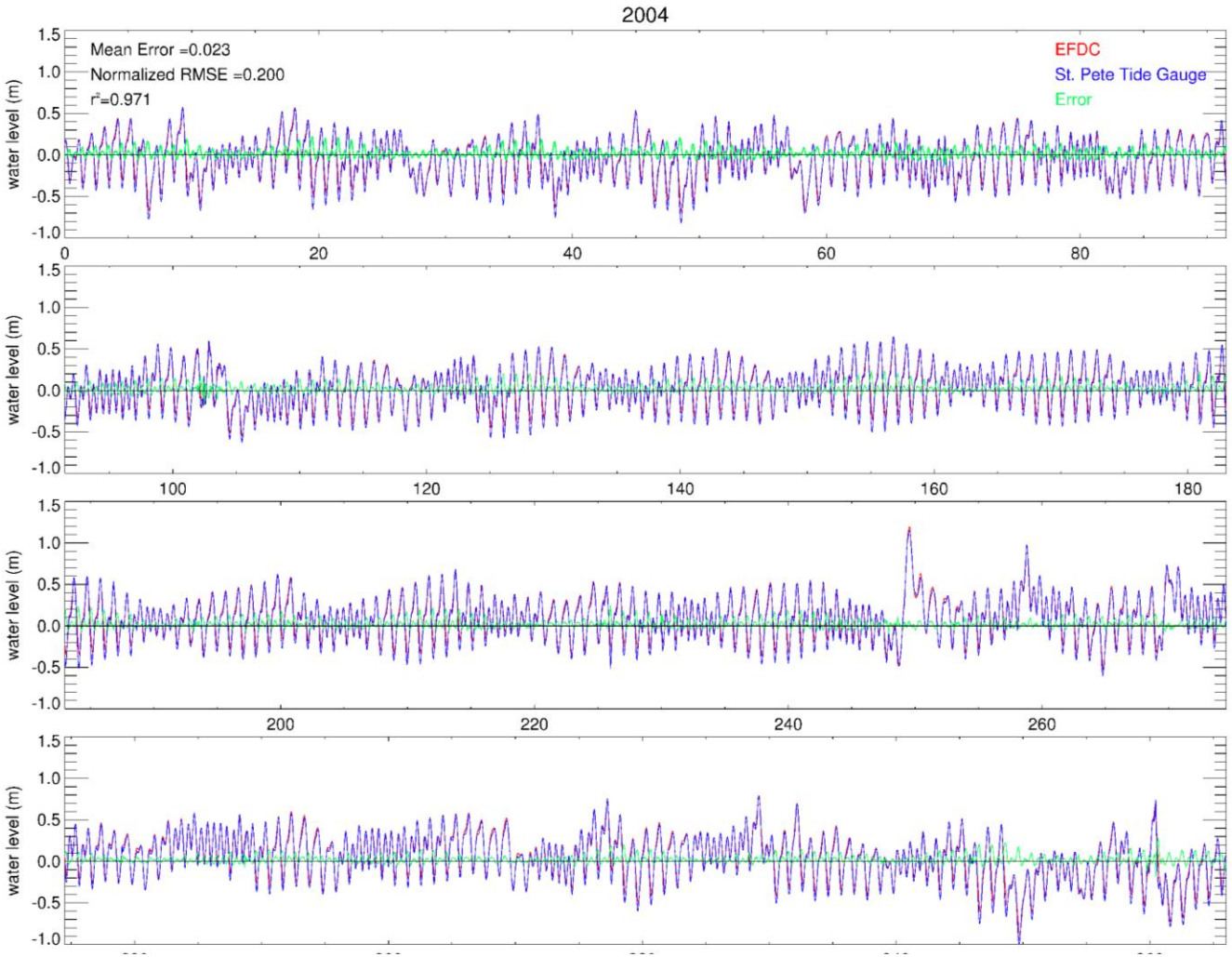

Figure 26. Elevation comparison between EFDC elevation (red) output and the St. Petersburg tide guage (blue) for 2004. Bias mean error, normalized RMSE, and r^2 values are shown

bathymetry. The ADCP is located in the middle of the shipping channel, and the model bathymetry is unable to replicate the steep and narrow channel. The shipping channel is wider in the model bathymetry, causing velocities to be slower than the ADCP at depth.

The bay volume is

$$V(t)_{total} = \sum_{i,j} \left[\left(e(t)_{i,j} + h_{i,j} \right) \times dx_{i,j} \times dy_{i,j} \right] \quad (12)$$

Model elevation (e) at location (i,j) is added to the mean model depth (h), multiplied by the area of each grid cell (dx,dy), and then summed up for all grid cells in the model grid. The same method is used to calculate predicted bay tidal volume:

$$V(t)_{tides} = \sum_{i,j} \left[\left(e_{tides}(t)_{i,j} + h_{i,j} \right) \times dx_{i,j} \times dy_{i,j} \right] \quad (13)$$

where e_{tides} consists of the sum of the eight primary tidal constituents for Tampa Bay plus the annual and semi-annual constituents. The amplitude and phase of each constituent (Table 4) is derived by performing a least square analysis on elevation at each i,j location for each tidal frequency. The difference yields bay volume anomalies for the entire 32 year period.

$$V(t)_{anomaly} = V(t)_{total} - V(t)_{tides} \quad (14)$$

Two main drivers of water volume in the bay are winds and tides, by removing the tides we can assume that $V(t)_{anomaly}$ is the wind-generated signal.

Volume anomalies are normalized by dividing by the mean bay volume, ~3.8 × 10^9 m^3. The time derivative of the normalized volume anomalies is used to calculate volumetric component of the flushing.

$$\frac{dV_{normalized}}{dt} = \text{flushing rate} \quad (15)$$

Table 4. Amplitude, epoch, and period for each tidal constituent used to perform a least square analysis.

Constituents	Amplitude (m)	Epoch (°)	Period (hr)
M_2	0.175	197	12.4206
S_2	0.057	211.7	12
N_2	0.03	191.3	12.6583
K_1	0.167	49.9	23.9345
O_1	0.155	37.7	25.8193
Q_1	0.029	26.2	26.8684
P_1	0.049	57.6	24.0659
K_2	0.025	215	11.9672
SSa	0.033	41	4382.9052
Sa	0.092	150.8	8765.8211

Positive flushing rates indicate inflow conditions and negative flushing rates indicate outflow conditions. Positive and negative flow conditions were integrated over time to produce total inflow (positive)/outflow (negative) flushing rates for each year of the 32-year record. Flushing rates are binned by month for the entire record and then averaged to produce a monthly climatology of the net average flushing rate.

Results

The results for two extratropical/winter storms and two hurricanes are discussed in detail below. The two extratropical/winter storms chosen occurred in March of 1993 named the Storm of the Century (Storm6) and in February of 1998 (Storm9). The hurricanes chosen are Hurricane Gabrielle that occurred in September of 2001 and Hurricane Frances that moved through the Tampa Bay area in September 2004. In March of 1993 an unnamed hurricane-like storm, known as the Storm of the Century, passed through the Tampa Bay

area. The storm had hurricane force winds, storm surges up to 12 feet, and created 14 tornadoes. Figure 27 shows the normalized bay volume anomalies and flushing rates for 1993. Results show that the Storm of the Century caused about a 25% increase above the mean in bay volume and then dropped to 15% below the mean, for a total change of 40% between peaks. It produced a peak inflow rate of 25% of bay volumes per day and a peak outflow rate of 35% of bay volumes per day (Figure 27). On February 2 of 1998 an area of severe weather moved across the Gulf of Mexico and through the south Florida region causing severe thunderstorms, winds, and tornadoes. This storm (Storm9) caused an increase of 13% above the mean in bay volume and then dropped to 1% below the mean, for a total volume change of 14%. Storm9 produced a peak inflow rate of 8% and a peak outflow rate of 12% of bay volumes per day (Figure 28).

In September of 2001 Hurricane Gabrielle made landfall on the west coast of Florida as a tropical storm with 60-knot sustained winds. It produced major river floods over west-central Florida. Gabrielle produced a loss of about 9% bay volume followed by an increase of 4%, for a total change of 13%. Outflow/inflow rates for Gabrielle were 11% bay volume per day in both directions (Figure 29). In 2004 Tampa Bay experienced 3 hurricanes in the course of 3 weeks. Hurricane Frances passed by the Tampa Bay area on September 6, Ivan occurred on September 15, and Jeanne came through on September 27. Wilson (2007), explains the individual impacts that Hurricane Frances and Jeanne had on the Bay area. As Hurricane Frances moved through the Bay there was a loss of 11% bay volume followed by a 25% gain for a total change of 36% between peaks. Frances produce a peak inflow rate of 30% of bay volume per day and a peak outflow rate of 20% bay volume per day (Figure 30). The total % volume changes and flushing

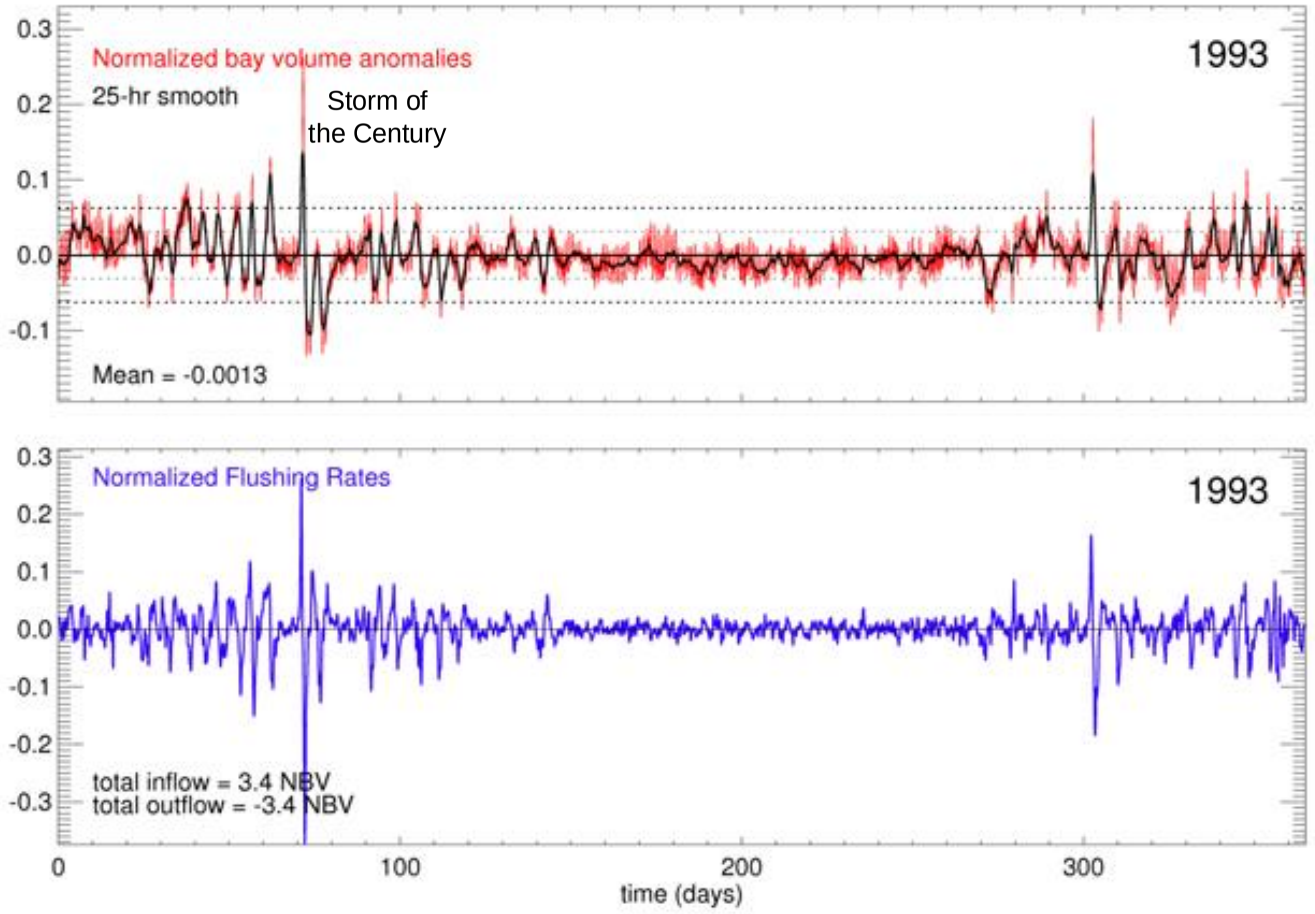

Figure 27. Normalized bay volume anomalies (top) and normalized flushing rates (bottom) for 1993.

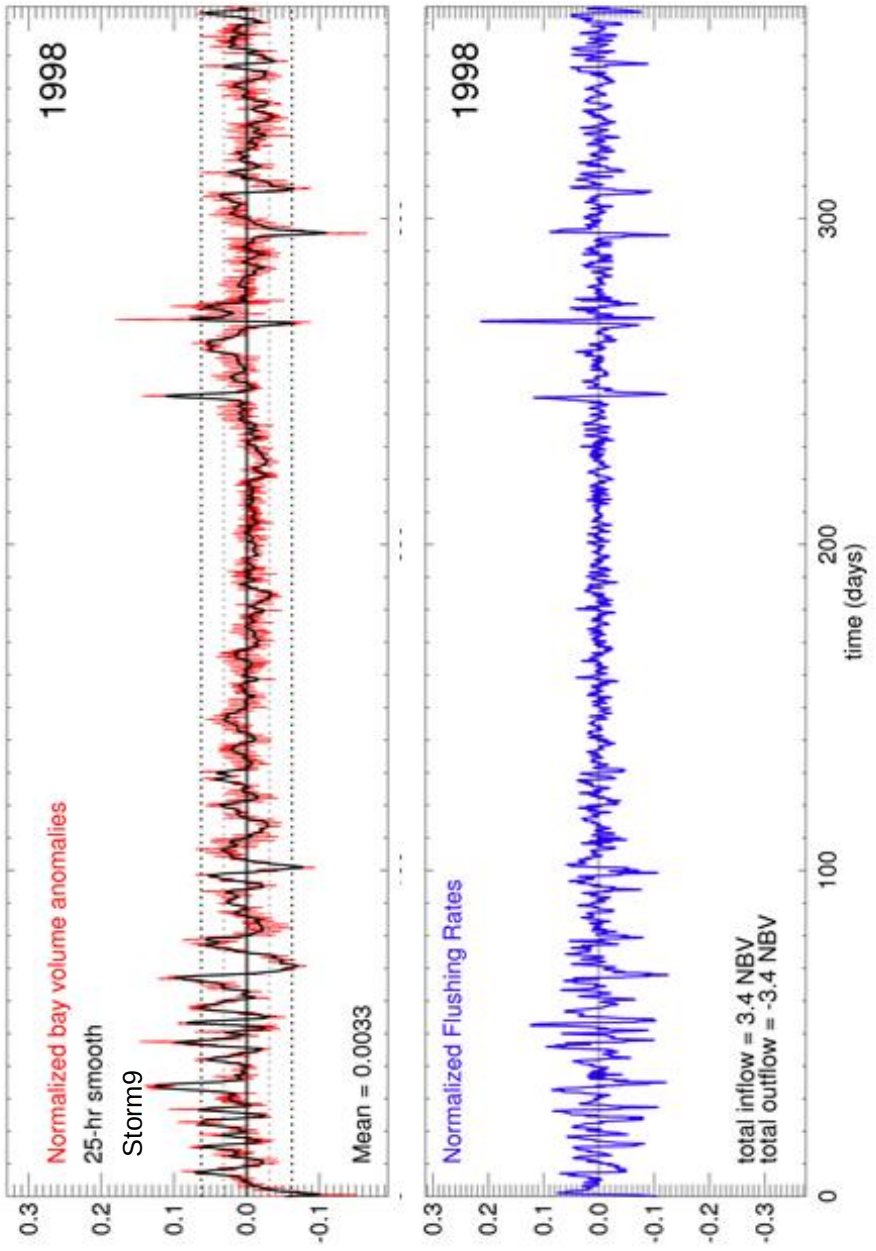

Figure 28. Same as figure 27, year 1998.

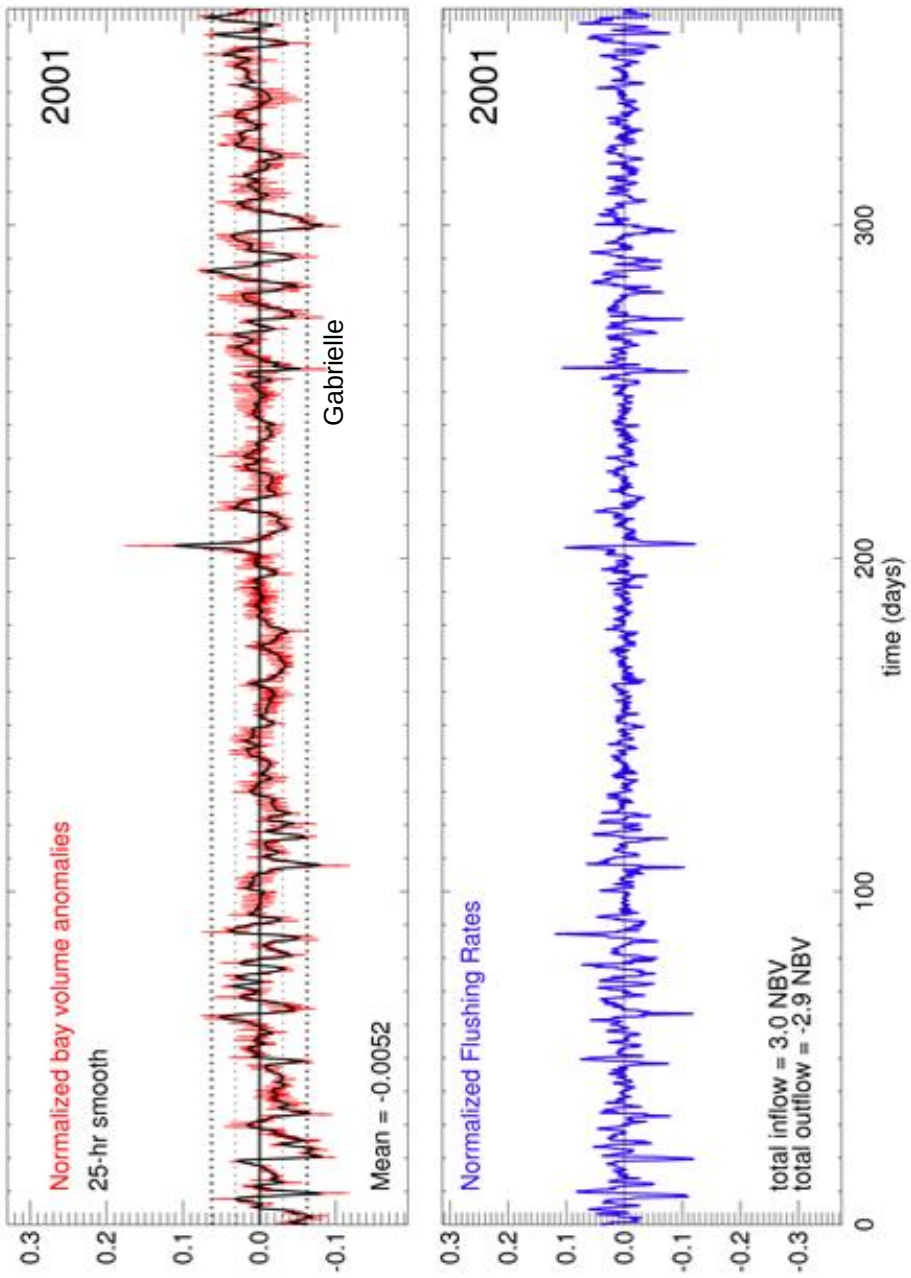

Figure 29. Same as figure 27, year 2001.

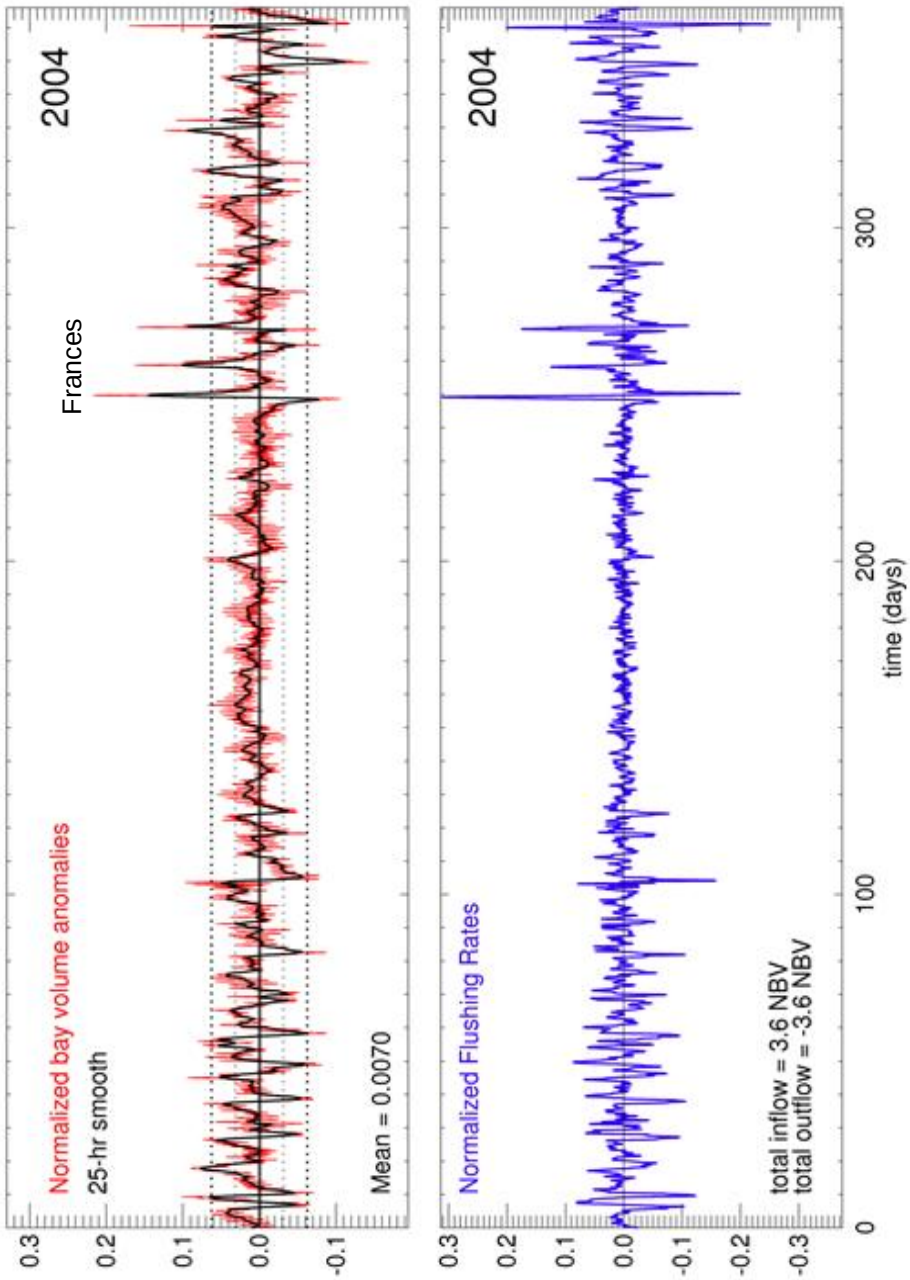

Figure 30. Same as figure 27, year 2004.

rates for all 10 extratropical/winter storms and 10 hurricanes are listed in tables 5 and 6. Bay volume anomalies and flushing rates for all other years can be seen in Appendices E and F. If we sum up the total normalized inflow and outflow rates from the tides we get a flushing of approximately 40 bay volumes per year. Once the tides are removed and we do the same calculation the total normalized inflow/outflow rates from the anomalies is 3.4±0.27 (standard deviation of annual total) bay volumes per year. This shows that approximately 9% of the volumetric changes in a year are due to winds.

Volume changes and flushing rates are then compared to the wind components. Scatter plots of normalized volume anomalies and normalized rates of change versus the zonal (u, east/west, x-axis) and meridional (v, north/south, y-axis) components of the wind for the extratropical/winter storms and hurricanes are shown in figures 31 - 34. The black line indicates the path of the storms, approximate start and end dates are indicated by the + and the *, and the color bar represents the volume anomalies and rates of change per day. Scatter plots for all extratropical/winter storms and hurricanes are shown in Appendix G. At the beginning of the Storm of the Century (Storm6) winds are fairly weak and are in the SE direction (Figure 31). As the winds begin to strengthen they rotate towards the NW direction and the normalized volume anomaly begins to increase. The anomalies reach their maximum value of about 25% when the winds are blowing towards the NE/E. The same occurs for the volume rate of change (Figure 31), there is a large positive rate of change when the winds are blowing towards the NE/E direction, but as the winds begin to slow slightly and blow towards the SE the rates of change switch from a positive to large negative rate of change. As soon as the winds begin to relax all the water that was being pushed into the Bay starts to make its way out. At the

Table 5. Total volume changes and flushing rates for all 10 extratropical storms. Negative flushing rates indicate outflow

Name	Start Date	End Date	Total Volume Change	Flushing rate
Storm1	1/11/1982	1/14/1982	20%	9%, -20%
Storm2	2/27/1983	2/27/1983	21%	16%, -12%
Storm3	11/22/1984	11/24/1984	25%	-9%, 9%
Storm4	12/22/1989	12/25/1989	17%	-8%, 10%
Storm5	3/8/1990	3/10/1990	22%	-12%, 16%
Storm6	3/11/1993	3/13/1993	40%	25%, -35%
Storm7	3/2/1994	3/2/1994	22%	14%, 16%
Storm8	2/5/1996	2/5/1996	27%	7%, -12%
Storm9	2/1/1998	2/3/1998	14%	8%, -12%
Storm10	12/26/2004	12/26/2004	29%	20%, -25%

Table 6. Same as table 6 for all 10 hurricanes.

Name	Start Date	End Date	Total Volume Change	Flushing rate
David	9/3/1979	9/4/1979	12%	-5%, 10%
Elena	8/31/1985	9/1/1985	35%	25%, -19%
Andrew	8/24/1992	8/25/1992	21%	-7%, 15%
Allison	6/5/1995	6/5/1995	20%	14%, -11%
Josephine	10/7/1996	10/8/1996	32%	22%, 26%
Gordon	9/17/2000	9/18/2000	26%	15%, -17%
Gabrielle	9/11/2001	9/15/2001	13%	-11%, 11%
Frances	9/5/2004	9/6/2004	36%	30%, -20%
Dennis	7/9/2005	7/10/2005	23%	22%, -15%
Alberto	6/10/2006	6/14/2006	26%	16%, -20%

start of Storm9 the winds stayed fairly weak, were blowing towards the SW, and the normalized volume anomalies were close to 0 (Figure 32). As the winds strengthened they began to blow towards the NW and normalized volume anomalies increased to their maximum values of 13%. The volume rates of change were low and negative at the beginning of the storm and transitioned to positive rates of change as the winds

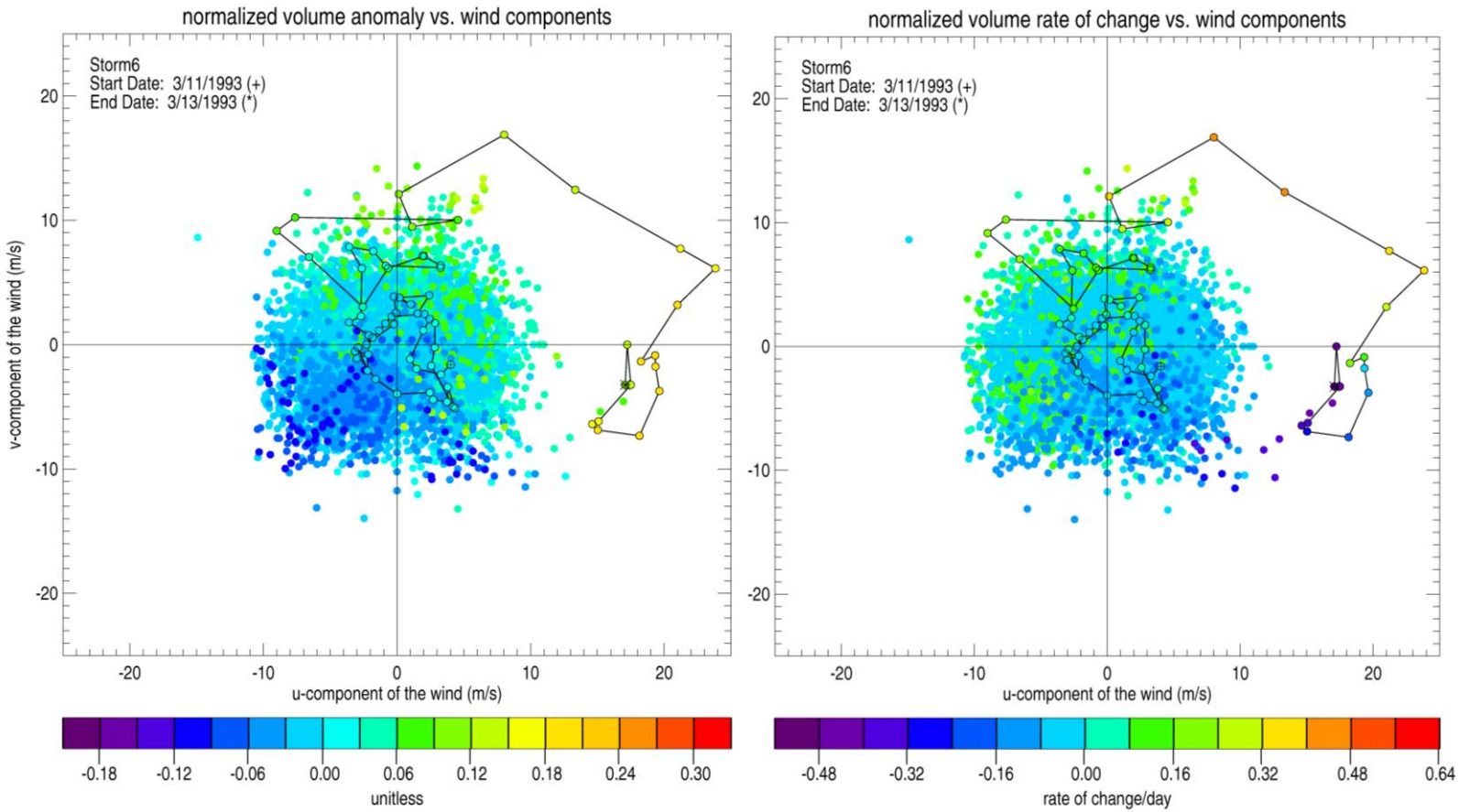

Figure 31. Scatter plot of normalized volume anomalies (left) and normalized volume rates of change (right) versus the zonal (v) and meridional (u) wind components for the year 1993. Outlined path represents the evolution of the Storm of the Century as it made its way through the Tampa Bay area. Colors represent normalized volume anomalies and rate of change per day.

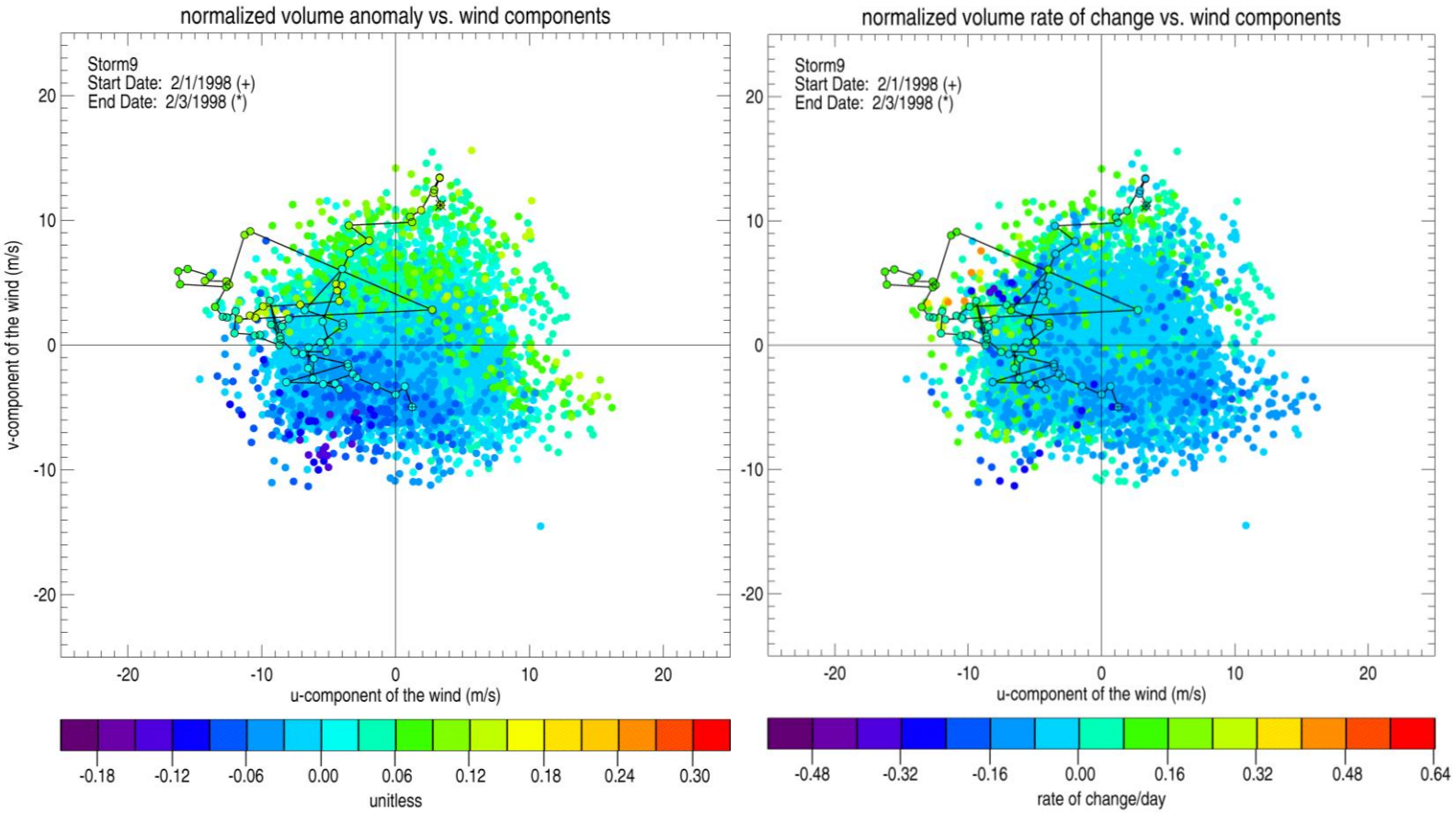

Figure 32. Same as figure 31, for Storm9 which occurred in February of 1998.

transitioned towards the NW. Towards the end of the storm the winds began to blow towards the NE and the rates of change switched back to negative values.

By the time Hurricane Gabrielle made landfall, it had been downgraded to a tropical storm. The winds were weak and blowing in the NW/W direction and the normalized volume anomalies stayed close to 0. The normalized volume anomalies began to transition to negative values and reach a maximum of 9% as the winds increased and shifted from the NW/W direction towards the S/SE direction. As the winds began to calm towards the end of Gabrielle, the volume anomalies began to weaken and go back towards a 0 value. The rates of changed during Gabrielle stayed close to 0 and in the positive direction at the beginning of the storm. The largest rates of changed occurred during the shifting of the winds from the NW/W to the S/SE direction as the winds blew towards the SW direction (out of the bay). The rates of change changed to positive values towards the end of the storm when the winds began to blow towards the SE and the water that had been flushed out began to make its way back into the Bay (Figure 33). Hurricane Frances lasted approximately 2.5 days and had two phases of strong winds (>20 m/s) with a short time of relaxed winds (9m/s) in between the two phases. In the beginning winds were blowing towards the SE causing about a 10% outflow of volume. As the winds relaxed and began rotating towards the NE, the volume anomalies begin to shift from outflow to inflow. As the second wind peak occurs winds begin to blow towards the NE direction causing the 25% increase in volume anomalies mentioned previously. As for the volume rates of change, we see the largest positive changes happening when the winds begin to transition from the SE to the NE. The largest volume

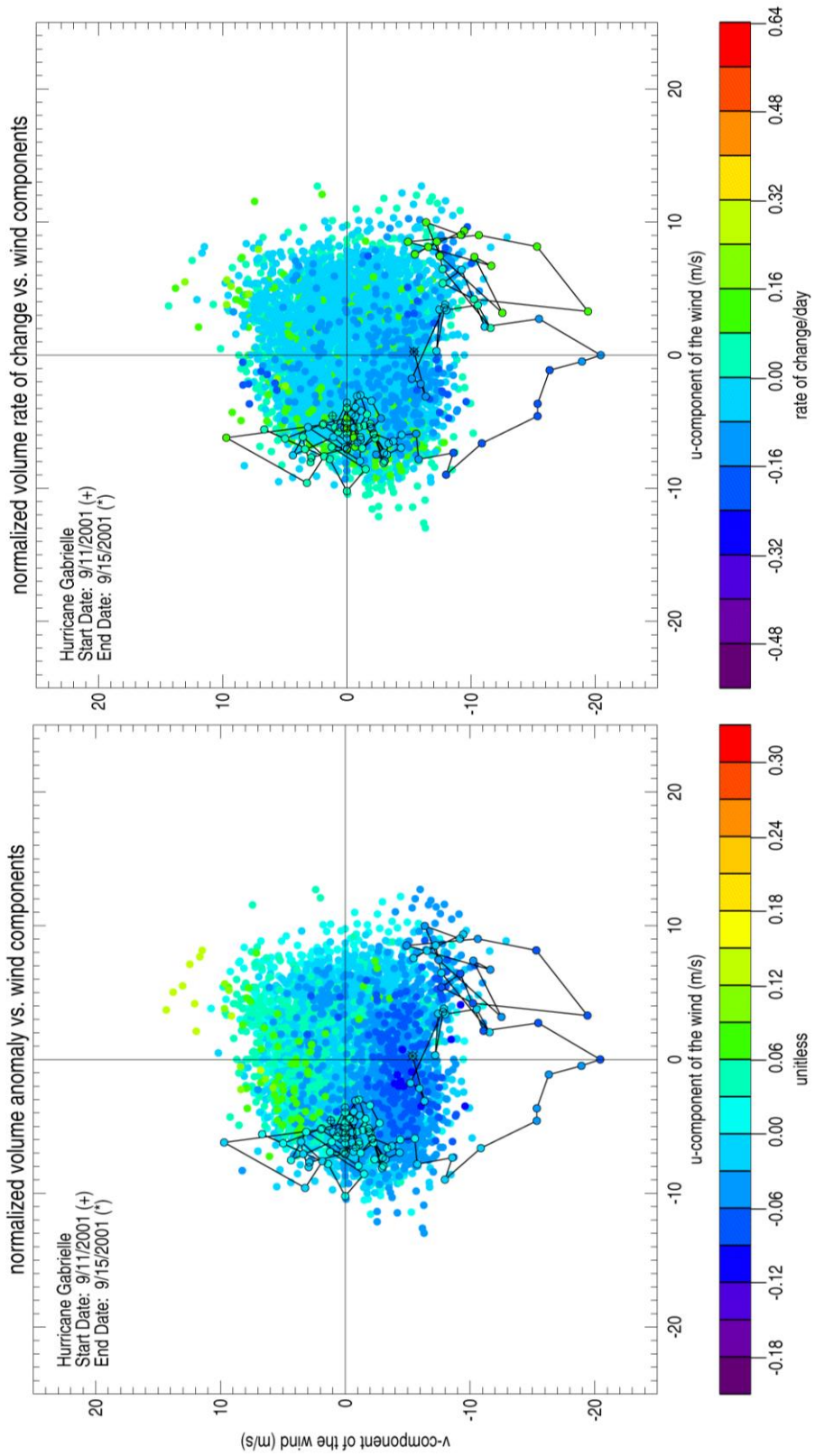

Figure 33. Same as figure 31, for Hurricane Gabrielle.

outflow occurs at the end of the storm when the winds begin to die down and the water begins to make its way out of the bay (Figure 34).

The scatter plots shown in figure 35 show the normalized volume anomalies and rates of change versus the wind components for the entire 32-year record. The largest outflows occur when the winds are blowing towards the southwest, out of the estuary, and the largest inflows are seen when the winds are blowing in the northeast direction up the main axis of the Bay. As previously stated, we see that the largest inflow/outflow rates of change occur when the winds are blowing towards the southeast and northwest.

Monthly climatologies of the net average flushing rates are shown in figure 36. The difference between the inflow and outflow shows that TB experiences a net inflow during the summer months and a net outflow during all other months. Figure 37 shows the year to year variability of total inflow/outflow flushing rates of the bay. The total inflow/outflow flushing rates appear to be symmetrical, and there is a definite year to year variability. The maximum and minimum total inflows are 3.9 and 2.7 bay volumes per year in 1983 and 1975, respectively. The maximum and minimum total outflows are -4 and -2.7 bay volumes per year in 1983 and 1975.

Summary and Discussion

Changes to the normalized volume anomalies and flushing rates of the Tampa Bay estuary caused by extratropical/winter storms and hurricanes is examined using numerical model output over a period of 32 years. The strong wind speeds, duration of the high winds, and wind direction during these extreme events has a direct impact on the amount of water that gets flushed in and out of the estuary. The wind induced total flushing rates

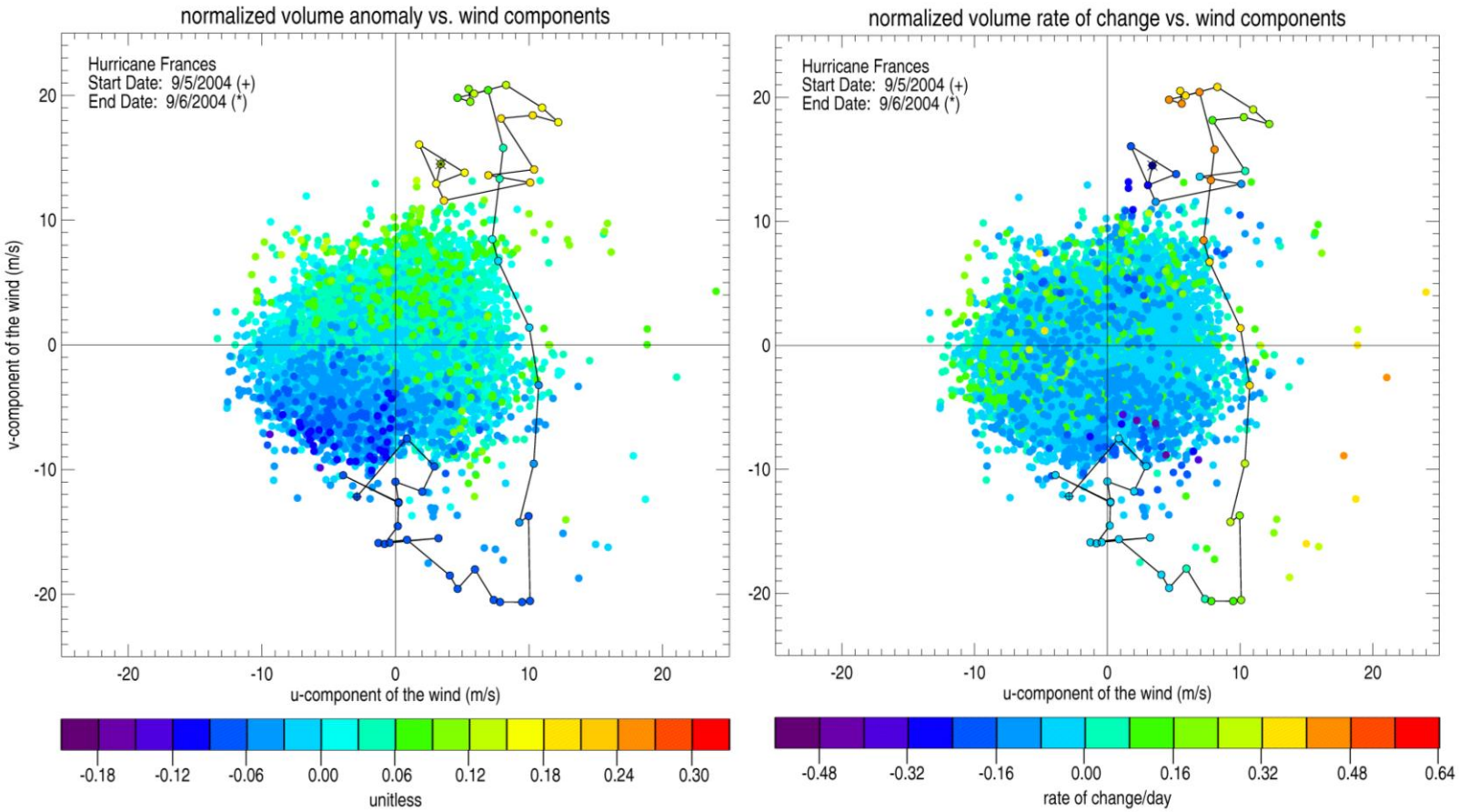

Figure 34. Same as figure 31, for Hurricane Frances.

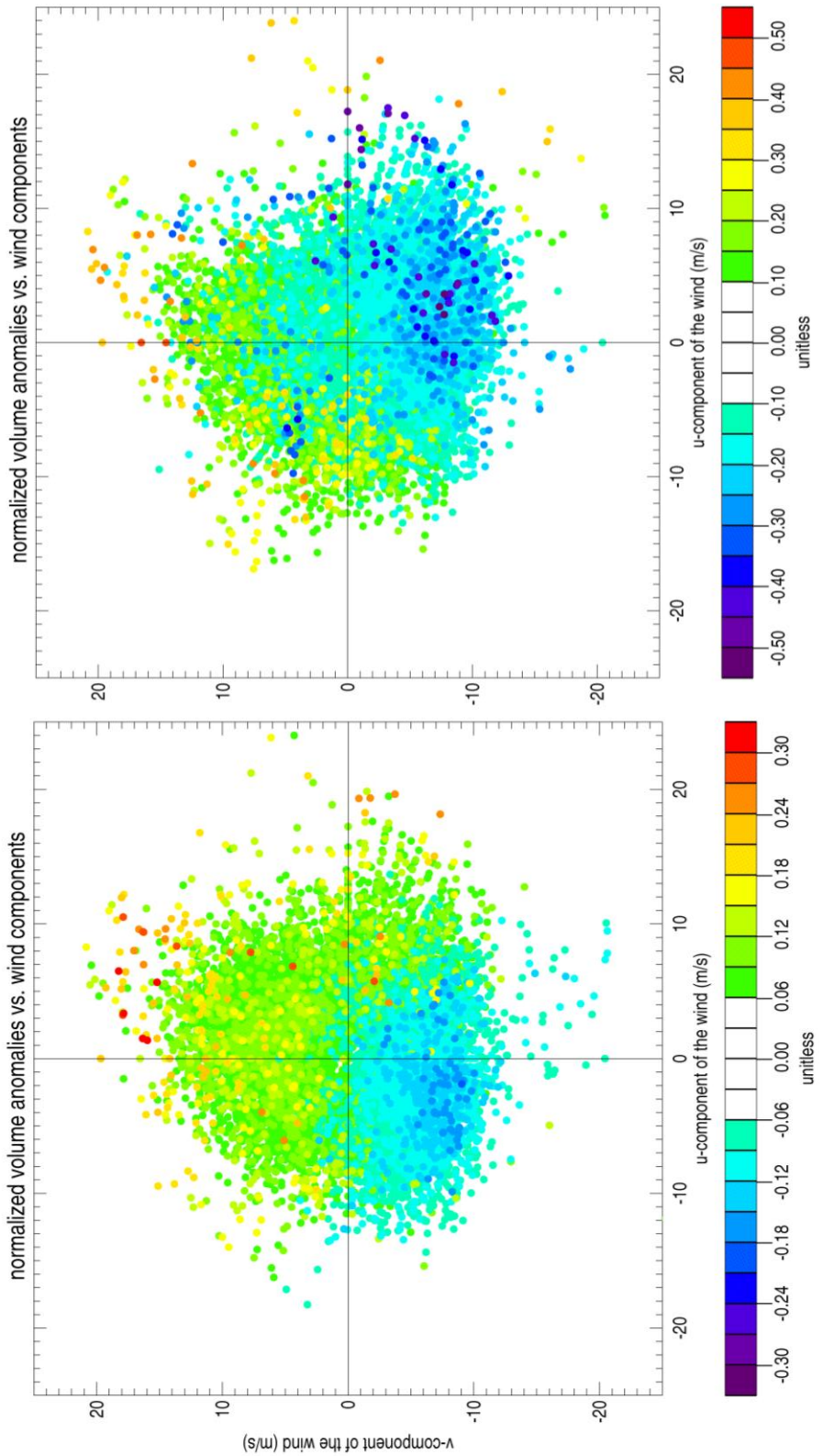

Figure 35. Normalized volume anomalies and volume rates of change versus wind components for the entire 32 year record.

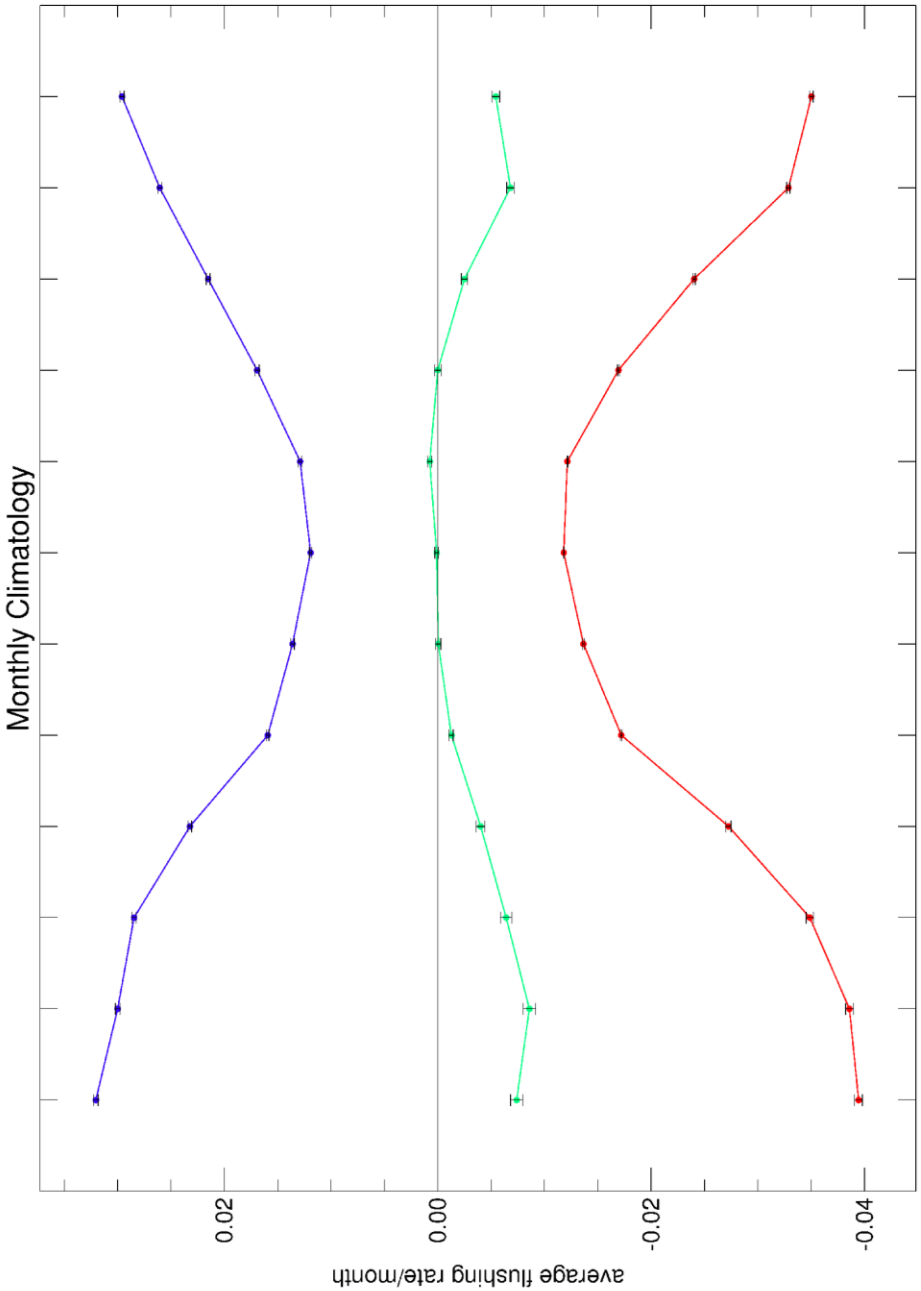

Figure 36. Monthly climatology for the entire 32 year record. Blue line represents inflow rates, red line, represents outflow rates, and green line represents the net difference between the two. Error bars represent standard error.

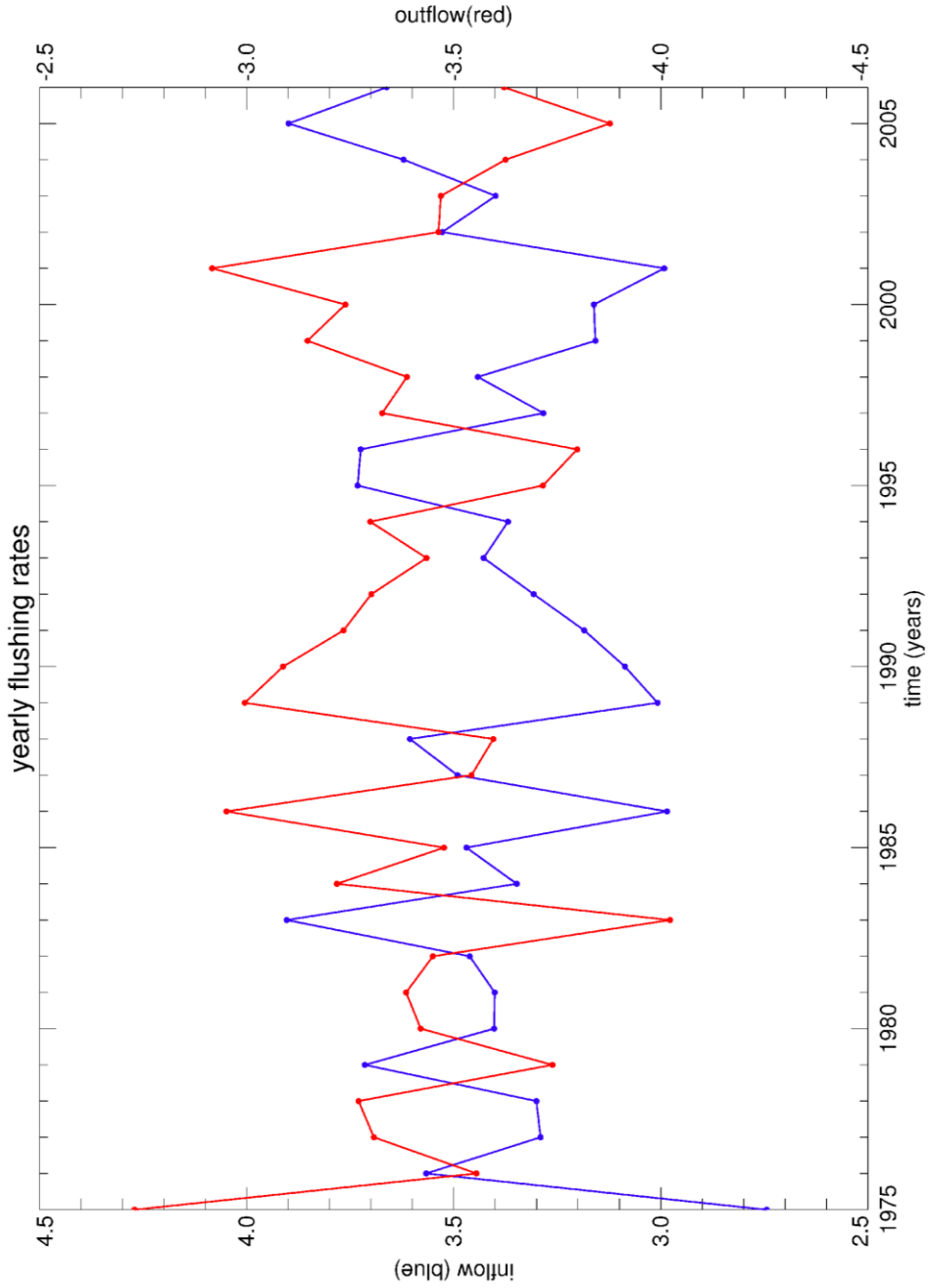

Figure 37. Year to year flushing rate variability. Inflow (blue) values are represented on the left y-axis. Outflow (red) values are represented the right y-axis.

for all 10 hurricanes range from 12% to 36%, and 14% to 40% for the extratropical/winter storms.

Although all the storms discussed here experienced high winds (> 15 m s^{-1}, ~30 knots), each individual storm experienced high winds blowing in different directions. As seen in figure 35, the largest volume anomalies occur mostly when the winds are blowing in the NE/SW direction along the main axis of the Bay. Storm9 and Hurricane Gabrielle had the smallest total volume changes of all storms, 14% and 13% respectively. Both Storm9 and Hurricane Gabrielle experienced relatively weak axial and co-axial winds compared to the Storm of the Century and Hurricane Frances (Figure 38). During both storms winds were blowing in directions off the main axis of the bay which is not optimal for large volume anomalies to occur, causing volume anomalies to be small. At the beginning of Storm9 axial winds were positive and co-axial winds were negative, causing winds to blow in the NW direction. This caused a slight positive increase in the volume anomalies. As the axial winds slowed and became negative, the co-axial winds became positive and the volume anomalies began to decrease. The initial decrease in the volume anomalies for Hurricane Gabrielle was caused by the sudden increase in the negative direction (out of the bay) of the axial winds. During the hurricane axial winds continued to blow out of the estuary causing water to flush out of the Bay. The outflow began to decrease and switched to inflow when the axial winds weakened. The Storm of the Century (Storm6) and Hurricane Frances had the highest total percent volume changes and strongest winds (40%, ~25 m/s and 36%, ~23 m/s, respectively) out of all extratropical/winter storms and hurricanes in this study. Just prior to the time of the maximum volume anomaly during the Storm of the Century, both the axial and co-axial

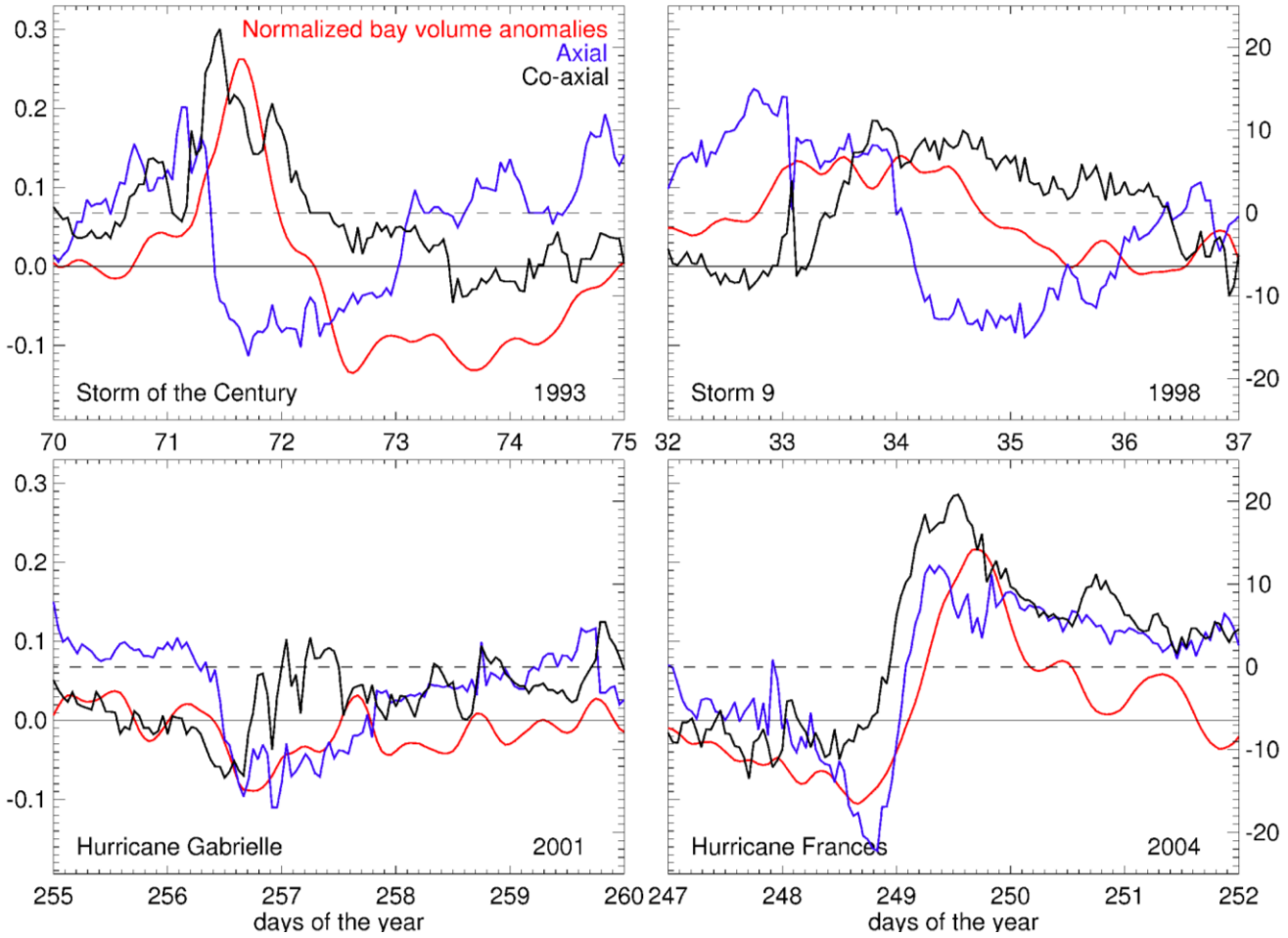

Figure 38. Unfiltered normalized bay volume anomalies (red), axial (blue) and co-axial winds (black) for all 4 extreme events. Left y-axis represents normalized volume anomaly values and right y-axis represents values for axial and co-axial wind components. Zero lines for volume anomalies (solid gray) and wind components (dashed gray) are also shown.

winds were positive (meaning winds blowing in the NE direction) which caused a large inflow of water into the bay (25% above the mean). At the time when the volume anomaly reached its peak, the axial winds began to shift and blow out of the Bay but the co-axial winds were still strongly positive. The volume anomaly began to decrease once the axial winds became strongly negative. The largest negative volume anomaly (15%) occurs when both the axial and co-axial winds are negative, causing winds to blow in the SW direction. As Hurricane Frances came through the Bay area, we experienced two wind peaks. During the first wind peak, both the axial and co-axial components were strongly negative causing winds to blow towards the S/SE and the outflow volume anomaly to reach its peak of 11%. As the winds shifted towards the E, they weakened and so did the outflow volume anomaly. When the winds peaked for a second time, both axial and co-axial winds were strongly positive, blowing towards the NE (optimal direction for large volume inflow) causing the positive volume anomalies to reach their maximum of 25%. The volume anomaly began to decrease when the winds weakened after the hurricanes passing. Tides could also be another factor affecting the volume changes, but they are not examined in this study.

Yearly total flushing in Tampa Bay is approximately 3.5 bay volumes per year (Figure 37). Total inflow flushing rates range from 2.75 to 3.9 bay volumes per year and total outflow rates range from -2.7 to -4. There is definitely year to year variability in the volume rates for Tampa Bay, FL. What the exact causes of this year to year variability is yet to be determined.

Flushing rates are a key variable for maintaining estuarine viability. Extreme events only occur a few times a year and are short lived, but they can cause large volumes

of water to flush in and out of the bay. By comparing 4 different extreme events that all experienced strong winds, we are able to conclude that different physical processes, specifically wind speed and direction, can cause large differences in the total volume anomaly changes and flushing rates. This flushing leads to large scale overturning of bay volume. Wind driven volume change is a significant fraction (~9%, (Wilson et al., 2013) of the total volume changes. Any type of change in storminess can have a huge impact on Bay health by altering the flushing rates.

Conclusion

Effects of wind events on estuarine flushing have been studied by many. Most studies mentioned here discuss the short term impacts of synoptic wind events on the flushing of an estuary, long-term studies are rare. In this study I used 55 years of observational data as well as the aid of a numerical model to investigate the synoptic to interannual variability in volumetric flushing in the Tampa Bay estuary caused by synoptic wind events.

Two separate analyses, volumetric analysis and wavelet analysis, are done on 55 years of observational data. Results from the first analysis show that at time scales longer than about one day, the synoptic scales dominate the variability of surface winds. The response of water level to local wind forcing along the axis of the estuary is in phase across the estuary, though the amplitude will vary, according to (1). This implies that elevation at any point is a good representation for the total bay volume. The strength of the axial wind component varies seasonally, driving a strong seasonal cycle of volumetric flushing (3) that is in phase with the wind. The long-term record of monthly normalized volume anomalies ($F_a(t)$) show that winter anomalies vary with the ENSO phase. Higher flushing is seen during warm phases and lower flushing during cool phases (Figure 23). Correlations between the ONI and the volume anomalies are low and lead us to believe that there is a seasonal dependence of the ENSO response. To understand the seasonal dependency, wavelet analysis is applied to the observational data and amplitudes are averaged between 2-20 days to isolate the synoptic scale variability. There is close

agreement in the monthly climatology between the synoptic wavelet variance of elevation and axial winds. Both the axial winds and elevation have single summer minimum and winter maximum. El Niño increases the synoptic variability in elevation during the winter but decreases it during the summer (Figure25). However, only in the winter season are the differences between ENSO phases statistically significant (table 4).

Winter extratropical storms and hurricanes have effects on the flushing rates of Tampa Bay. All 4 events examined in this study show how the individual characteristics of each storm can cause differences in the total volume changes and flushing rates. Storm9 and Hurricane Gabrielle had winds that were greater than 15 m s^{-1}, however due to the wind speed, direction, duration, and tidal phase, total volume changes were the lowest of all 20 storms studied (Figures 32 and 33). The Storm of the Century and Hurricane Frances had the highest total volume changes of all the storms (tables 6 and 7). High winds were blowing in the NE/E direction (Figures 31 and 34) and volume anomalies were in phase with the tides. Winter extratropical storms cause total volume changes to range from 14% to 40%, and hurricanes from 12% to 40%.

Annual flushing in Tampa Bay is approximately 3.5 bay volumes per year. Figure 37 shows that total inflow/outflow rates are almost symmetrical and that there is definite year to year variability. The exact causes of this year to year variability have yet to be examined, however, any type of change in storminess can alter the flushing rates in the estuary.

These studies conclude that synoptic wind events affect the overall flushing of the estuary. Flushing can have large impacts on multiple aspects of an estuary. Flushing can influence the mixing and transport within the Bay and by extention the circulation as

well. Circulation plays a key role in the distribution of nutrients and pollutants, as well as the transportation or retention of sediments and waste. The overall water quality and health of an estuary is dependent upon how an estuary flushes out pollutants or waste and how it recycles its nutrients. The rates of estuarine flushing can be a determining factor for the presence of phytoplankton and other biological organisms within an estuary. It is important to understand the details of how flushing is affected or altered to help aid in determining and improving water quality within an estuarine system.

Future Studies

Possible directions for future research include:

1) Using velocity model output other short/long term studies can be done to get a better understanding of how circulation is being altered during extreme events. This could be done on portions of the Bay or the estuary as a whole.

2) Using the salinity model output, investigations on baywide salinity or salinity gradients between the head and the mouth can be done to get a better understanding of the density-driven circulation of the Bay and how that varies on long term scales and short term scales.

3) Direct links between extreme events and water quality of the Bay can be examined. Water quality measurements before and after an extreme event can help understand if the flushing that occurs during these events is helping flush out pollutants or causing them to reside longer in the estuary.

4) Lagrangian studies can also be done to examine the spatial displacement of water, mixing, and retention.

References

Angelovic, J.W., 1976. Environmental Studies of the South Texas Outer Continental Shelf, 1975, 2. Physical Oceanography, 2.

Arnott, K.D., Valle-Levinson, A. and Luther, M., 2012. Friction dominated exchange in a Florida estuary. Estuarine, Coastal and Shelf Science, 113(0): 248-258.

Blumberg, A.F., 1990. A Primer for ECOM-3D. Hydroqual, Inc, Mahway, New Jersey, pp. 58.

Boler, R., 1992. Surface water quality 1990-91 Hillsborough County, Florida.

Bove, M.C., O'Brien, J.J., Eisner, J.B., Landsea, C.W. and Niu, X., 1998. Effect of El Niño on U.S. Landfalling Hurricanes, Revisited. Bulletin of the American Meteorological Society, 79(11): 2477-2482.

Burwell, D., 2001. Modeling the Spatial Structure of Estuarine Residence Time: Eulerian and Lagrangian Approaches. Dissertation Thesis, University of South Florida, St. Petersburg, FL, 251 pp.

Comrie, A.C. and Yarnal, B., 1992. Relationships between synoptic-scale atmospheric circulation and ozone concentrations in Metropolitan Pittsburgh, Pennsylvania. Atmospheric Environment. Part B. Urban Atmosphere, 26(3): 301-312.

Critchfield, H., 1983. General Climatology. Prentice Hall, Enlewood Cliffs, New Jersey.

Dagg, M.J., 1988. Physical and biological responses to the passage of a winter storm in the coastal and inner shelf waters of the northern Gulf of Mexico. Continental Shelf Research, 8(2): 167-178.

Davis, R.E. and Dolan, R., 1993. Nor'easters. American Scientist, 81(5): 428-439.

Dyer, K.R., 1973. Estuaries: a physical introduction. John Wiley, 140 pp.

Emery, W.J. and Thomson, R.E., 2001. Data analysis methods in physical oceanography. Elsevier, New York.

Enloe, J., O'Brien, J.J. and Smith, S.R., 2004. ENSO Impacts on Peak Wind Gusts in the United States. Journal of Climate, 17(8): 1728-1737.

Farge, M., 1992. Wavelet Transforms and their Applications to Turbulence. Annual Review of Fluid Mechanics, 24(1): 395-458.

Feng, Z., 2009. Hydrodynamic response to cold fronts along the Louisiana coast, Louisiana State University, 119 pp.

Galperin, B., Blumberg, A.F. and Weisberg, R.H., 1991. A time-dependent three-dimensional model of circulation in Tampa, Bay. In: S. Treat and P. Clark (Editors), Proceedings Tampa Bay Area Scientific Information Synposium 2, Tampa, FL, pp. 67-75

Galperin, B., Blumberg, A.F., Weisberg, R.H. , 1991. A time-dependent three-dimensional model of circulation in Tampa Bay. In: S.T.a.P. Clark (Editor), Tampa Bay Area Scientific Information Symposium 2, Tampa, FL.

Geyer, W.R. and Signell, R.P., 1992. A reassessment of the role of tidal dispersion in estuaries and bays. Estuaries, 15(2): 97-108.

Goodwin, C.R., 1987. Tidal flow, circulation, and flushing changes caused by dredge and fill in Tampa Bay, Florida. In: U.S.G.S. (Editor), U. S. Geological Survey Water Supply Paper pp. 88.

Goring, D.G. and Bell, R.G., 1999. El Niño and decadal effects on sea-level variability in northern New Zealand: A wavelet analysis. New Zealand Journal of Marine and Freshwater Research, 33(4): 587-598.

Gray, W.M., 1984. Atlantic Seasonal Hurricane Frequency. Part I: El Niño and 30 mb Quasi-Biennial Oscillation Influences. Monthly Weather Review, 112(9): 1649-1668.

Greening, H., Doering, P. and Corbett, C., 2006. Hurricane impacts on coastal ecosystems. Estuaries and Coasts, 29(6): 877-879.

Grinsted, A., Moore, J.C. and Jevrejeva, S., 2004. Application of the cross wavelet transform and wavelet coherence to geophysical time series. Nonlin. Processes Geophys., 11(5/6): 561-566.

Hamrick, J.M., 1992. A three-dimensional environmental fluid dynamics computer code: theoretical and computational aspects, Virginia Institute of Marine Science.

Hamrick, J.M., 1996. Users manual for the environmental fluid dynamic computer code, Virginia Institute of Marine Science.

Harwell, M.A., Ault, J.S. and Gentile, J.H., 1995. Comparison of the Ecological Risks to the Tampa Bay Ecosystem from Spills of Fuel Oil #6 and Orimulsion, Center for Marine and Environmental Analyses, Univeristy of Miami, Miami, Florida, Comparative Ecological Risk Assessment.

Hsu, S.A., 1988. Coastal Meteorology. Academic Press, San Diego, CA, 260 pp.

Janzen, C.D. and Wong, K.C., 2002. Wind-forced dynamics at the estuary-shelf interface of a large coastal plain estuary. J. Geophys. Res., 107(C10): 3138.

Kennedy, A.J., Griffin, M.L., Morey, S.L., Smith, S.R. and O'Brien, J.J., 2007. Effects of El Niño–Southern Oscillation on sea level anomalies along the Gulf of Mexico coast. Journal of Geophysical Research: Oceans, 112(C5): C05047.

Ketchum, B.H., 1954. Relation between Circulation and Planktonic Populations in Estuaries. Ecology, 35(2): 191-200.

Knudsen, M., 1900. Ein hydrographischer lehrsatz. Ann. Hydrogr. mar. Meterol, 28: 316-320.

Kruskal, W.H. and Wallis, W.A., 1952. Use of Ranks in One-Criterion Variance Analysis. Journal of the American Statistical Association, 47(260): 583-621.

Lewis, R., Whitman, Jr., R., 1982. A new geographic description of the boundaries and subdivisions of Tampa Bay. In: S.F.e.a. Treat (Editor), Tampa Bay Area Scientific Information Symposium. Bellwether Press, Tampa, Florida, pp. 10-18.

Lewis, R.R., Clark, P.A., Fehring, W.K., Greening, H.S., Johansson, R.O. and Paul, R.T., 1999. The Rehabilitation of the Tampa Bay Estuary, Florida, USA, as an Example of Successful Integrated Coastal Management. Marine Pollution Bulletin, 37(8-12): 468-473.

Li, Z., 1993. Circulation of Tampa Bay in Relation to Tides, Winds and Buoyancy Driven Convection, University of South Florida, St. Petersburg, FL.

Liu, Y., San Liang, X. and Weisberg, R.H., 2007. Rectification of the Bias in the Wavelet Power Spectrum, pp. 2093-2102.

Meyers, S.D., Kelly, B.G. and O'Brien, J.J., 1993. An Introduction to Wavelet Analysis in Oceanography and Meteorology: With Application to the Dispersion of Yanai Waves. Monthly Weather Review, 121(10): 2858-2866.

Meyers, S.D., Linville, A. and Luther, M.E., 2013. Changes in Residence Time due to Large-Scale Infrastructure in a Coastal Plain Estuary. Estuaries and Coasts: submitted.

Meyers, S.D., Luther, M.E., Wilson, M., Havens, H., Linville, A. and Sopkin, K., 2007. A numerical simulation of residual circulation in Tampa bay. Part I: Low-frequency temporal variations. Estuaries and Coasts, 30(4): 679-697.

Percival, D.B. and Mofjeld, H.O., 1997. Analysis of Subtidal Coastal Sea Level Fluctuations Using Wavelets. Journal of the American Statistical Association, 92(439): 868-880.

Pritchard, D.W., 1956. The Dynamic Structure of a Coastal Plain Estuary. Journal of Marine Research, 15(1): 33-42.

Rasmusson, E.M. and Carpenter, T.H., 1982. Variations in Tropical Sea Surface Temperature and Surface Wind Fields Associated with the Southern Oscillation/El Niño. Monthly Weather Review, 110(5): 354-384.

Ryan, H.F. and Noble, M.A., 2007. Sea level fluctuations in central California at subtidal to decadal and longer time scales with implications for San Francisco Bay, California. Estuarine, Coastal and Shelf Science, 73(3–4): 538-550.

Schmidt, N., Lipp, E.K., Rose, J.B. and Luther, M.E., 2001. ENSO influences on seasonal rainfall and river discharge in Florida. Journal of Climate, 14(4): 615-628.

Schmidt, N. and Luther, M.E., 2002. El Niño/Southern Oscillation impacts on salinity in Tampa Bay, Florida. Estuaries, 25: 976-984.

Schoellhamer, D.H., 1995. Sediment Resuspension Mechanisms in Old Tampa Bay, Florida. Estuarine, Coastal and Shelf Science, 40(6): 603-620.

Shi, H. and Singh, H., 2003. Status and Interconnections of Selected Environmental Issues in the Global Coastal Zones. AMBIO: A Journal of the Human Environment, 32(2): 145-152.

Sittel, M.C., 1994. Differences in the means of ENSO extremes for maximum temperature and precipitation in the United States, Florida State University.

Smith, S.R., Brolley, J., O'Brien, J.J. and Tartaglione, C.A., 2007. ENSO's Impact on Regional U.S. Hurricane Activity. Journal of Climate, 20(7): 1404-1414.

Smith, S.R., Green, P.M., Leonardi, A.P. and O'Brien, J.J., 1998. Role of Multiple-Level Tropospheric Circulations in Forcing ENSO Winter Precipitation Anomalies. Monthly Weather Review, 126(12): 3102-3116.

Soulé, P.T., 1998. Some Spatial Aspects of Southeastern United States Climatology. Journal of Geography, 97(4-5): 142-150.

Statham, P.J., 2012. Nutrients in estuaries — An overview and the potential impacts of climate change. Science of The Total Environment, 434(0): 213-227.

Swenson, E.M. and Chuang, W.-S., 1983. Tidal and subtidal water volume exchange in an estuarine system. Estuarine, Coastal and Shelf Science, 16(3): 229-240.

Torrence, C. and Compo, G.P., 1998. A Practical Guide to Wavelet Analysis. Bulletin of the American Meteorological Society, 79(1): 61-78.

Trenberth, K.E., 1997. The Definition of El Niño. Bulletin of the American Meteorological Society, 78(12): 2771-2777.

Valle-Levinson, A., Wong, K.C. and Bosley, K.T., 2001. Observations of the wind-induced exchange at the entrance to Chesapeake Bay. Journal of Marine Research, 59(3): 391-416.

Valle-Levinson, A., Wong, K.C. and Bosley, K.T., 2002. Response of the lower Chesapeake Bay to forcing from Hurricane Floyd. Continental Shelf Research, 22(11-13): 1715-1729.

Vincent, M.S., 2001. Development, Implementation and Analysis of the Tampa Bay Coastal Prediction System. Dissertation Thesis, College of Engineering, University of South Florida, Tampa, FL, 252 pp.

Walker, N., 2001. Tropical Storm and Hurricane wind effects on water level, salinity, and sediment transport in the river-influenced Atchafalaya-Vermilion Bay System, Louisiana, USA. Estuaries, 24(4): 498-508.

Walker, N.D. and Hammack, A.B., 2000. Impacts of Winter Storms on Circulation and Sediment Transport: Atchafalaya-Vermilion Bay Region, Louisiana, U.S.A. Journal of Coastal Research, 16(4): 996-1010.

Weisberg, R.H. and Sturges, W., 1976. Velocity Observations in the West Passage of Narragansett Bay: A Partially Mixed Estuary. Journal of Physical Oceanography, 6(3): 345-354.

Weisberg, R.H. and Williams, R.G., 1991. Initial findings on the circulation of Tampa Bay, Tampa Bay Area Scientific Information Symposium 12, Tampa, Florida, pp. 77-89.

Weisberg, R.H. and Zheng, L.Y., 2006. Circulation of Tampa Bay driven by buoyancy, tides, and winds, as simulated using a finite volume coastal ocean model. Journal of Geophysical Research-Oceans, 111(C1).

Wilson, M., 2007. Effects of Extreme Events on Residual Circulation for Tampa Bay, Florida, University of South Florida, 145 pp.

Wilson, M., Meyers, S.D. and Luther, M.E., 2006. Changes in the Circulation of Tampa Bay Due to Hurricane Frances as Recorded by ADCP Measurements and Reproduced with a Numerical Ocean Model. Estuaries and Coasts, 29: 914-918.

Wilson, M., Meyers, S.D. and Luther, M.E., 2013. Synoptic volumetric variations and flushing of the Tampa Bay estuary. Climate Dynamics.

Wong, K.-C., 2002. On the wind-induced exchange between Indian River Bay, Delaware and the adjacent continental shelf. Continental Shelf Research, 22(11–13): 1651-1668.

Wong, K.-C. and Moses-Hall, J.E., 1998. On the relative importance of the remote and local wind effects to the subtidal variability in a coastal plain estuary. Journal of Geophysical Research: Oceans, 103(C9): 18393-18404.

Wong, K.C. and Valle-Levinson, A., 2002. On the relative importance of the remote and local wind effects on the subtidal exchange at the entrance to the Chesapeake Bay. Journal of Marine Research, 60(3): 477-498.

Zervas, C.E., 1993. Tampa Bay Oceanography Project: Physical Oceanographic Synthesis. In: M. Office of Ocean and Earth Sciences Silver Spring (Editor), pp. 175.

Appendices

Appendix A: Comparison of monthly observation and model salinity

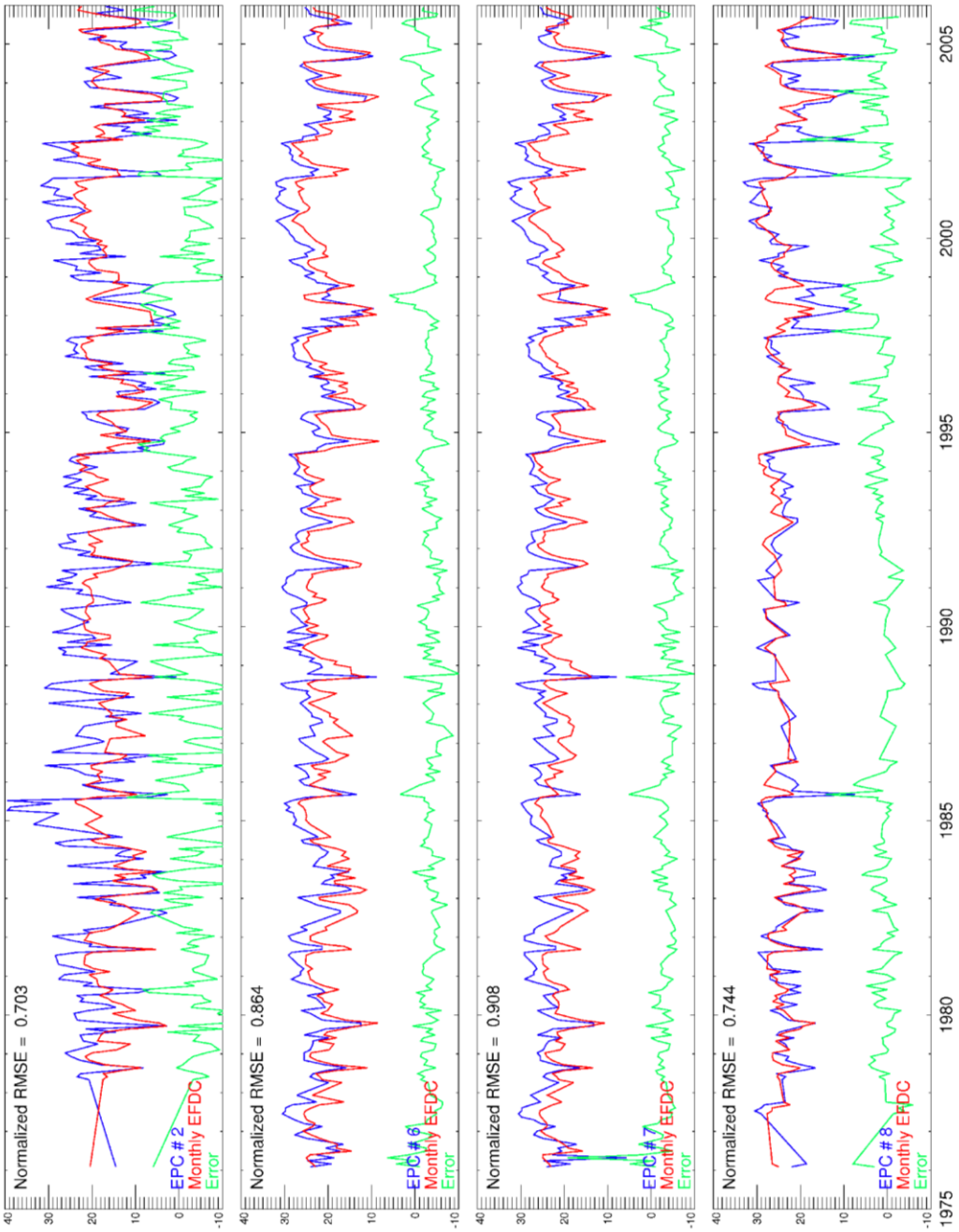

Figure A1. Monthly comparison of observational (blue) and model (red) salinity. Difference is shown in green. Normalized RMSE values are shown.

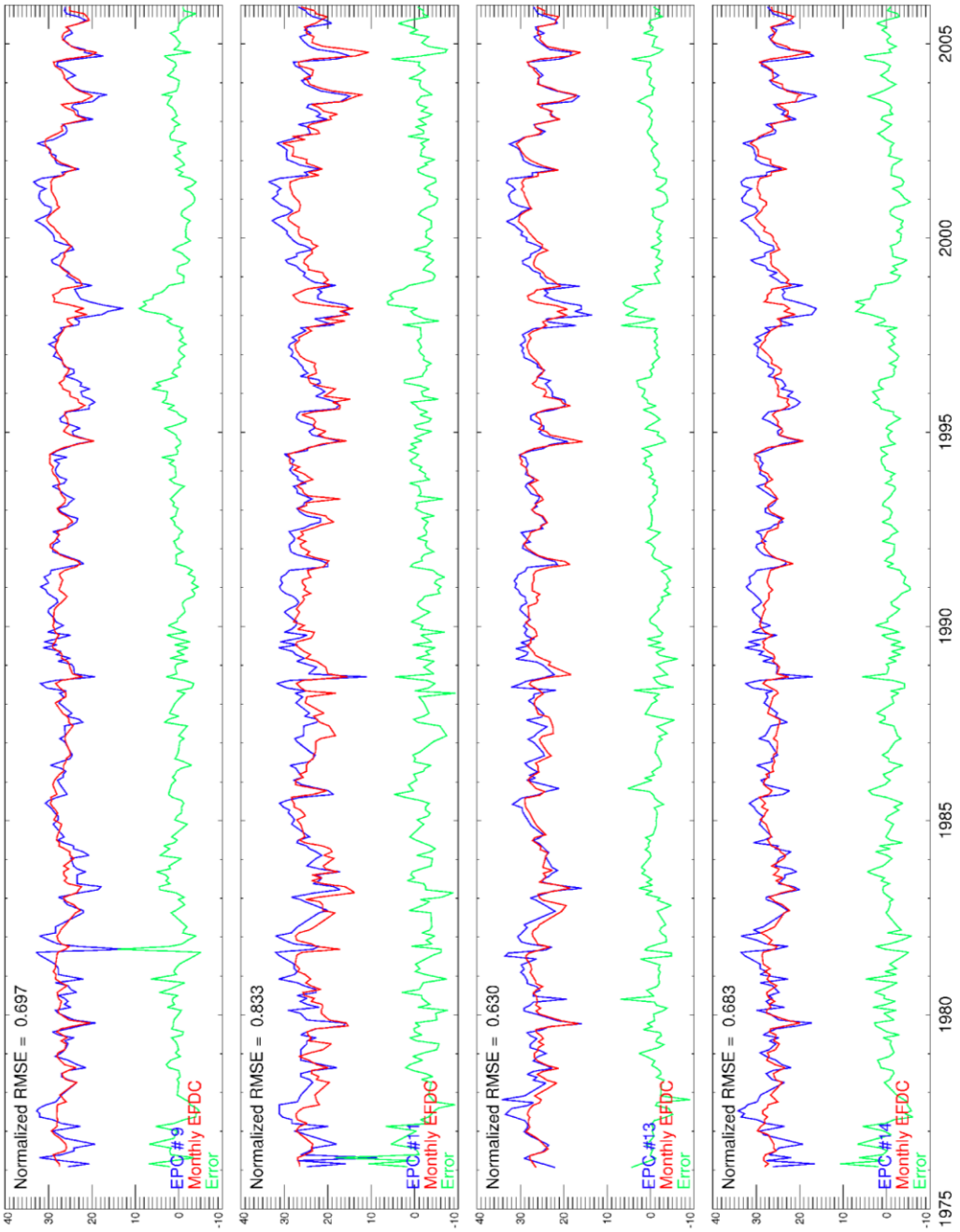

Figure A2. Same as figure A1.

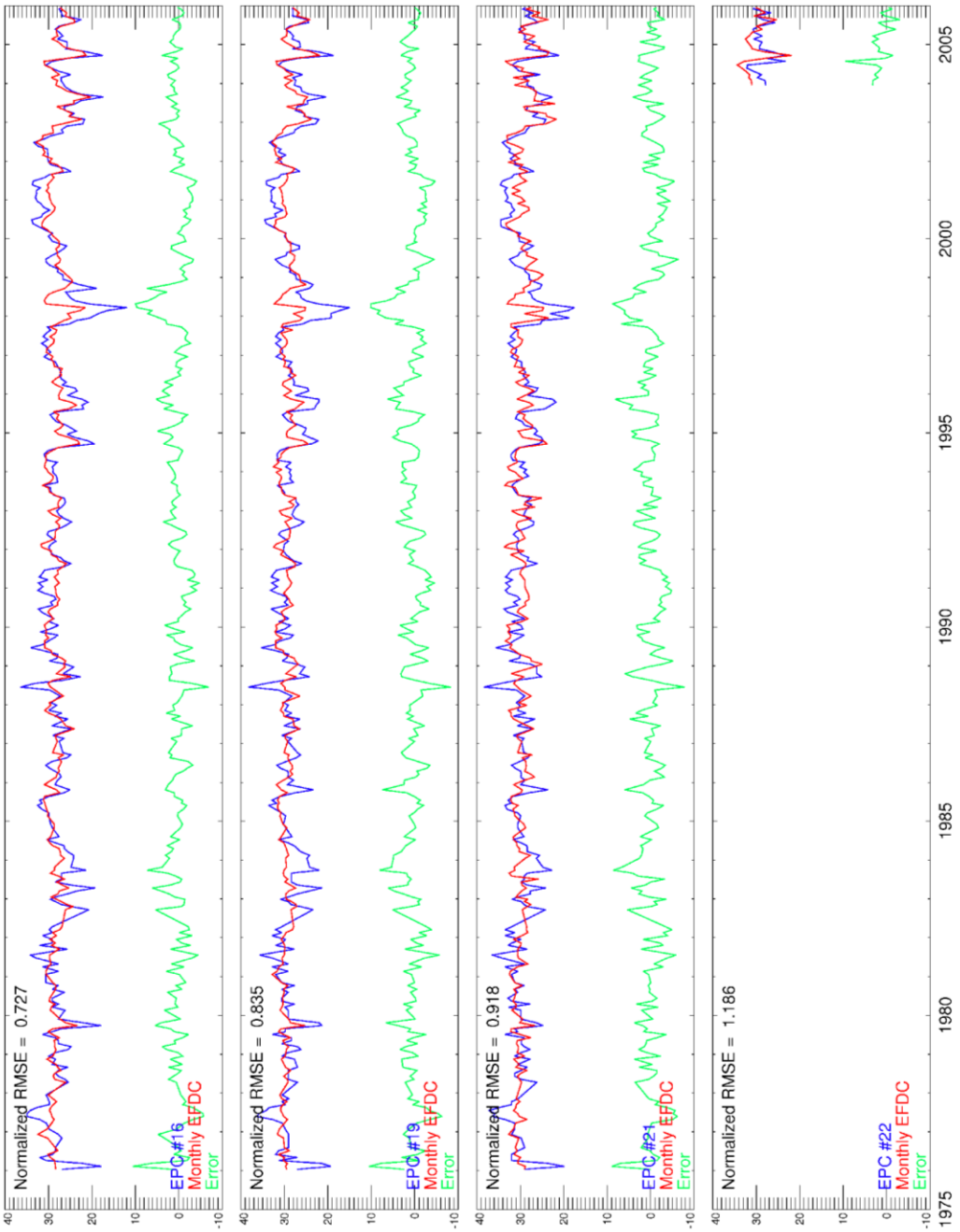

Figure A3. Same as figure A1.

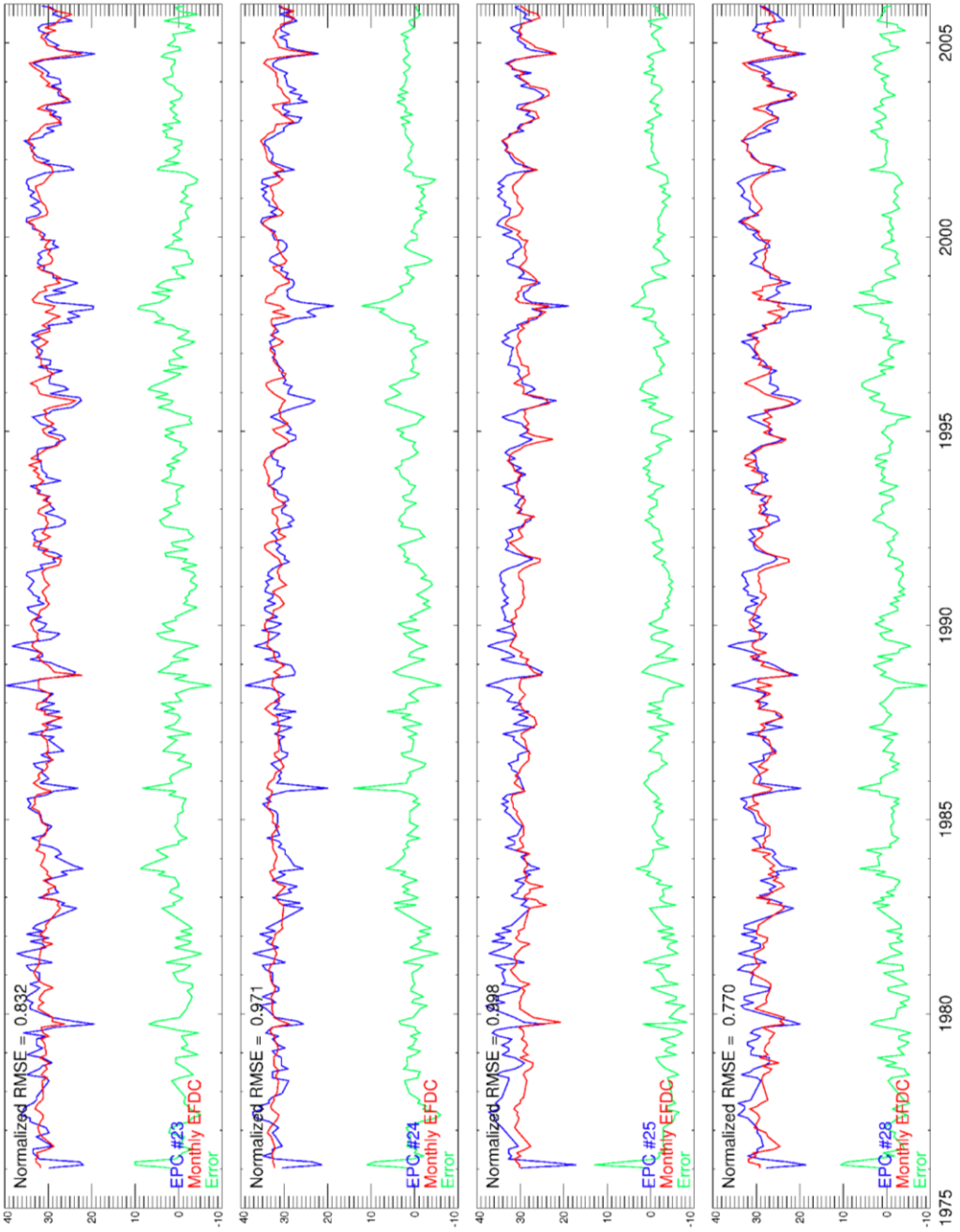

Figure A4. Same as figure A1.

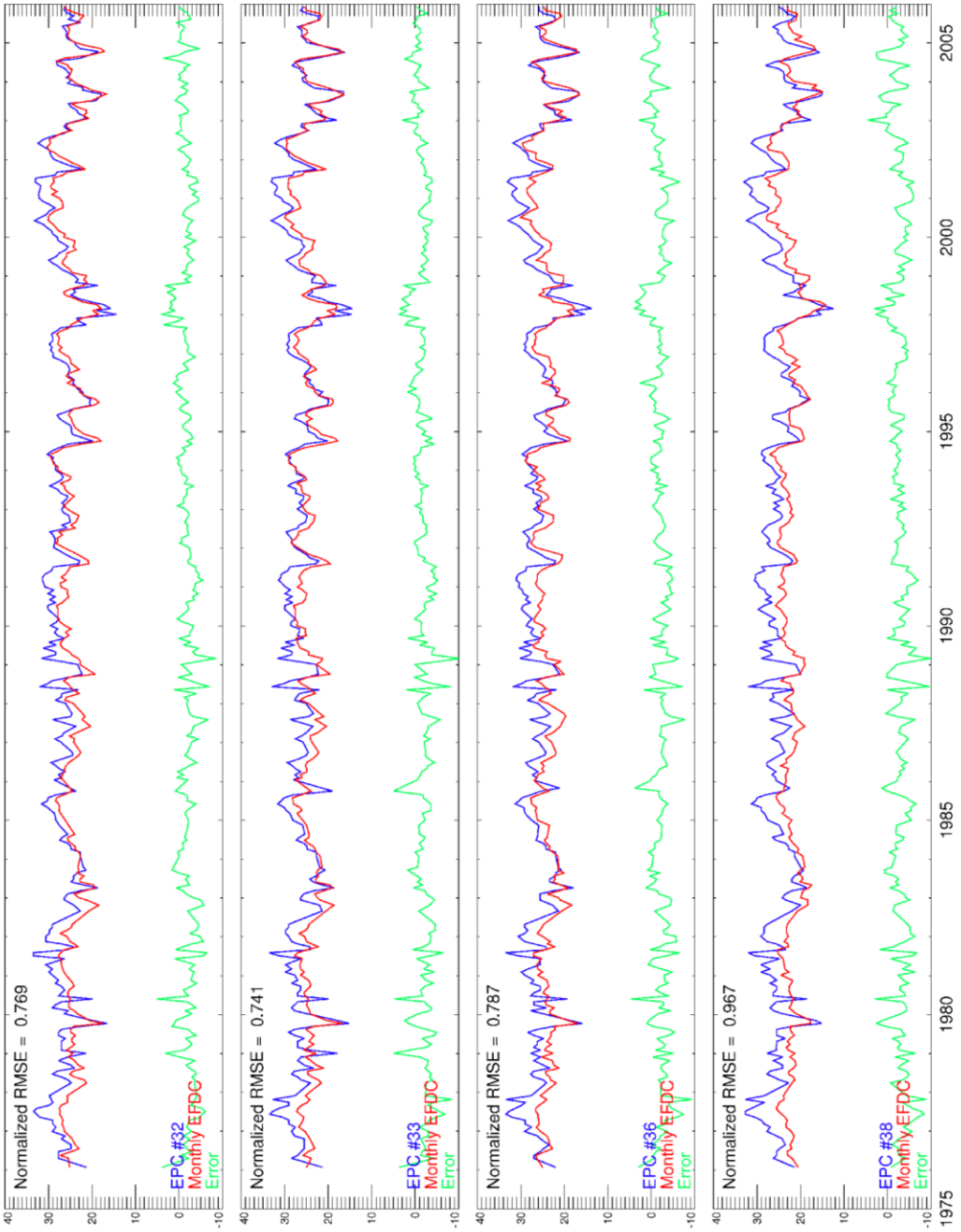

Figure A5. Same as figure A1.

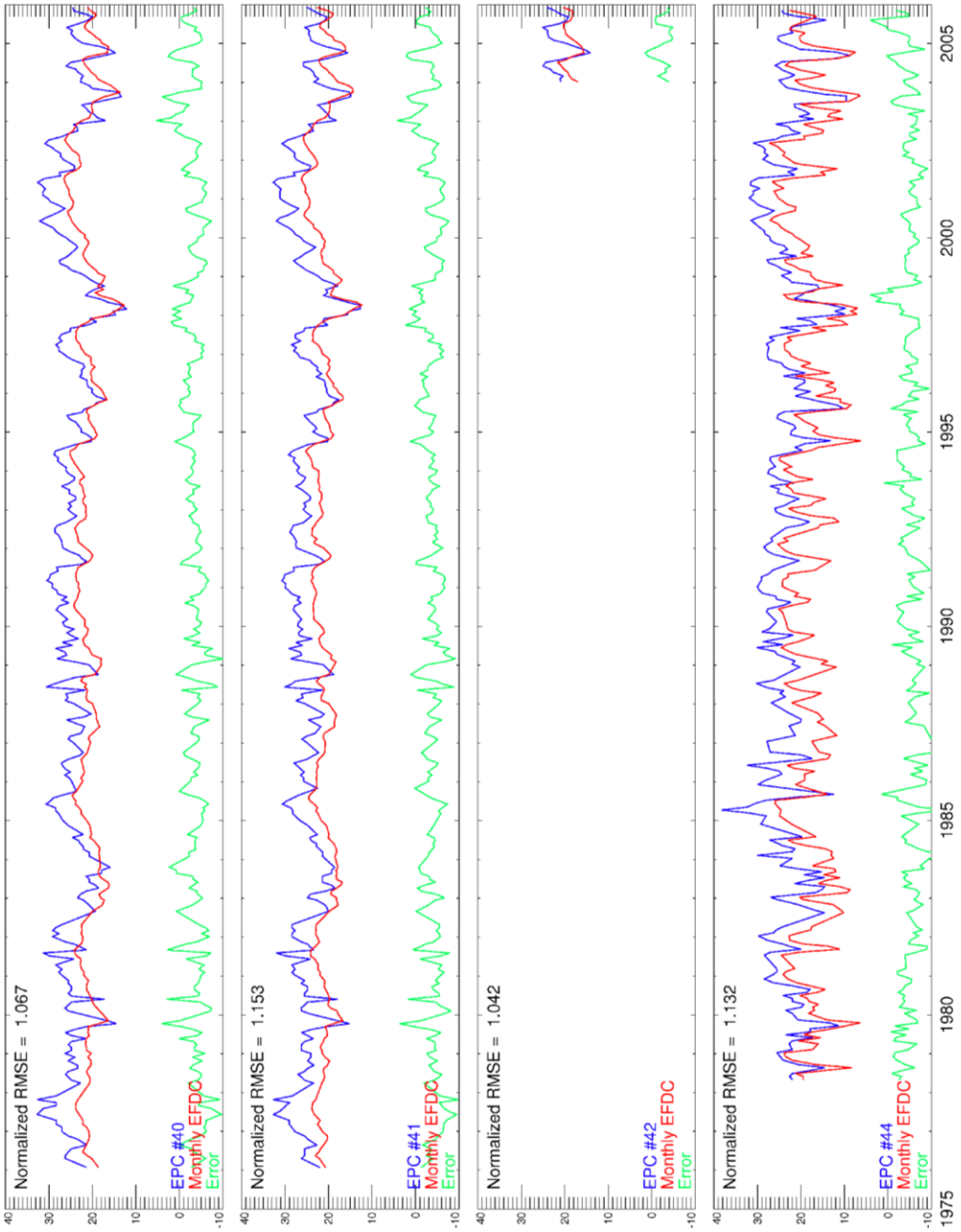

Figure A6. Same as figure A1.

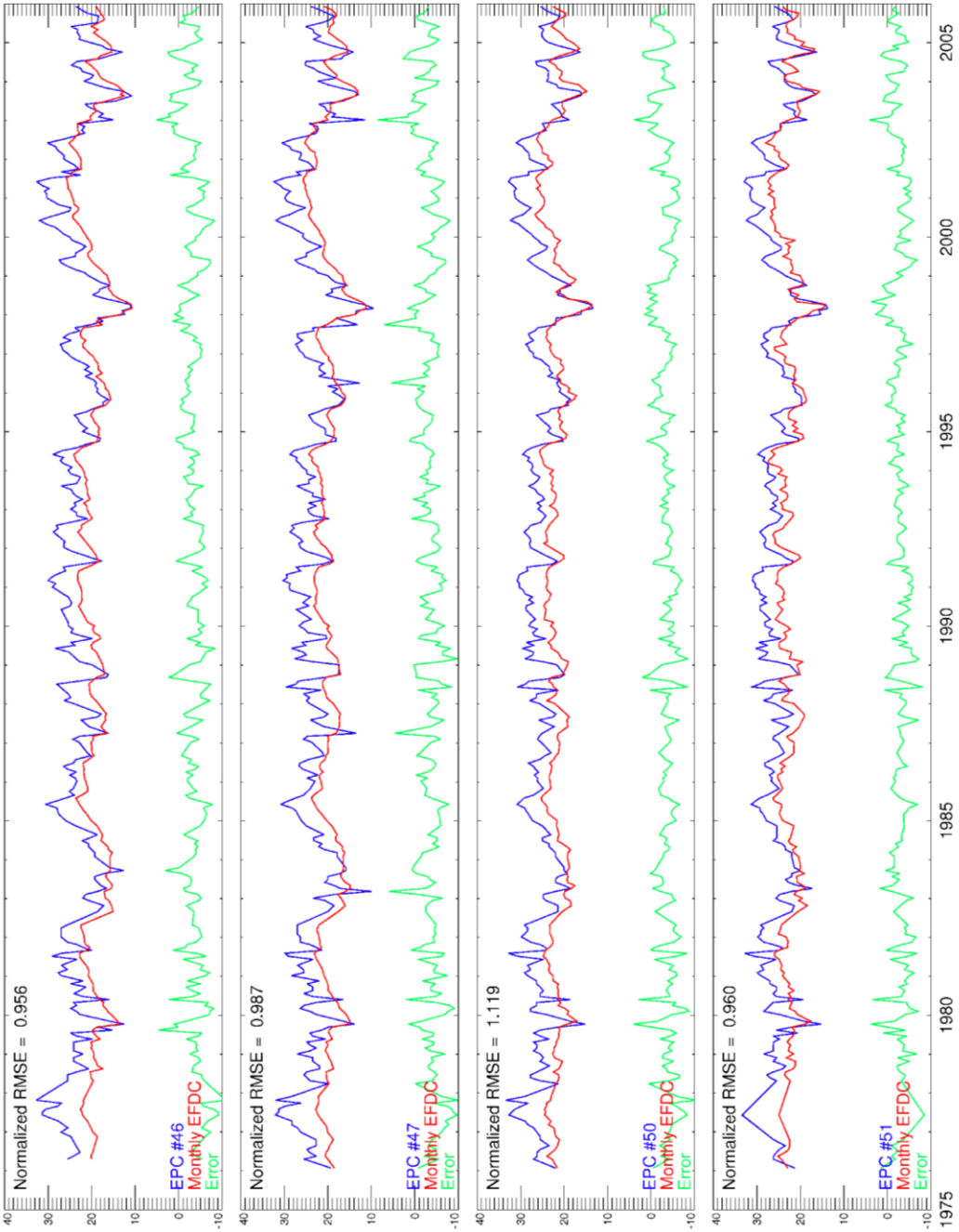

Figure A7. Same as figure A1.

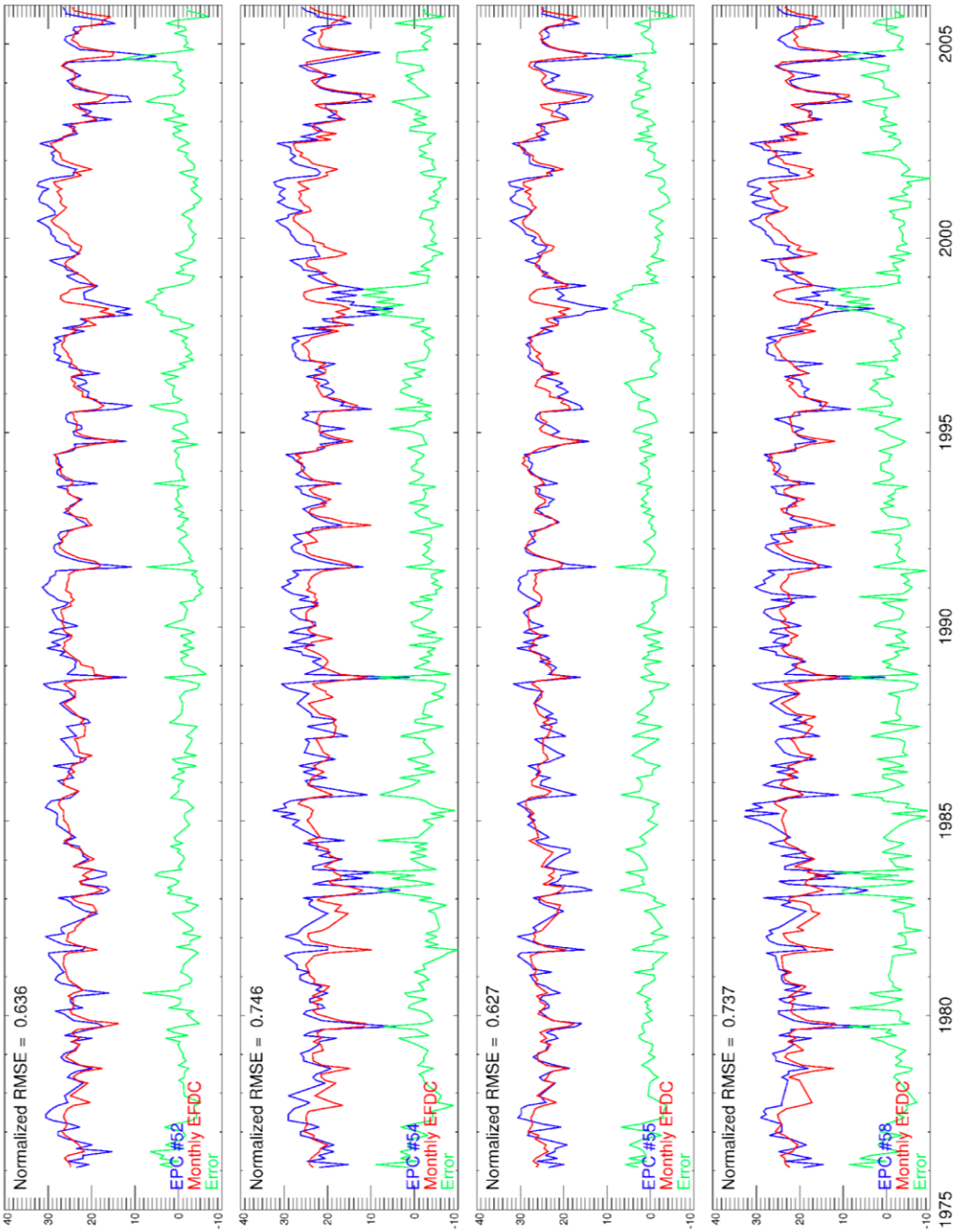

Figure A8. Same as figure A1.

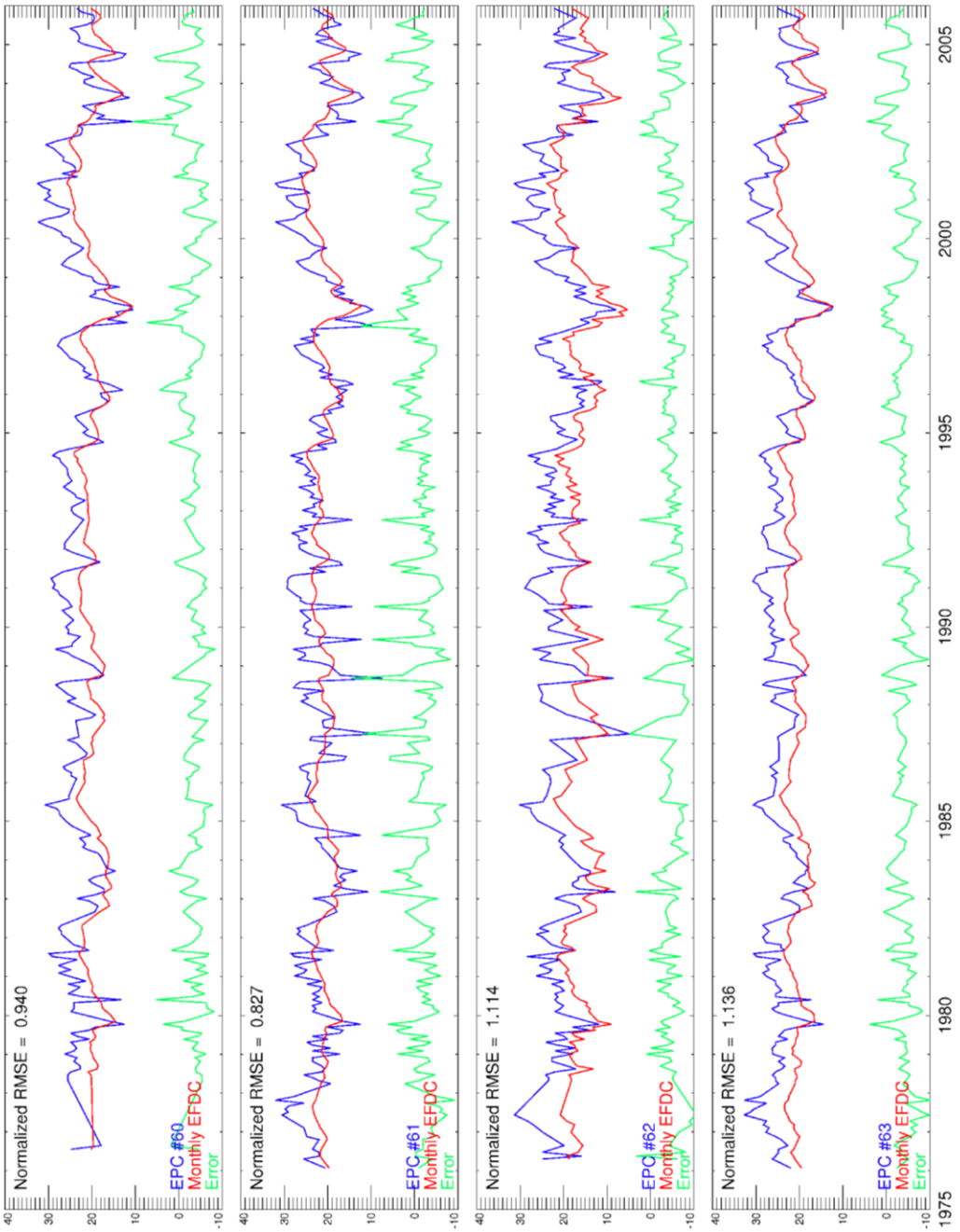

Figure A9. Same as figure A1.

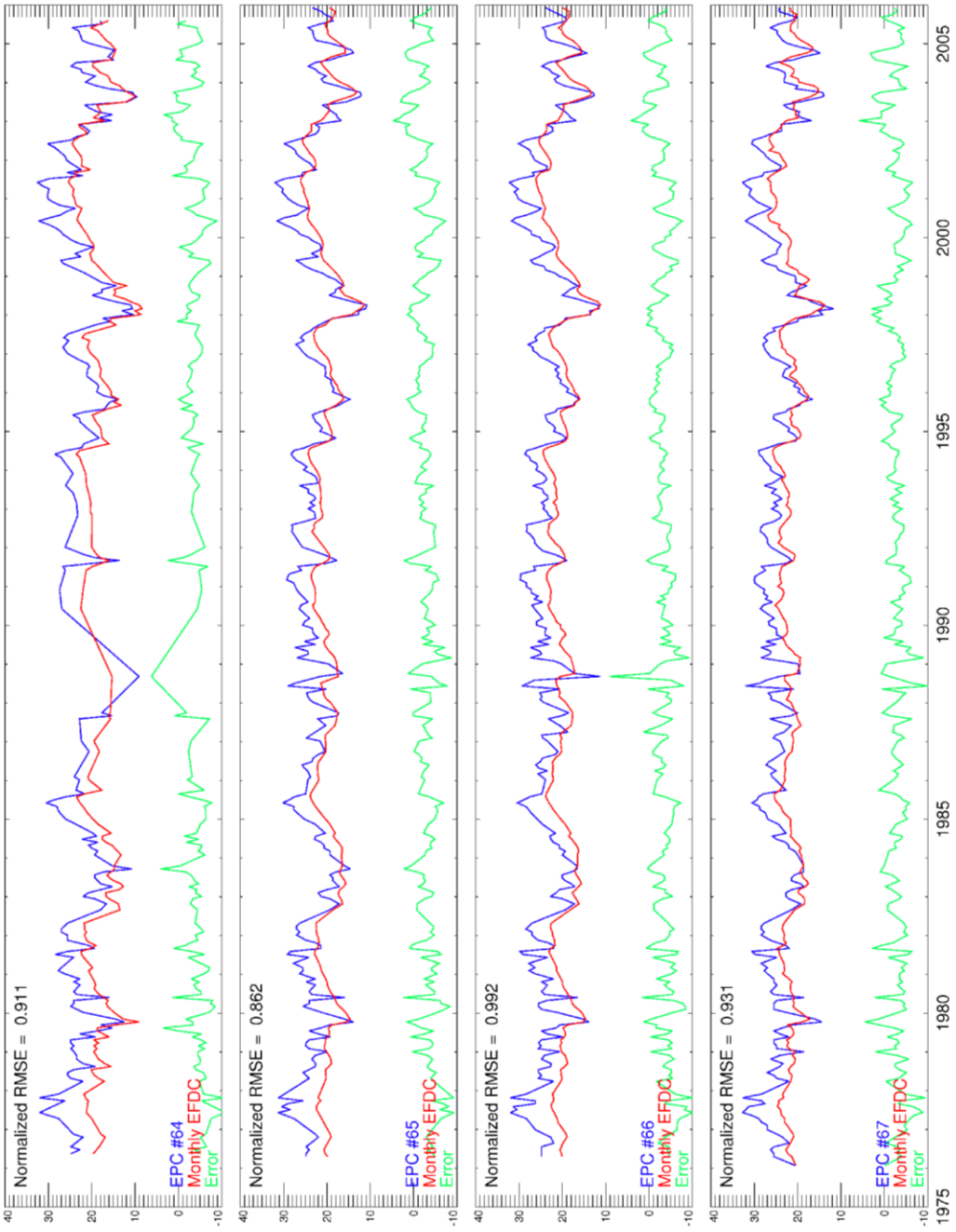

Figure A10. Same as figure A1.

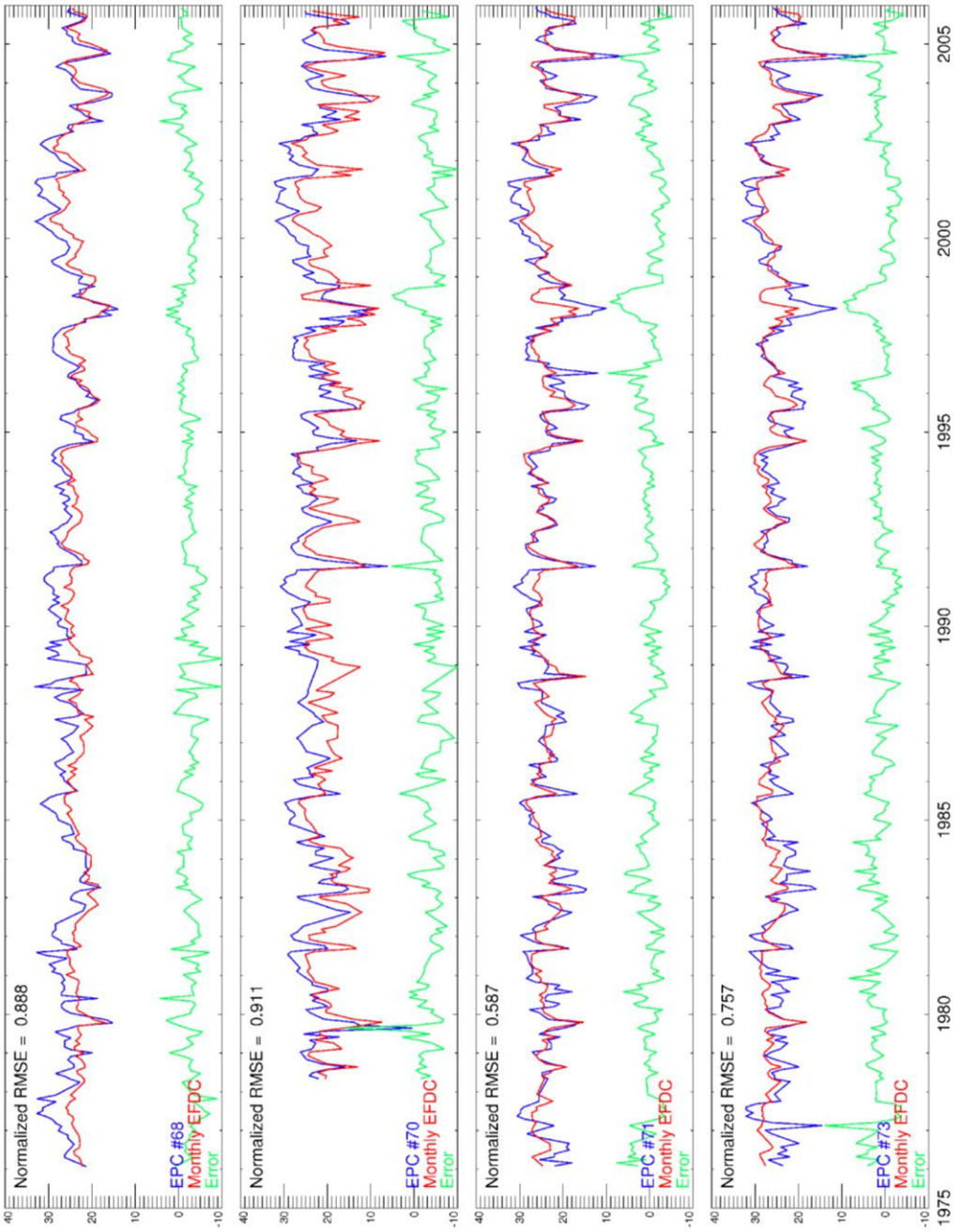

Figure A11. Same as figure A1.

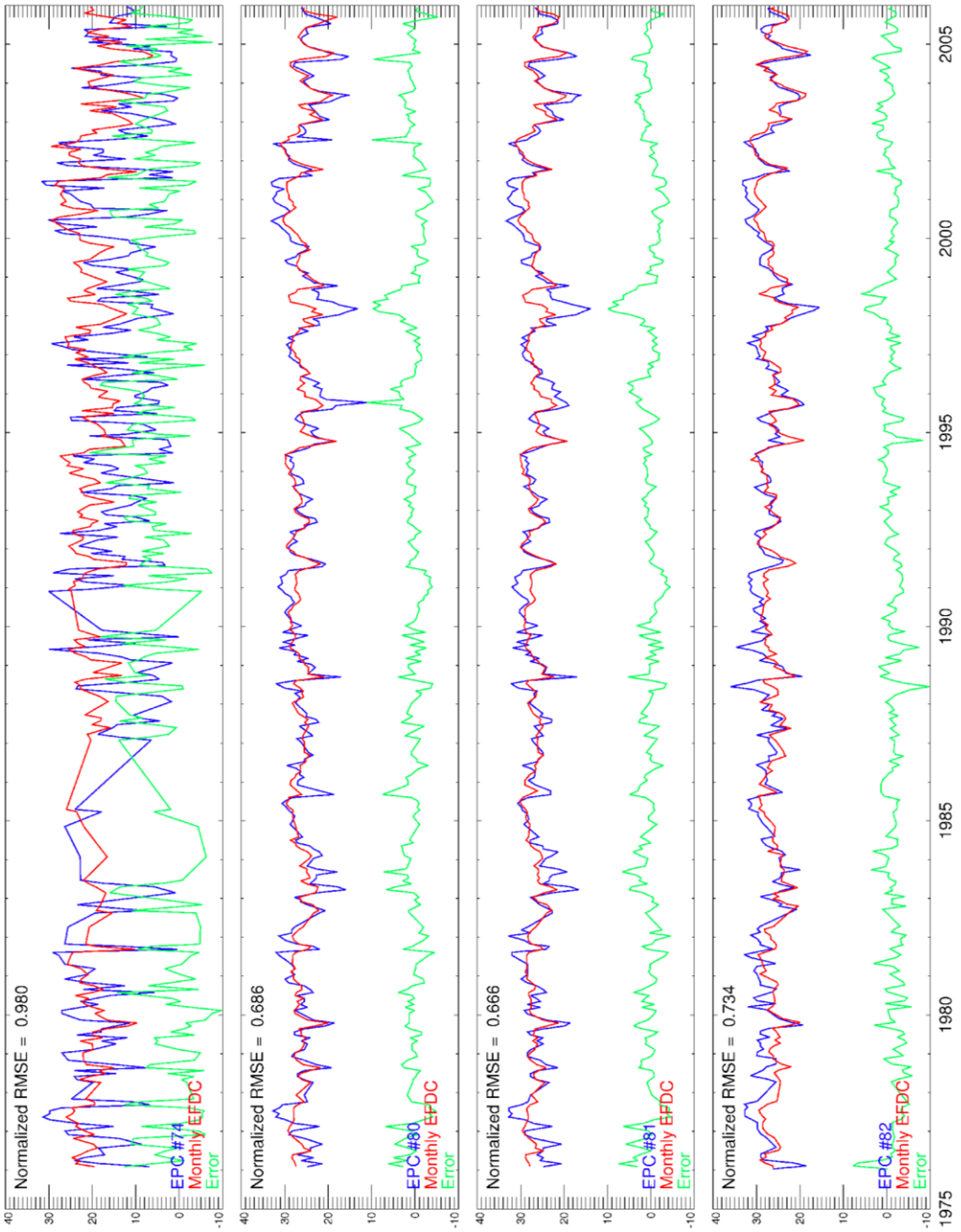

Figure A12. Same as figure A1.

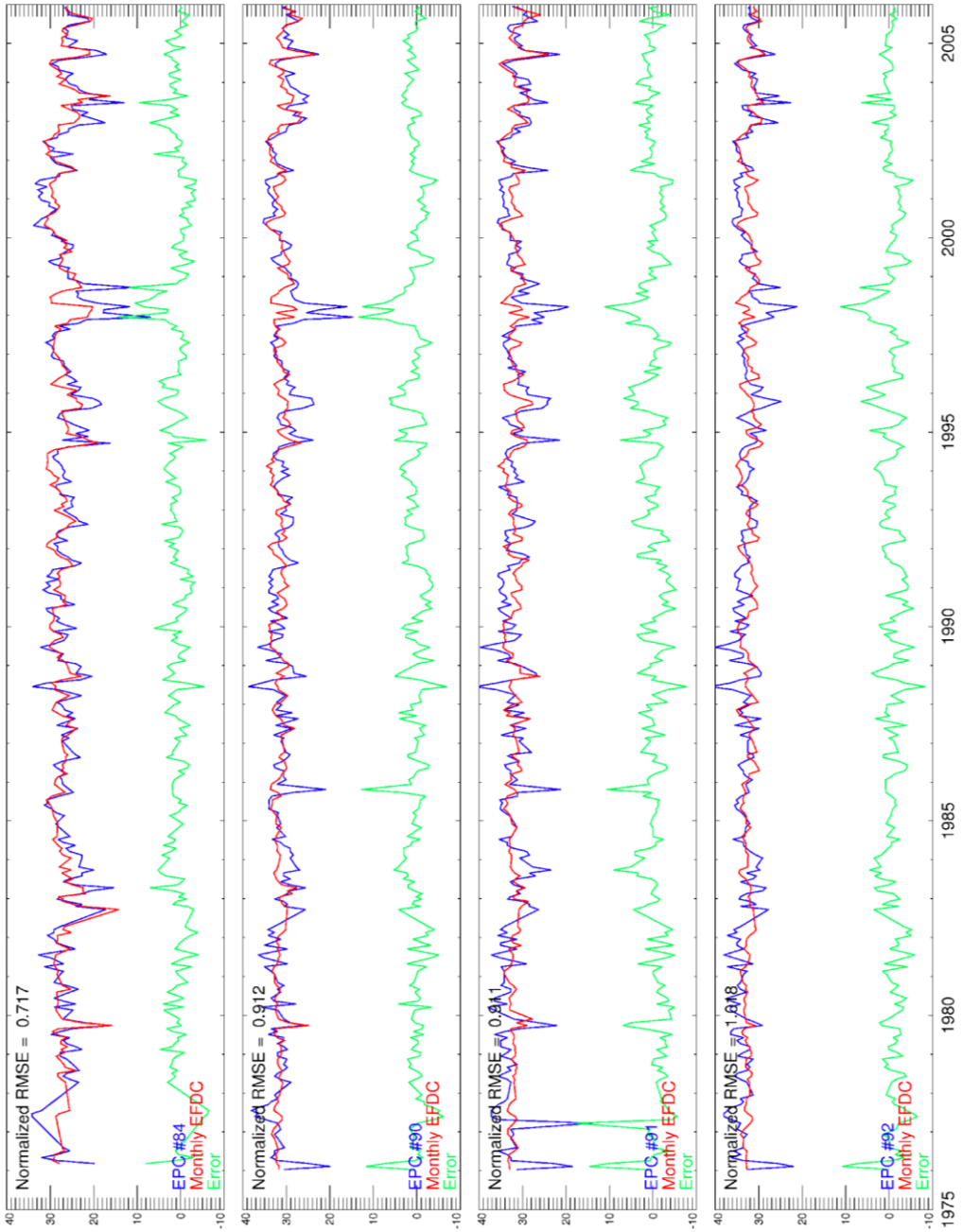

Figure A13. Same as figure A1.

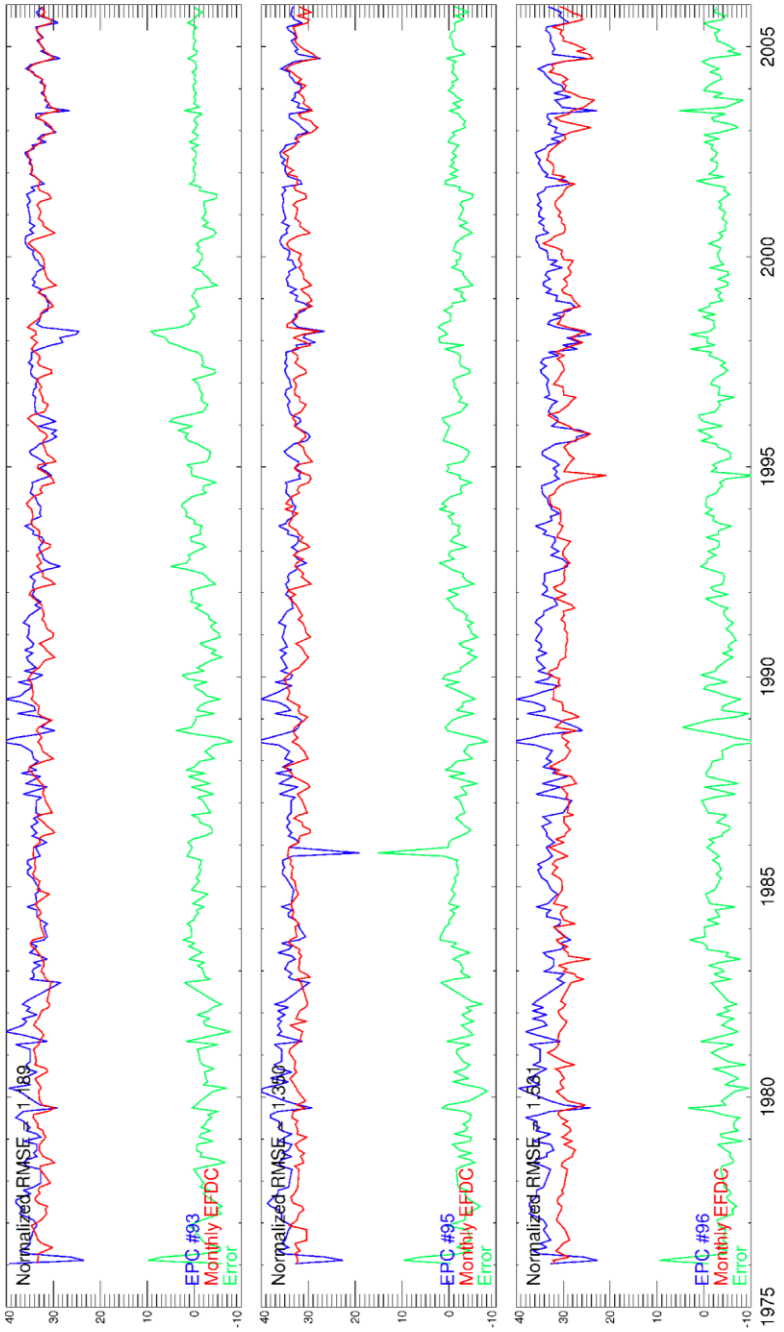

Figure A14. Same as figure A1.

Appendix B: Yearly bias bay mean error and normalized RMSE

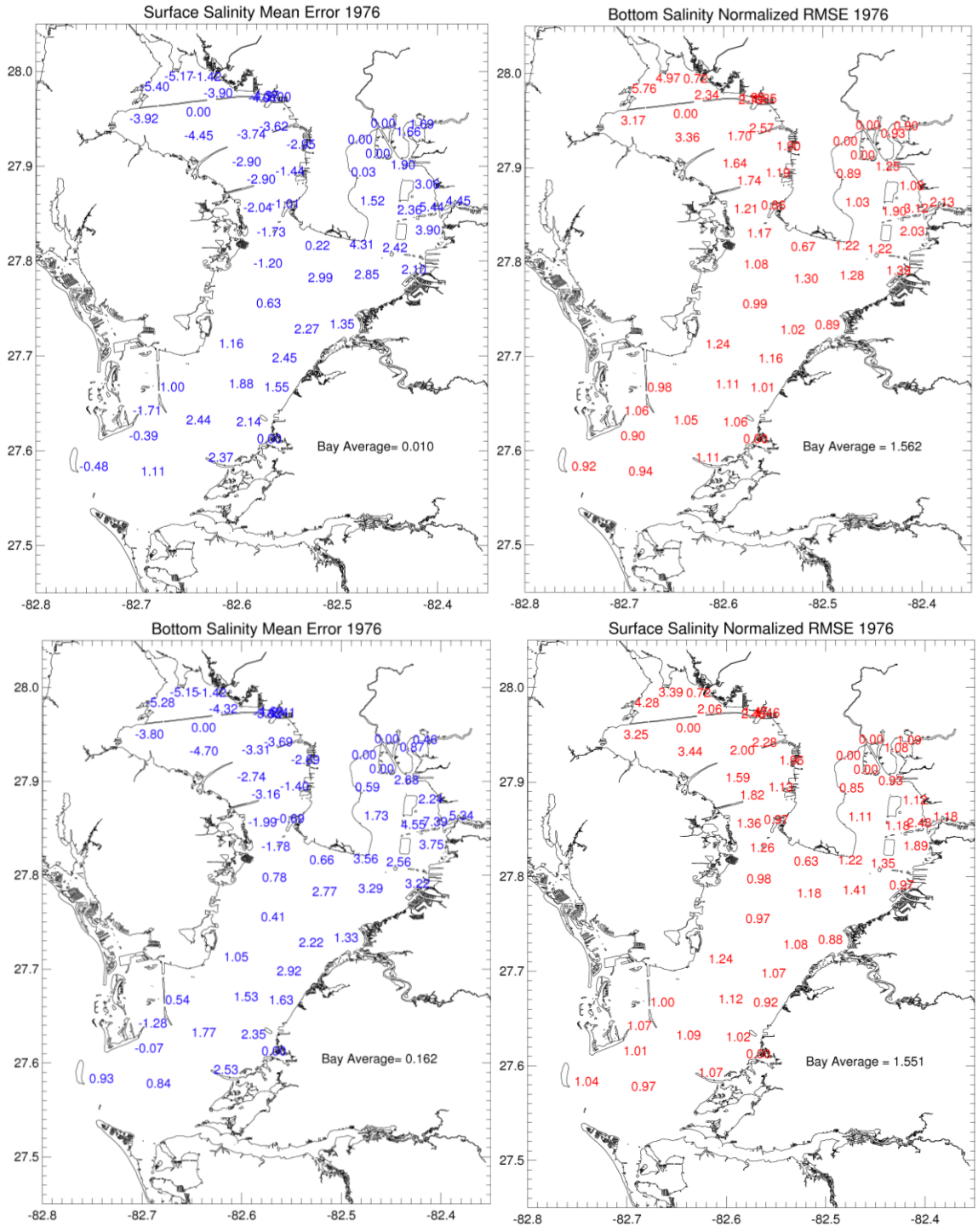

Figure A15. Near surface (top row) and bottom (bottom row) salinity bias mean errors and normalized RMSE for 1976

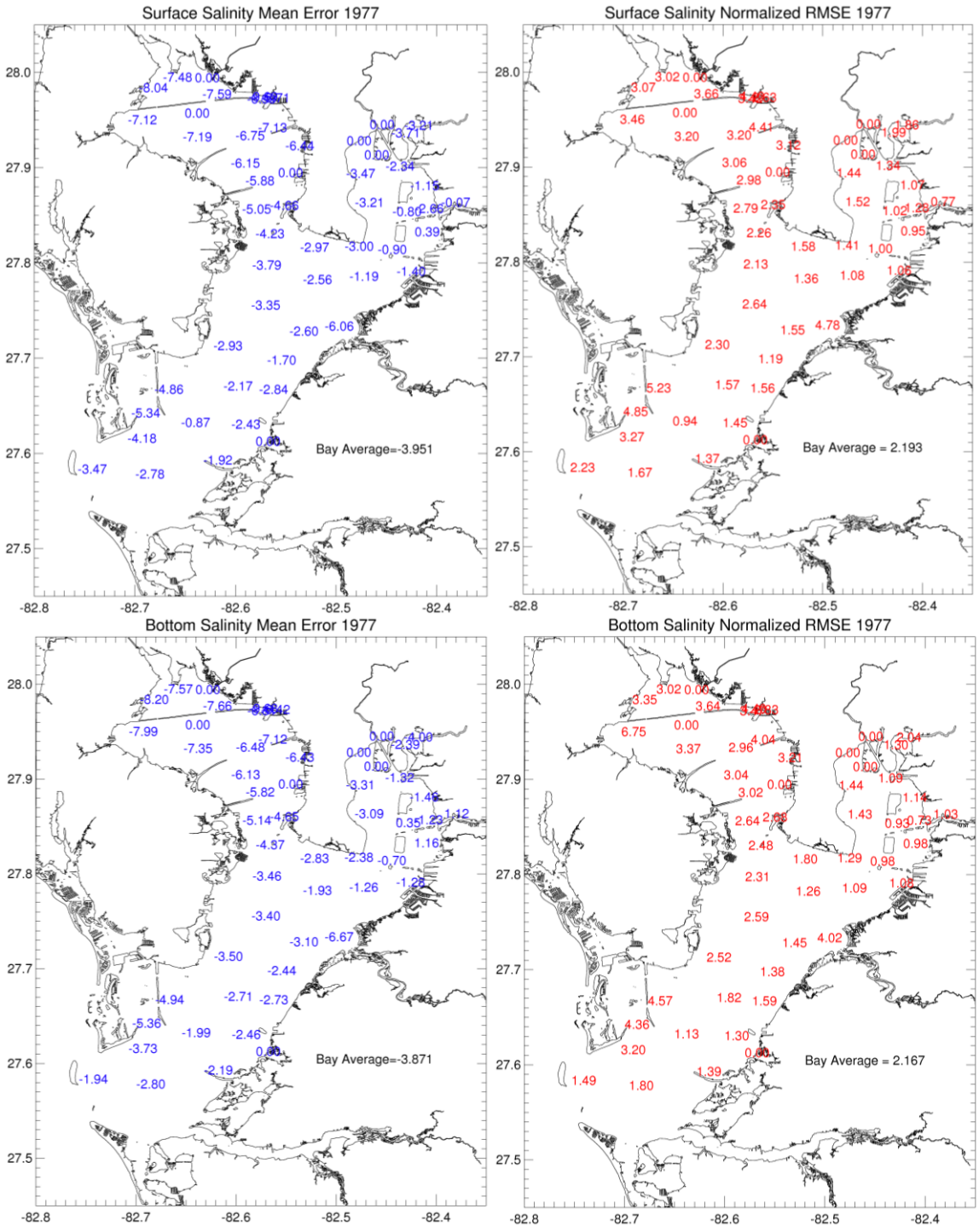

Figure A16. Same as figure A15 for 1977.

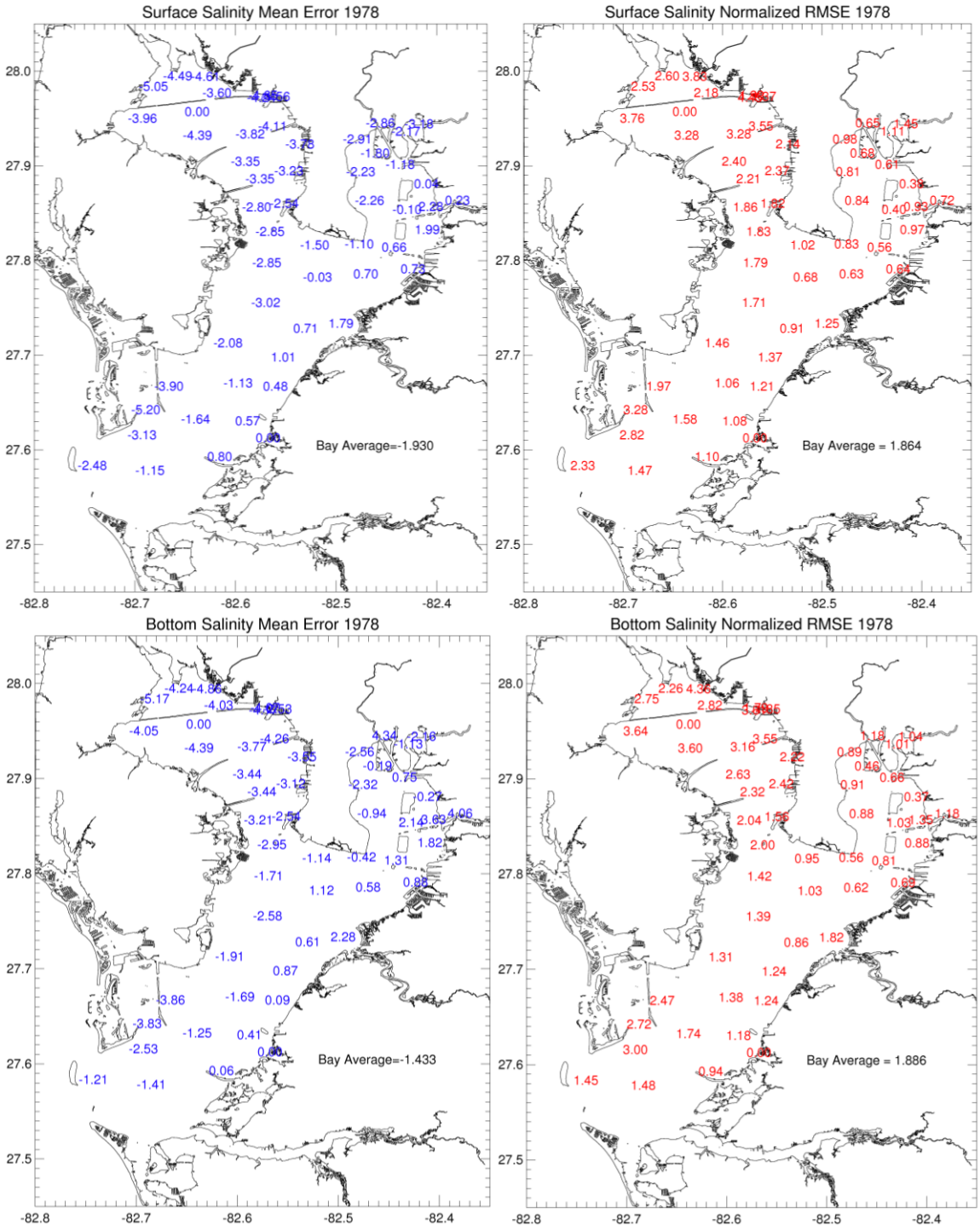

Figure A17. Same as figure A15 for 1978.

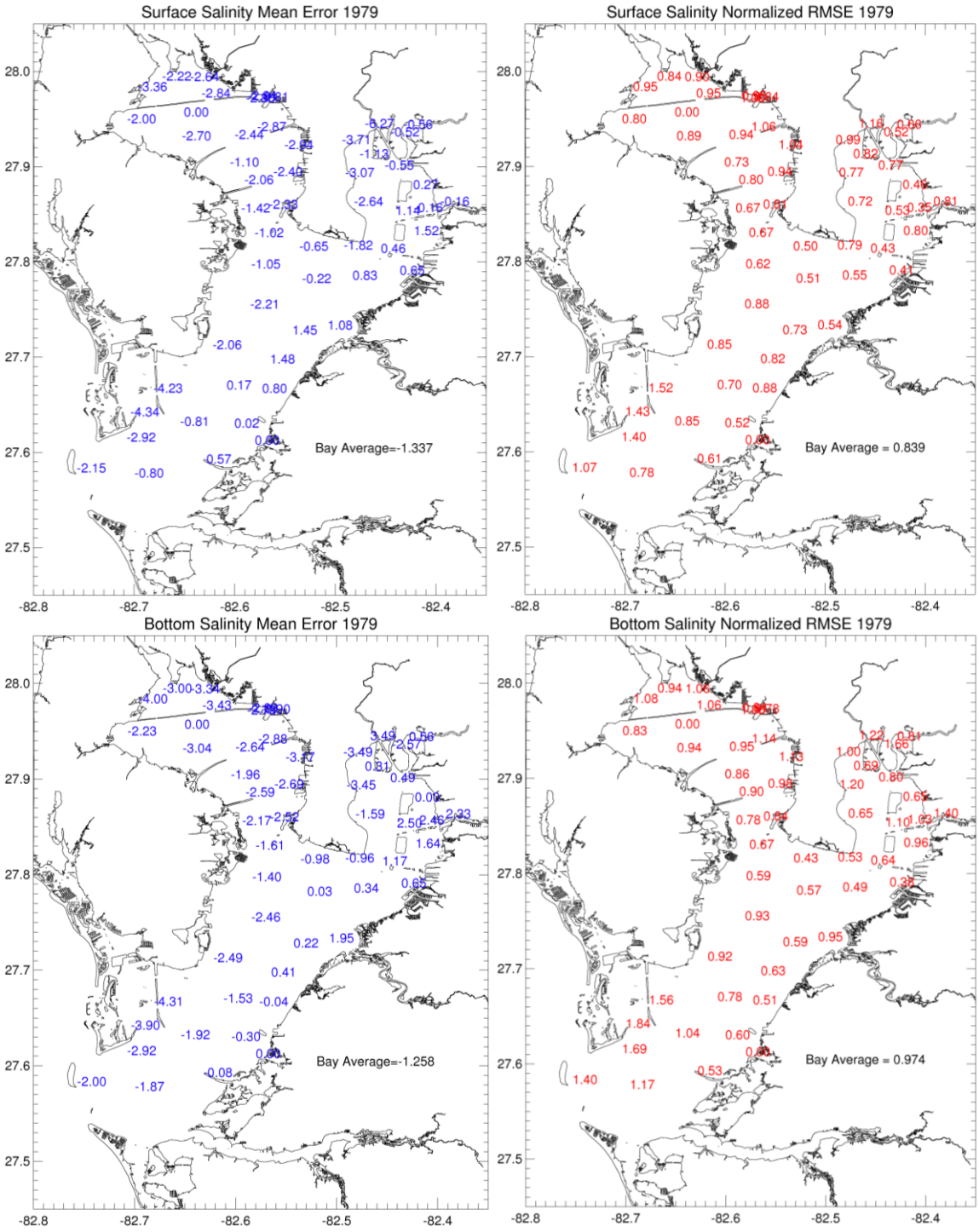

Figure A18. Same as figure A15 for 1979.

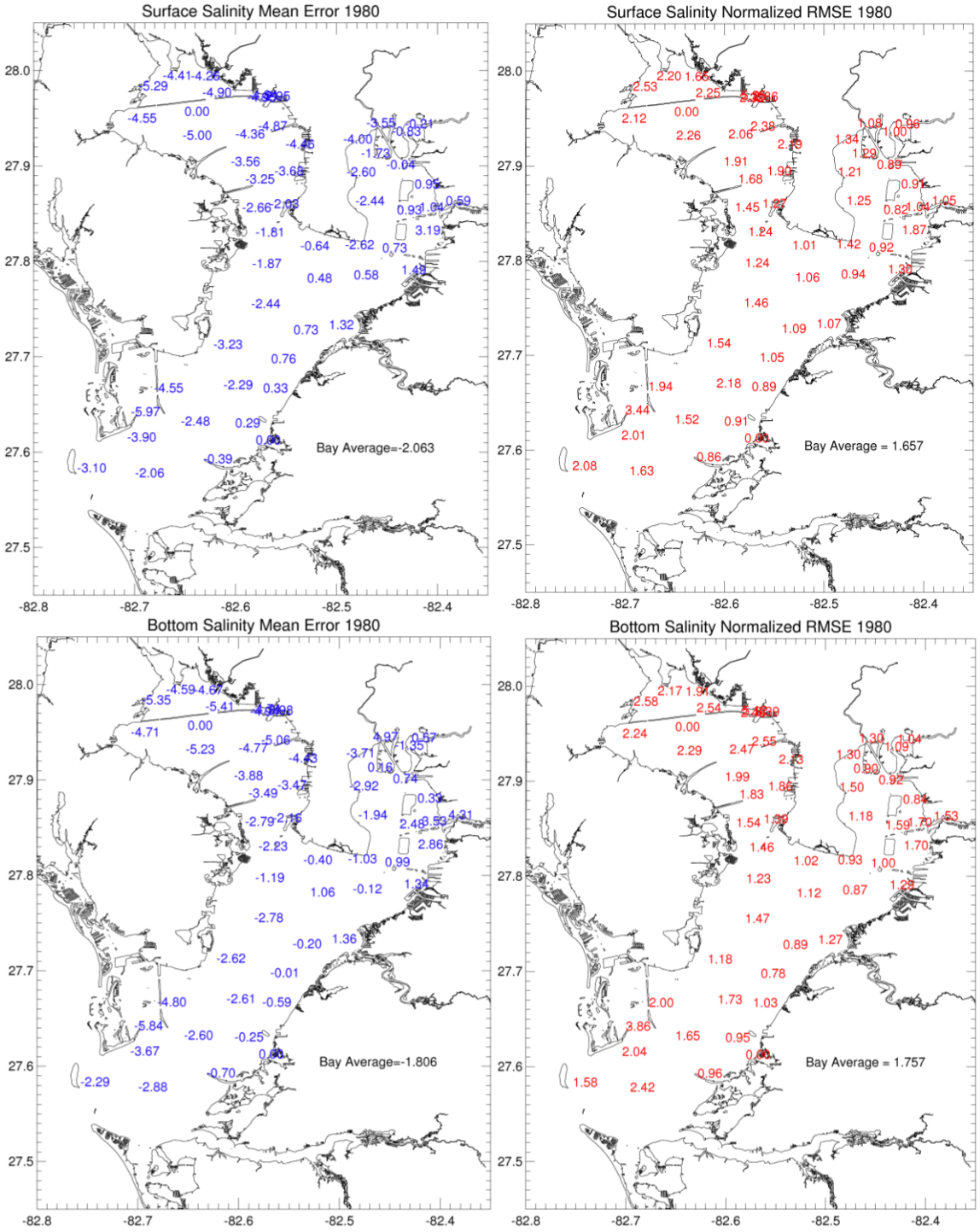

Figure A19. Same as figure A15 for 1980.

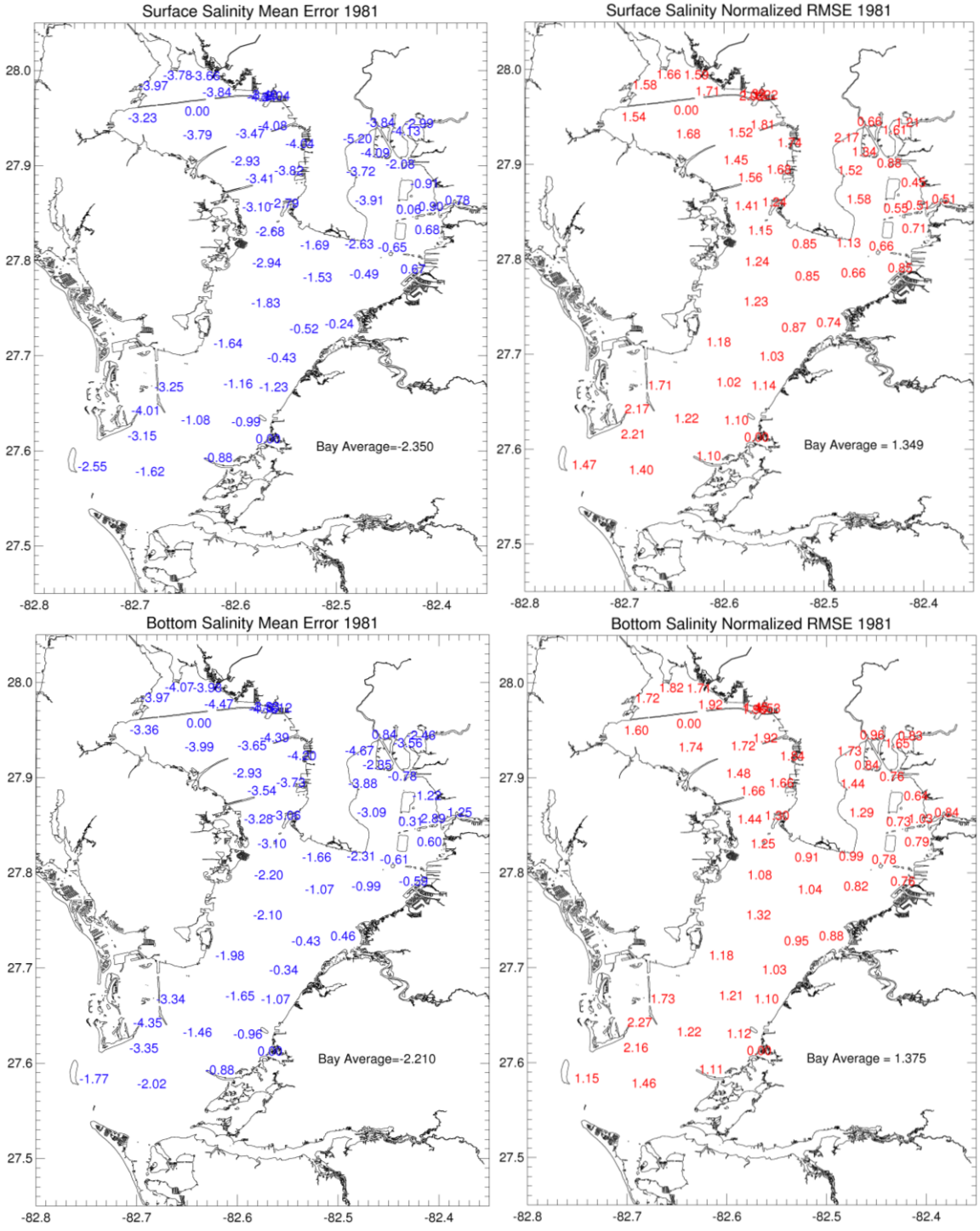

Figure A20. Same as figure A15 for 1981.

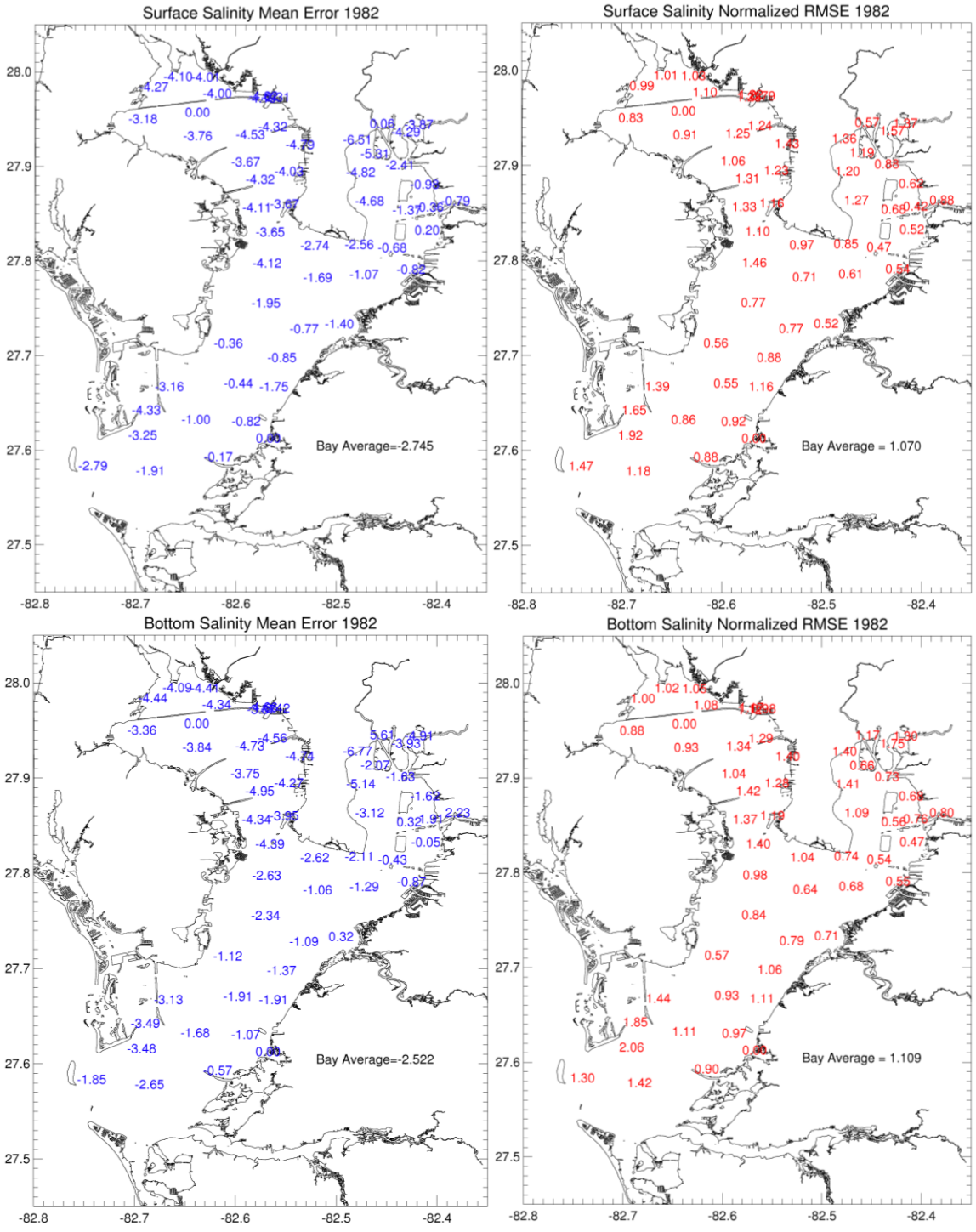

Figure A21. Same as figure A15 for 1982.

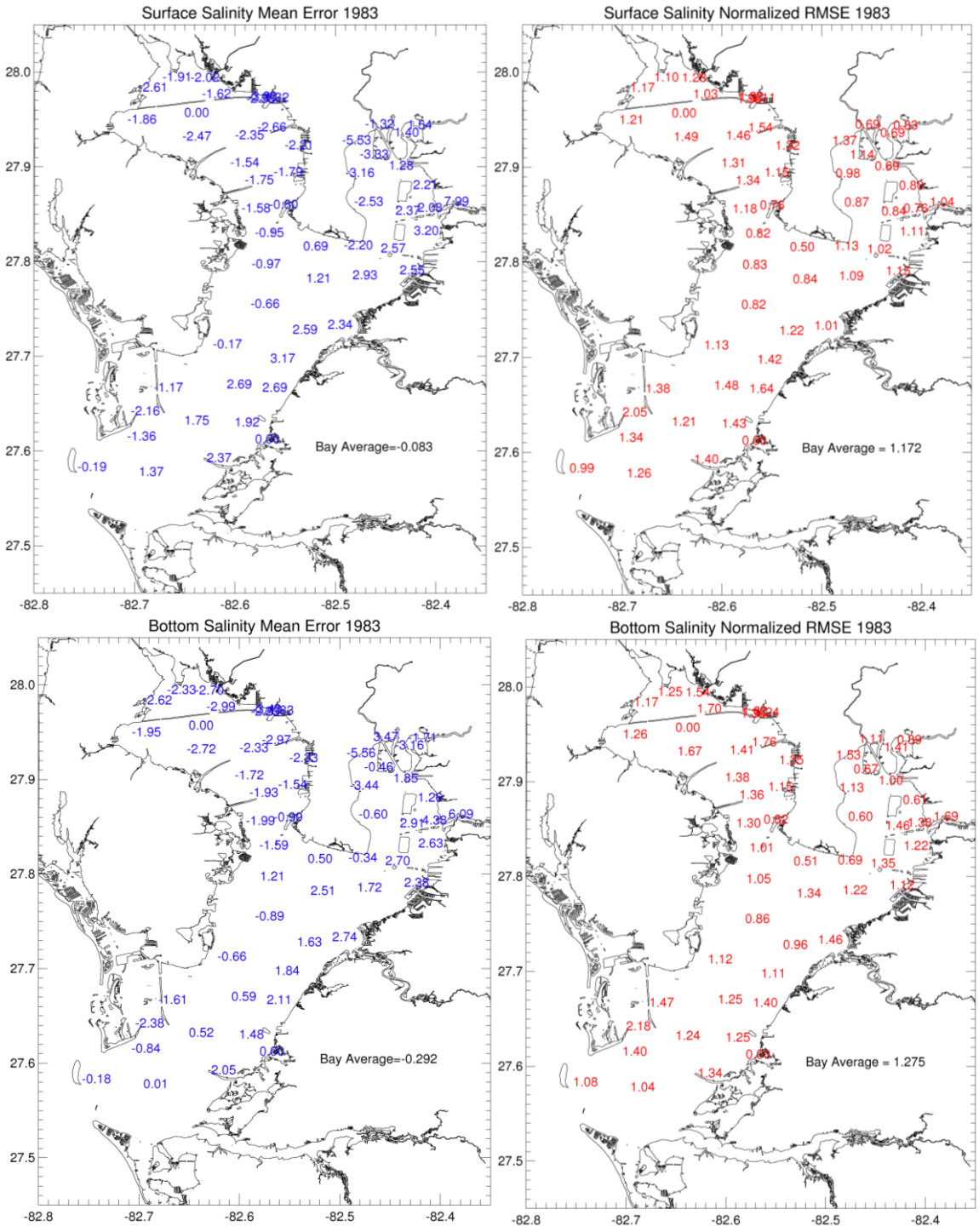

Figure A22. Same as figure A15 for 1983.

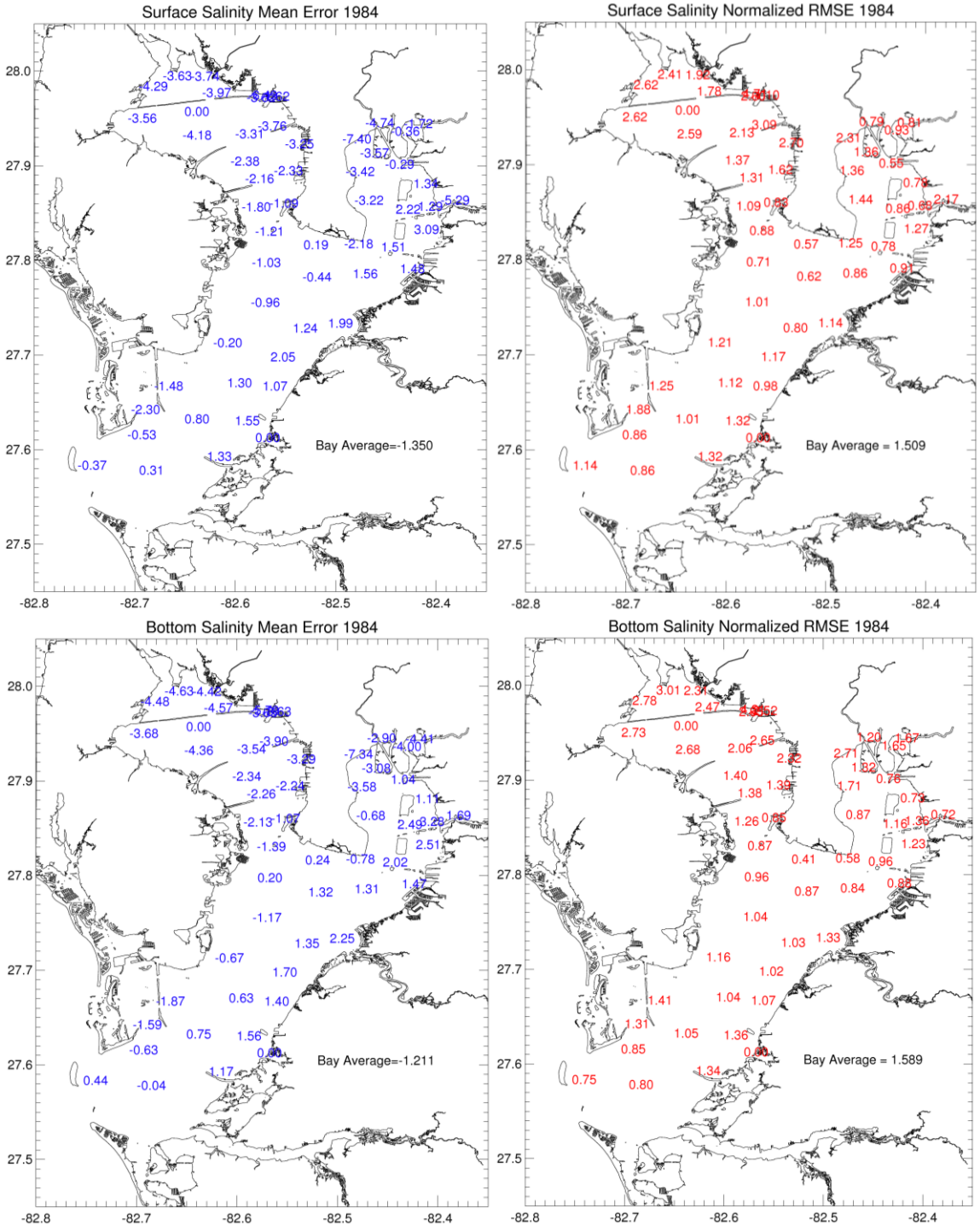

Figure A23. Same as figure A15 for 1984.

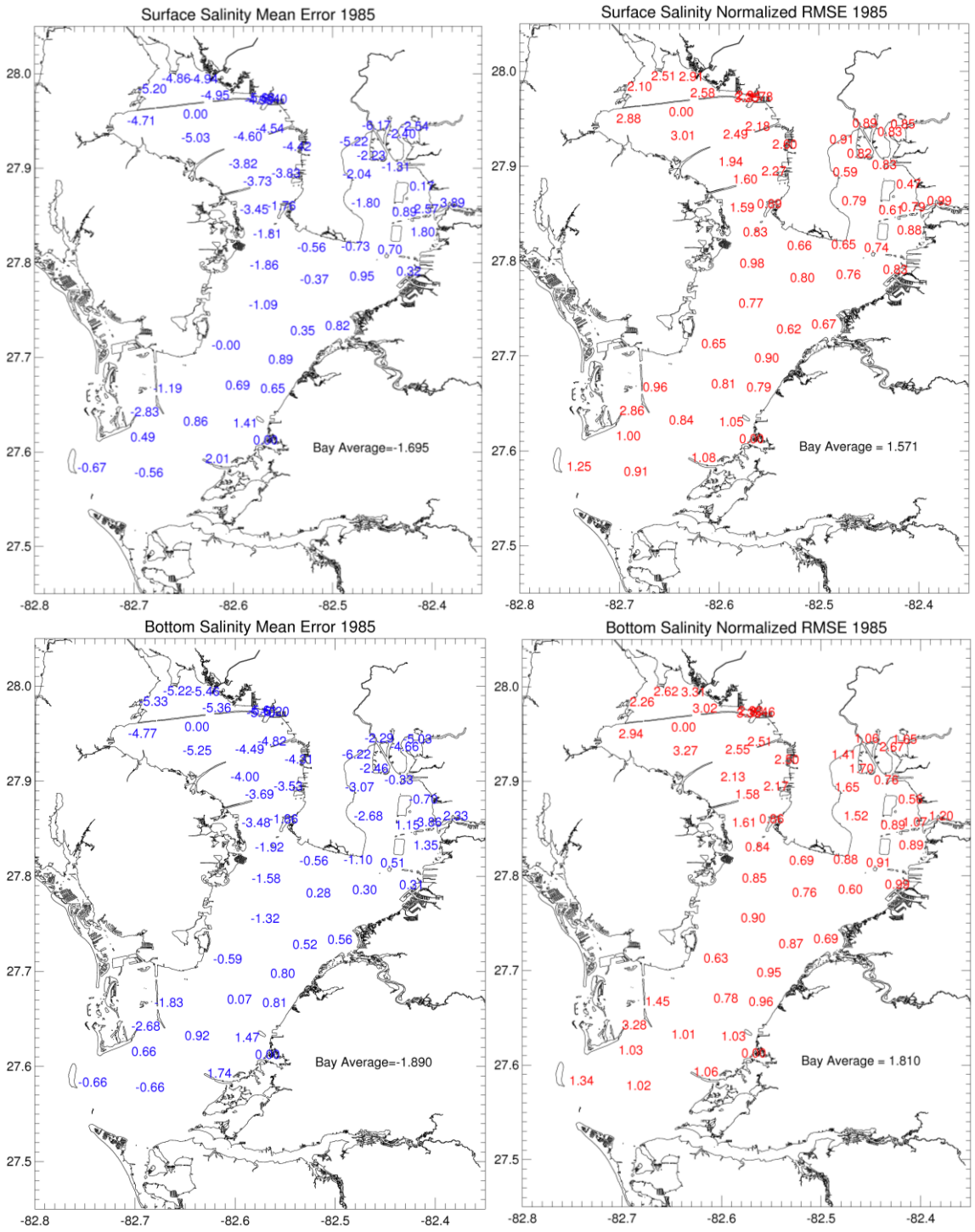

Figure A24. Same as figure A15 for 1985.

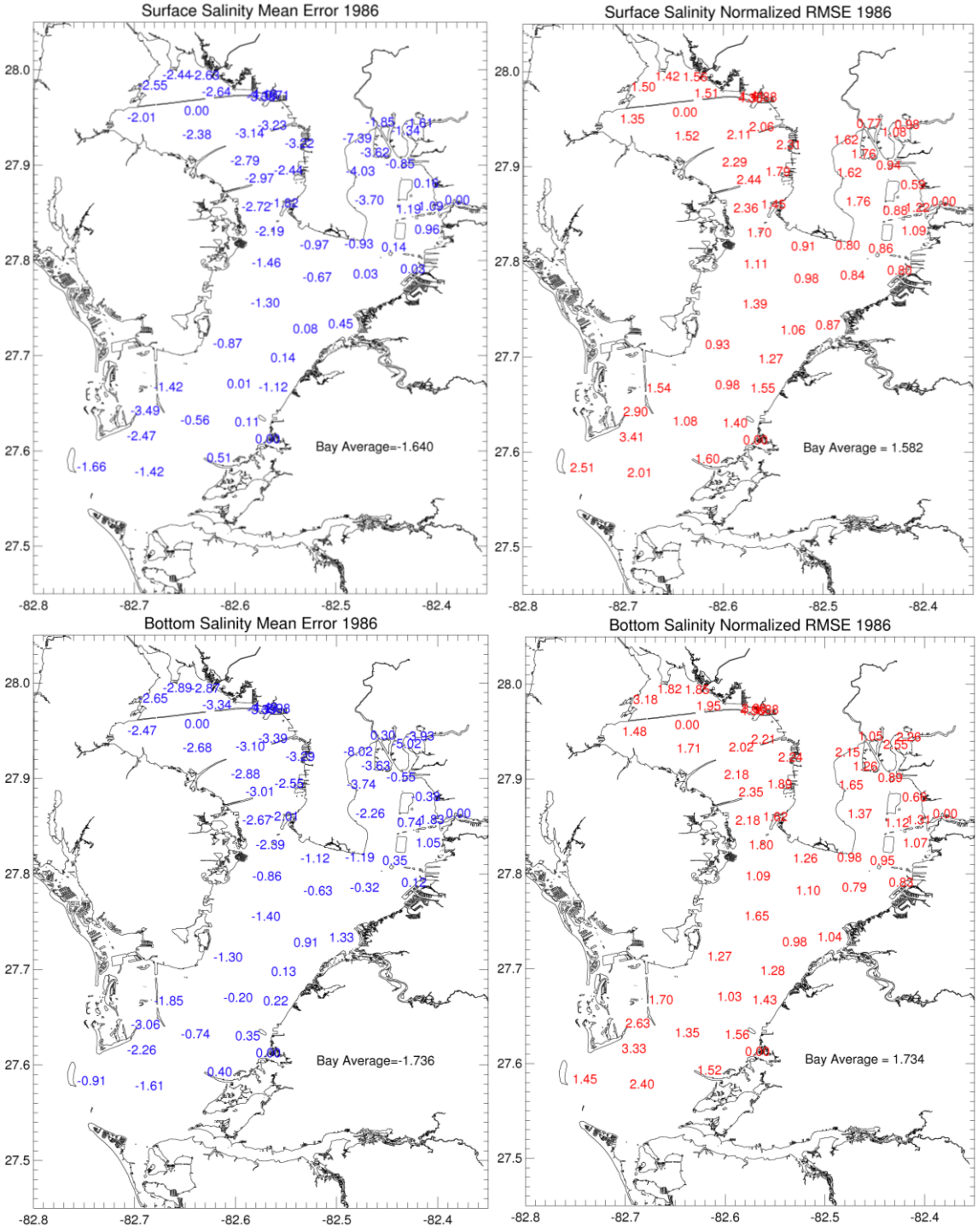

Figure A25. Same as figure A15 for 1986.

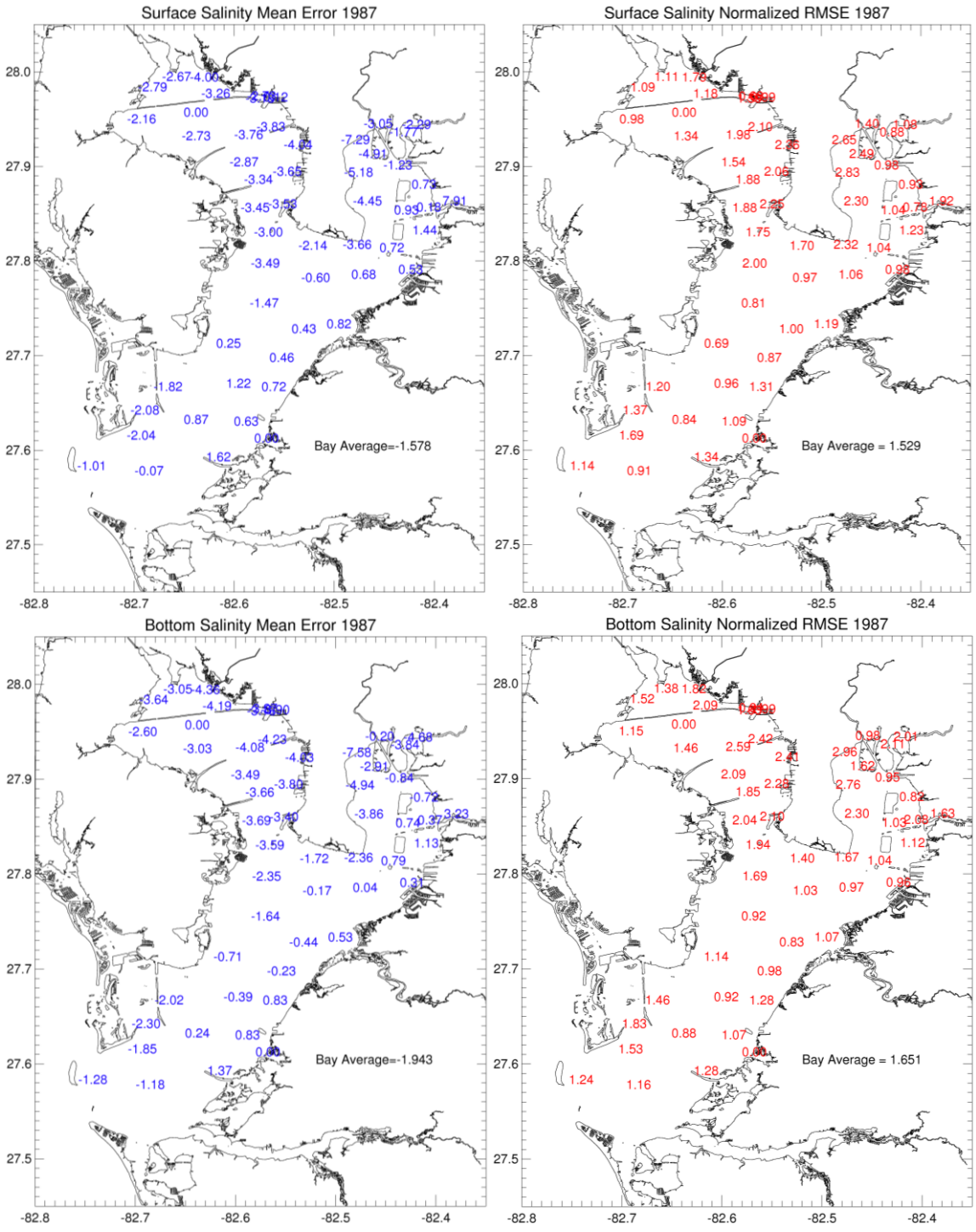

Figure A26. Same as figure A15 for 1987.

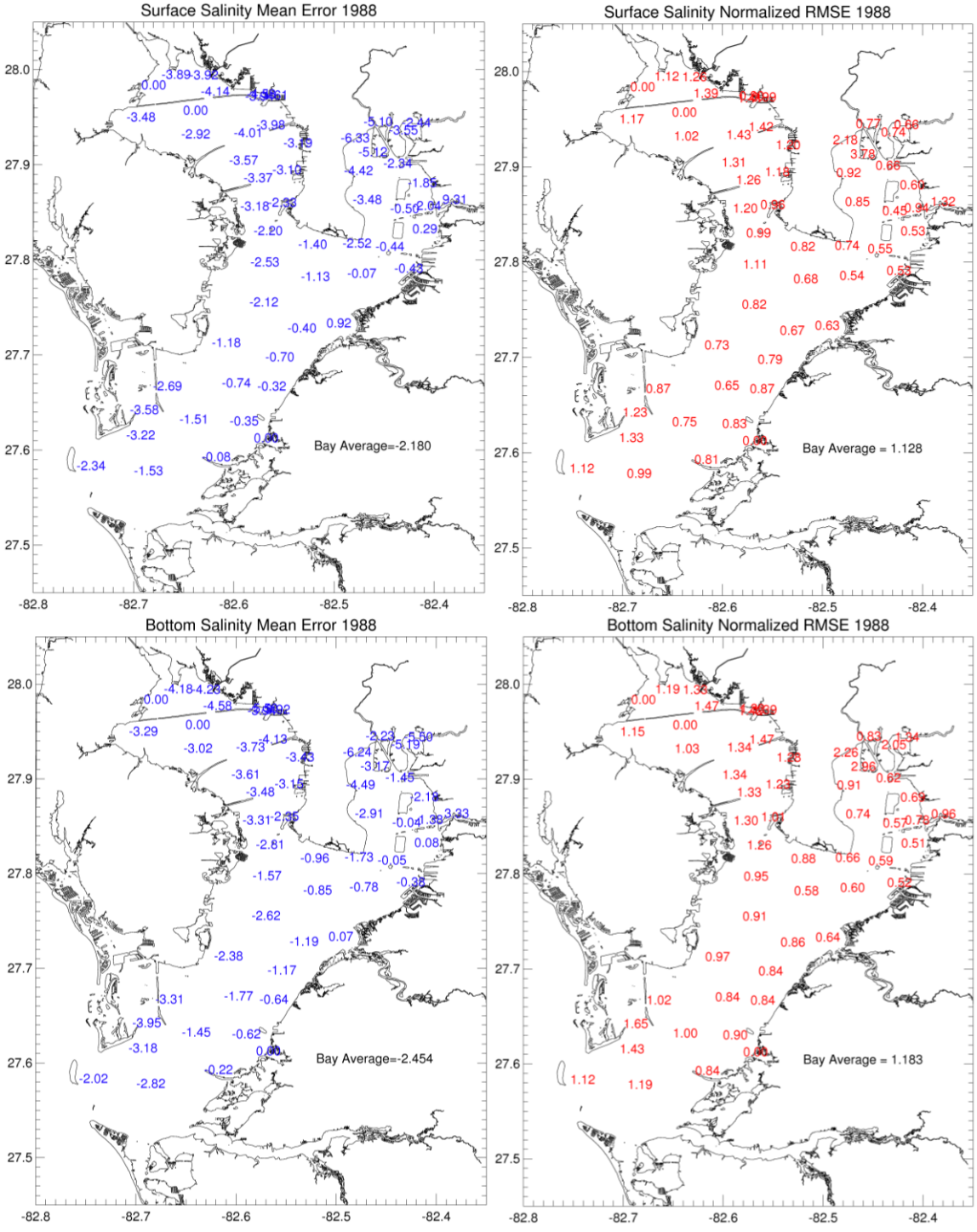

Figure A27. Same as figure A15 for 1988.

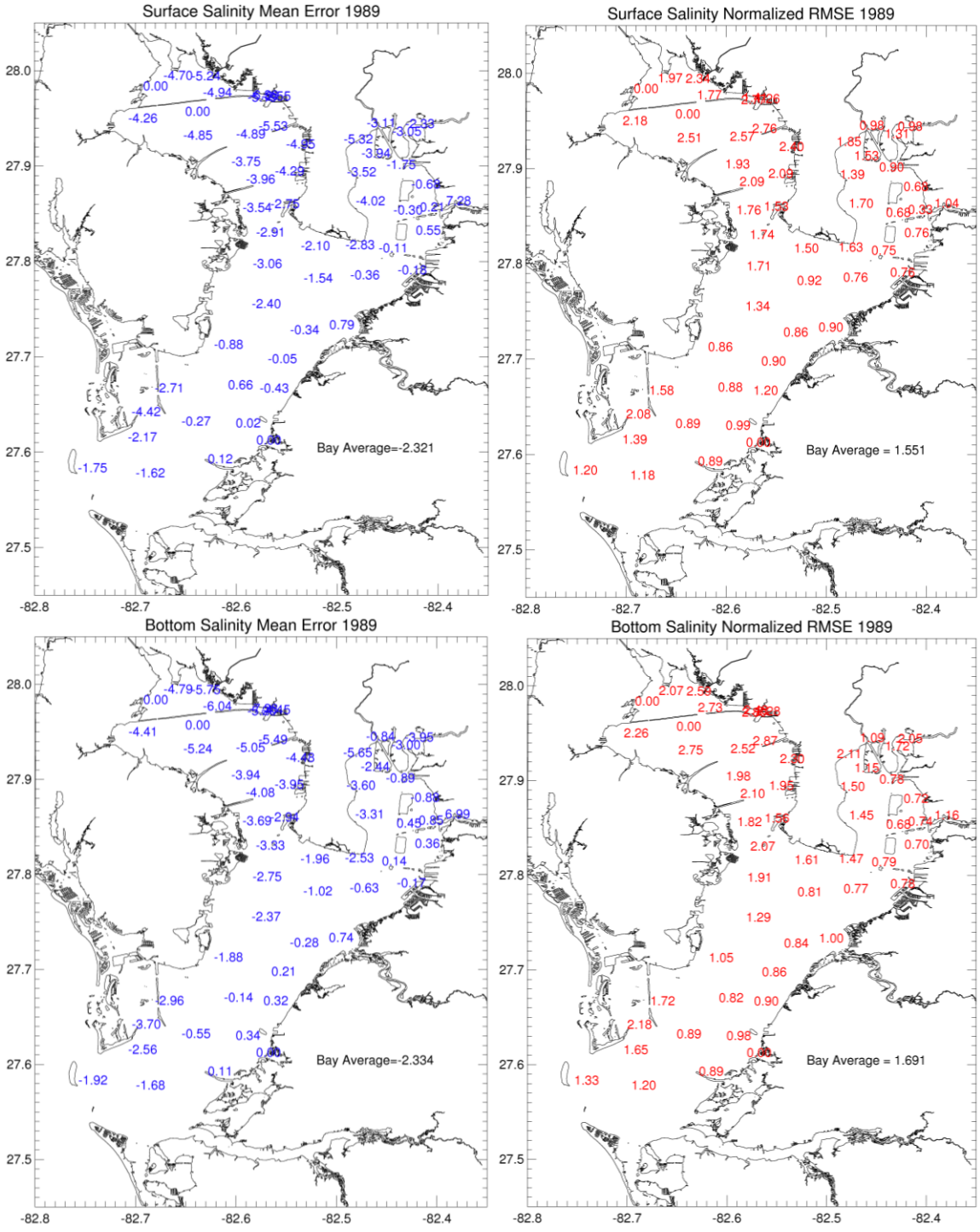

Figure A28. Same as figure A15 for 1989.

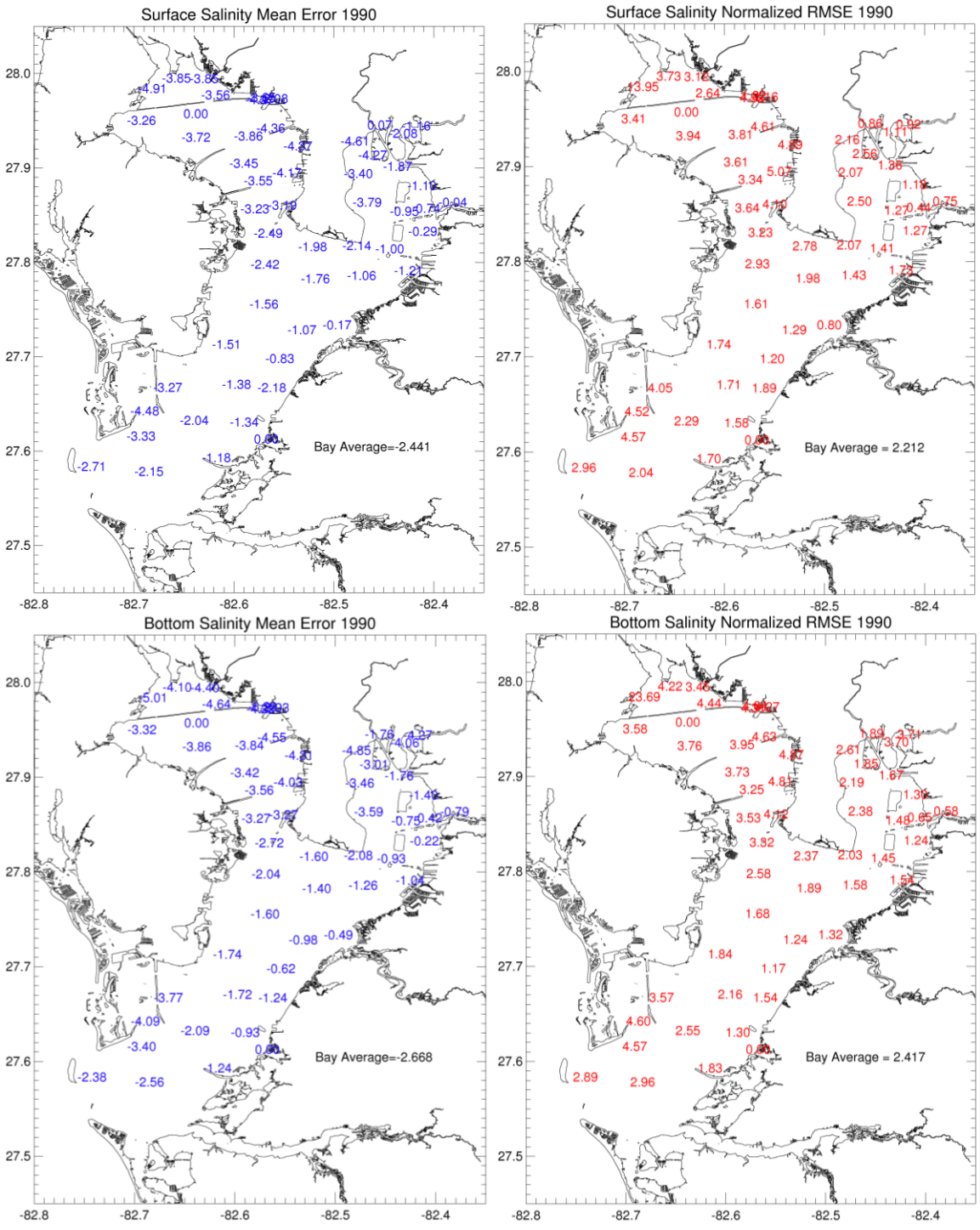

Figure A29. Same as figure A15 for 1990.

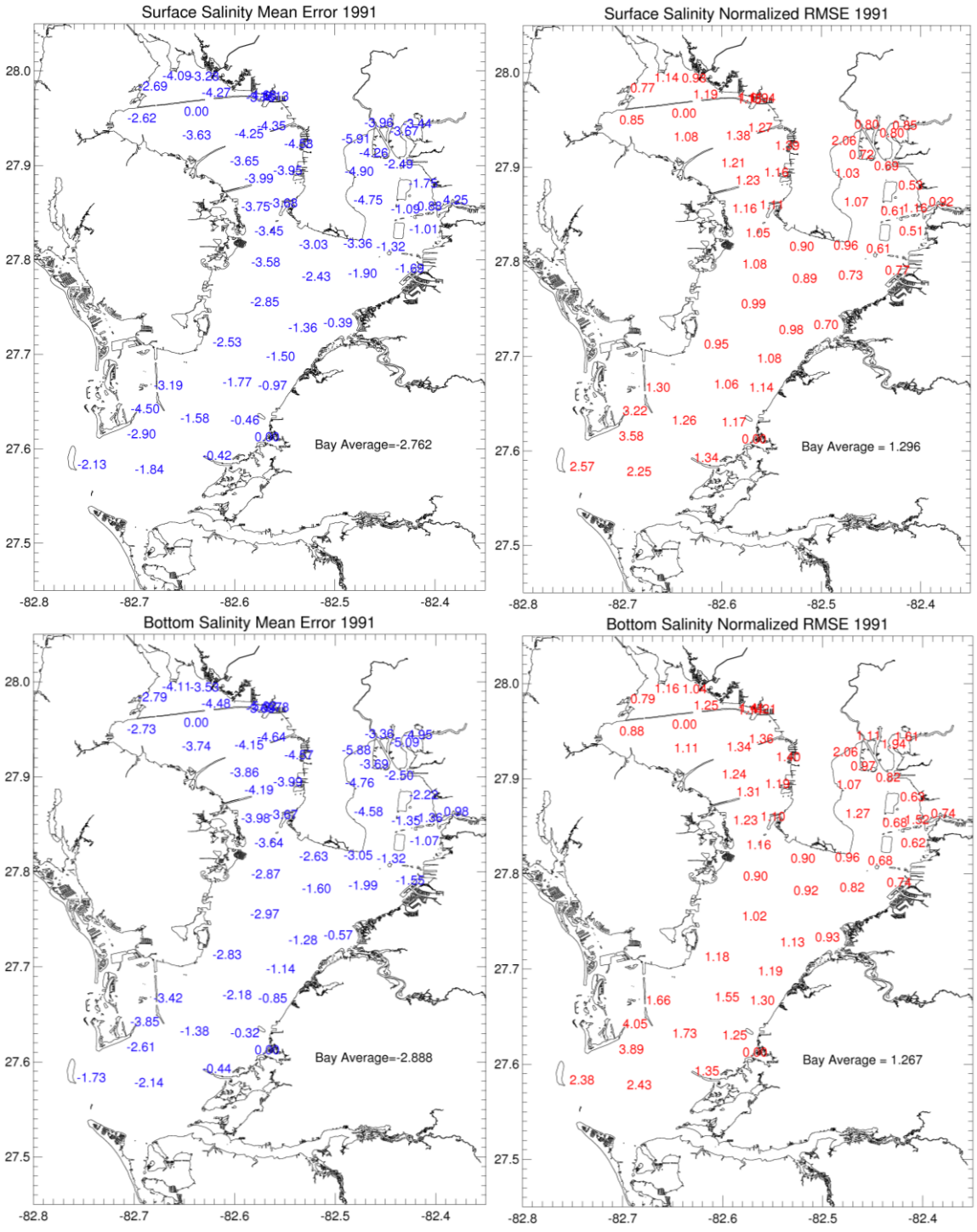

Figure A30. Same as figure A15 for 1991.

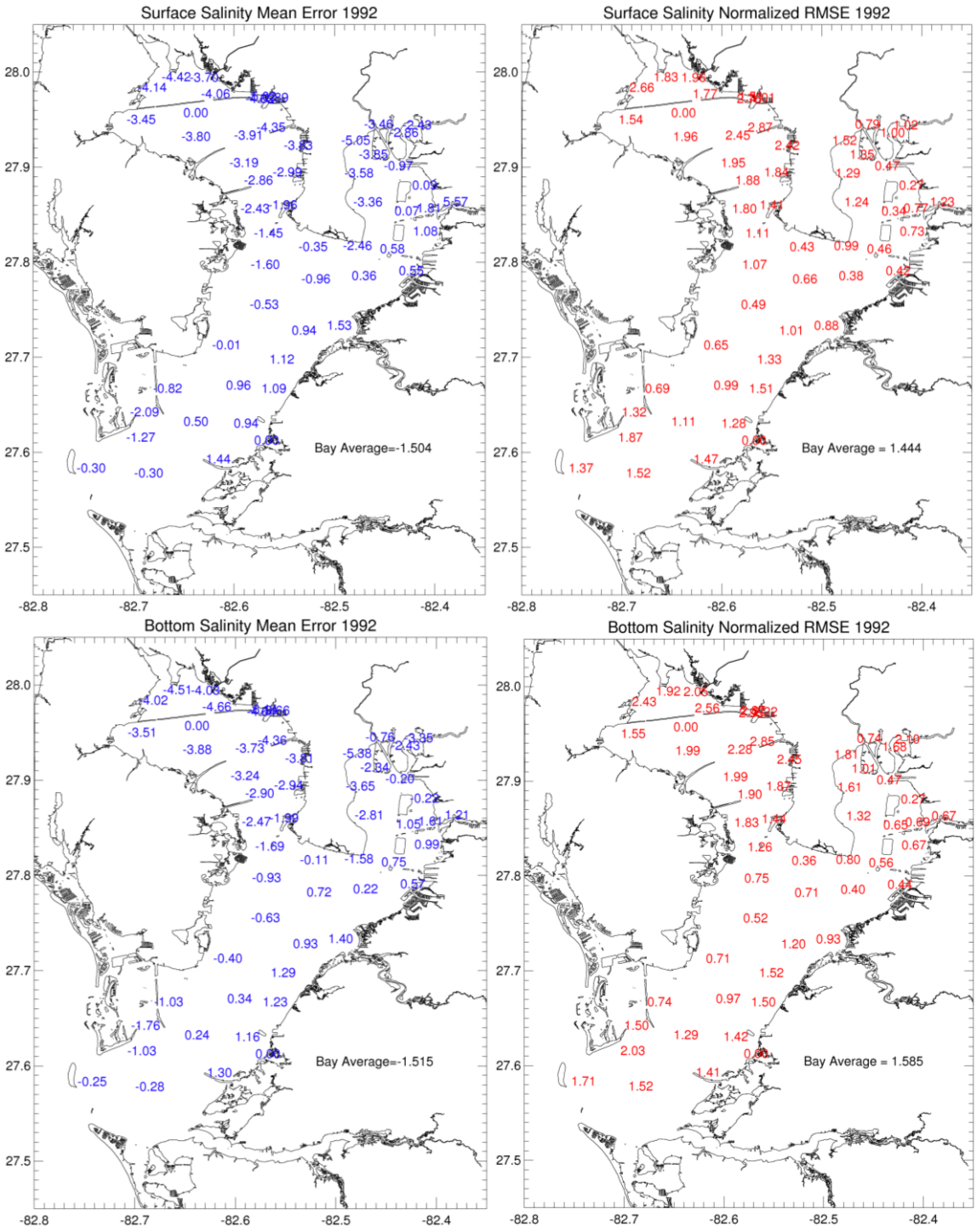

Figure A31. Same as figure A15 for 1992.

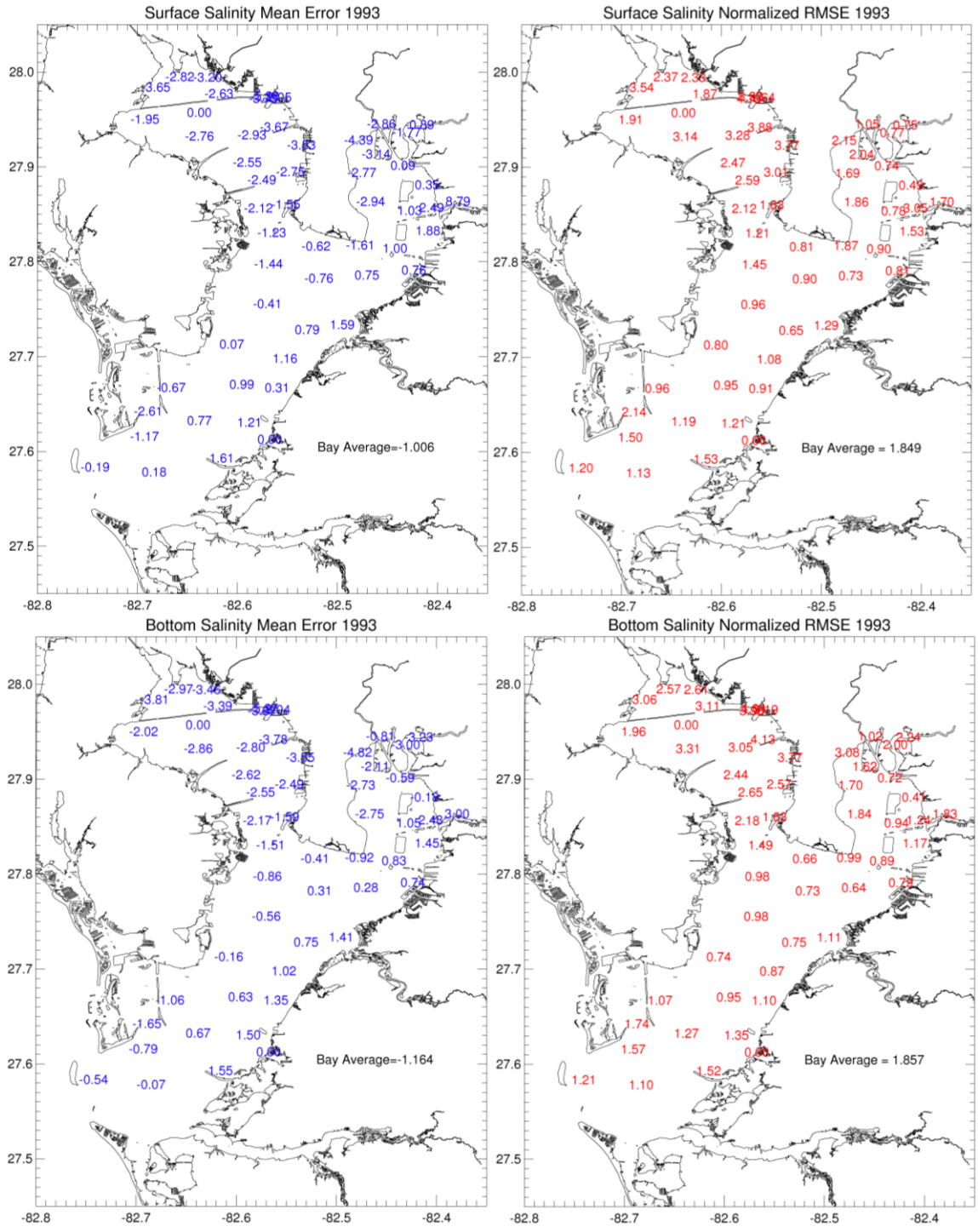

Figure A32. Same as figure A15 for 1993.

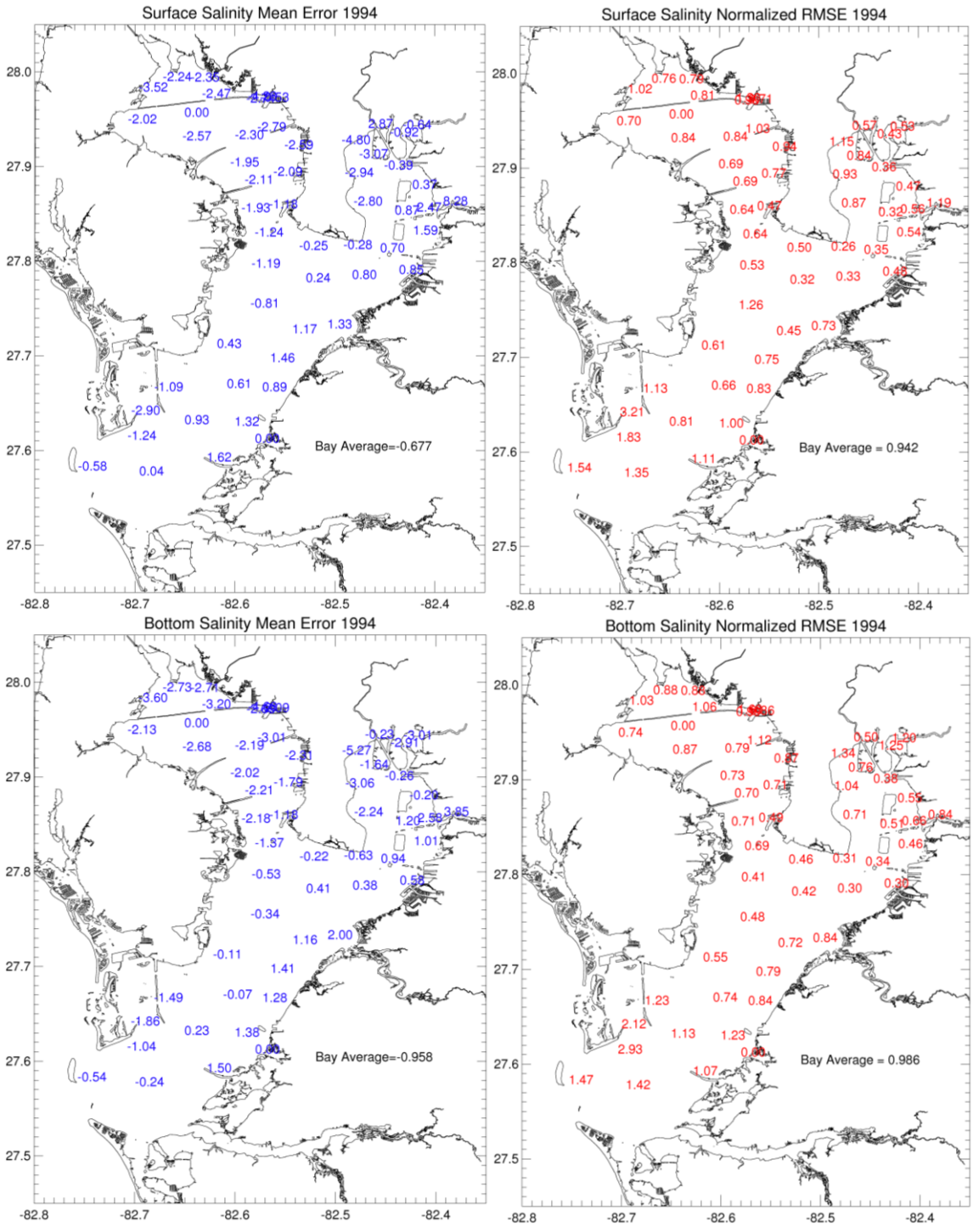

Figure A33. Same as figure A15 for 1994.

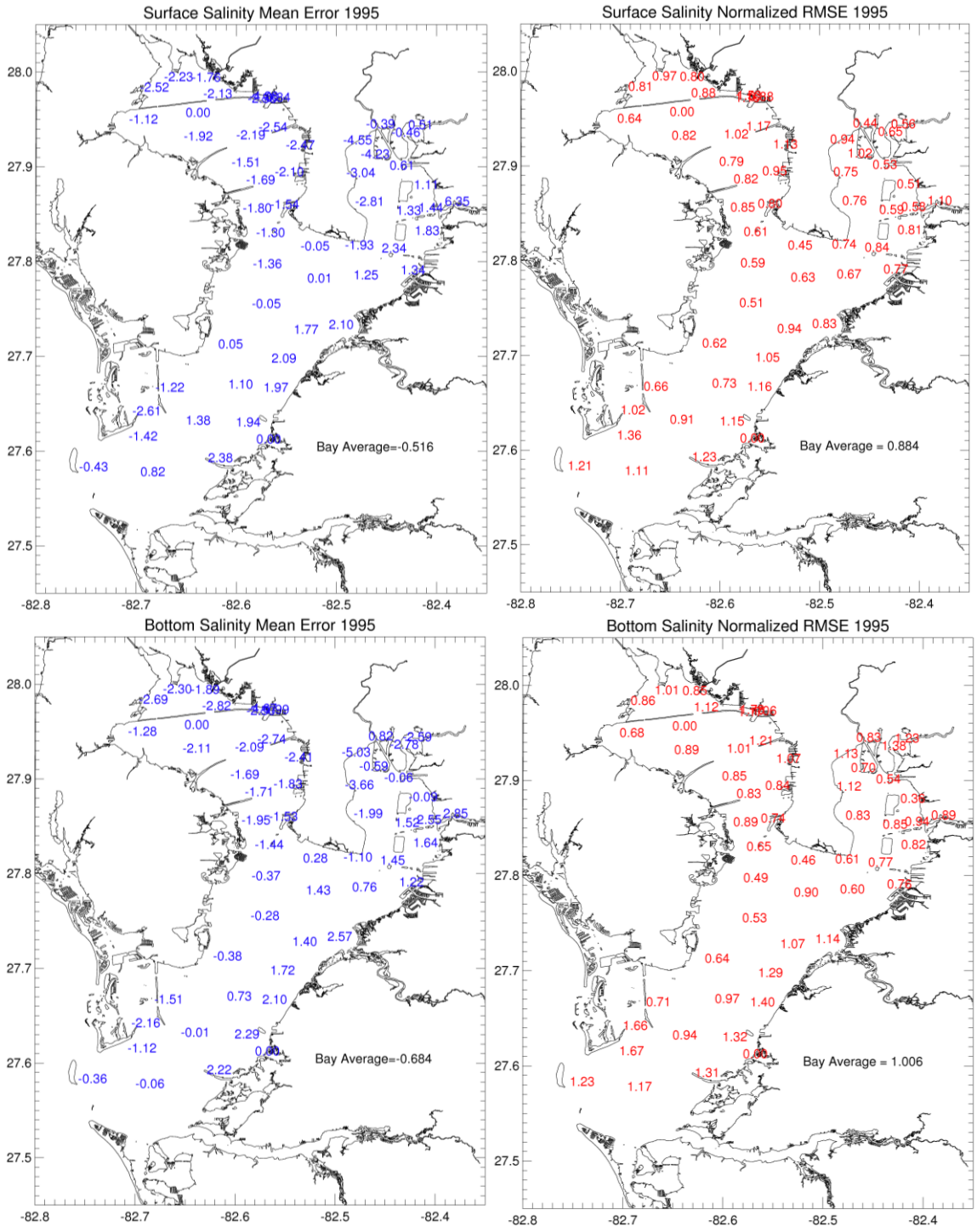

Figure A34. Same as figure A15 for 1995.

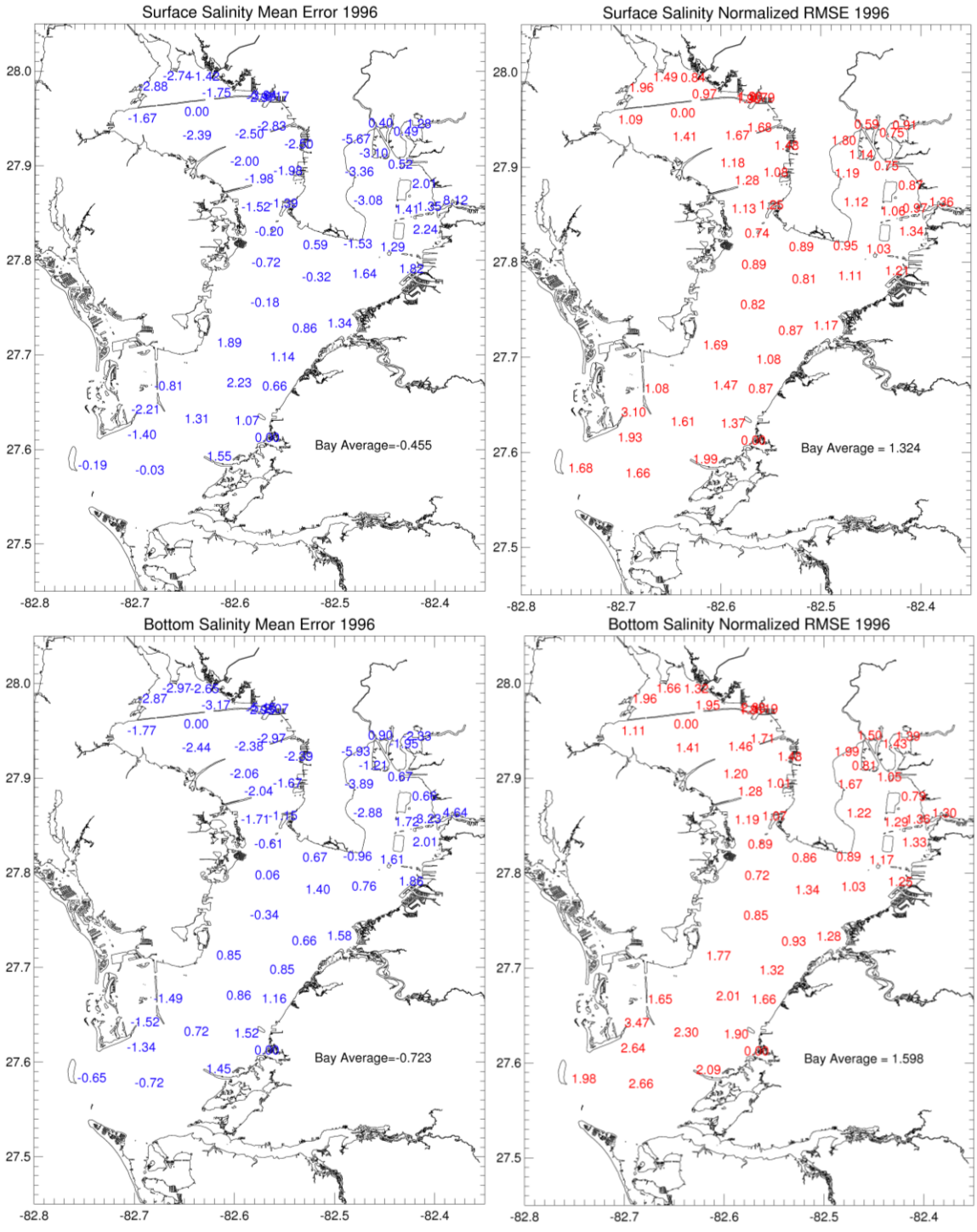

Figure A35. Same as figure A15 for 1996.

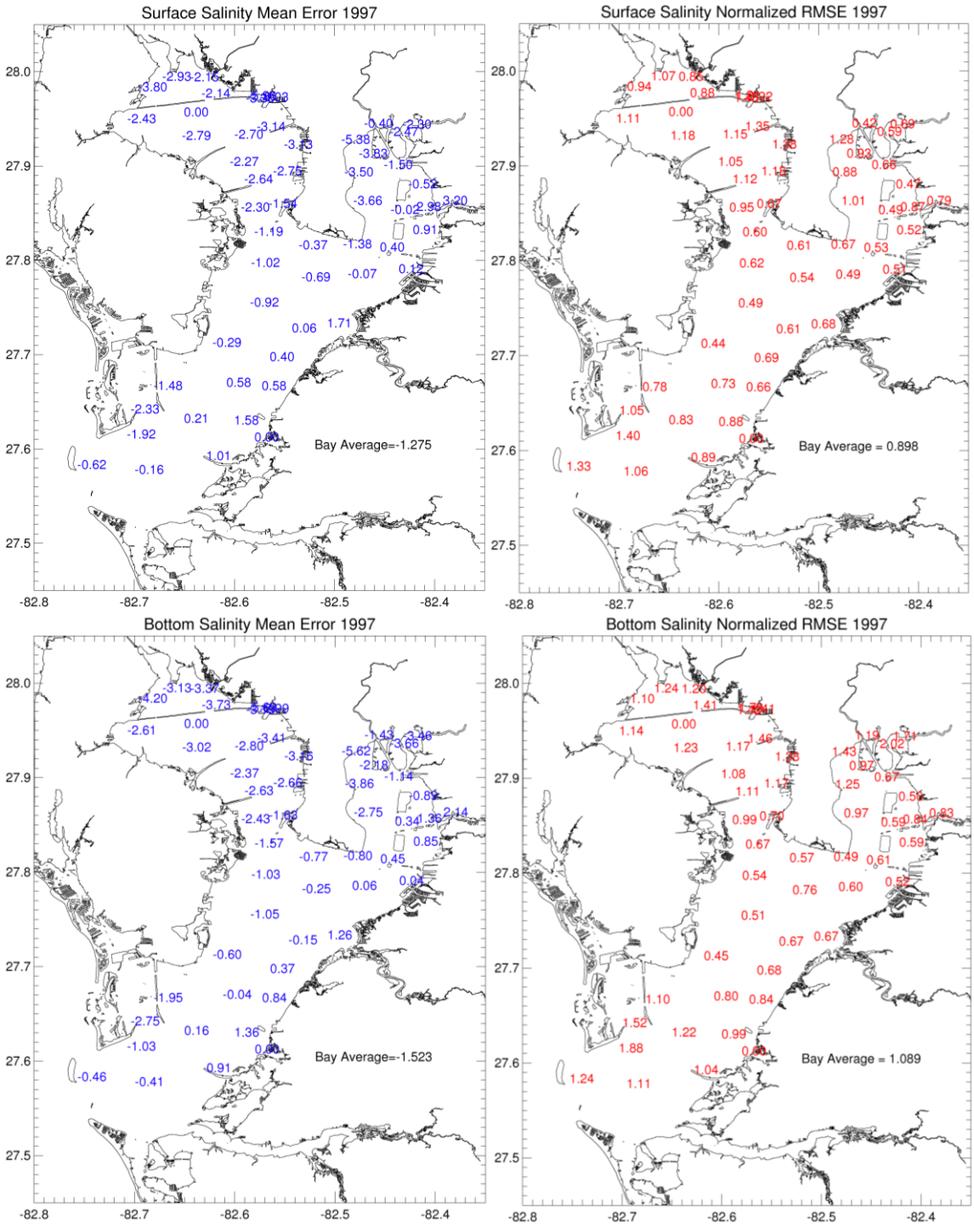

Figure A36. Same as figure A15 for 1997.

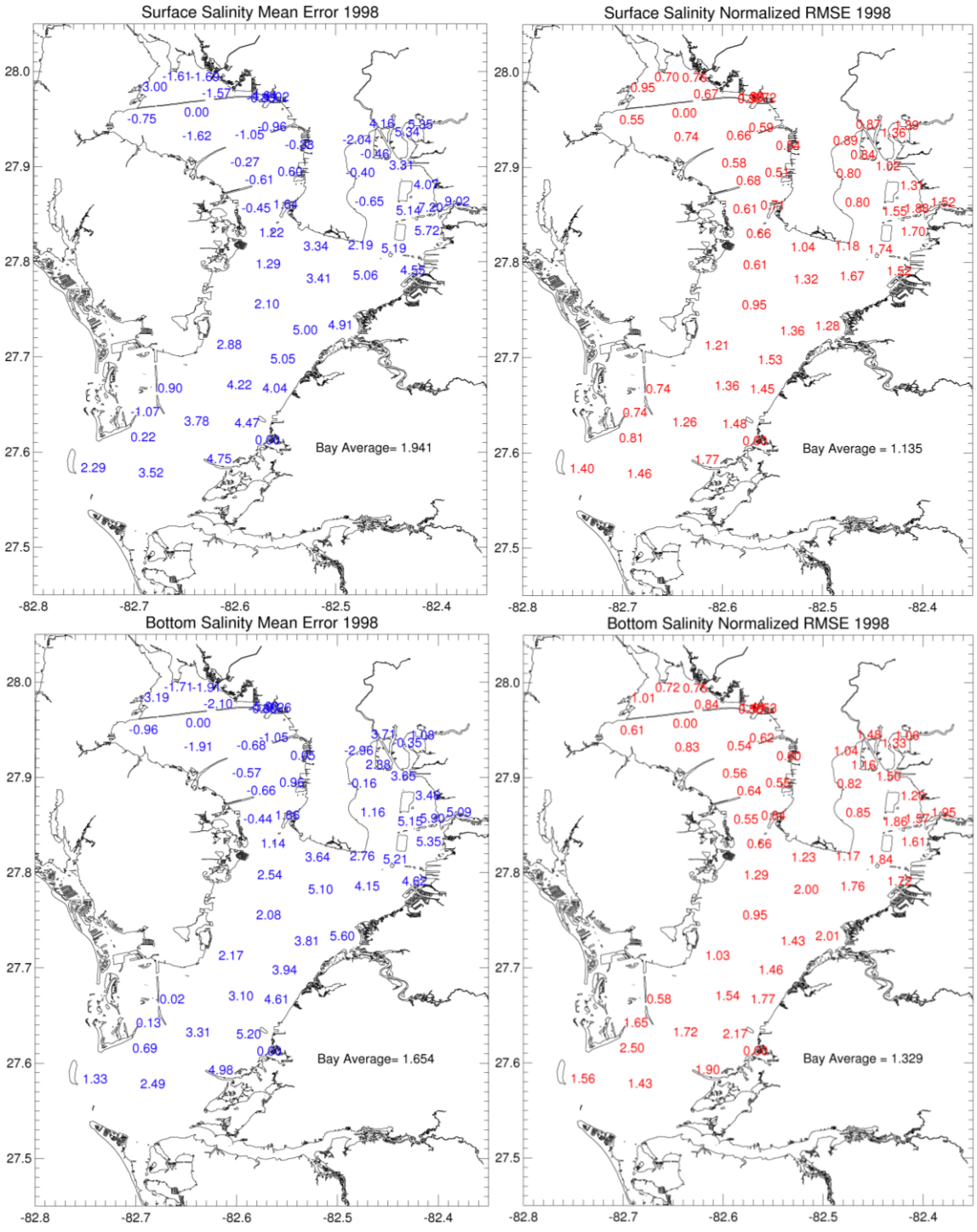

Figure A37. Same as figure A15 for 1998.

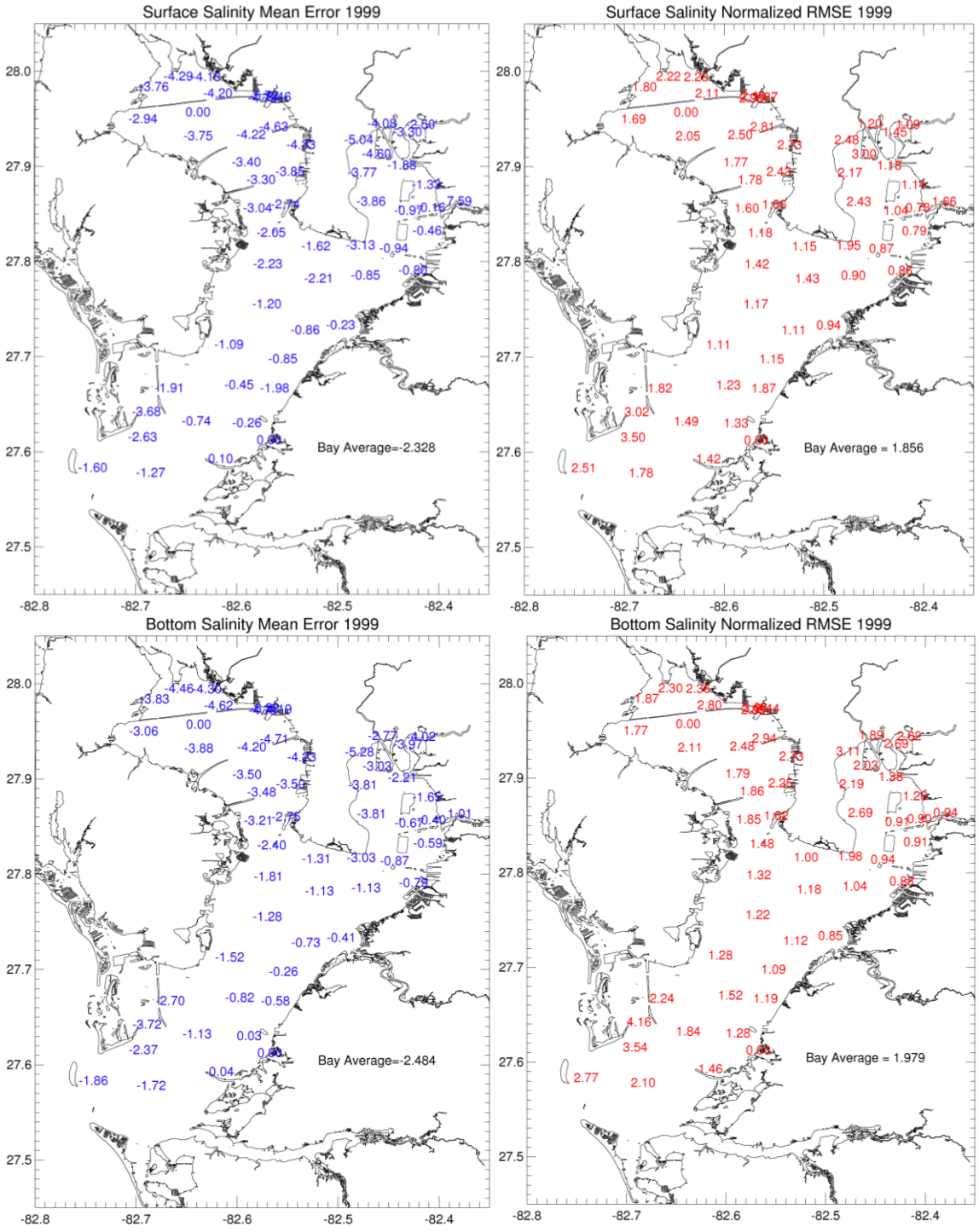

Figure A38. Same as figure A15 for 1999.

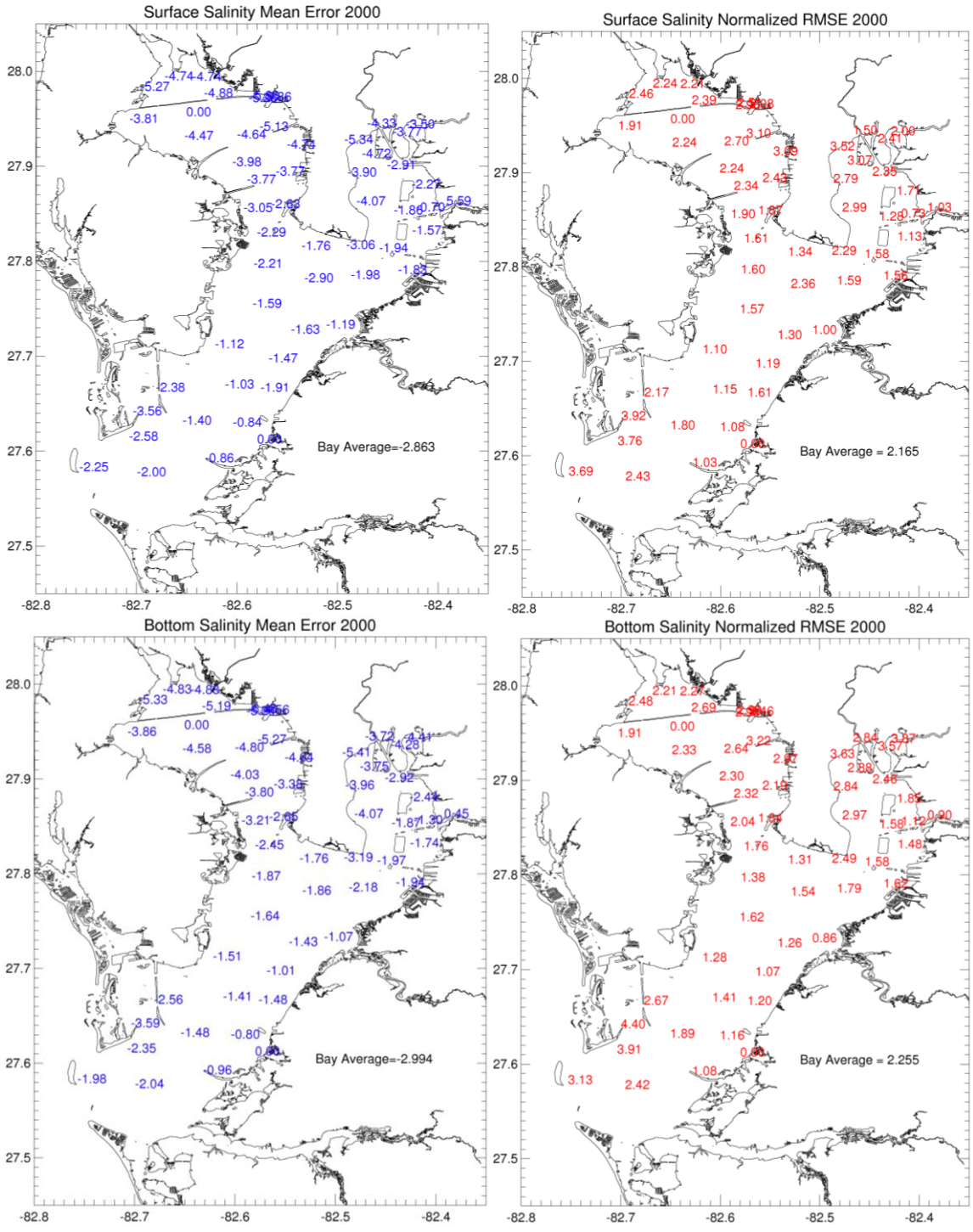

Figure A39. Same as figure A15 for 2000.

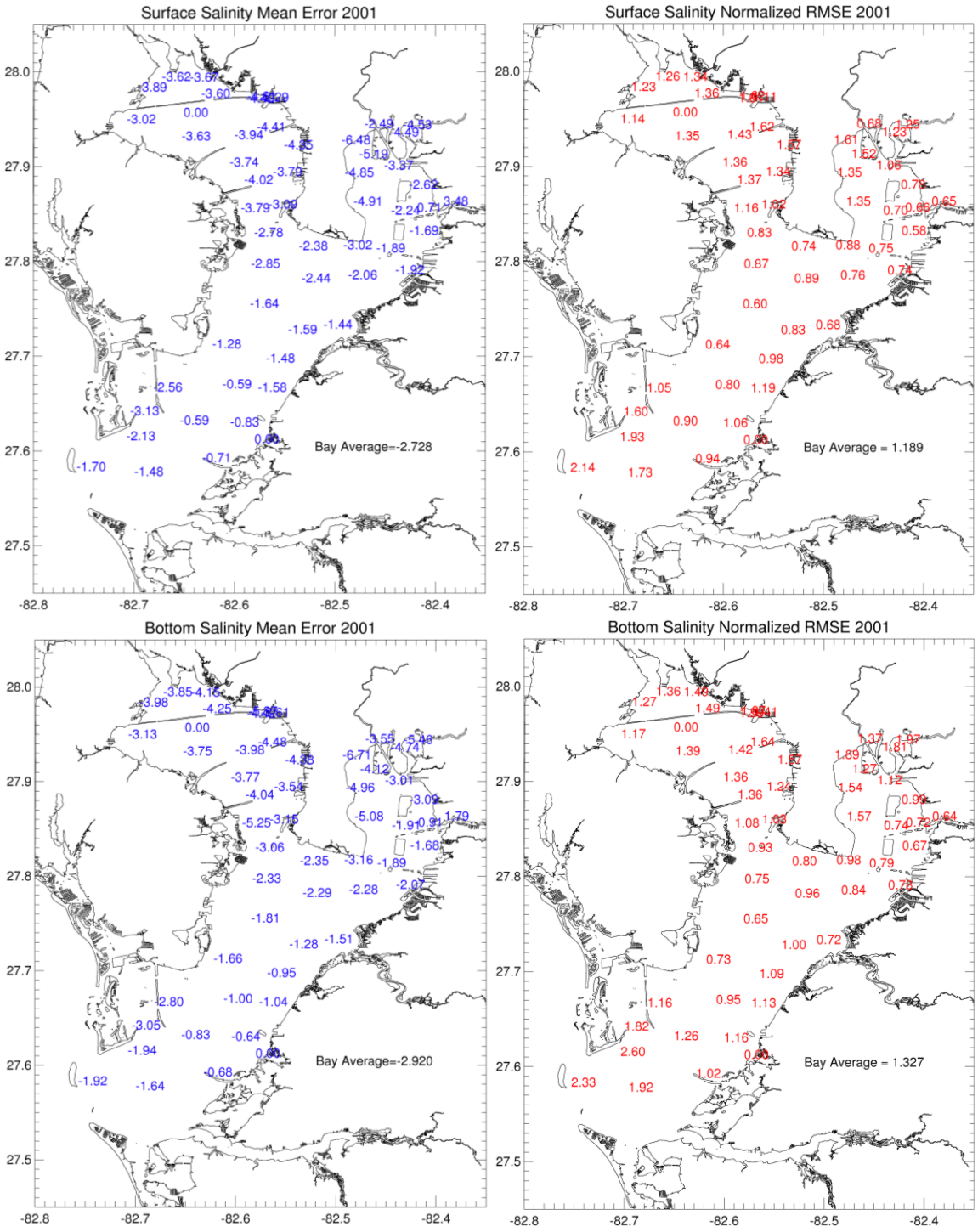

Figure A40. Same as figure A15 for 2001.

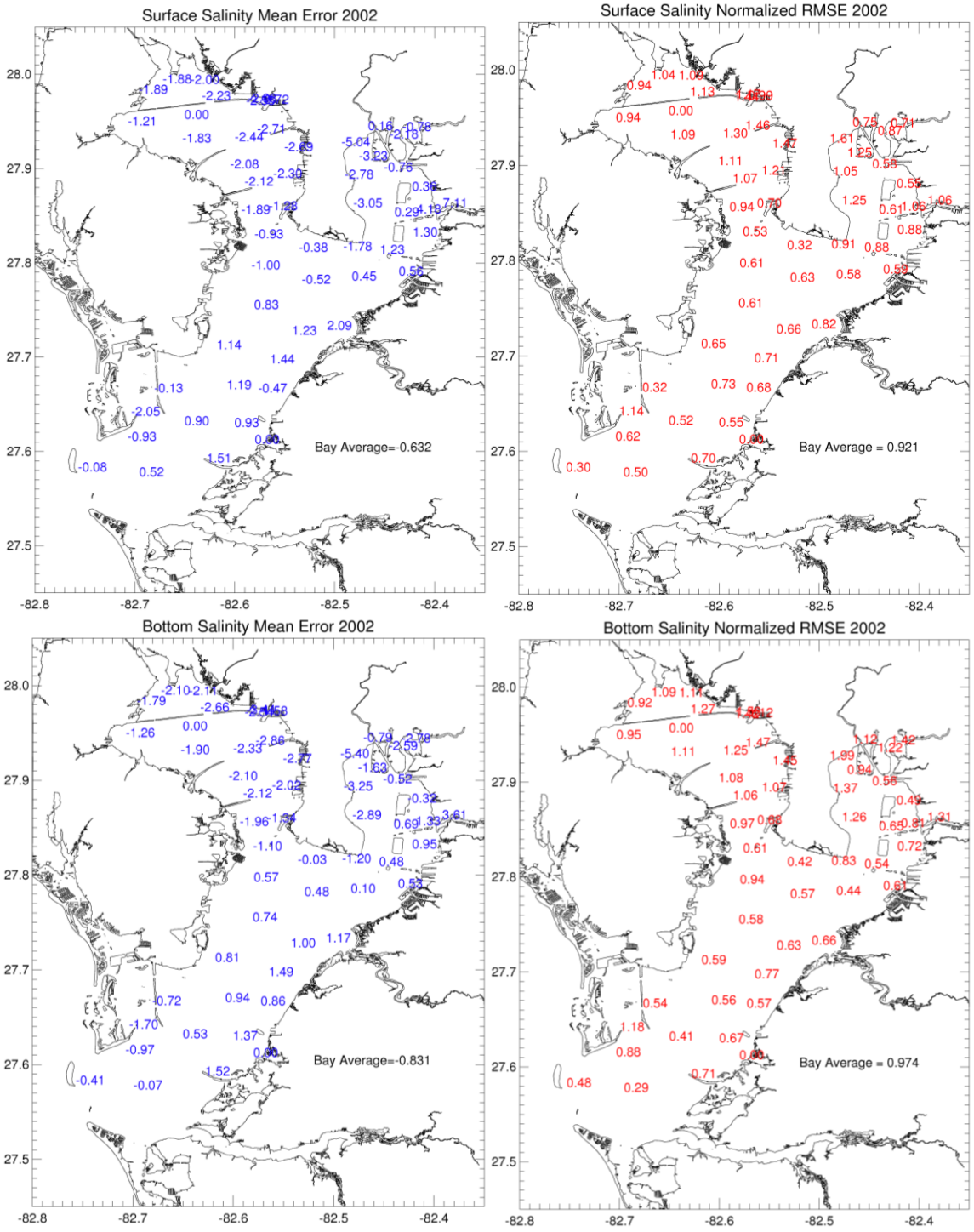

Figure A41. Same as figure A15 for 2002.

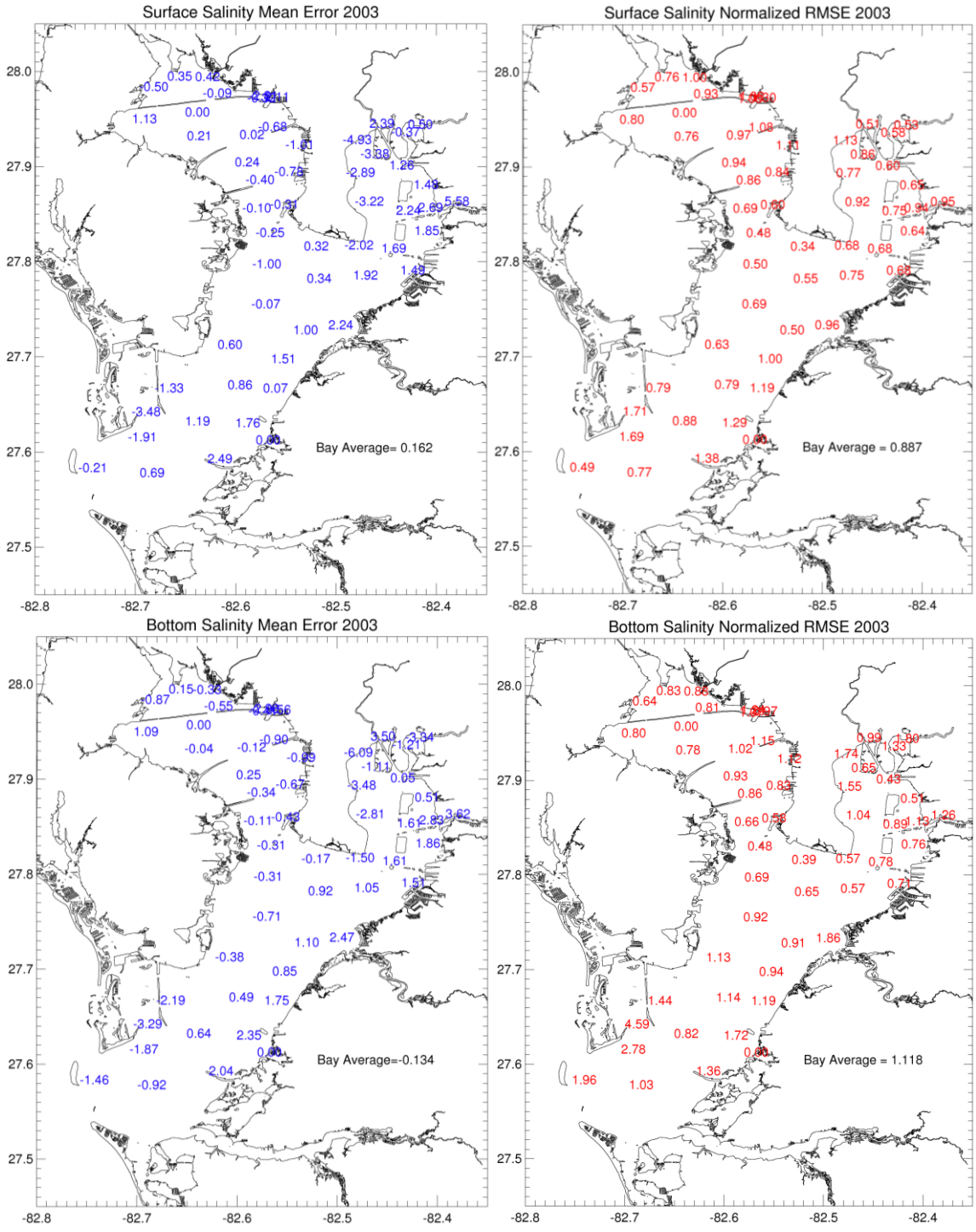

Figure A42. Same as figure A15 for 2003.

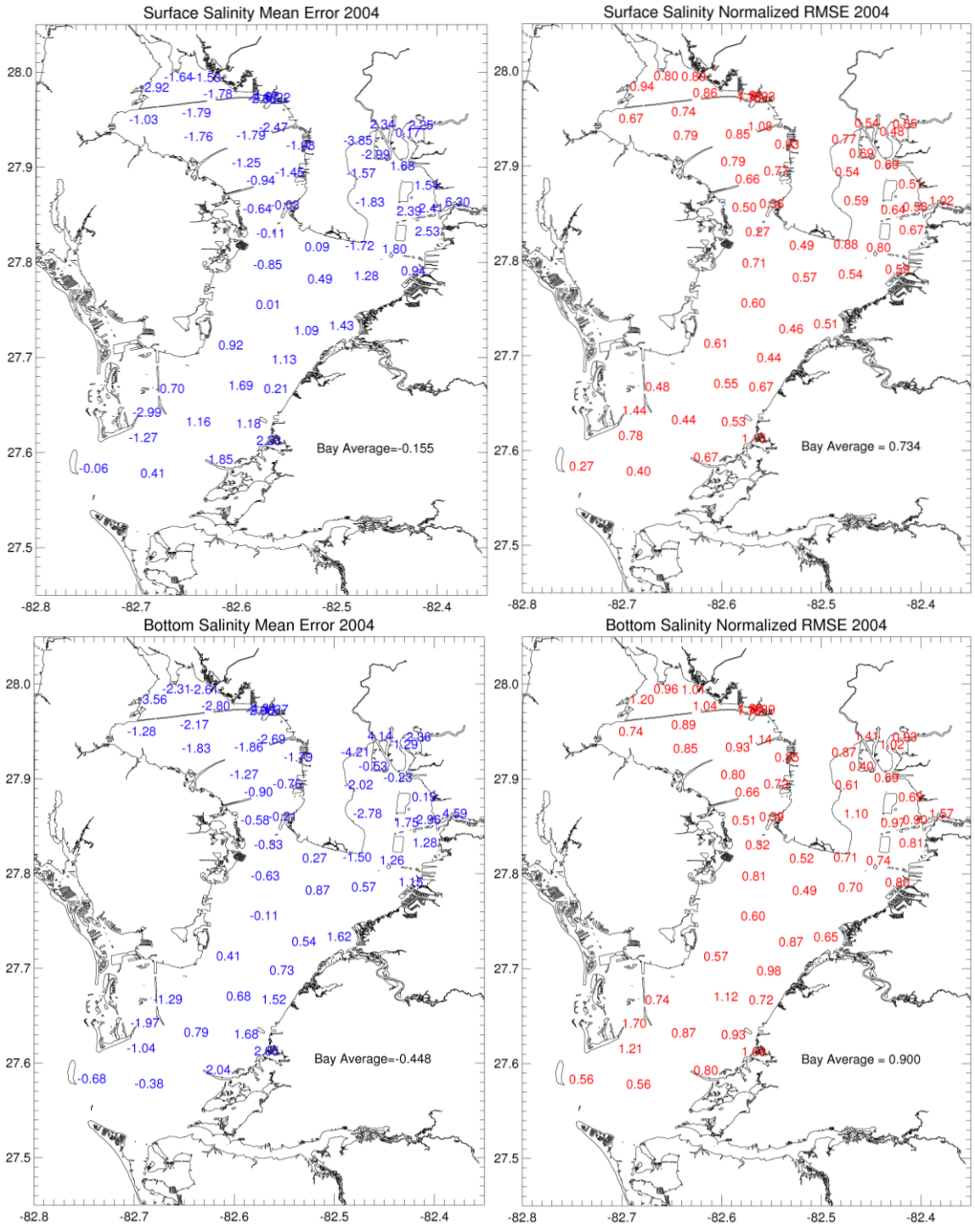

Figure A43. Same as figure A15 for 2004.

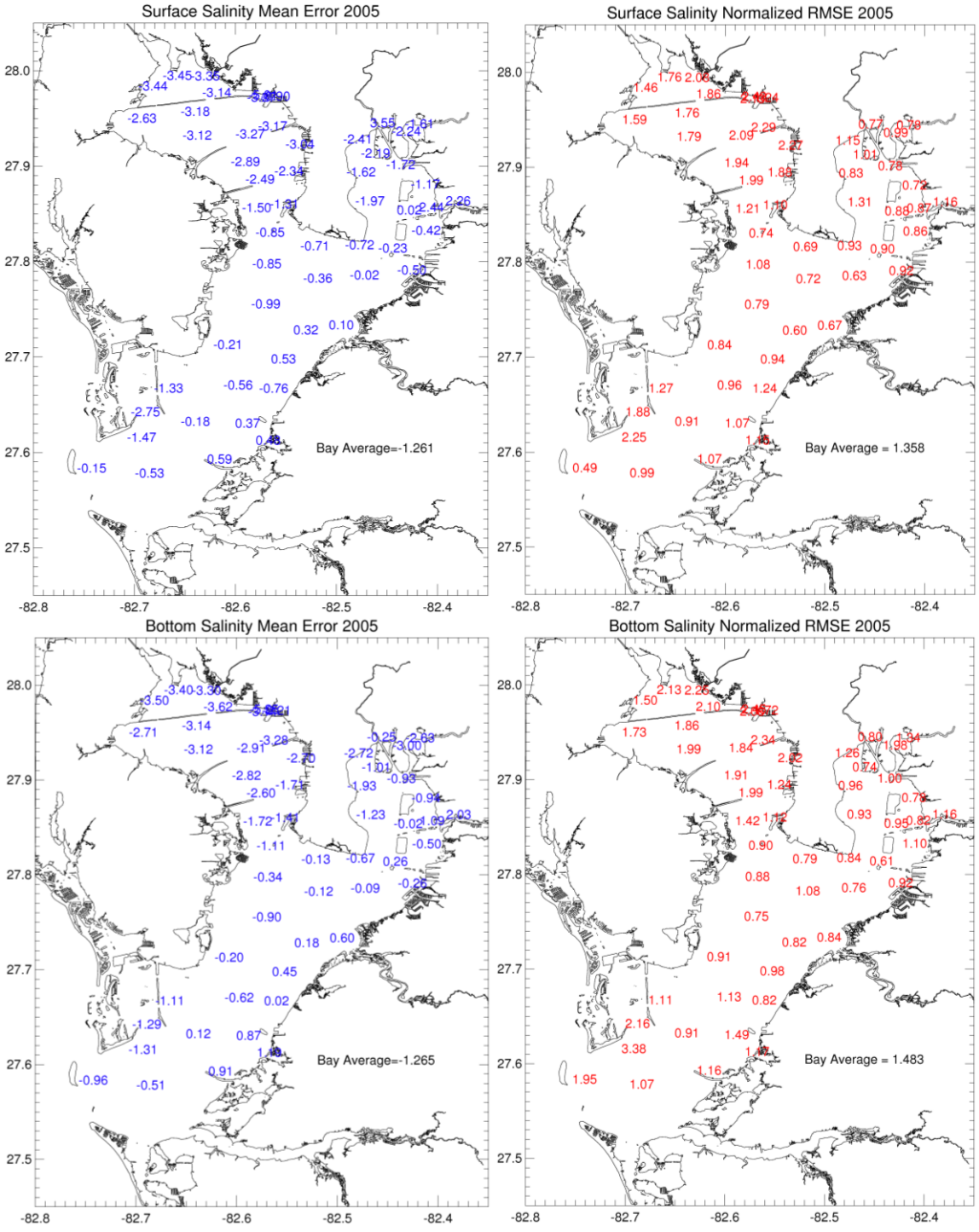

Figure A44. Same as figure A15 for 2005.

Appendix C: Yearly comparison of observational and model elevation

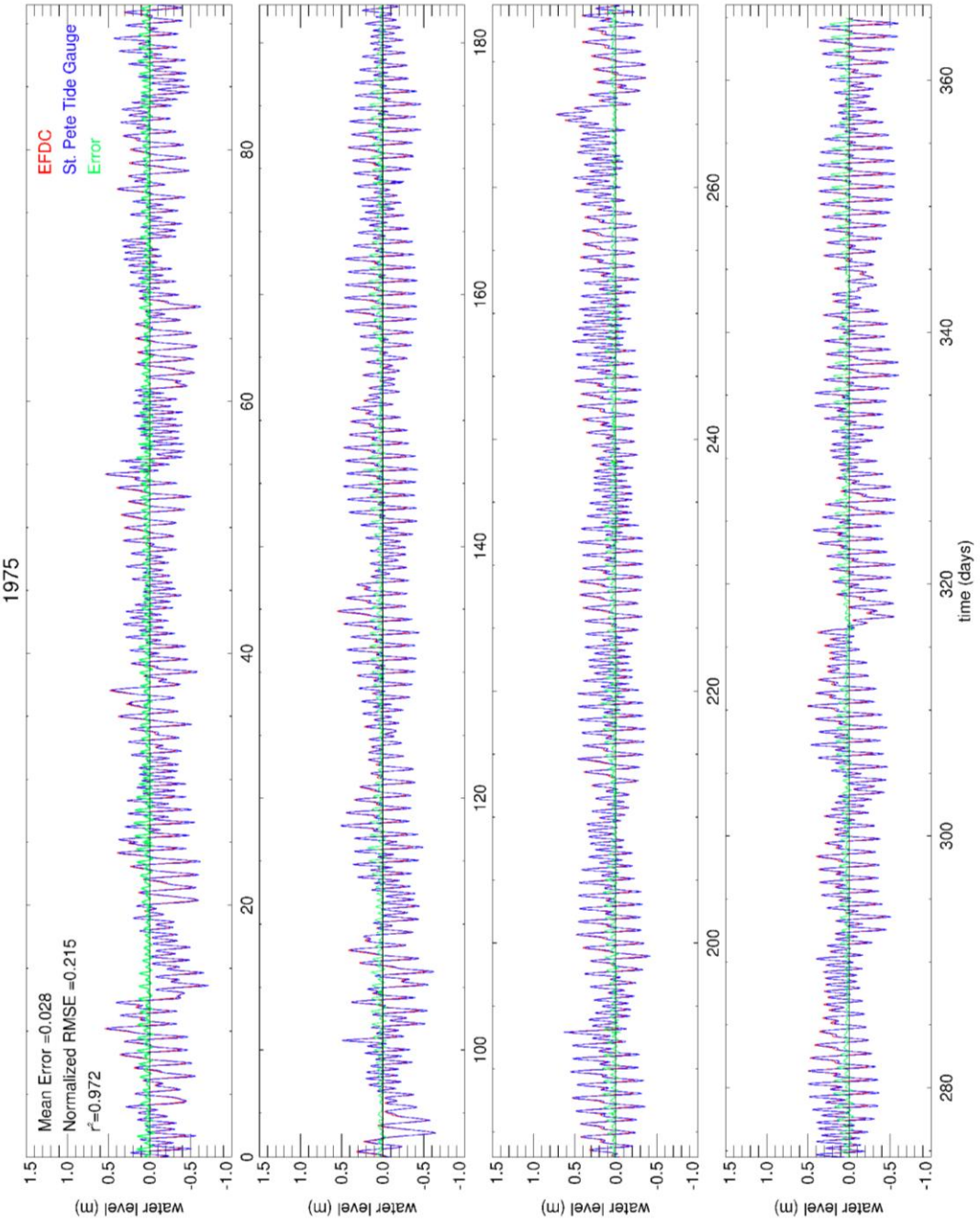

Figure A45. Observational elevation (blue) versus model elevation (red) for 1975. Difference is shown in green.

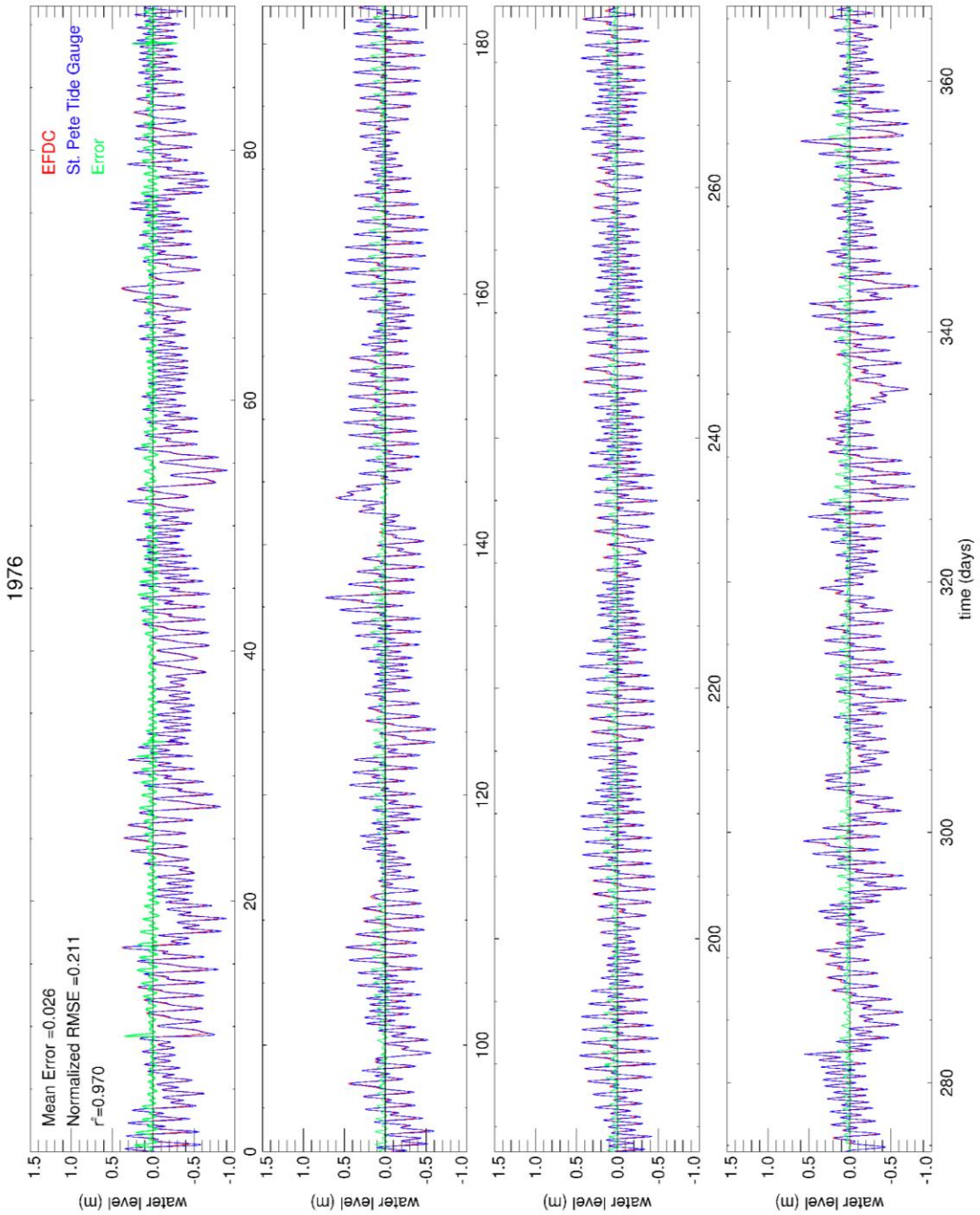

Figure A46. Same as figure A45 for 1976.

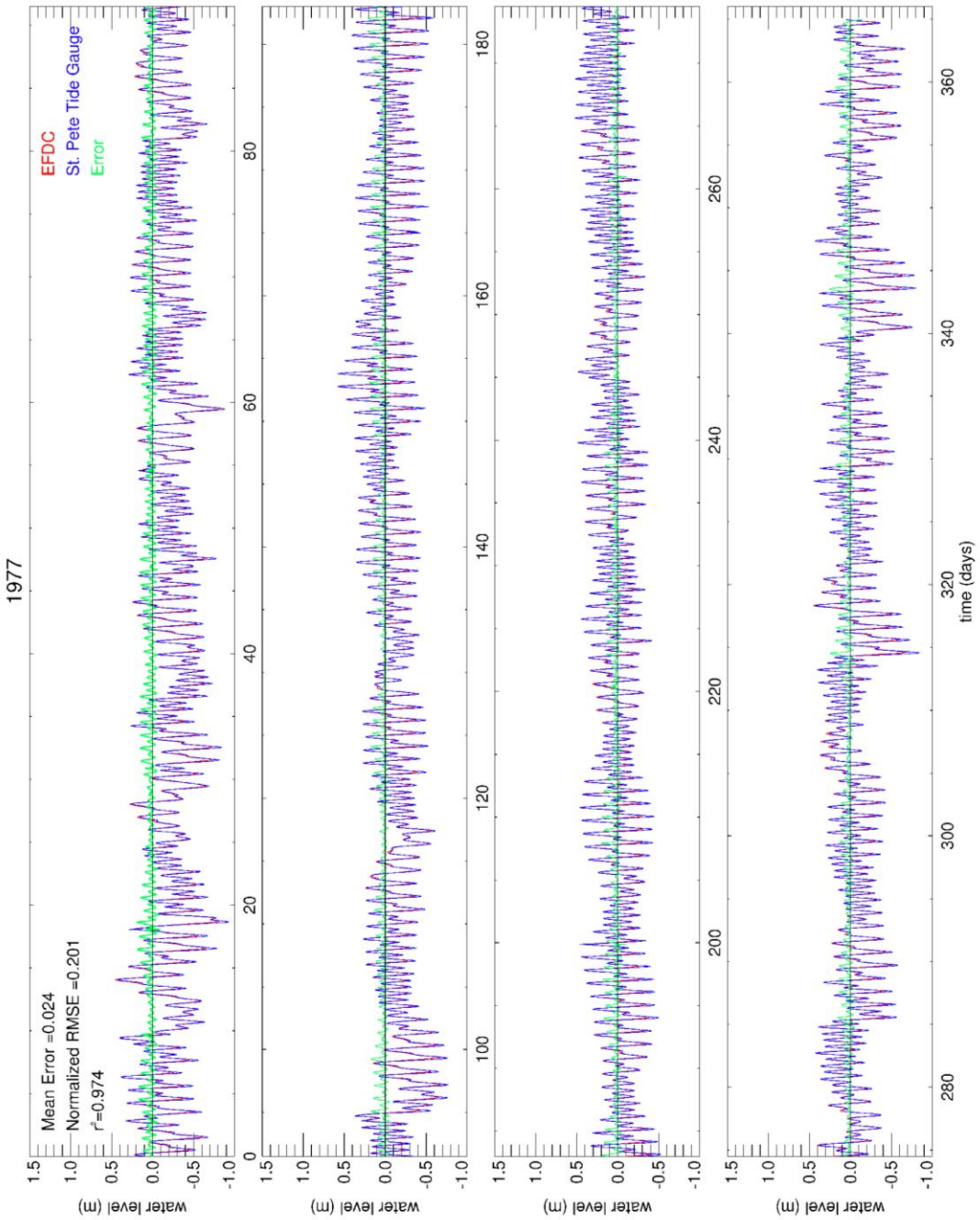

Figure A47. Same as figure A45 for 1977.

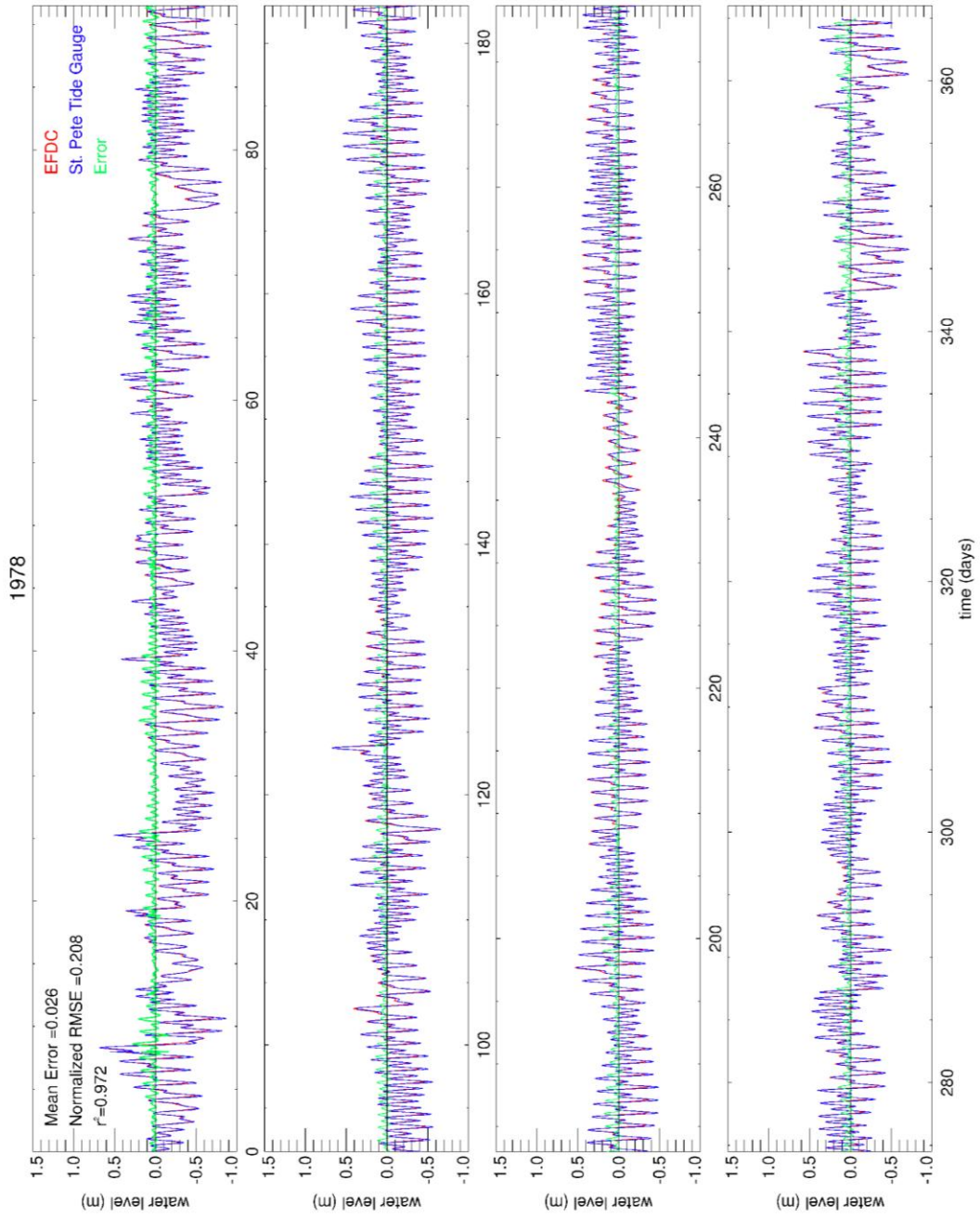

Figure A48. Same as figure A45 for 1978.

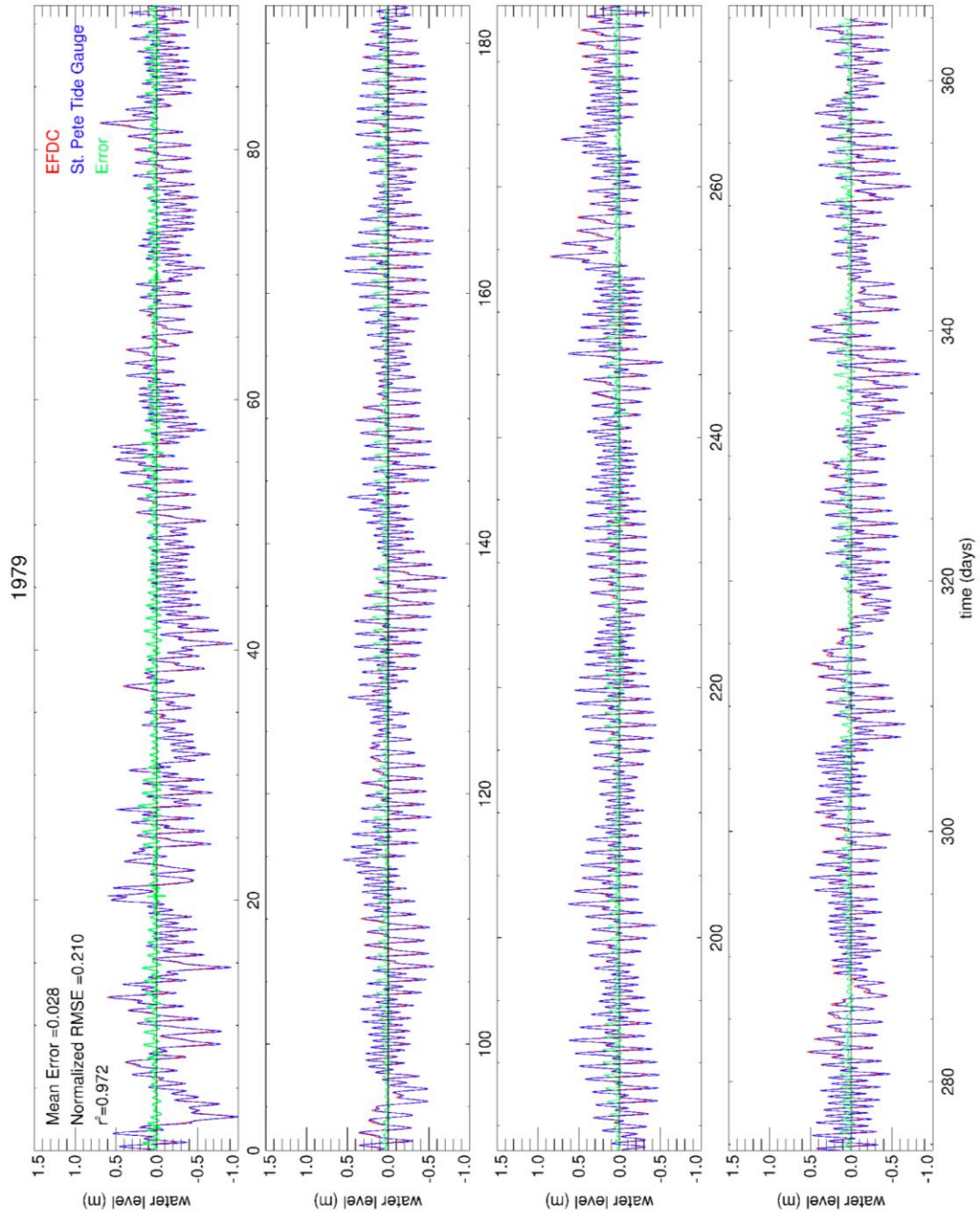

Figure A49. Same as figure A45 for 1979.

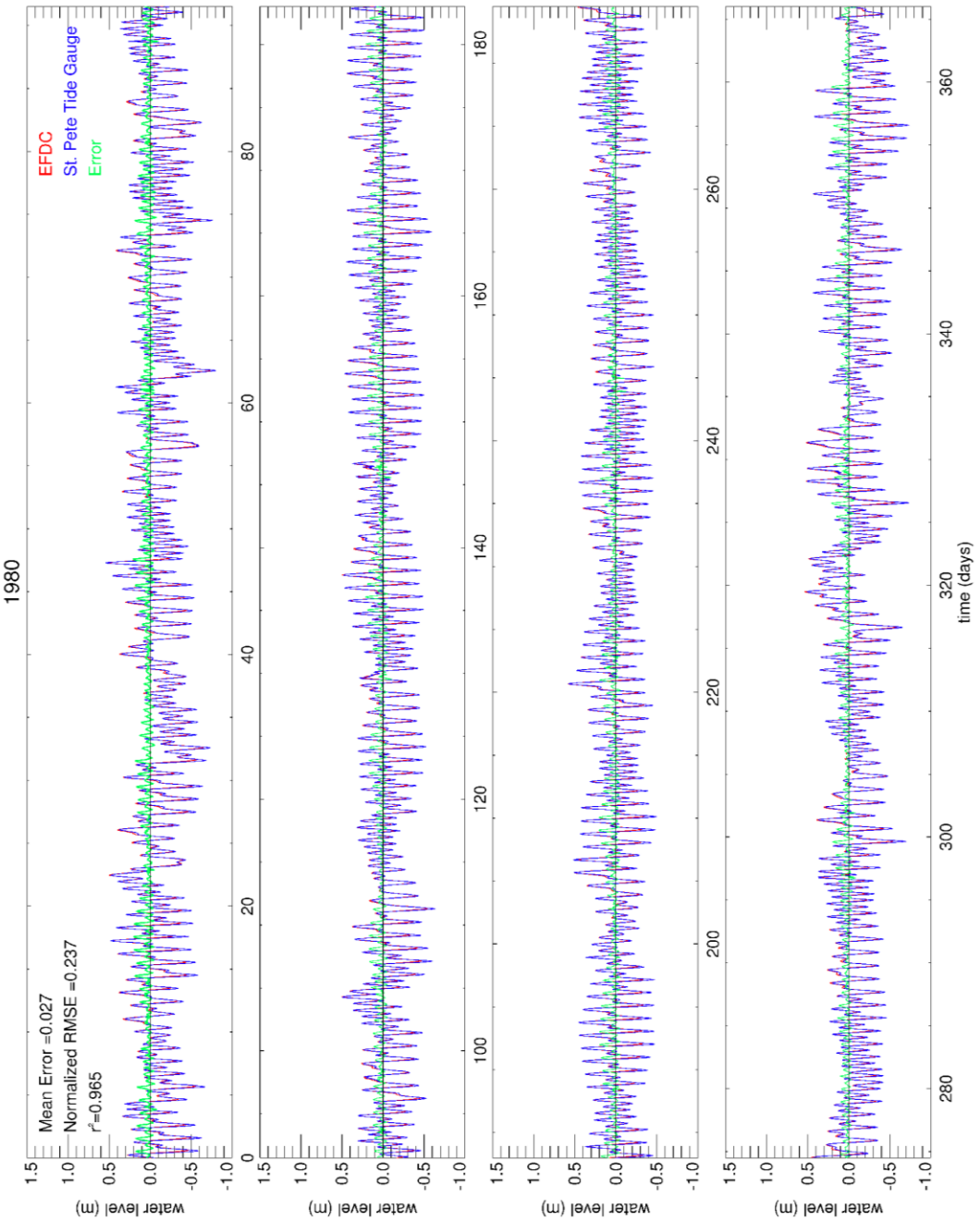

Figure A50. Same as figure A45 for 1980.

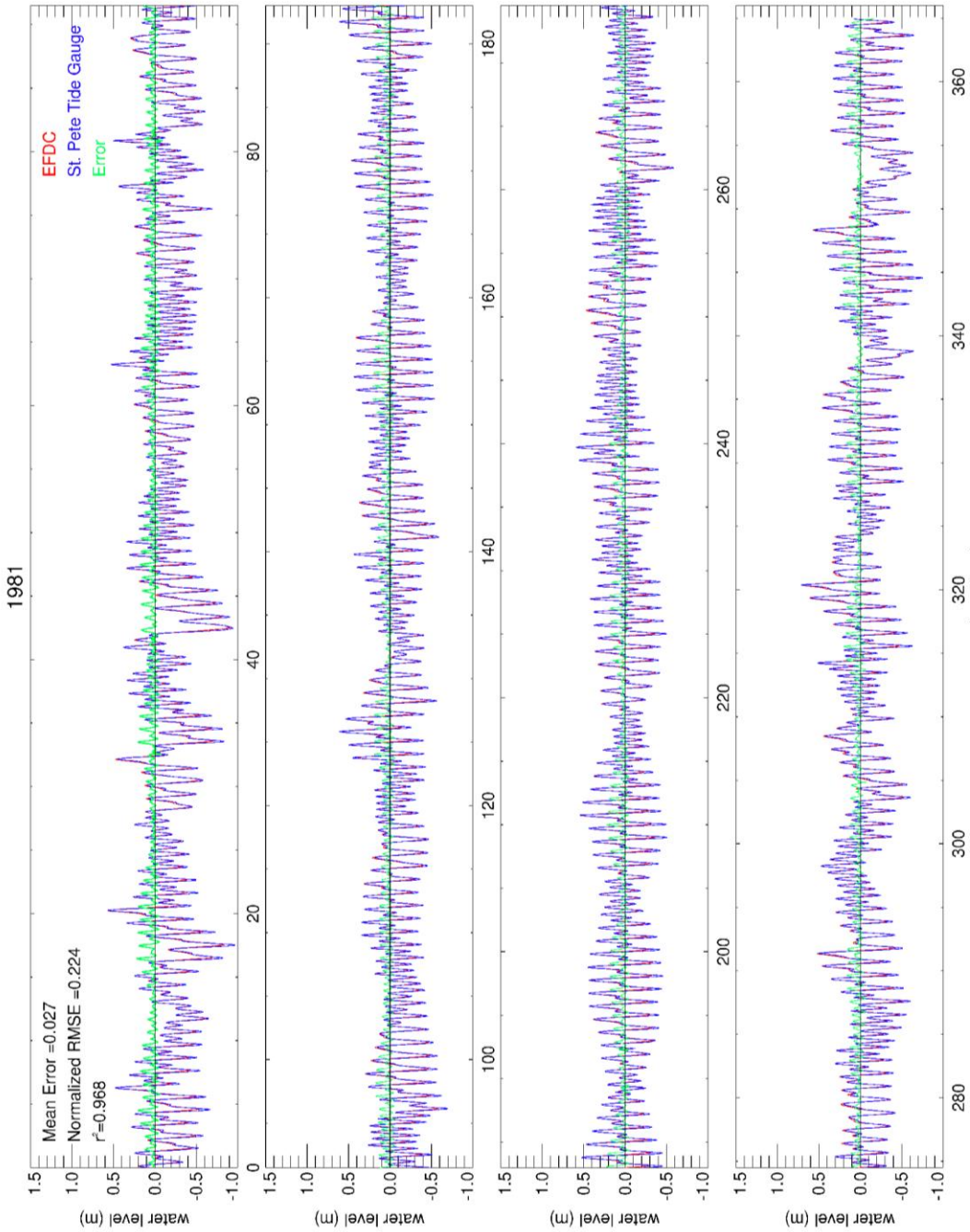

Figure A51. Same as figure A45 for 1981.

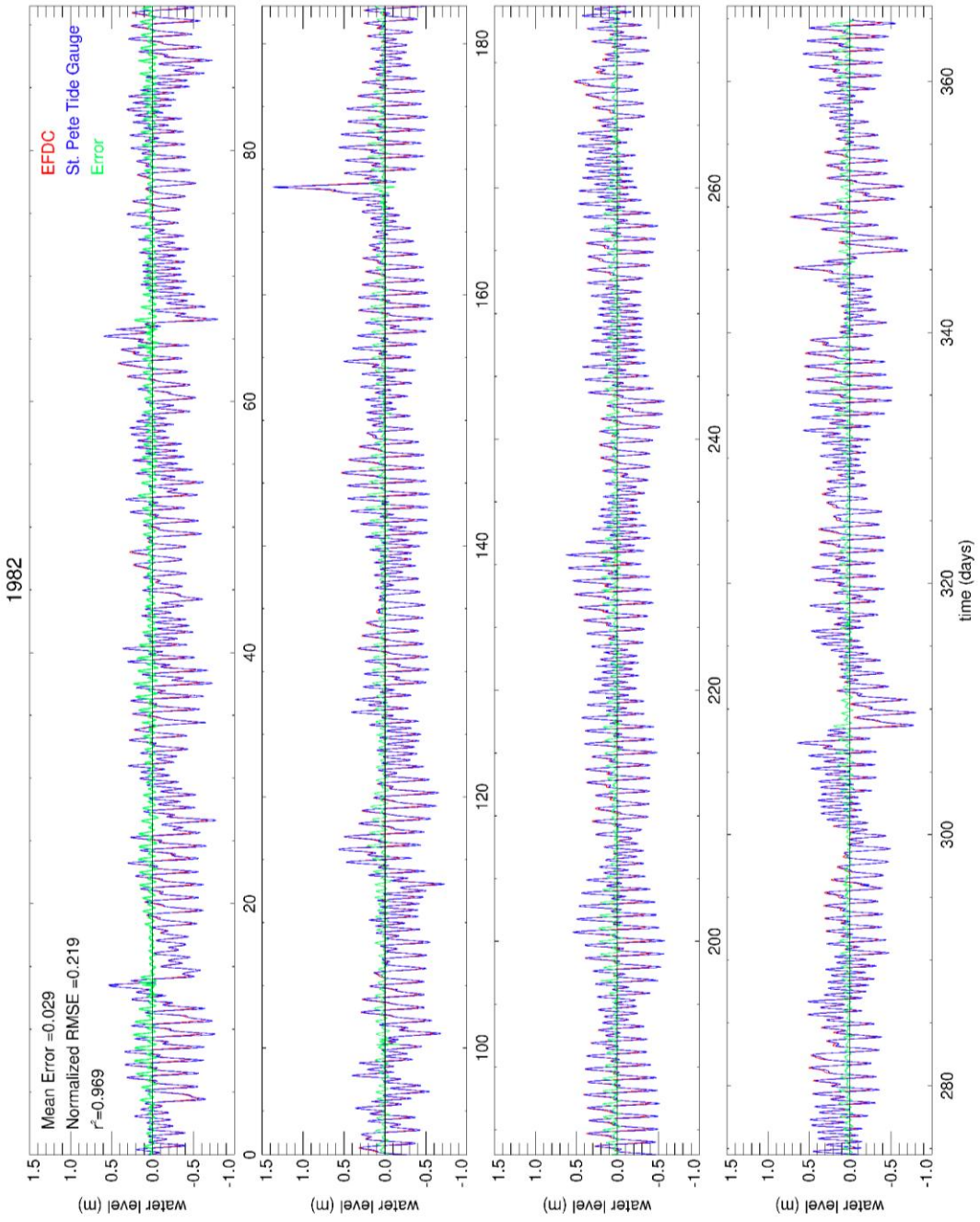

Figure A52. Same as figure A45 for 1982.

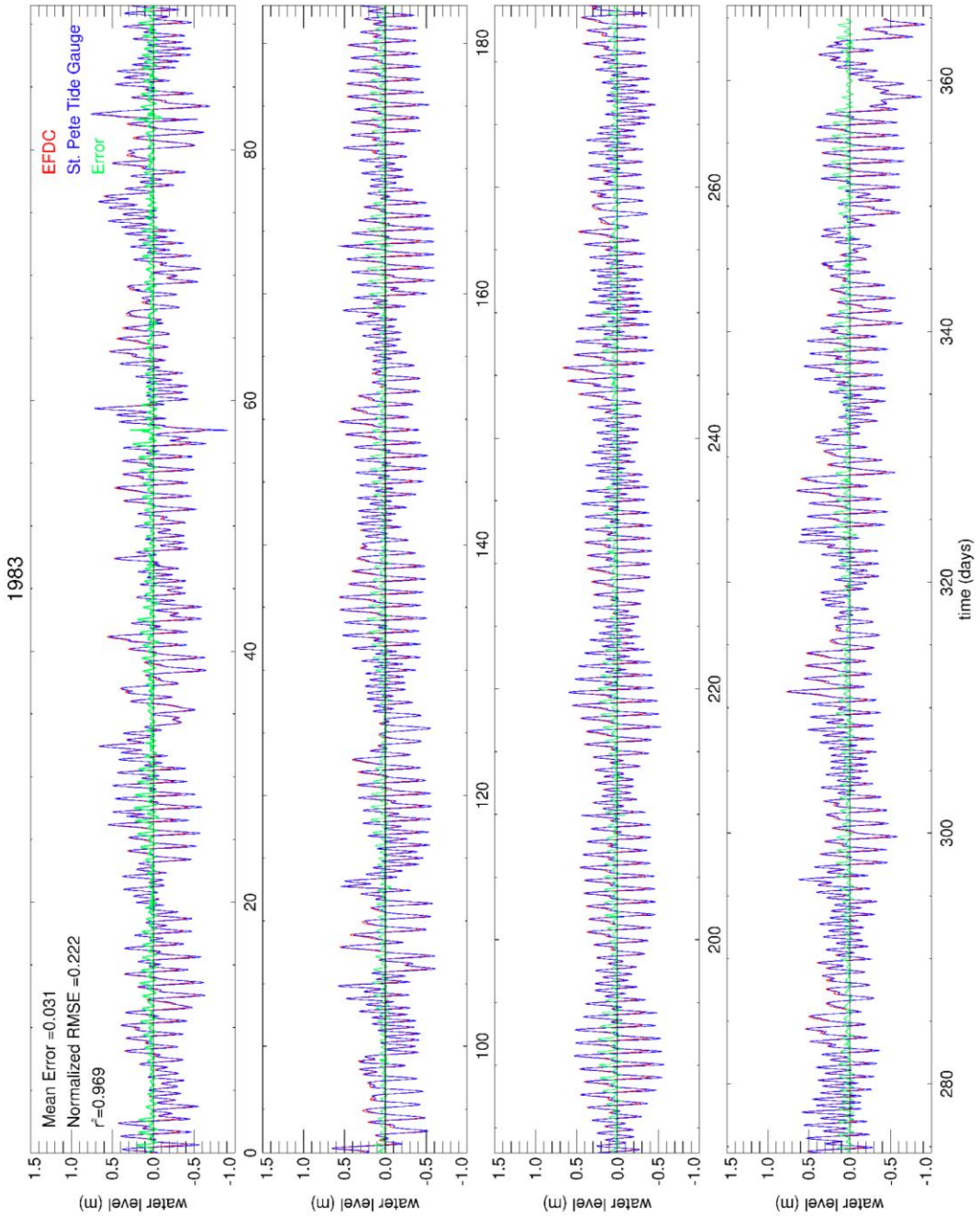

Figure A53. Same as figure A45 for 1983.

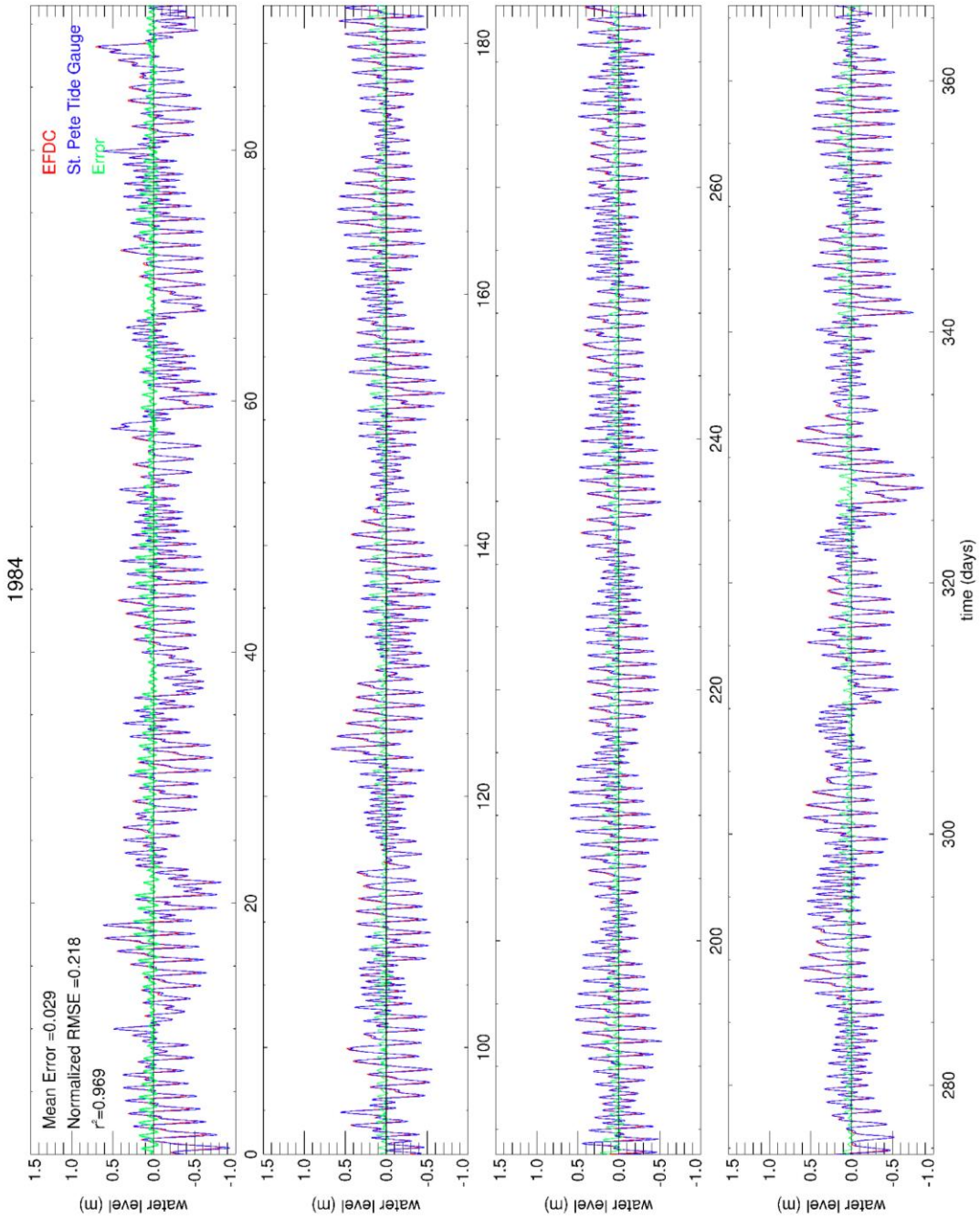

Figure A54. Same as figure A45 for 1984.

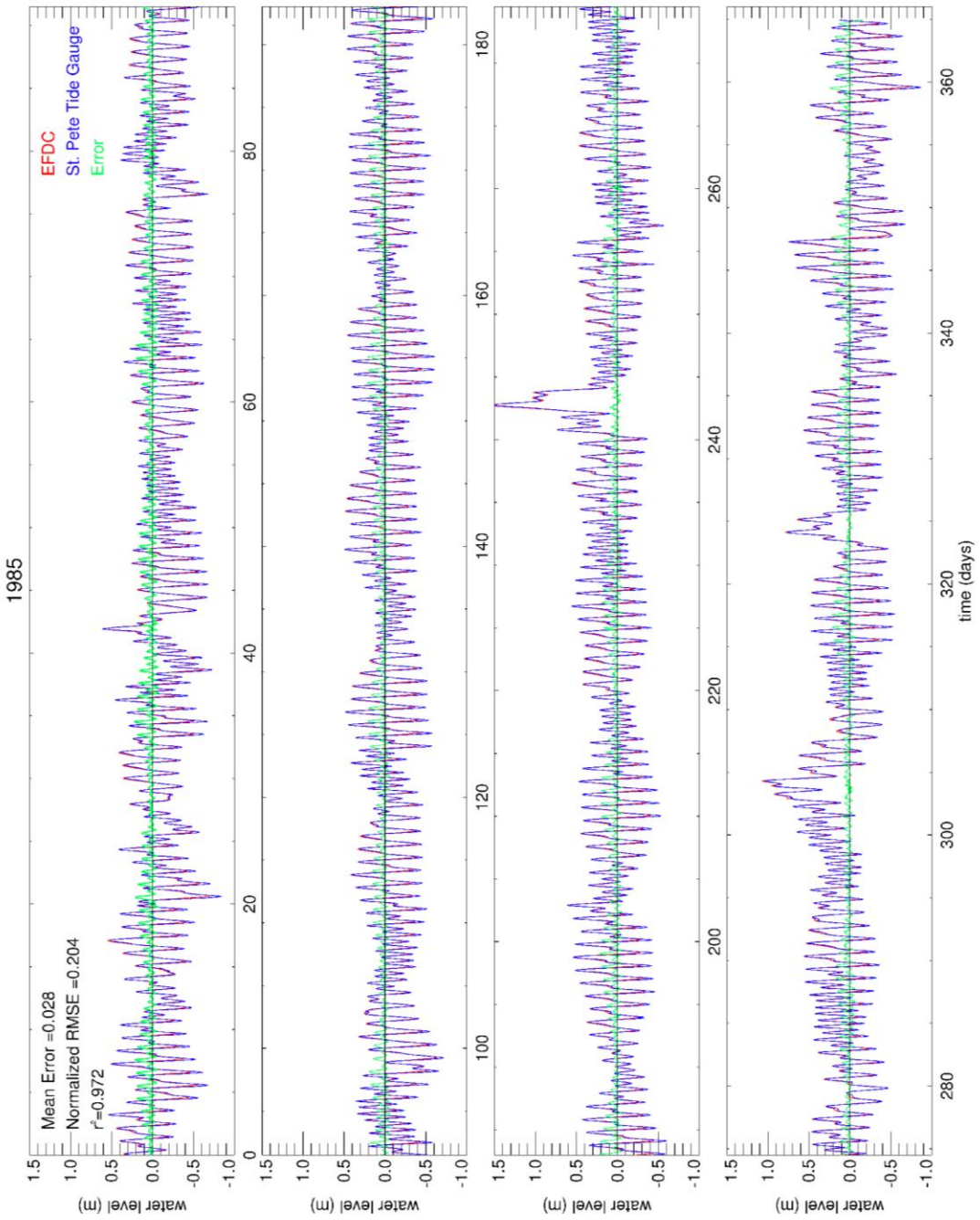

Figure A55. Same as figure A45 for 1985.

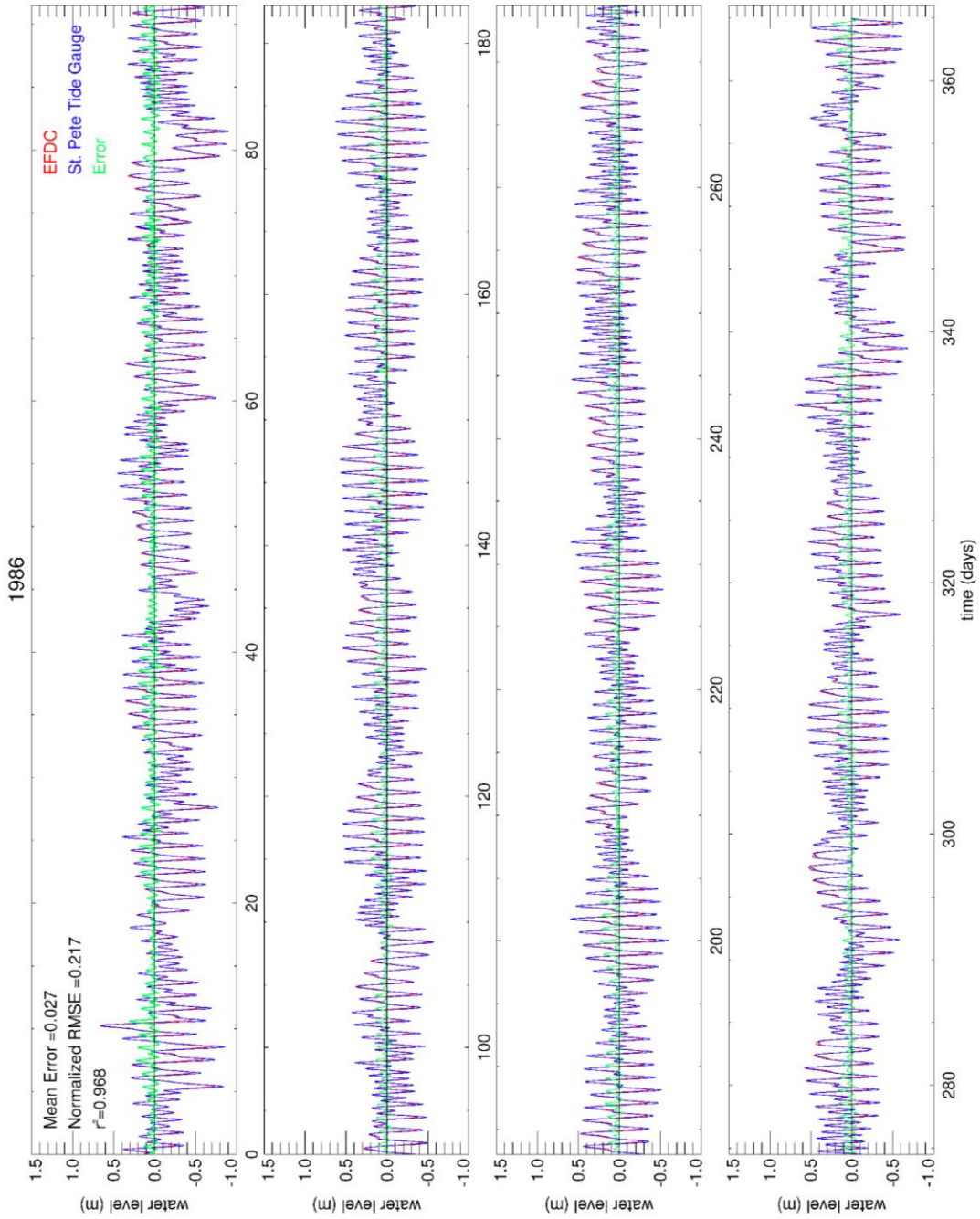

Figure A56. Same as figure A45 for 1986.

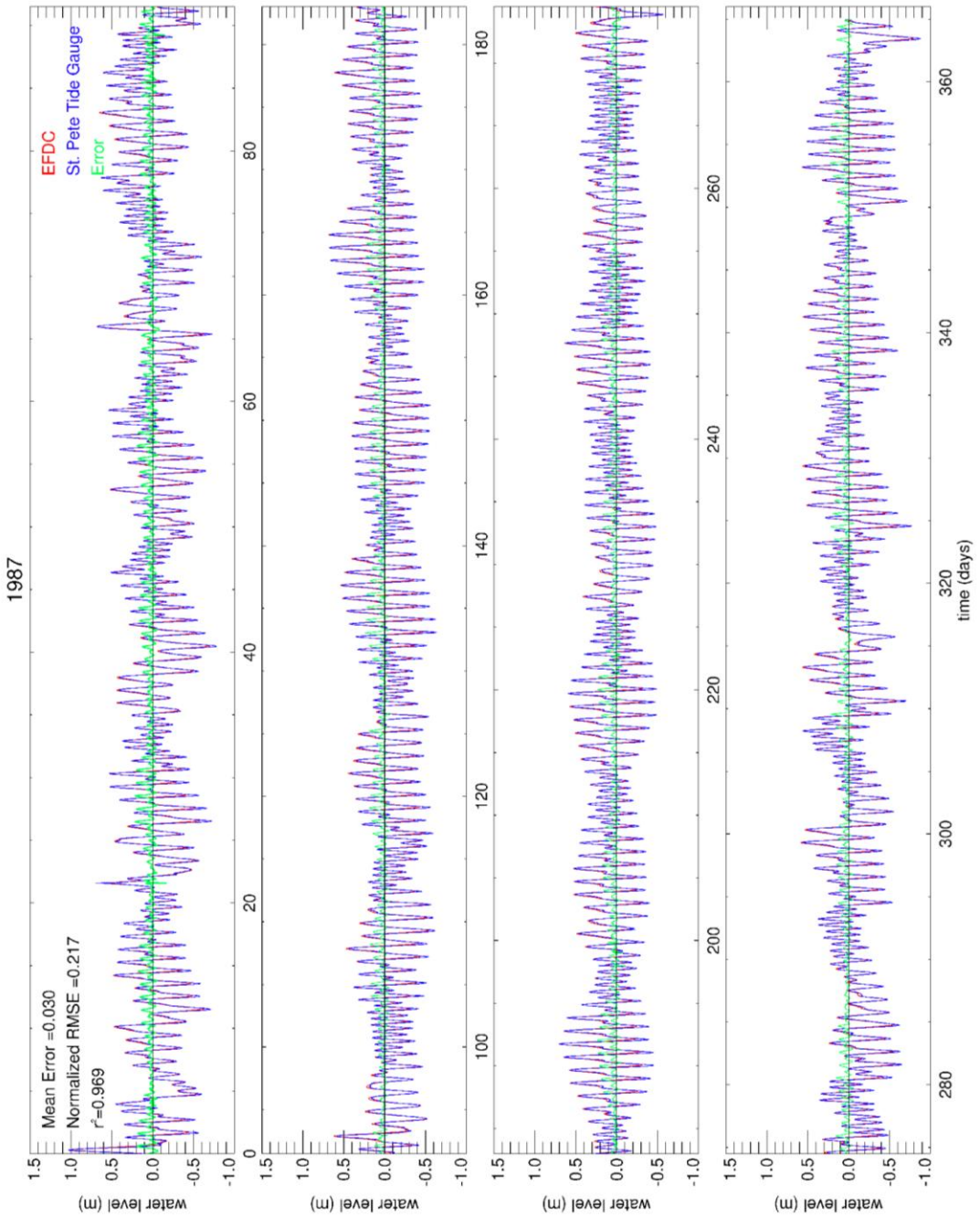

Figure A57. Same as figure A45 for 1987.

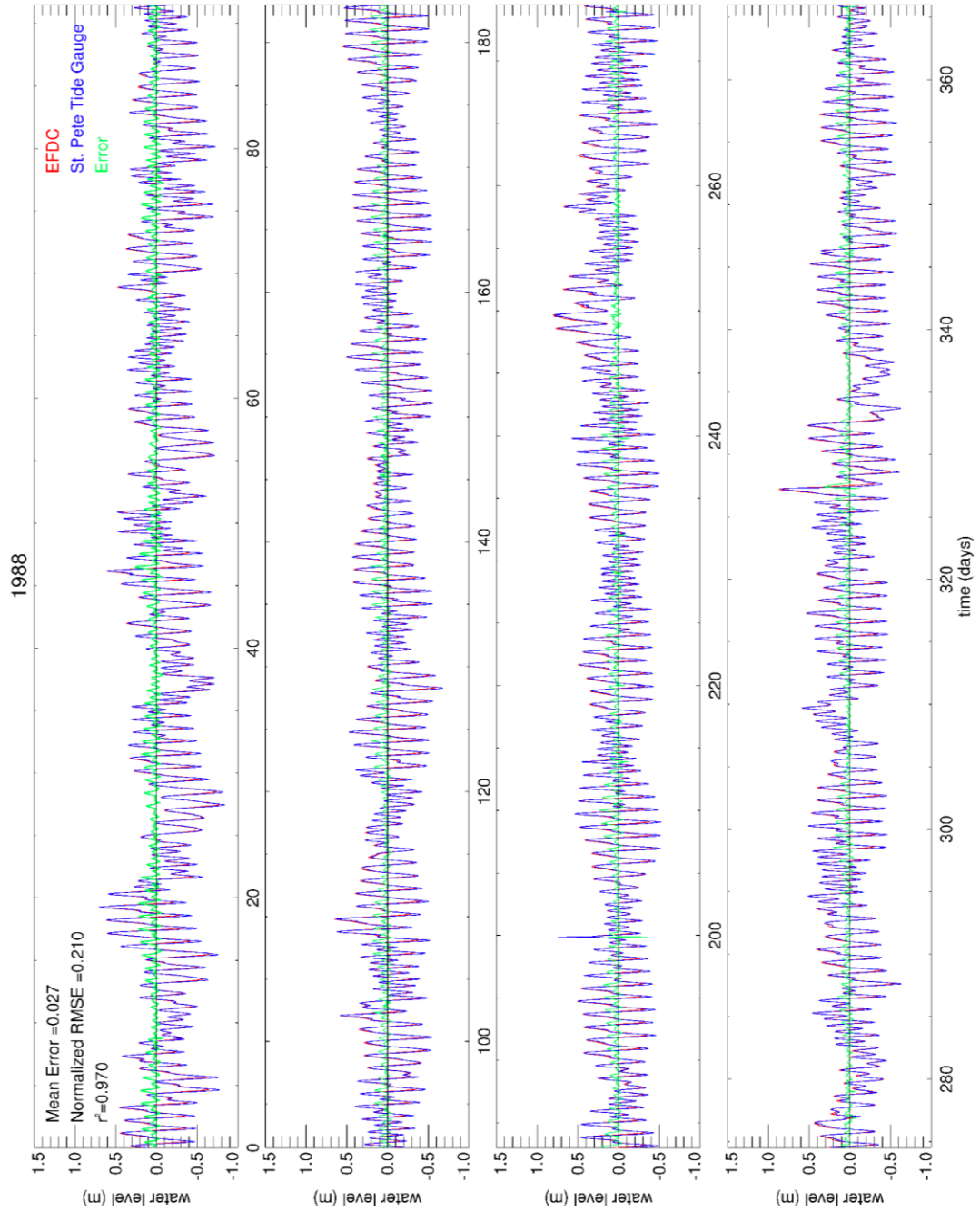

Figure A58. Same as figure A45 for 1988.

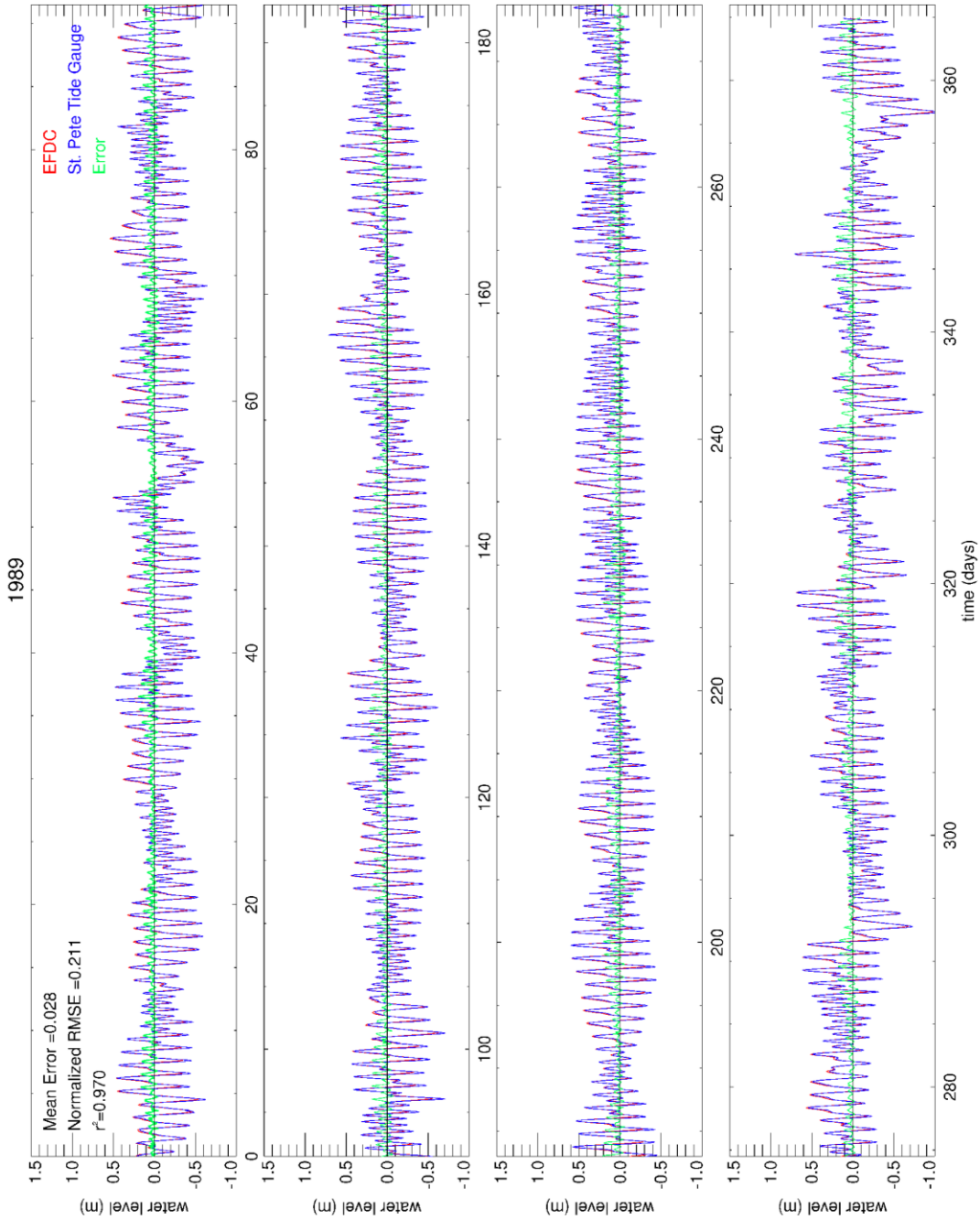

Figure A59. Same as figure A45 for 1989.

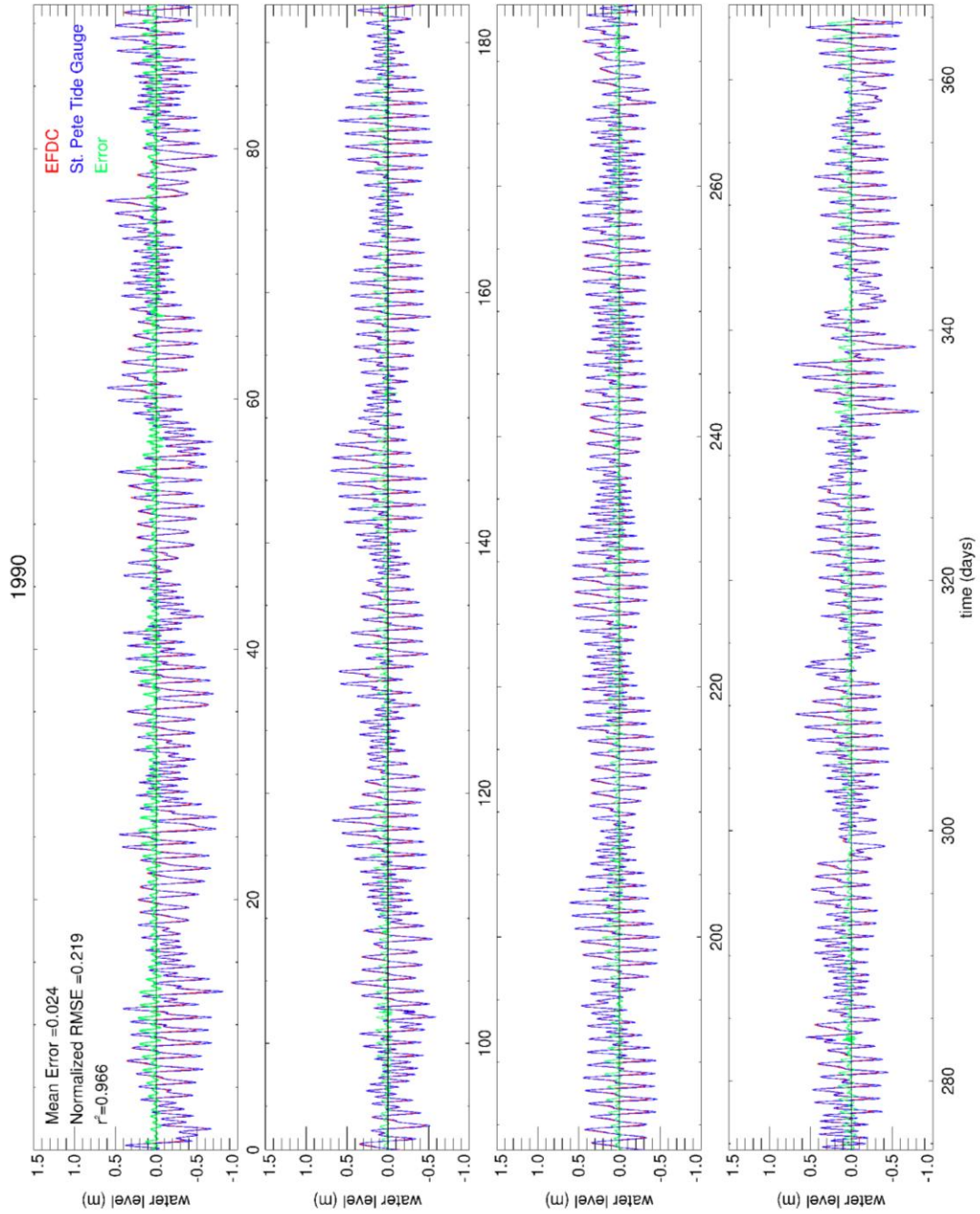

Figure A60. Same as figure A45 for 1990.

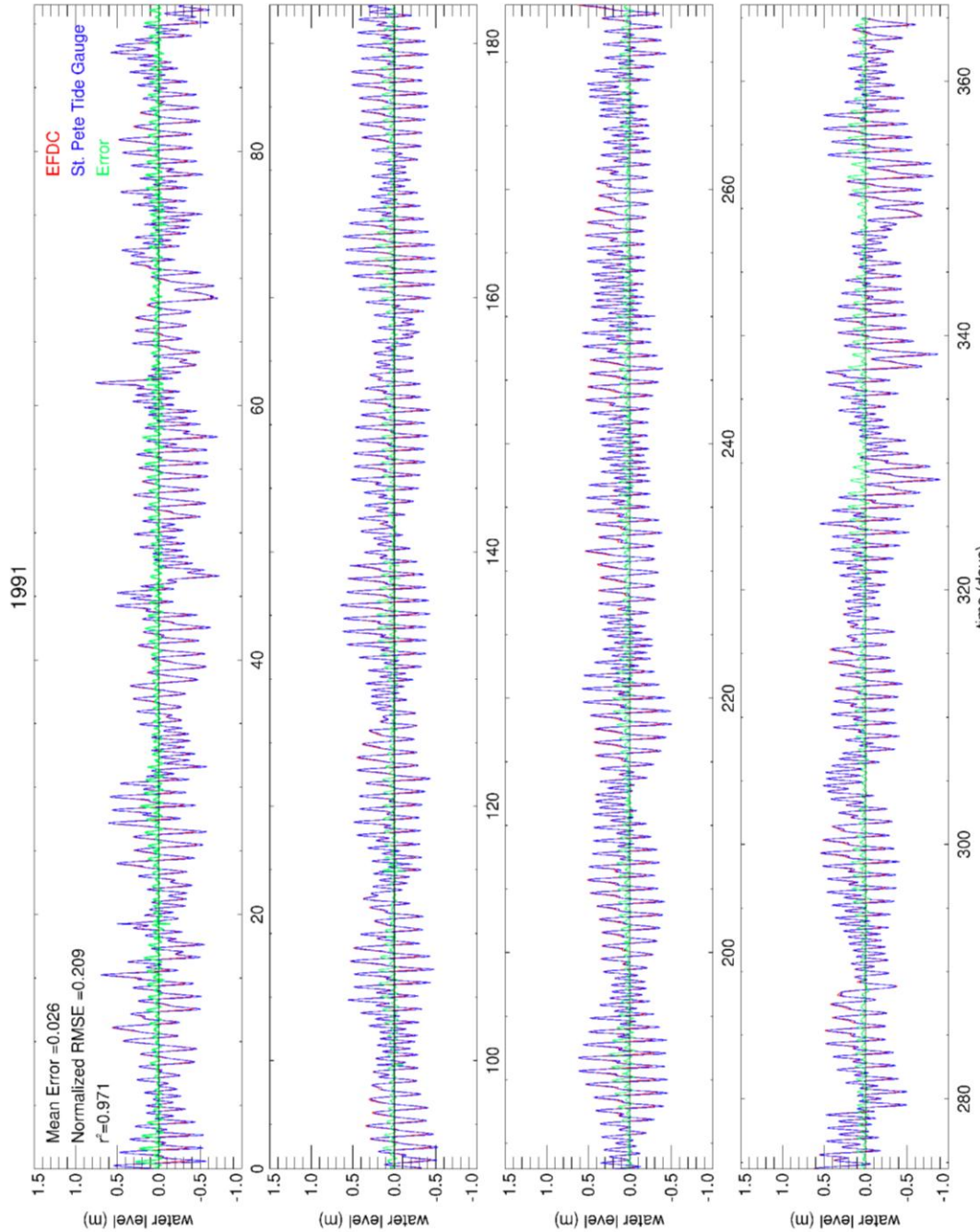

Figure A61. Same as figure A45 for 1991.

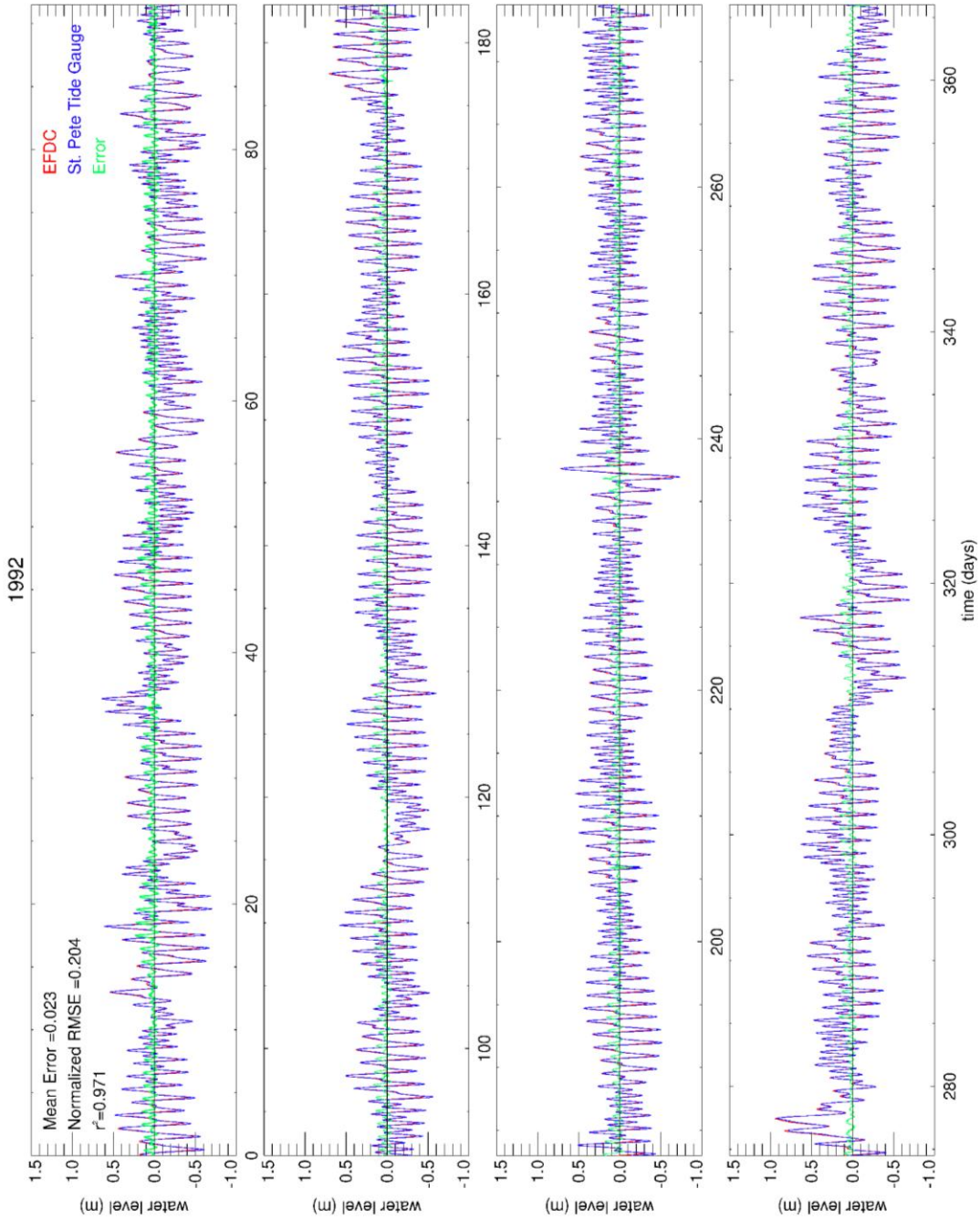

Figure A62. Same as figure A45 for 1992.

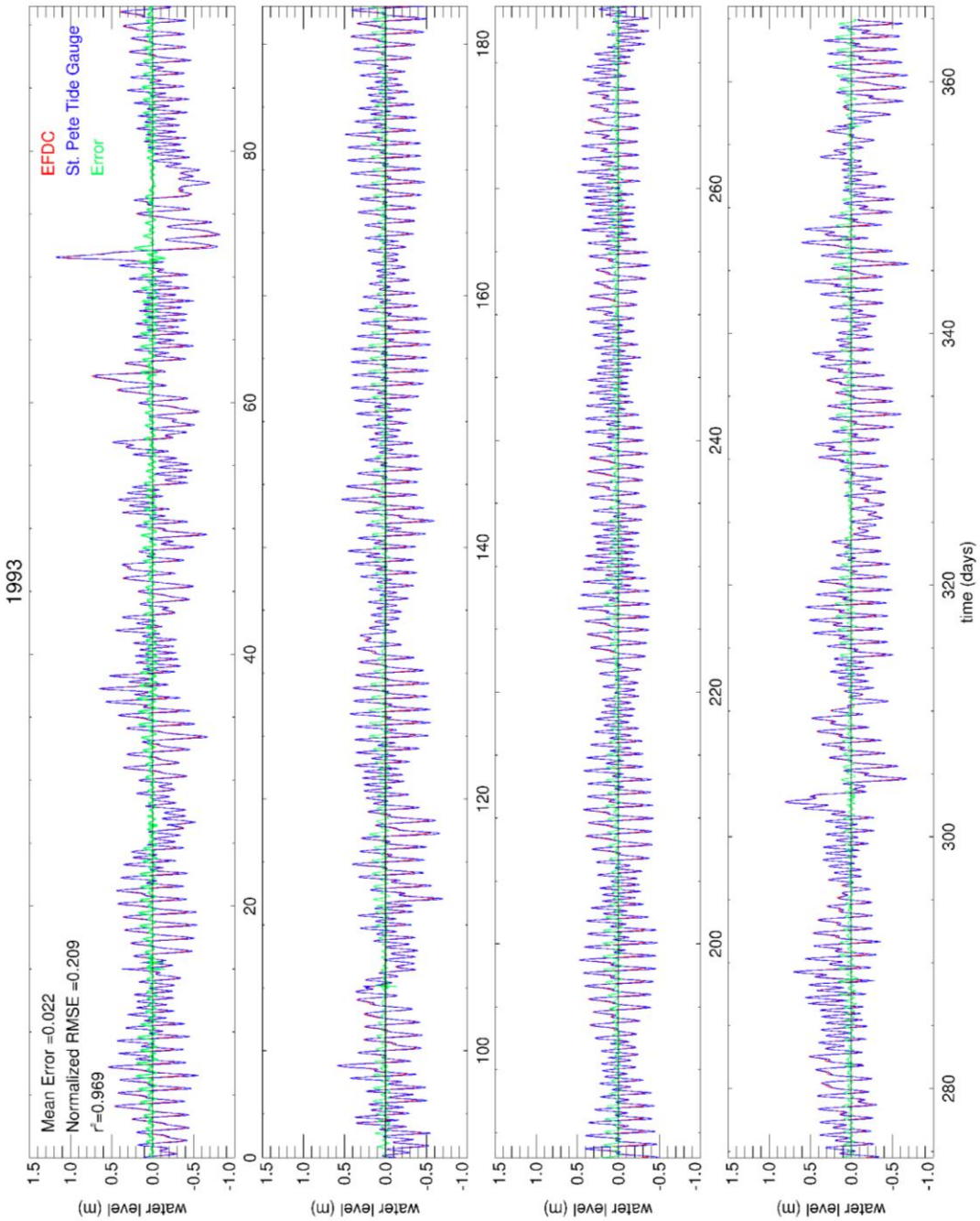

Figure A63. Same as figure A45 for 1993.

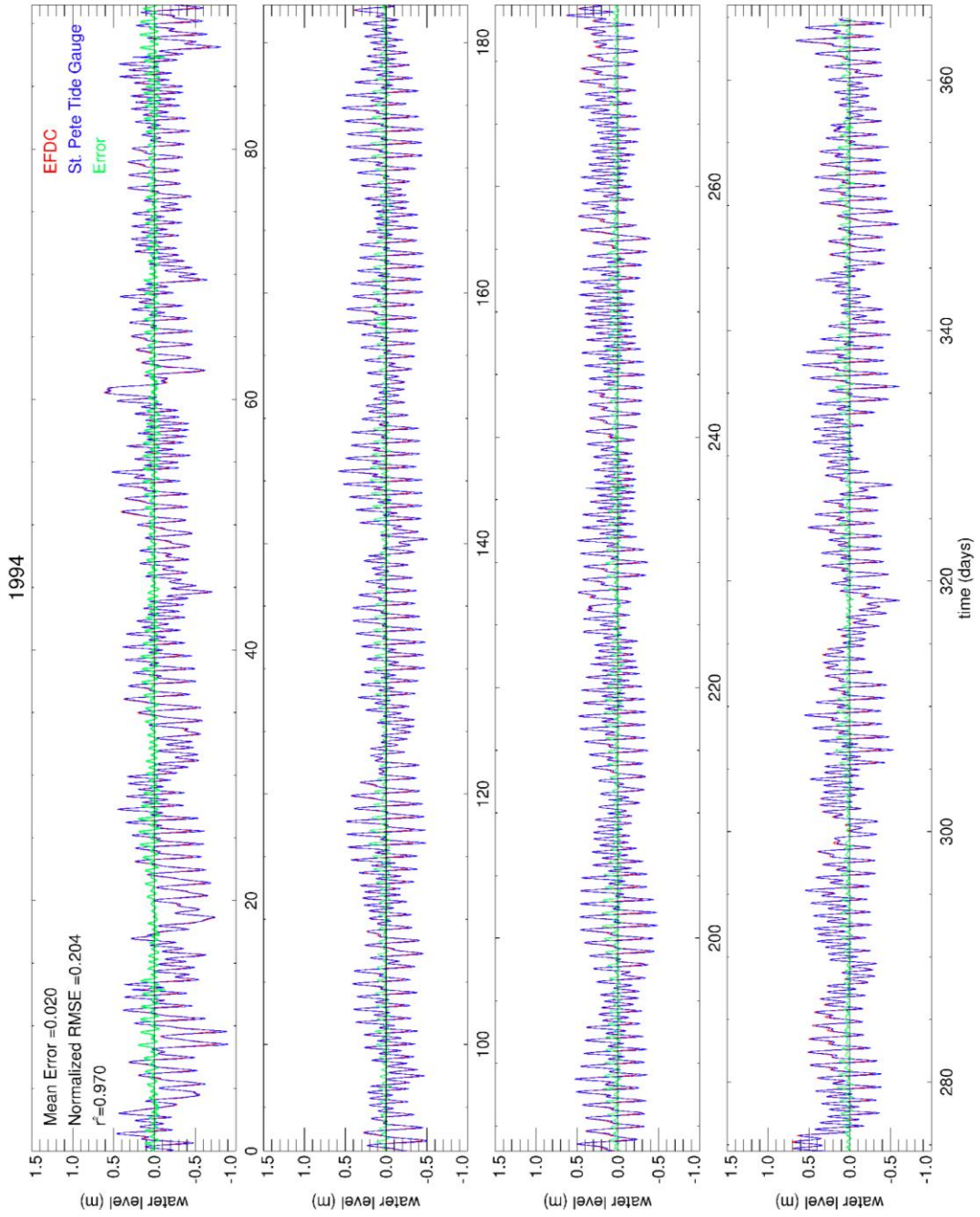

Figure A64. Same as figure A45 for 1994.

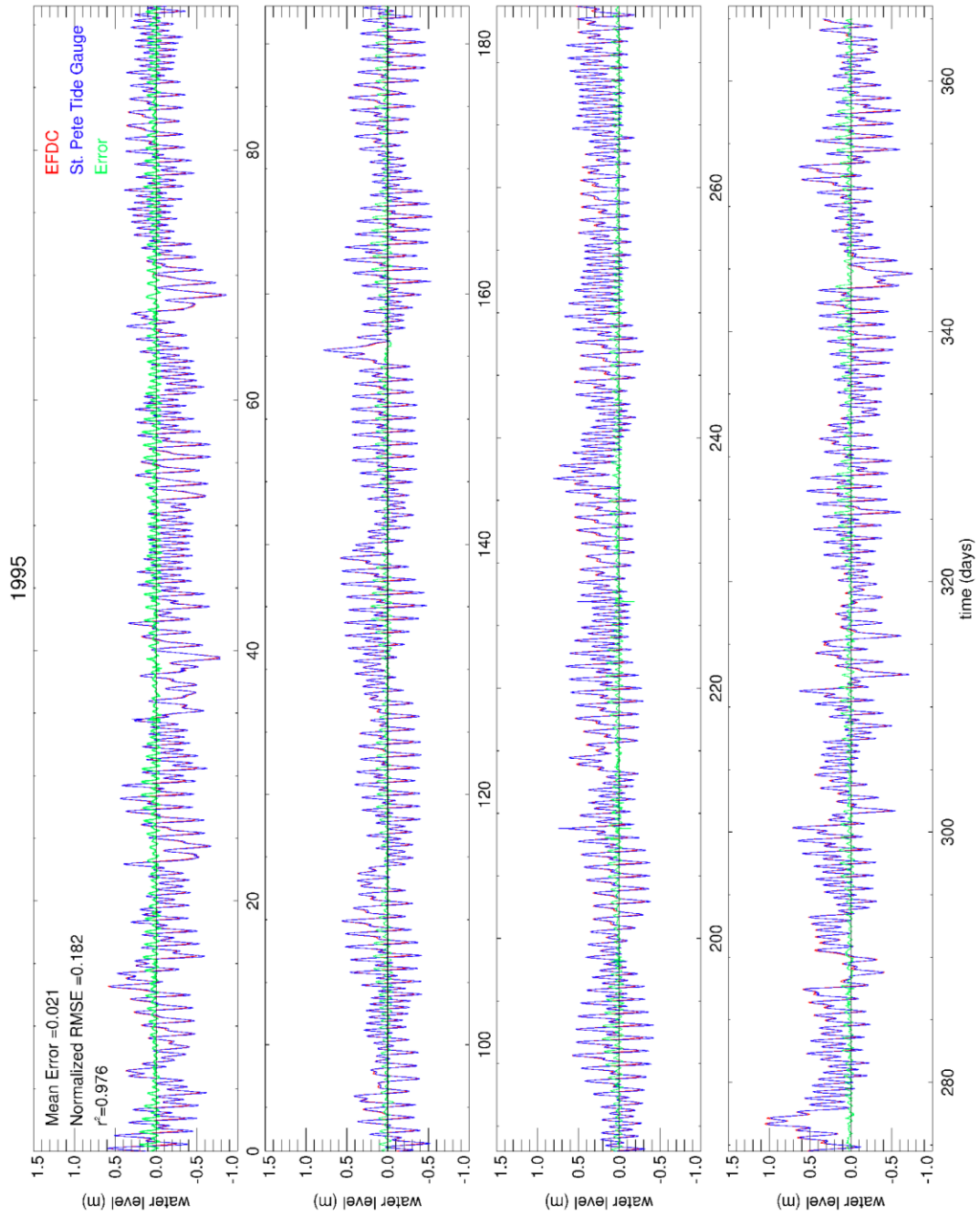

Figure A65. Same as figure A45 for 1995.

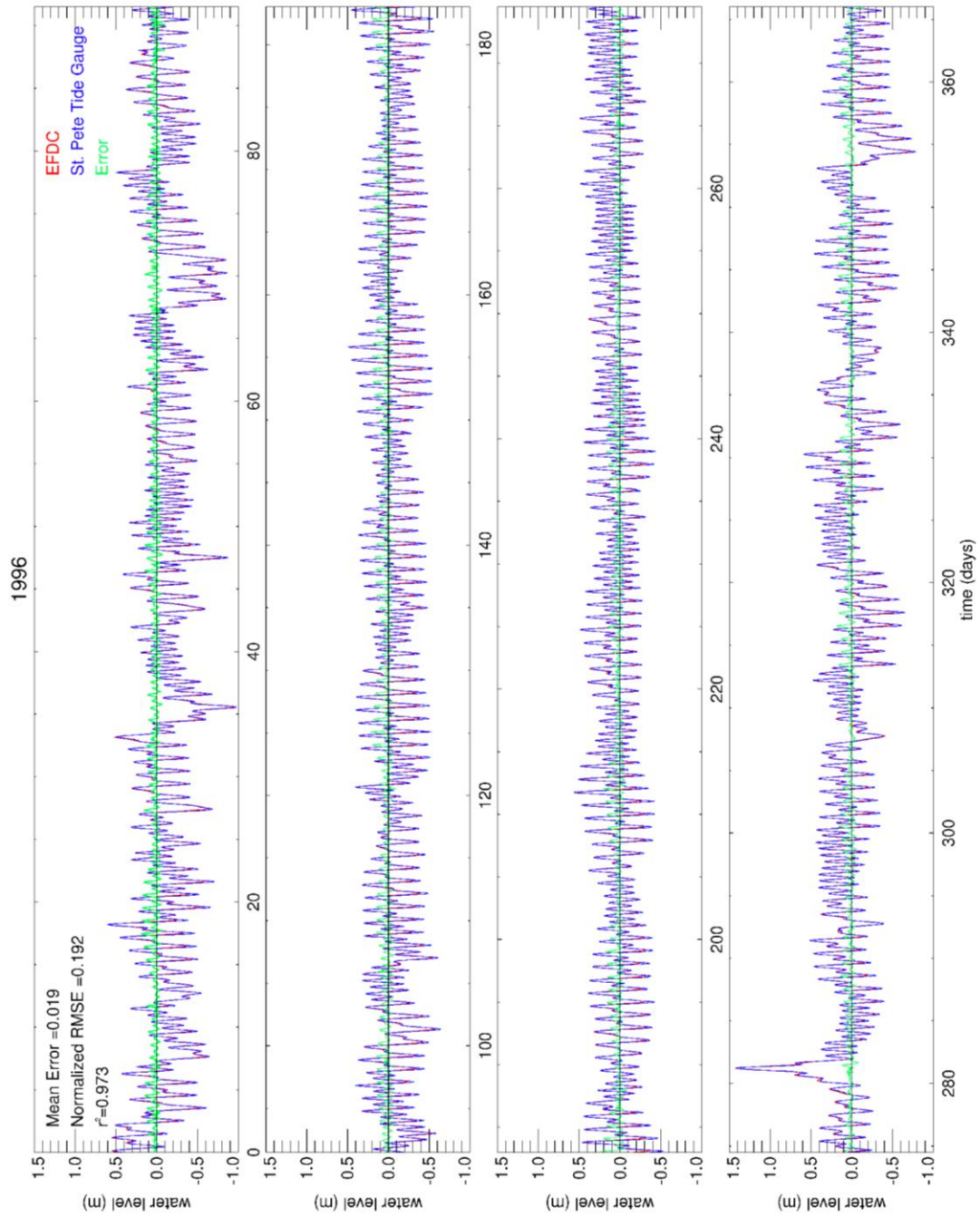

Figure A66. Same as figure A45 for 1996.

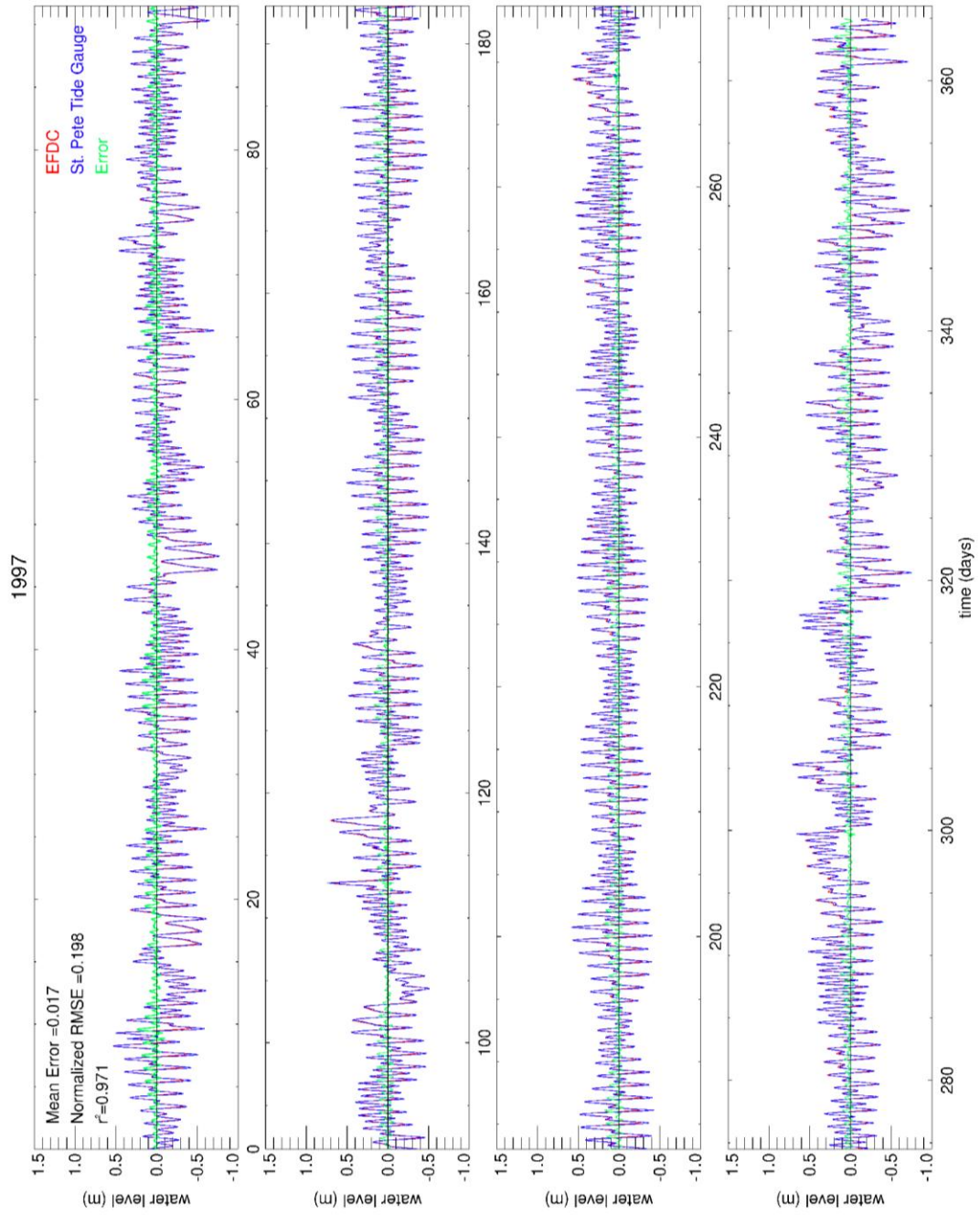

Figure A67. Same as figure A45 for 1997.

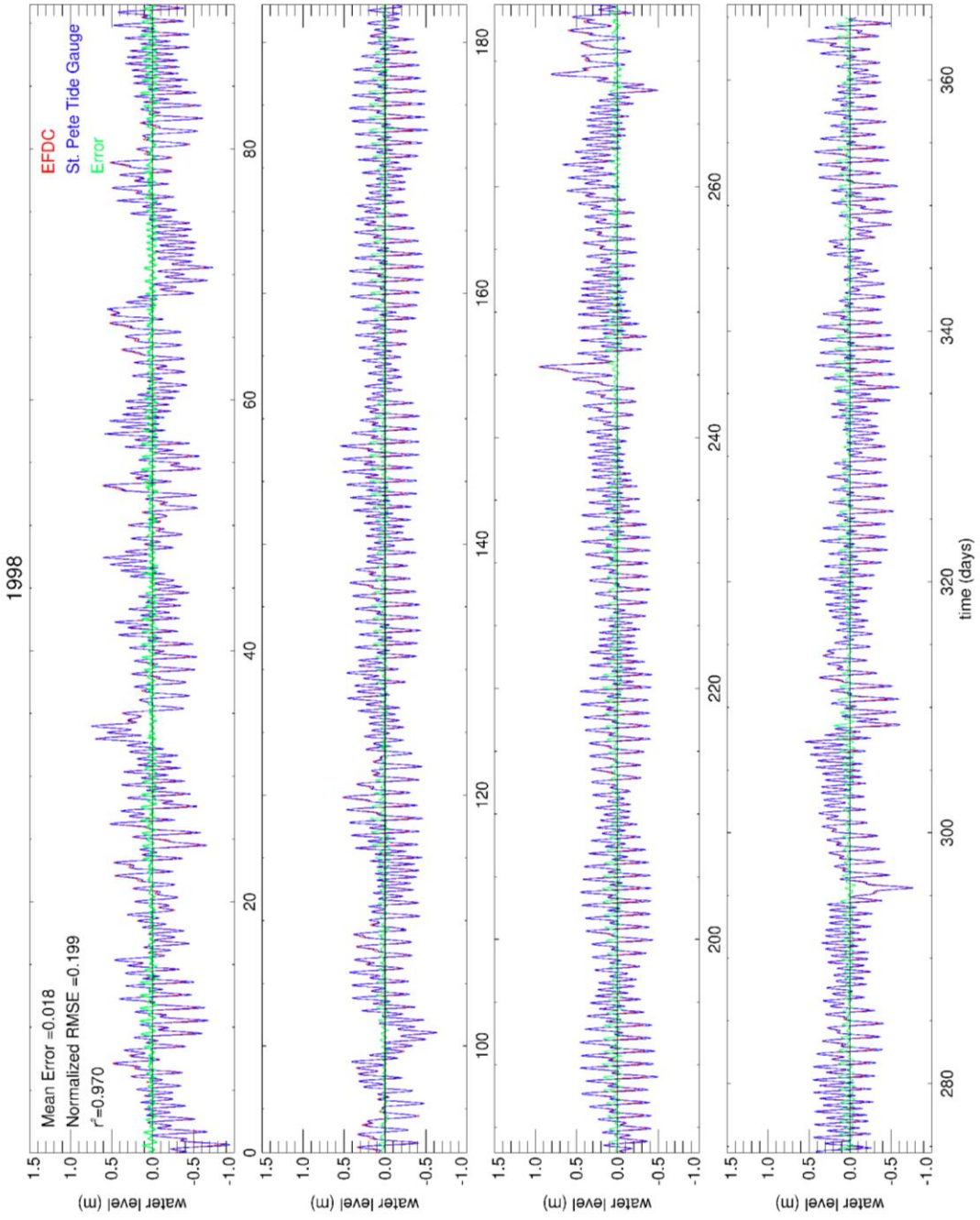

Figure A68. Same as figure A45 for 1998.

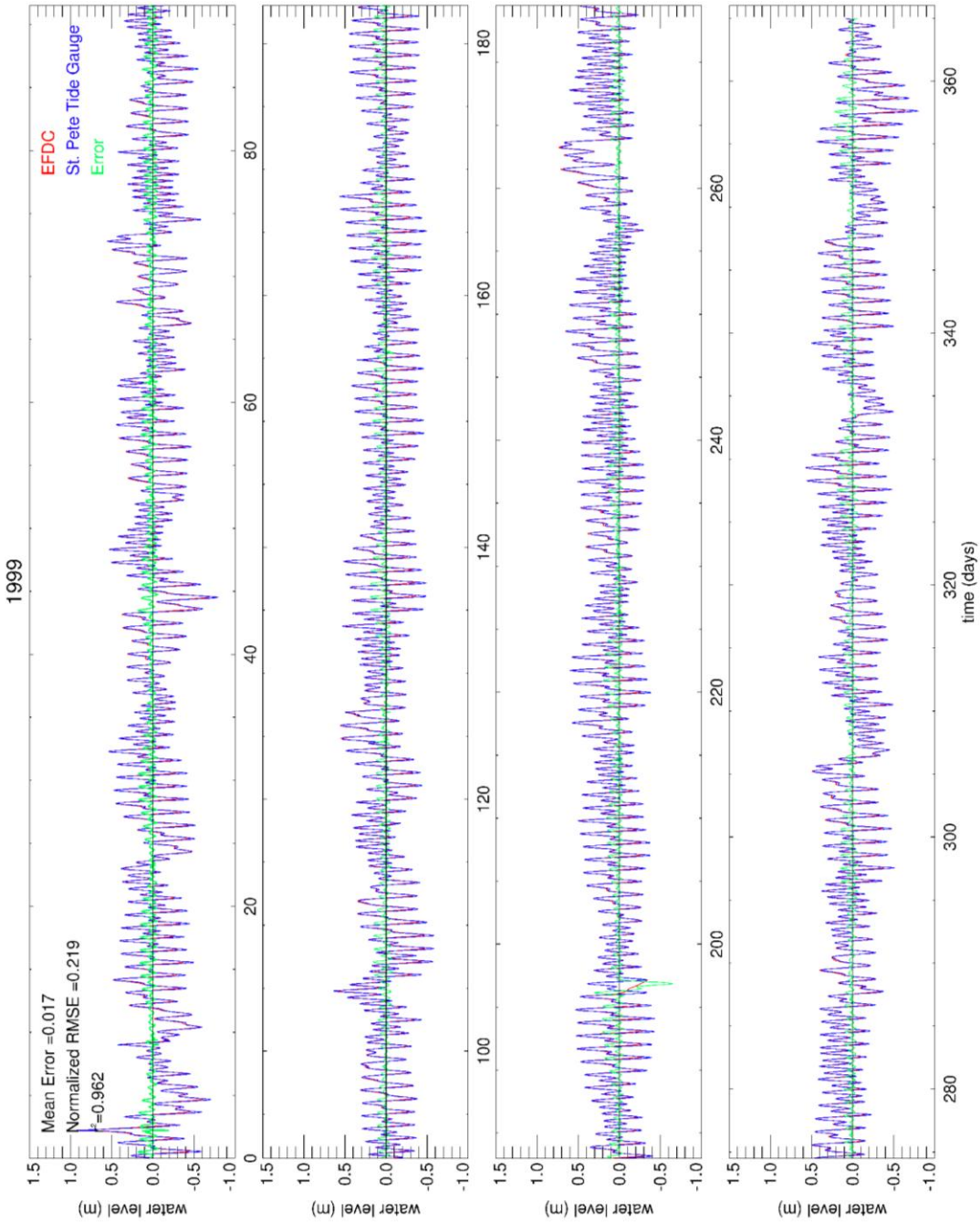

Figure A69. Same as figure A45 for 1999.

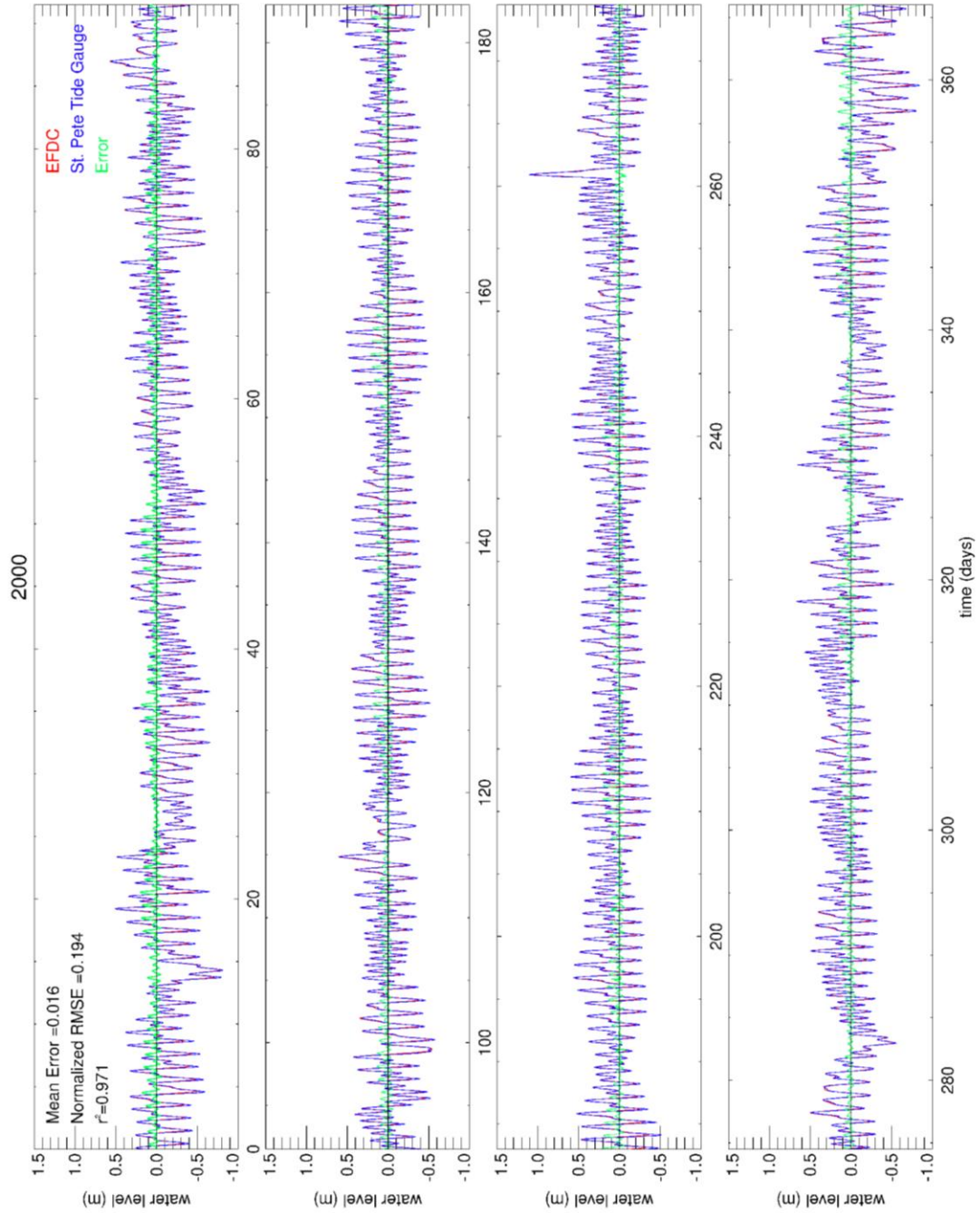

Figure A70. Same as figure A45 for 2000.

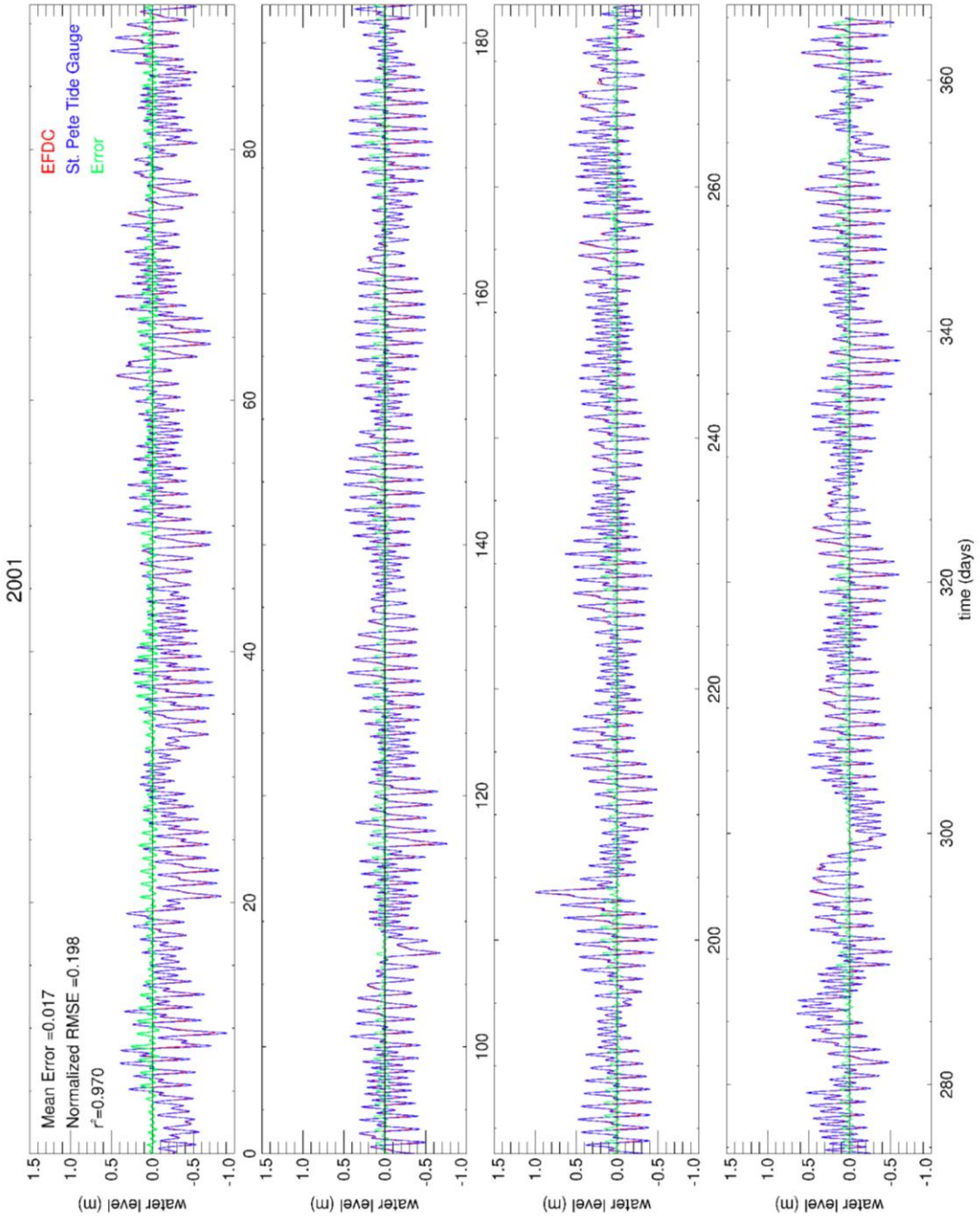

Figure A71. Same as figure A45 for 2001.

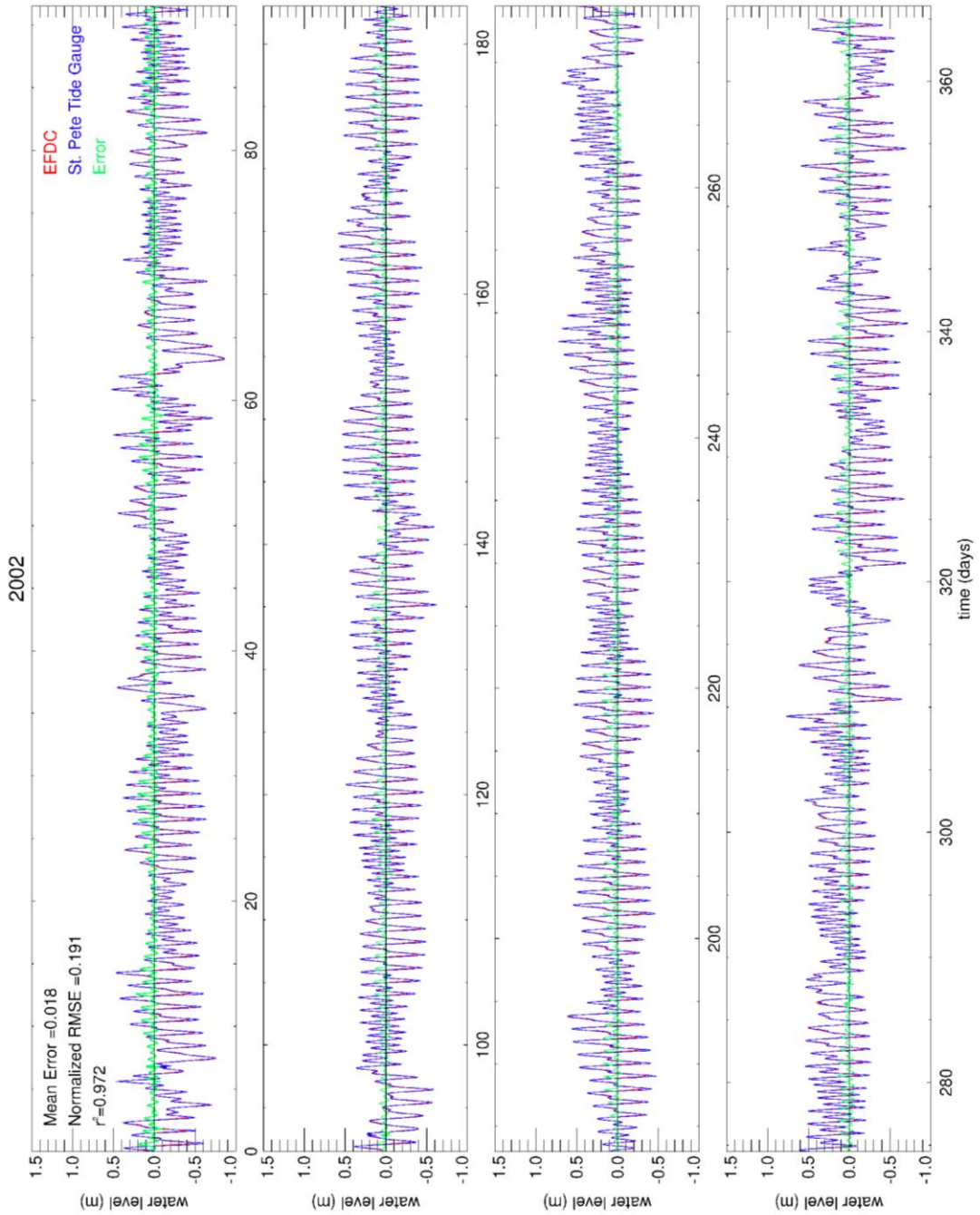

Figure A72. Same as figure A45 for 2002.

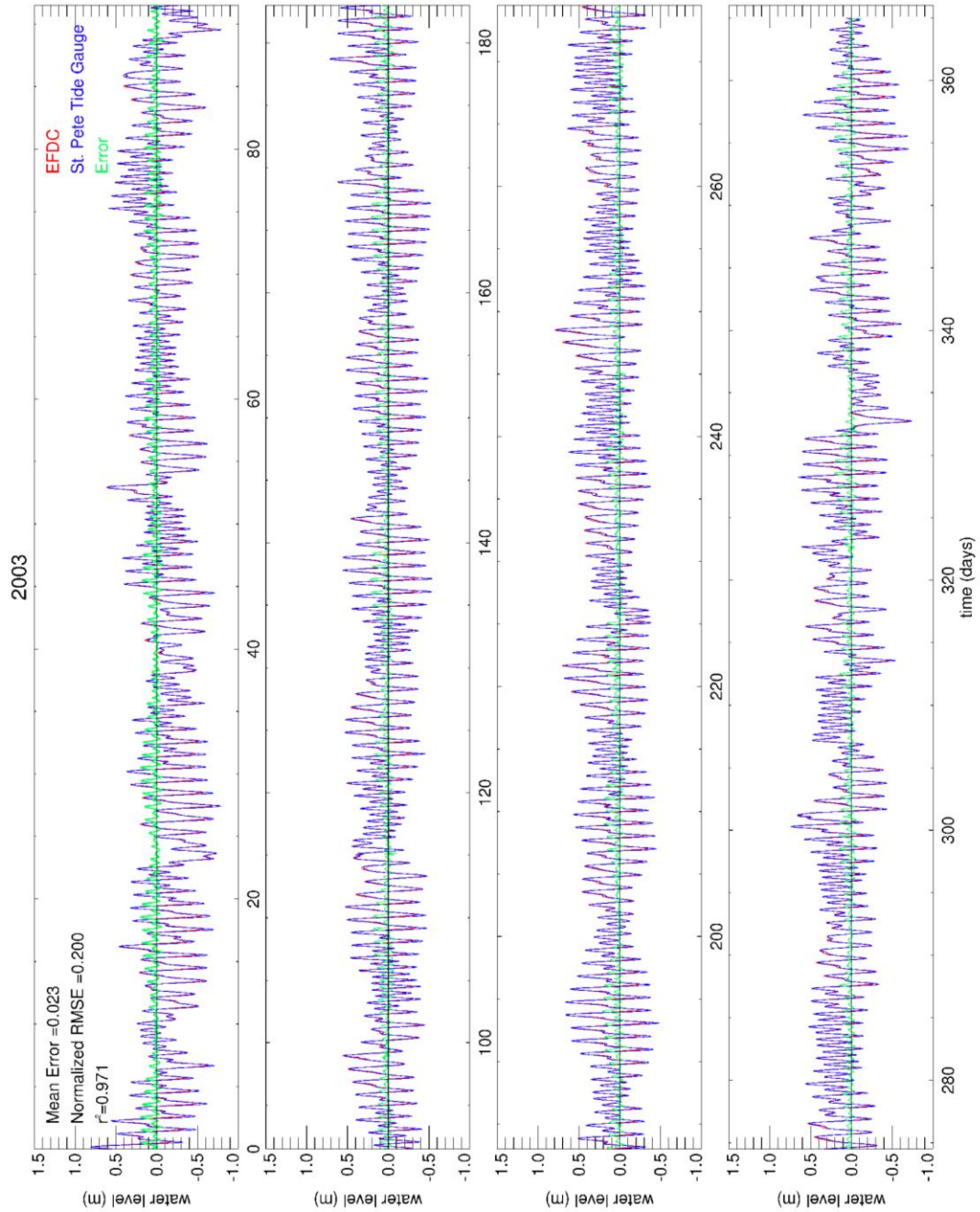

Figure A73. Same as figure A45 for 2003.

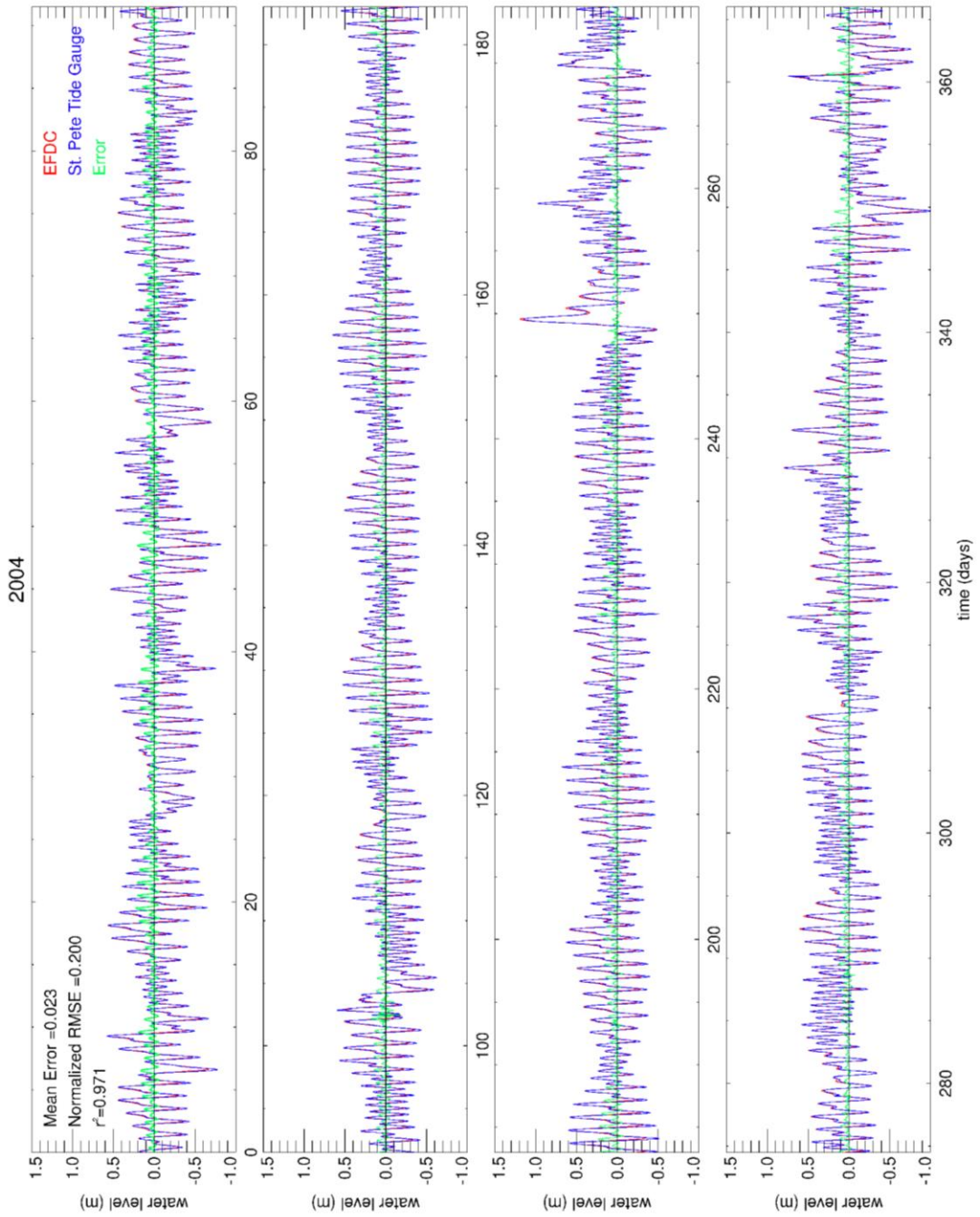

Figure A74. Same as figure A45 for 2004.

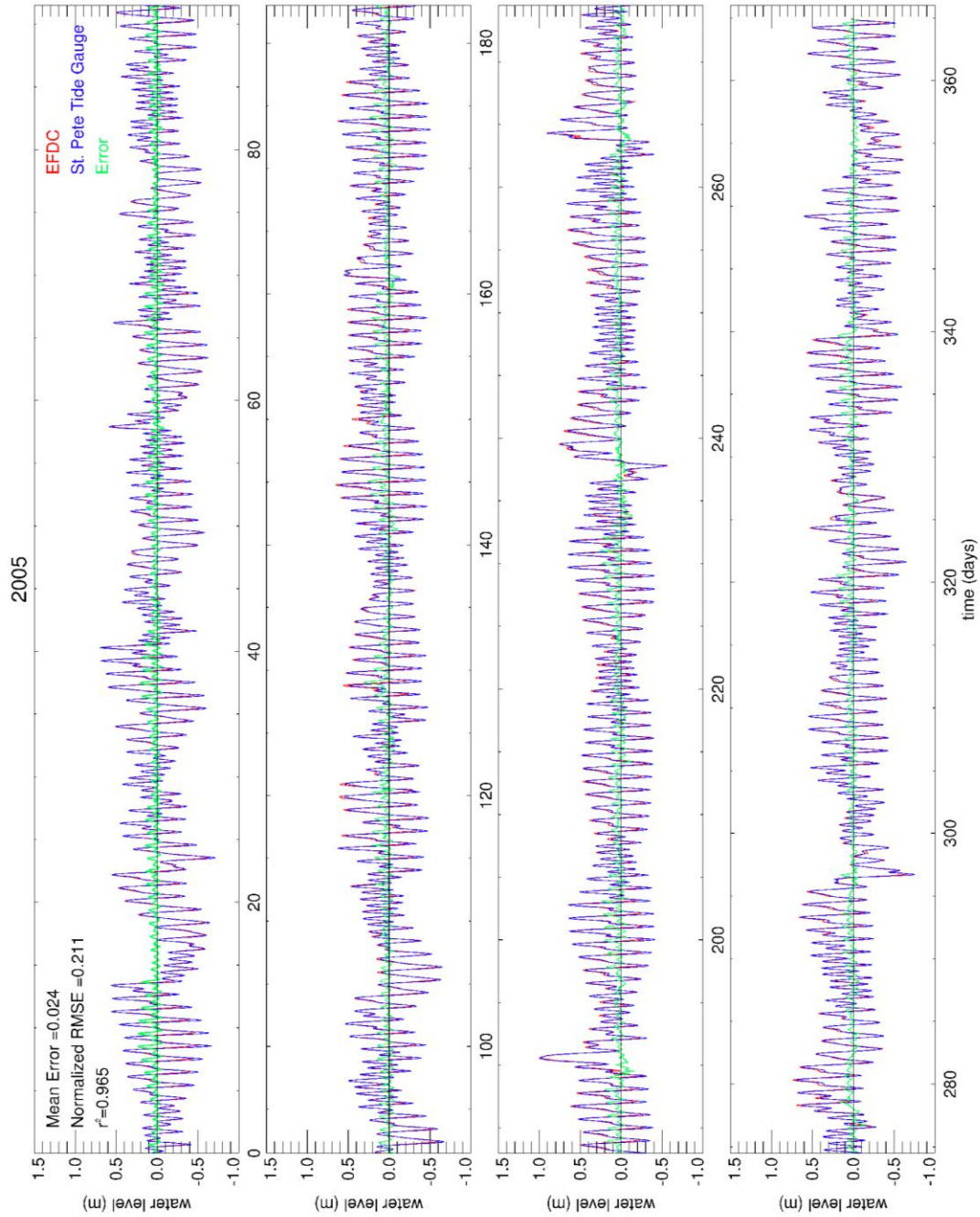

Figure A75. Same as figure A45 for 2005.

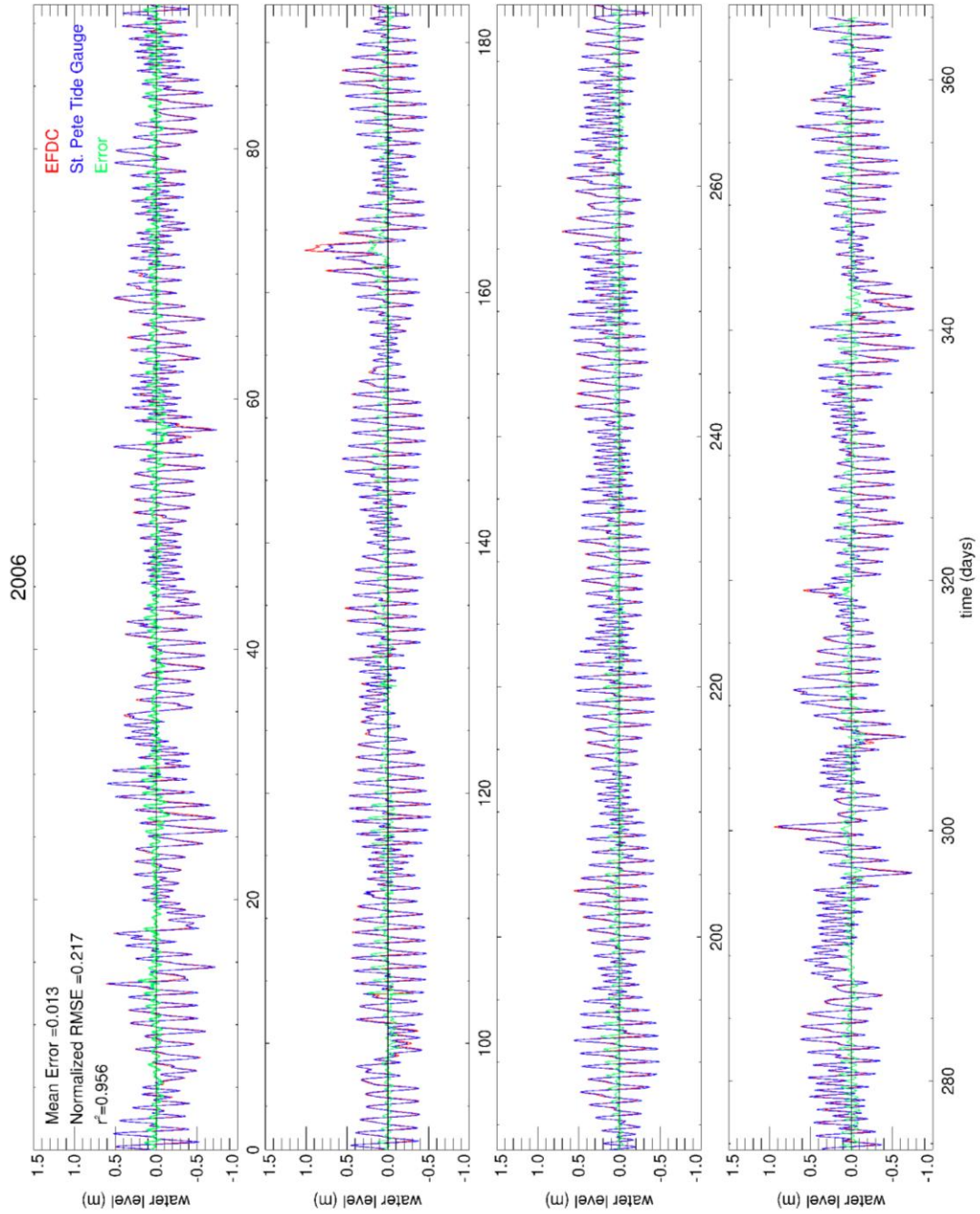

Figure A76. Same as figure A45 for 2006.

Appendix D: Yearly wavelet transforms for elevation, axial, and co-axial wind components

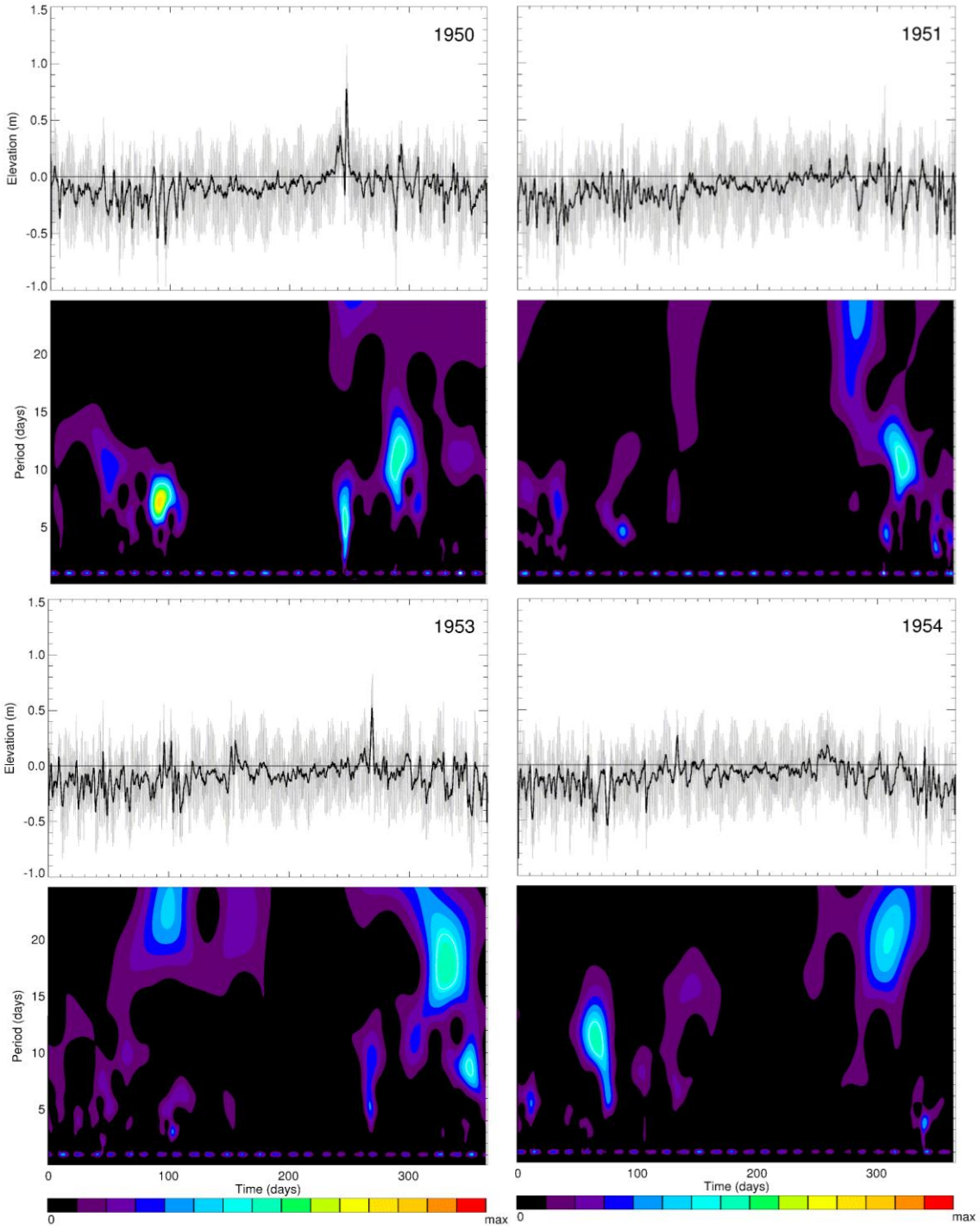

Figure A77. Instantaneous elevation (gray) and 25-hr smoothed elevation (thick black). Elevation wavelet transform for 1950, 1951, 1953, and 1954 with 80% significance levels (white lines) and 95% significance levels (black lines) shown.

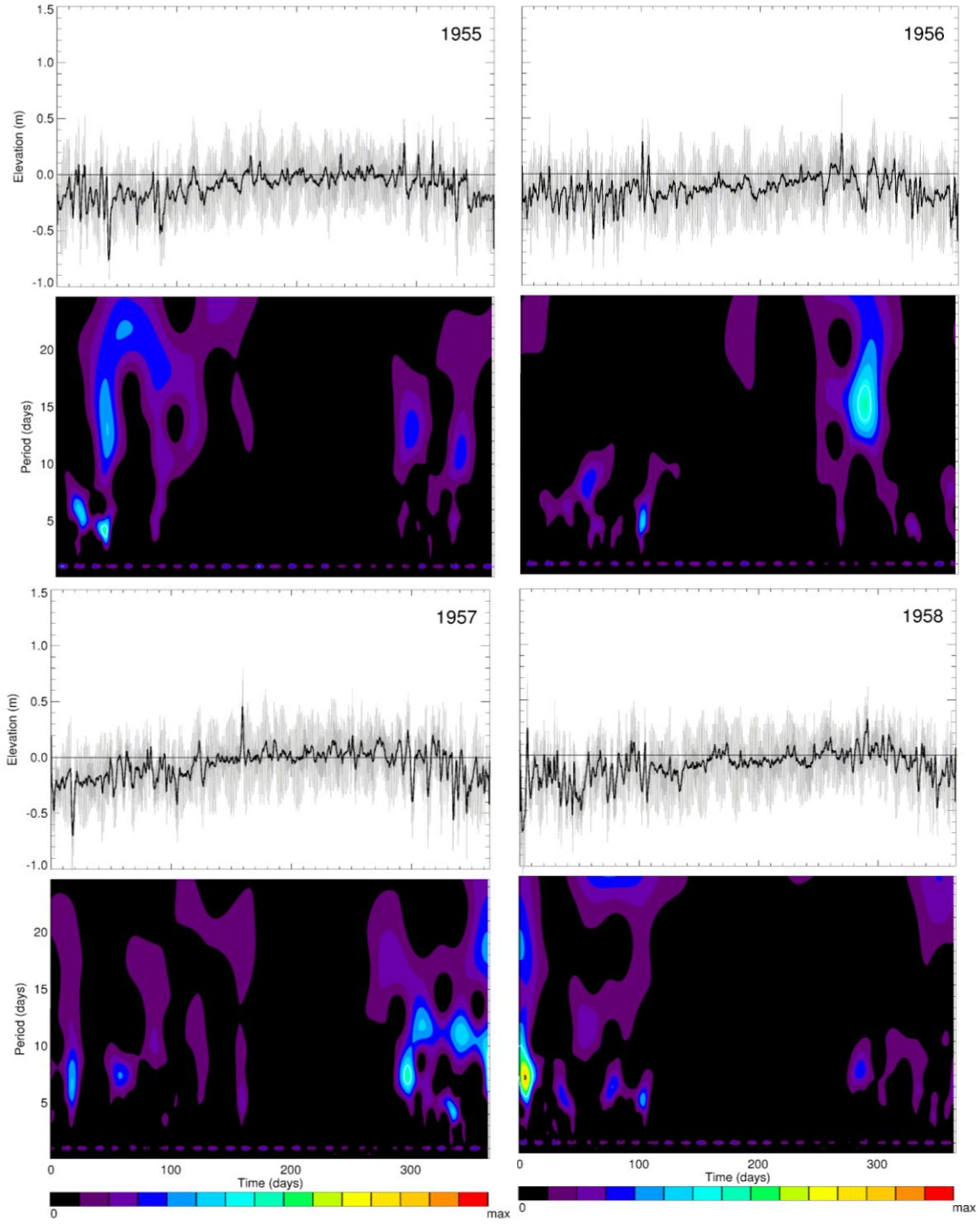

Figure A78. Same as figure A77, 1955-1958.

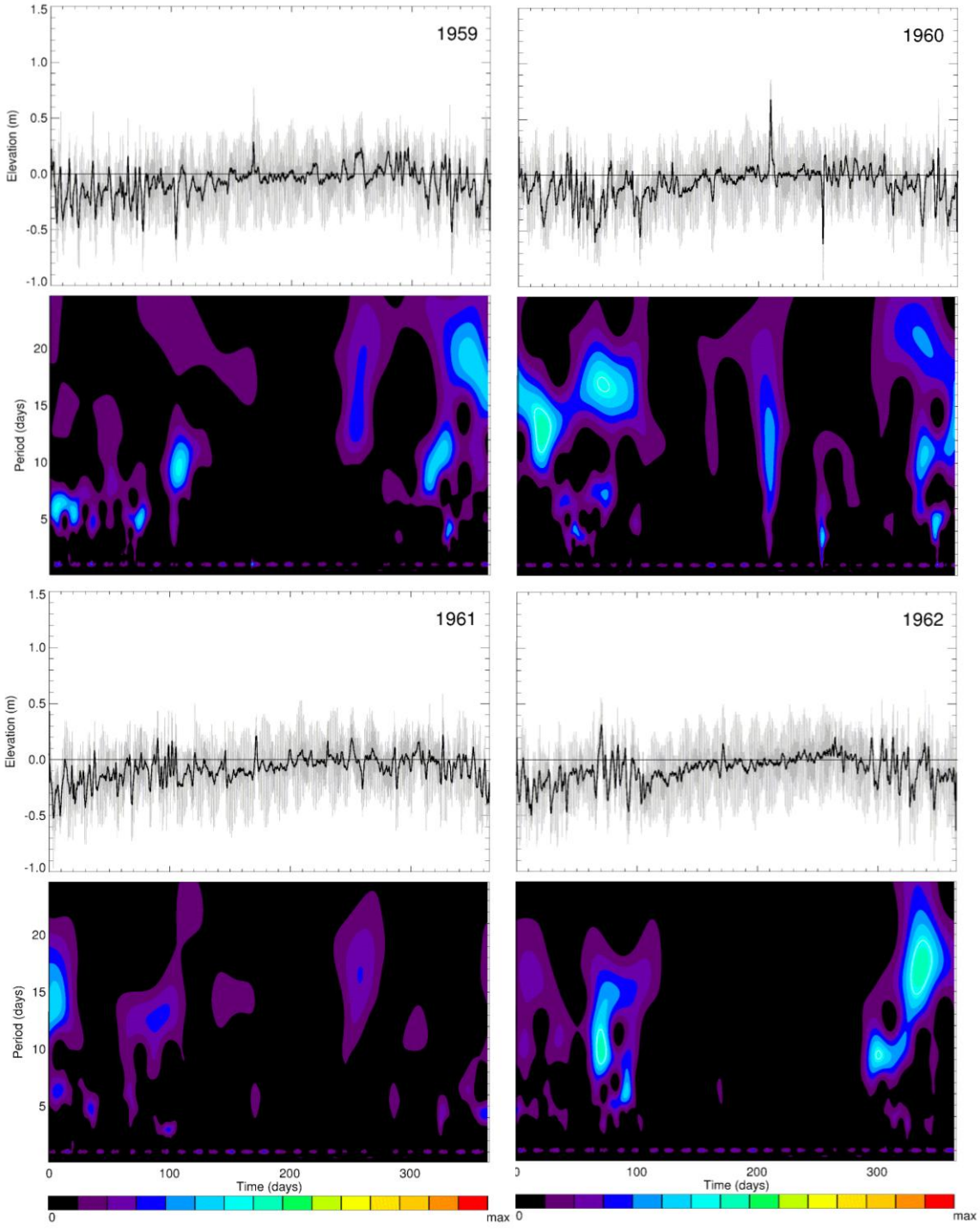

Figure A79. Same as figure A77, 1959-1962.

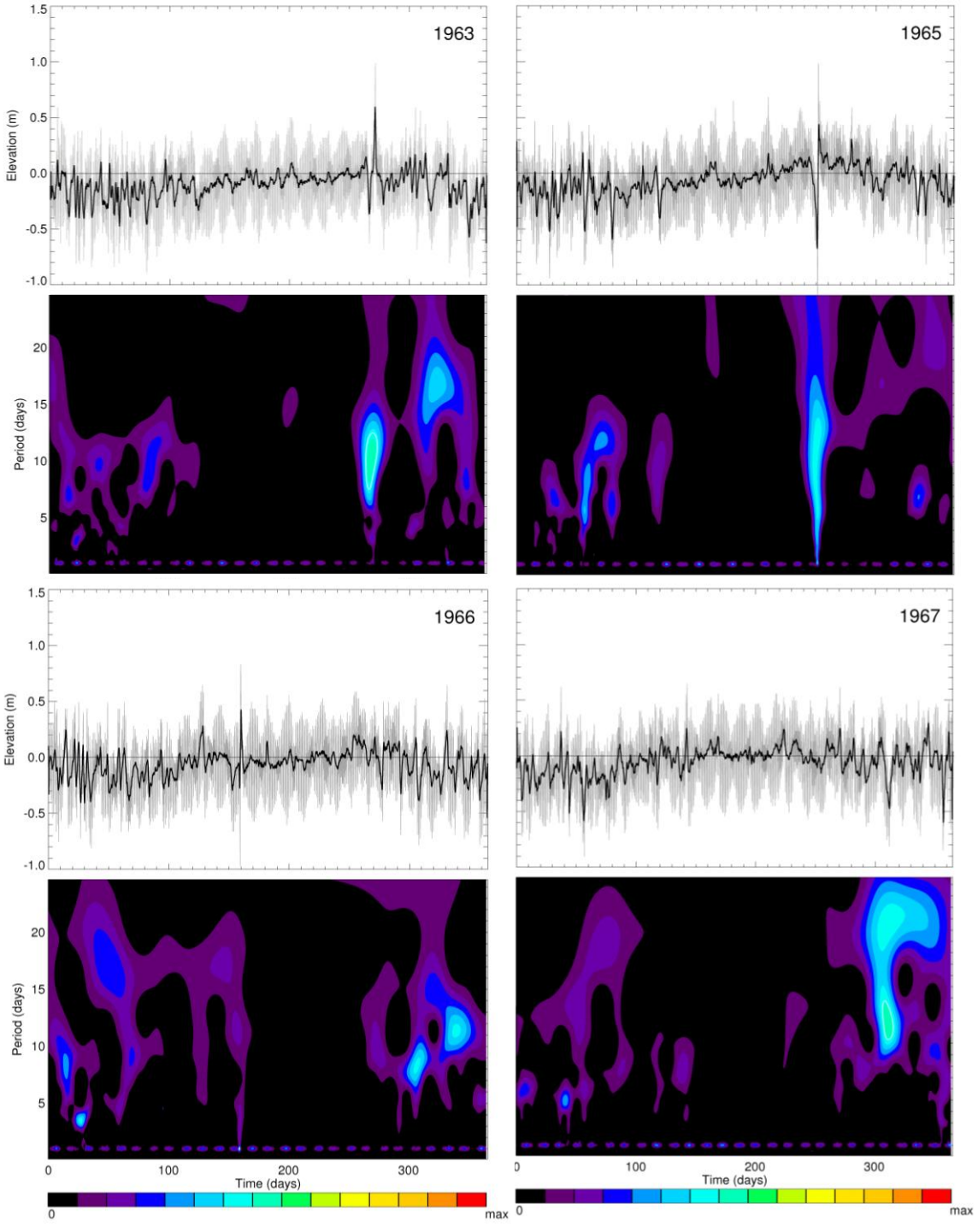

Figure A80. Same as A77, 1963, 1965, 1966, and 1967.

Appendix D (Continued)

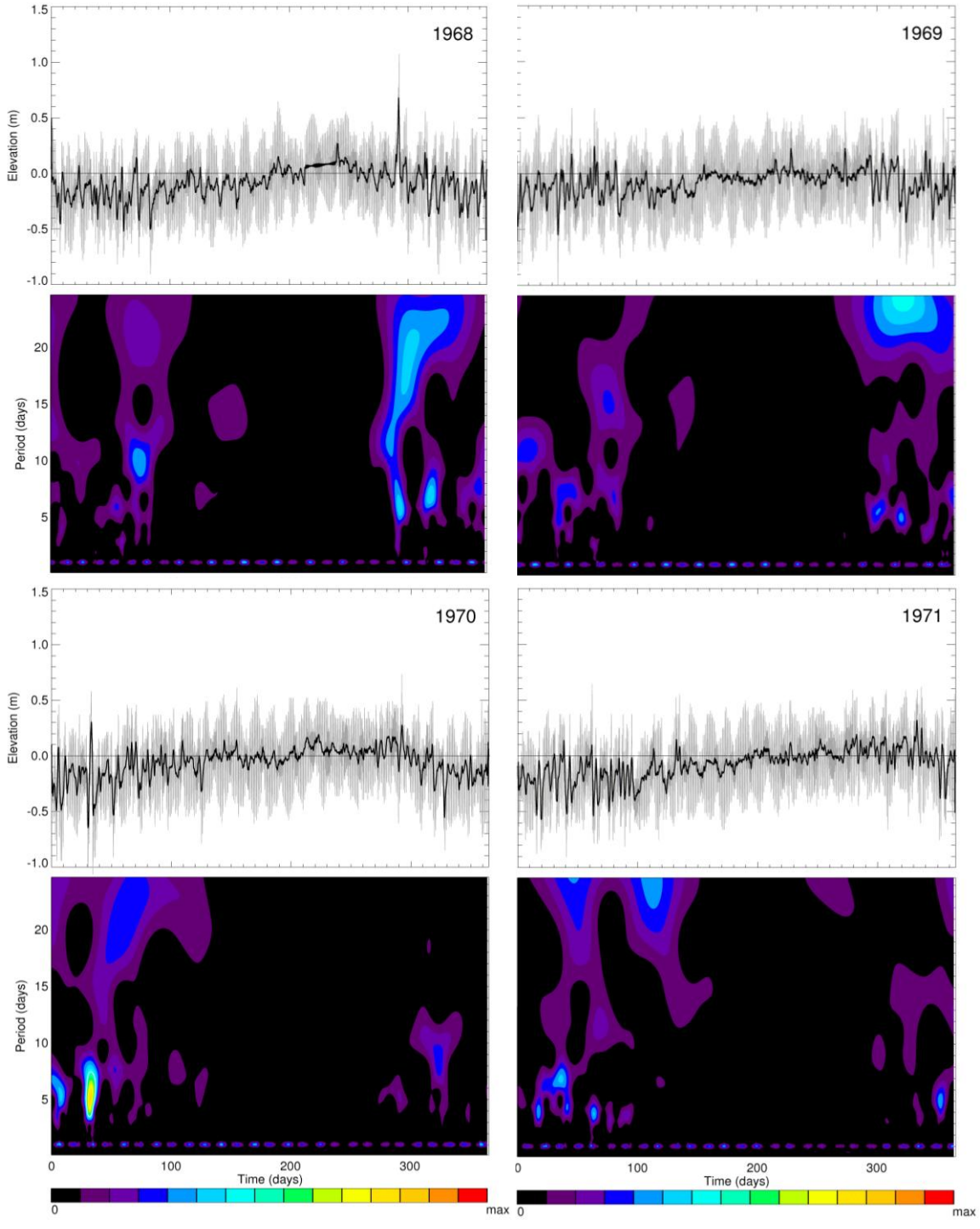

Figure A81. Same as figure A77, 1968-1971.

Appendix D (Continued)

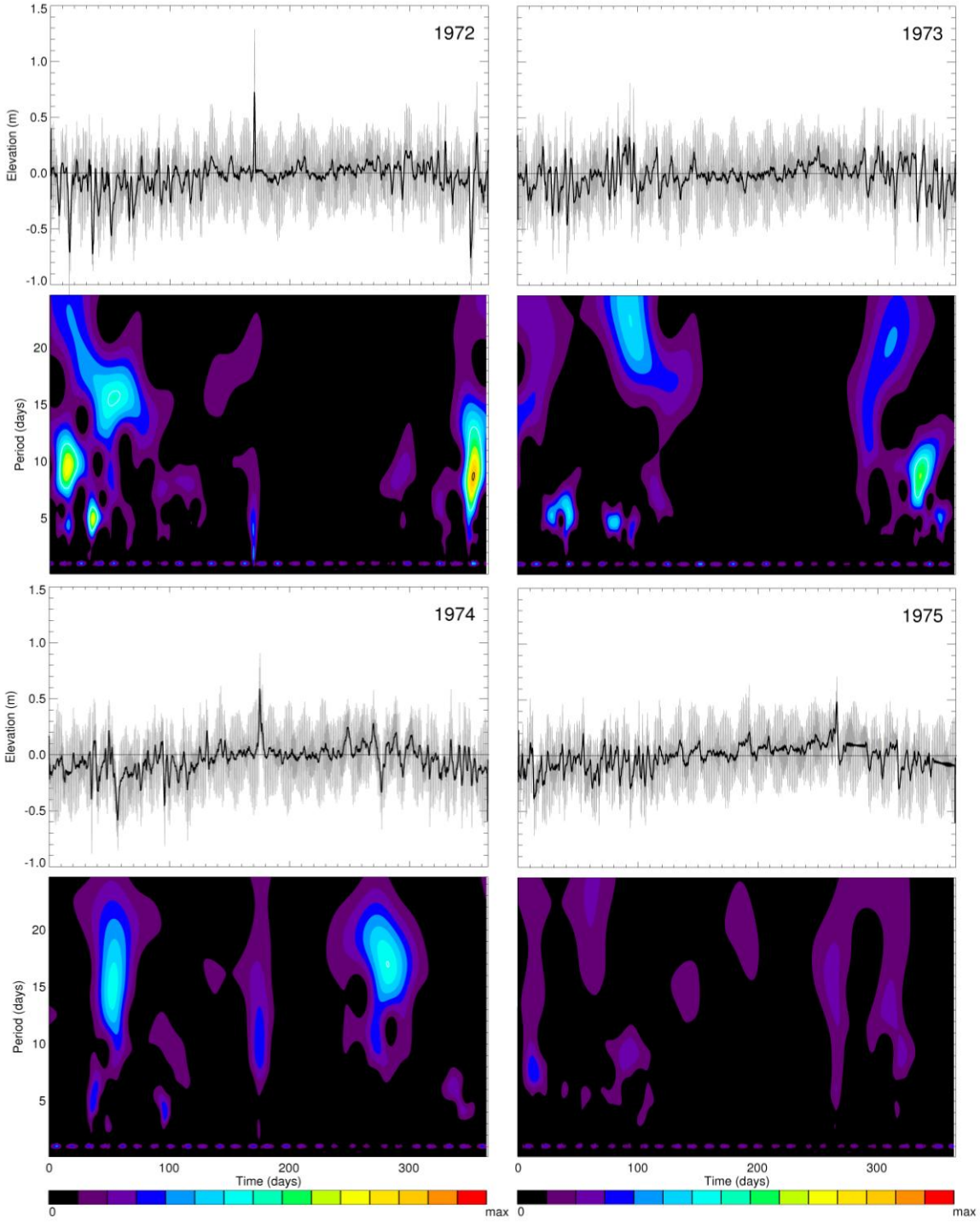

Figure A82. Same as figure A77, 1972-1975.

Appendix D (Continued)

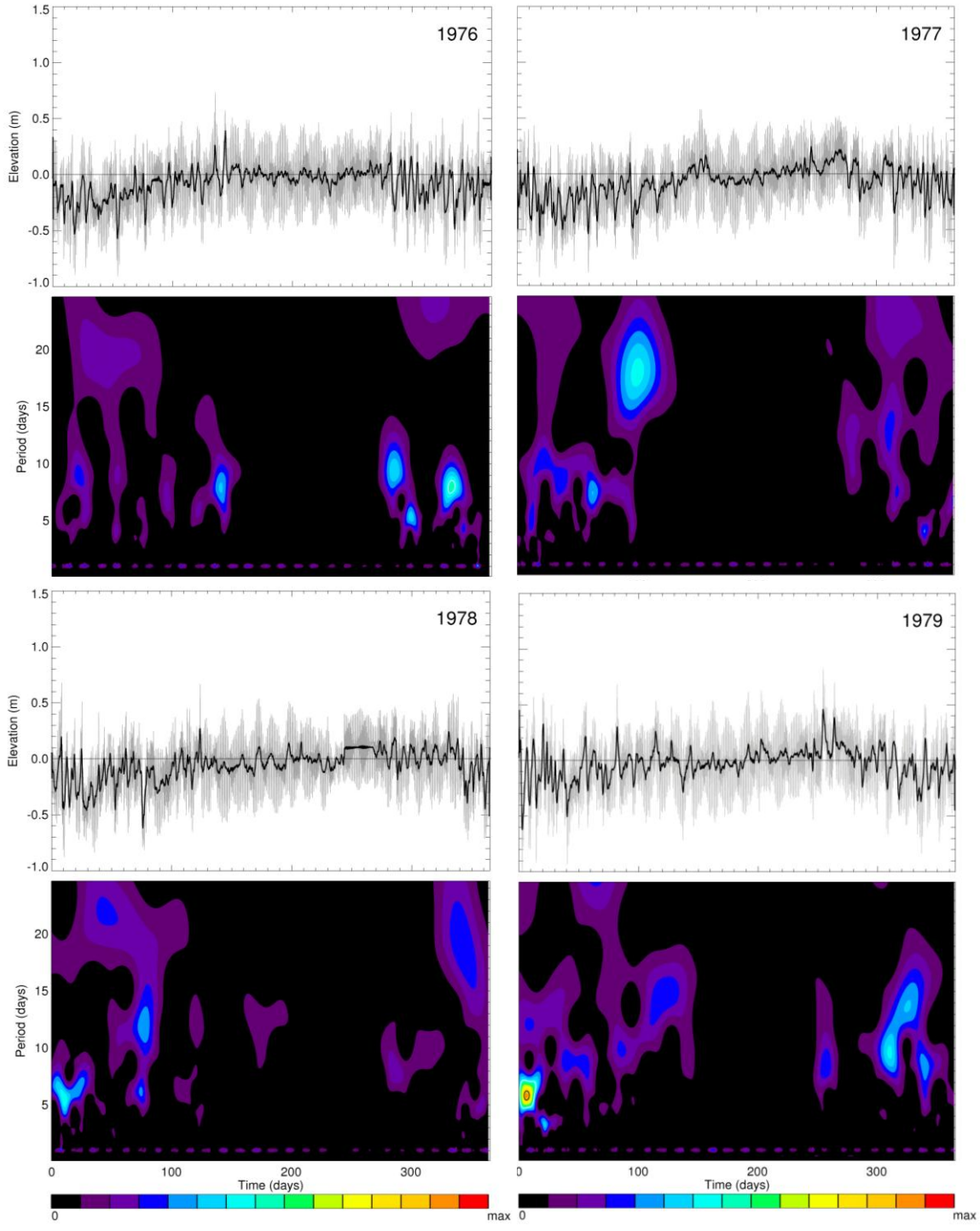

Figure A83. Same as figure A77, 1976-1979.

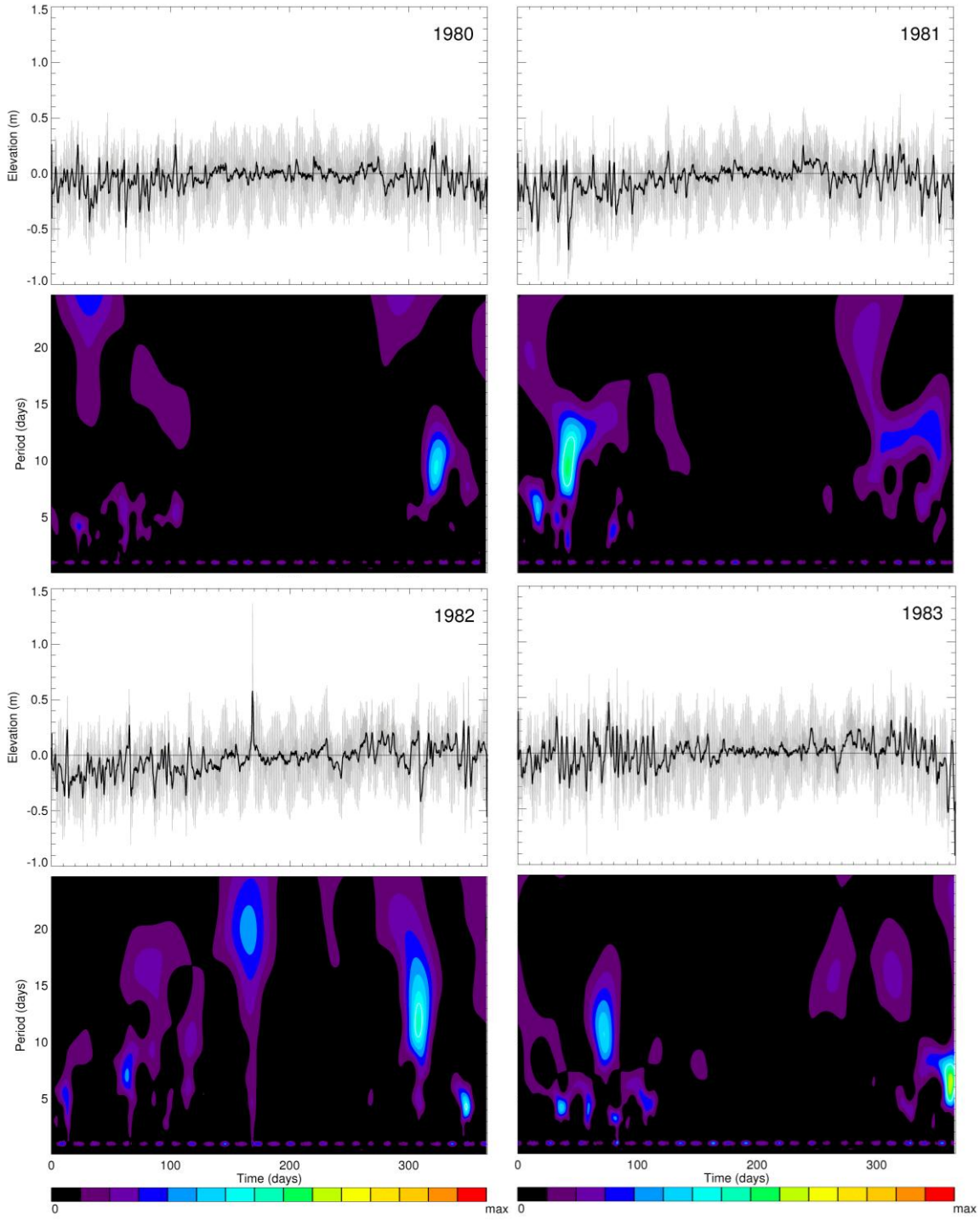

Figure A84. Same as figure A77, 1980-1983.

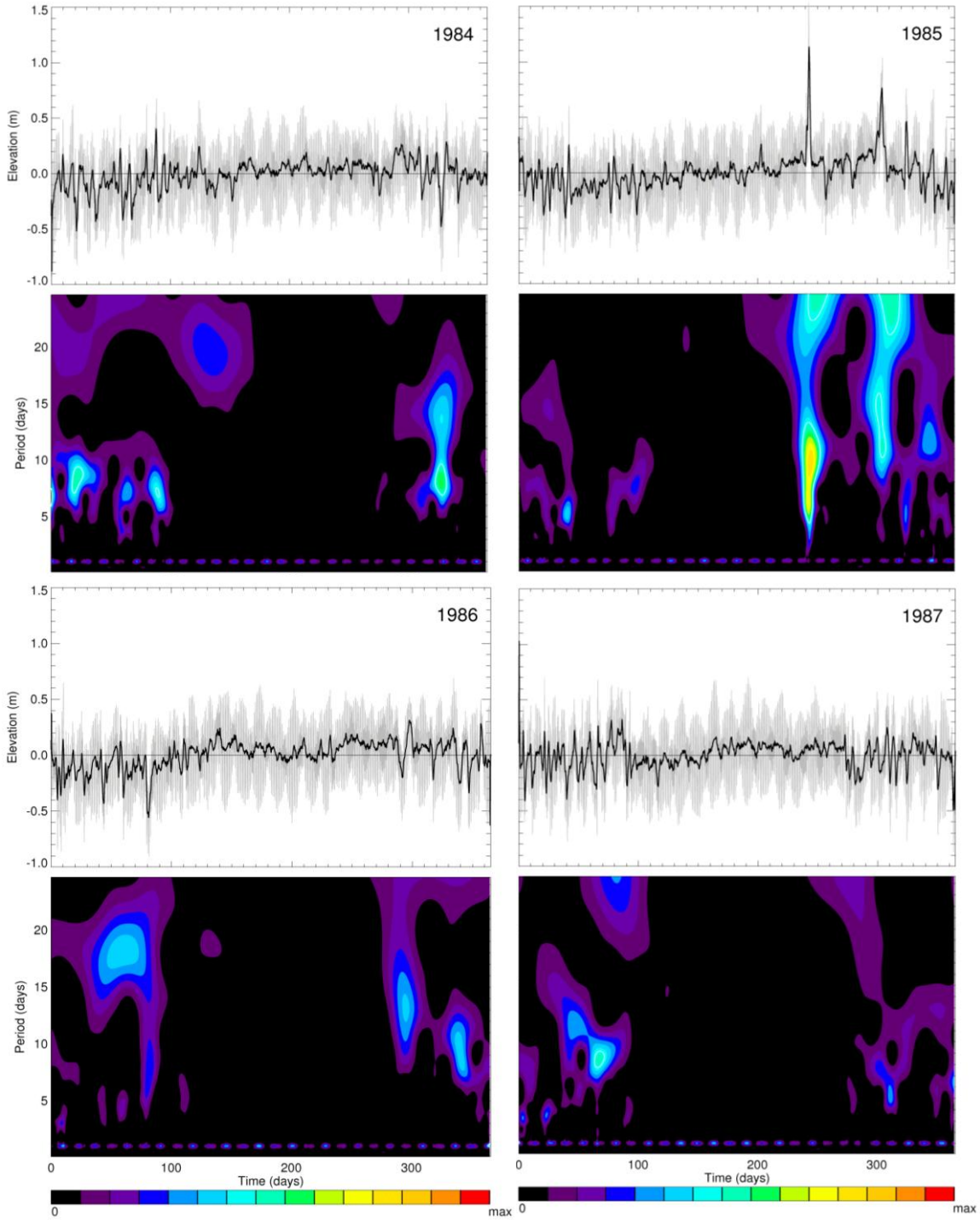

Figure A85. Same as figure A77, 1984-1987.

Appendix D (Continued)

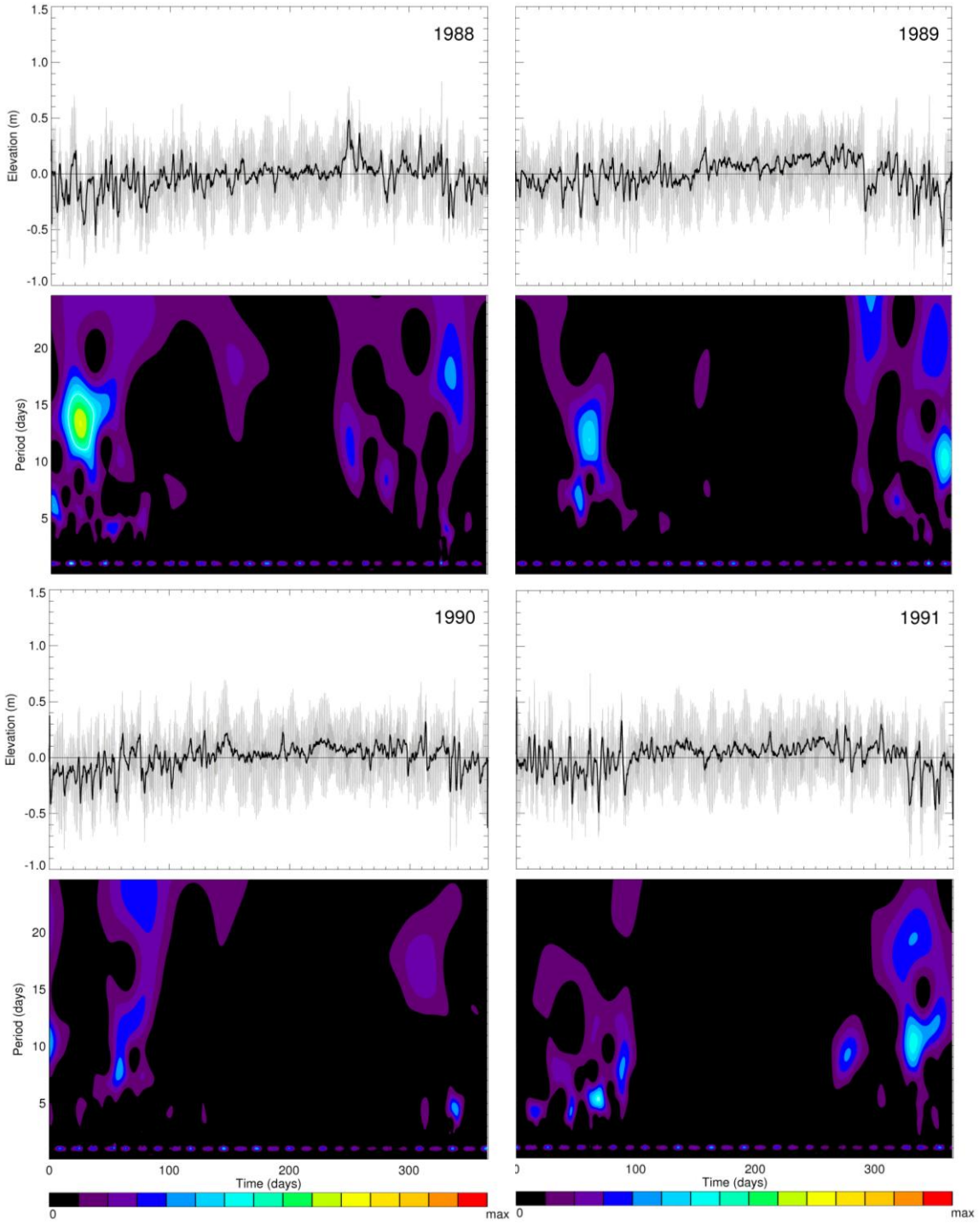

Figure A86. Same as figure A77, 1988-1991.

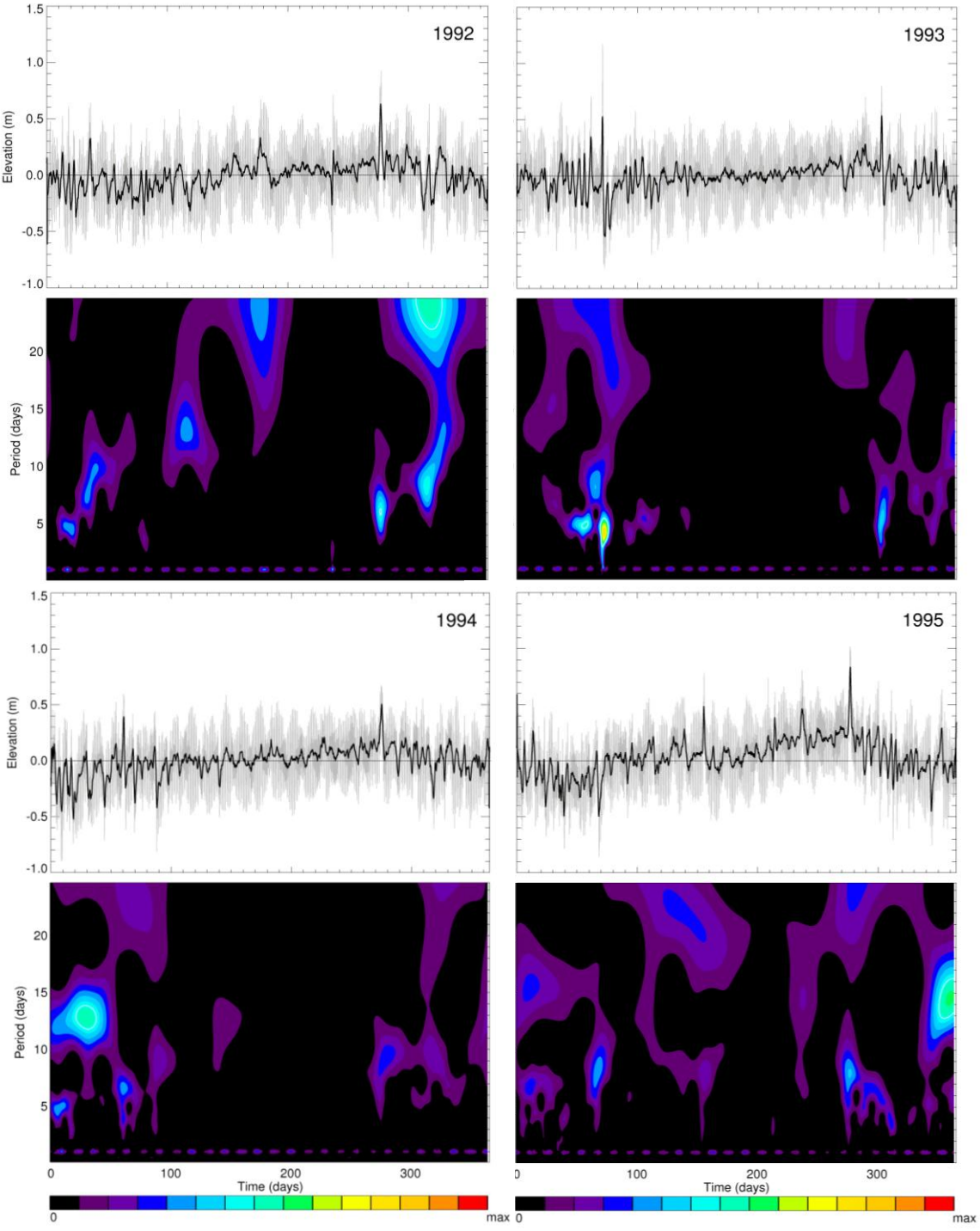

Figure A87. Same as figure A77, 1992-1995.

Appendix D (Continued)

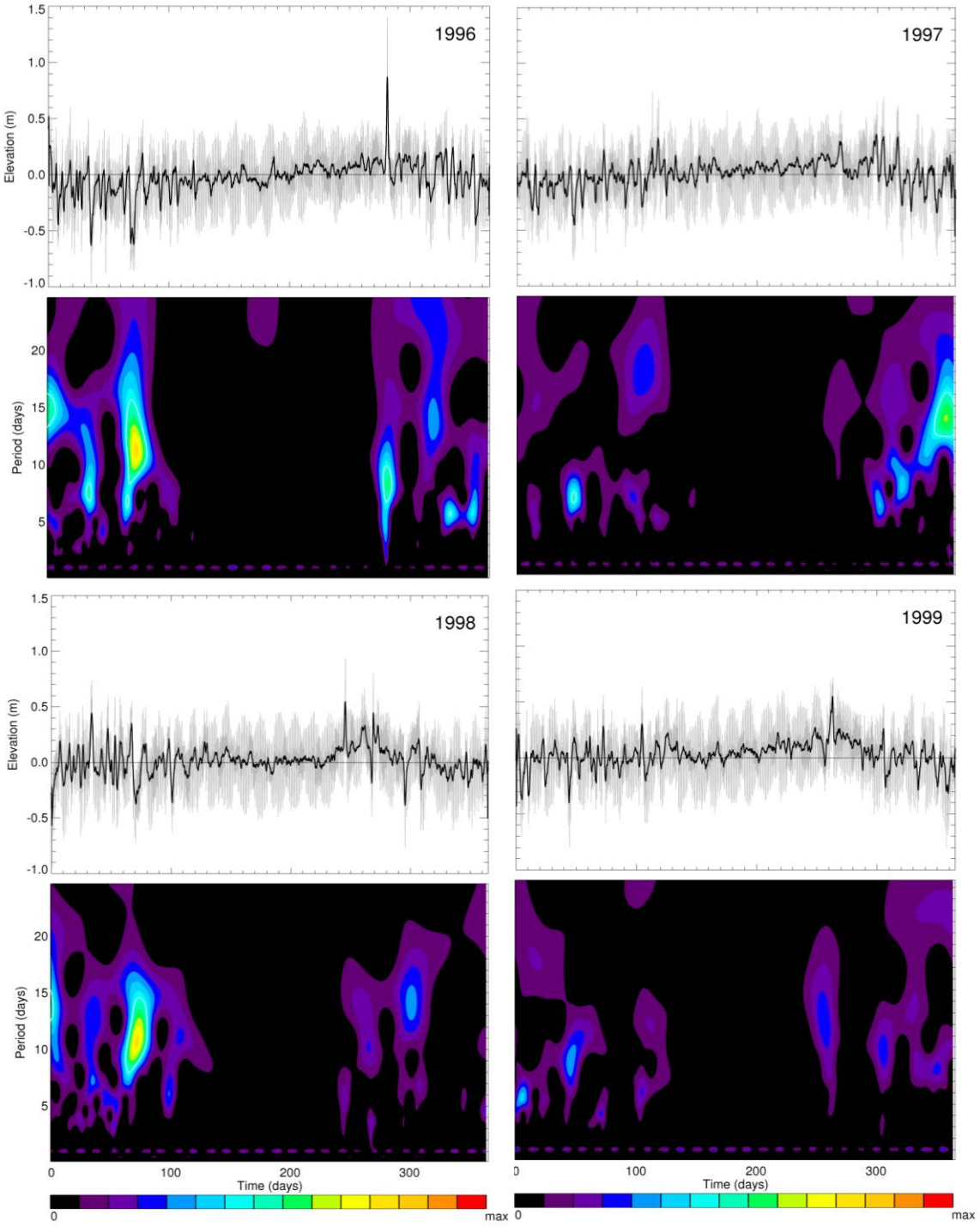

Figure A88. Same as figure A77, 1996-1999.

Appendix D (Continued)

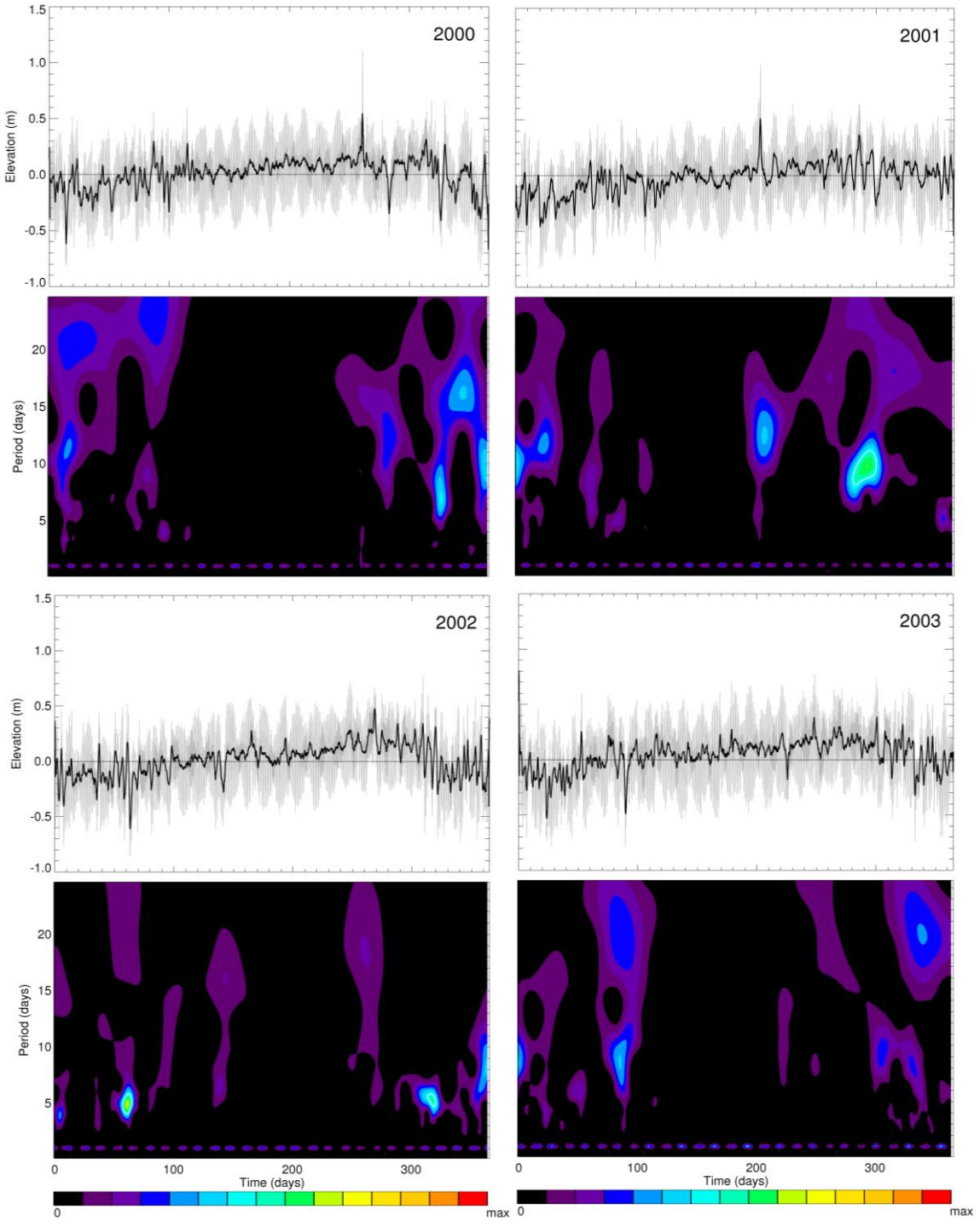

Figure A89. Same as figure A77, 2000-2003.

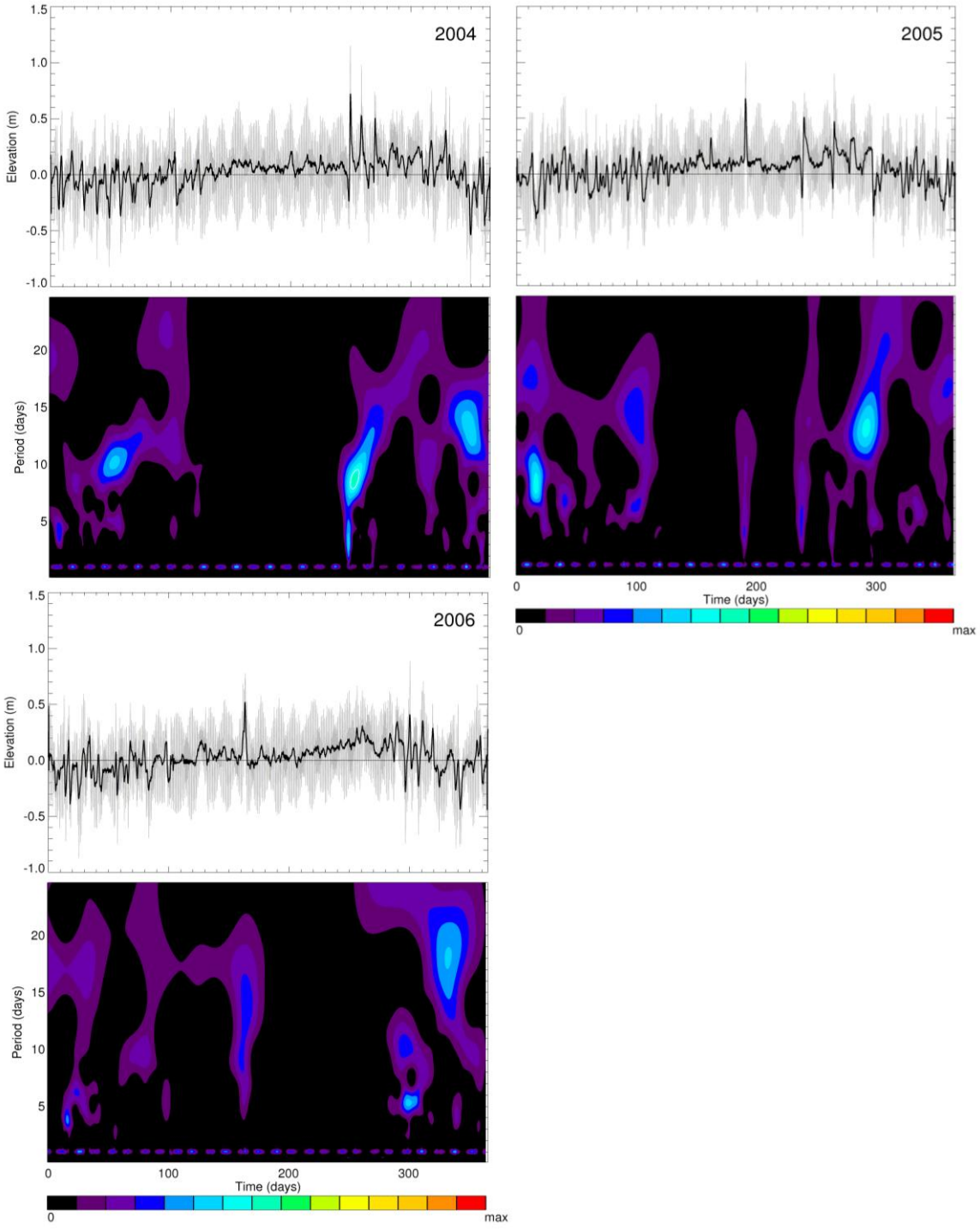

Figure A90. Same as figure A77, 2004-2006.

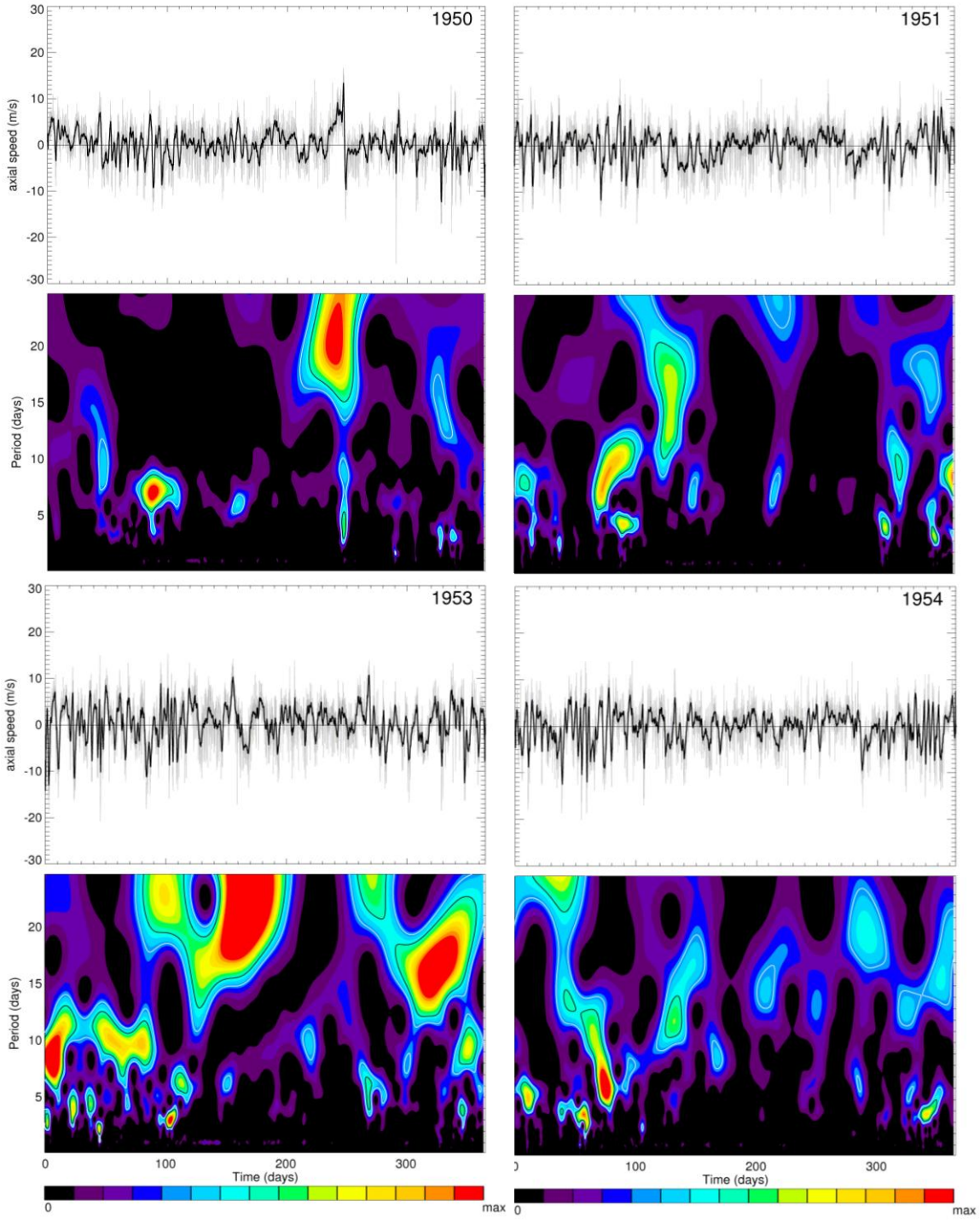

Figure A91. Instantaneous axial wind component (gray) and 25-hr smoothed axial wind component (thick black). Axial wind component wavelet transform for 1950, 1951, 1953, and 1954, with 95% significance levels (white lines) and 99% significance levels (black lines) shown.

Appendix D (Continued)

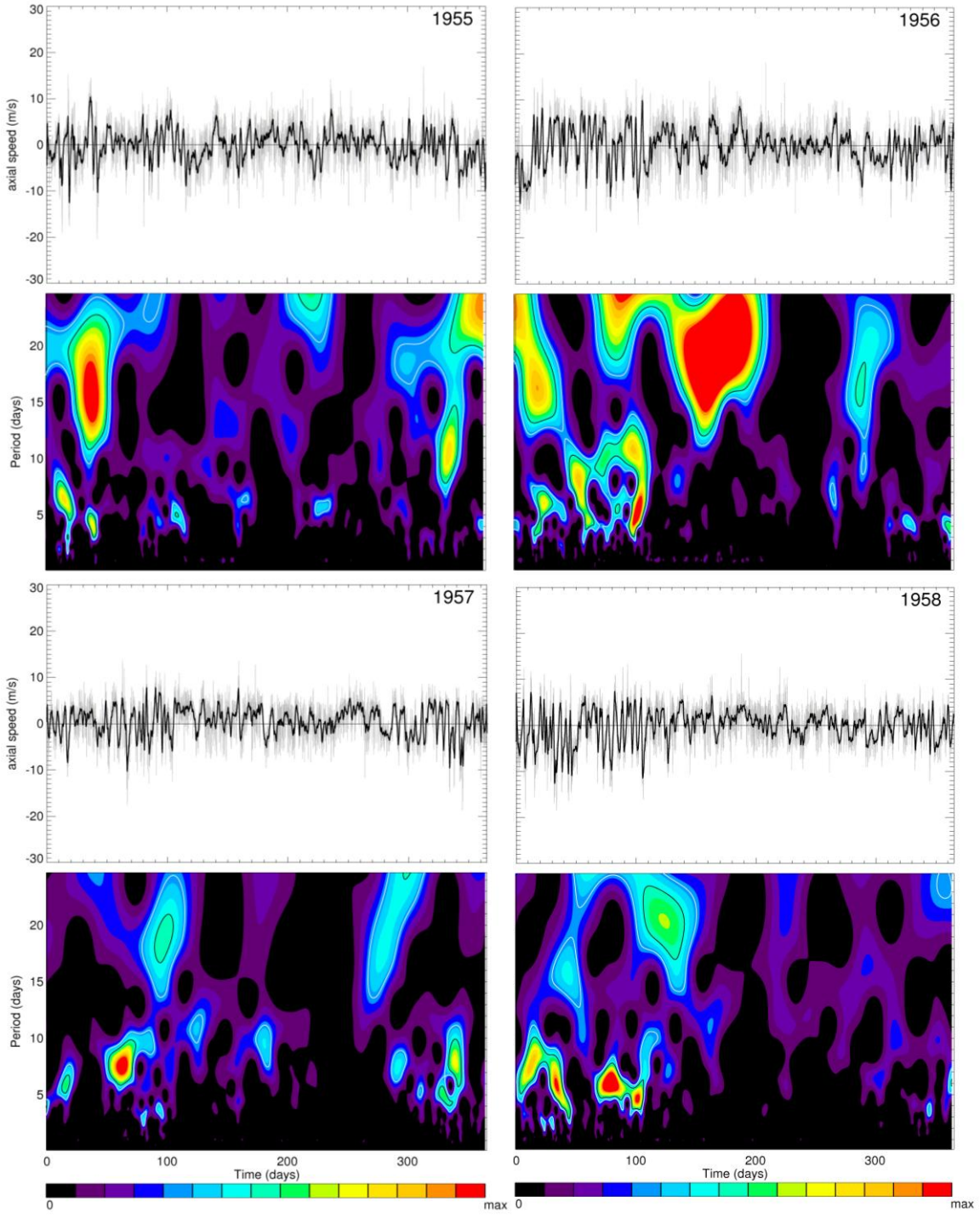

Figure A92. Same as figure A91, 1955-1958.

Appendix D (Continued)

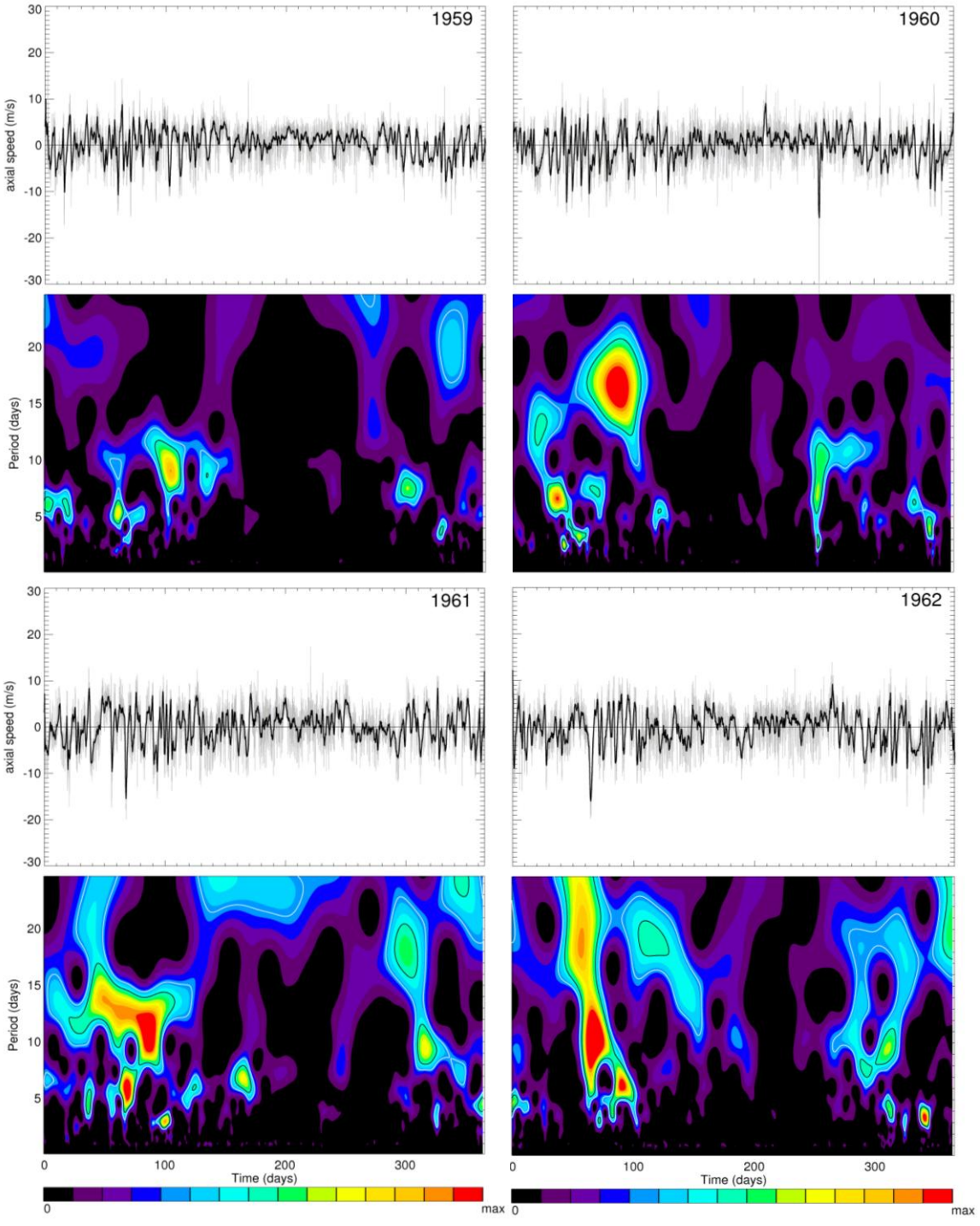

Figure A93. Same as figure A91, 1959-1962.

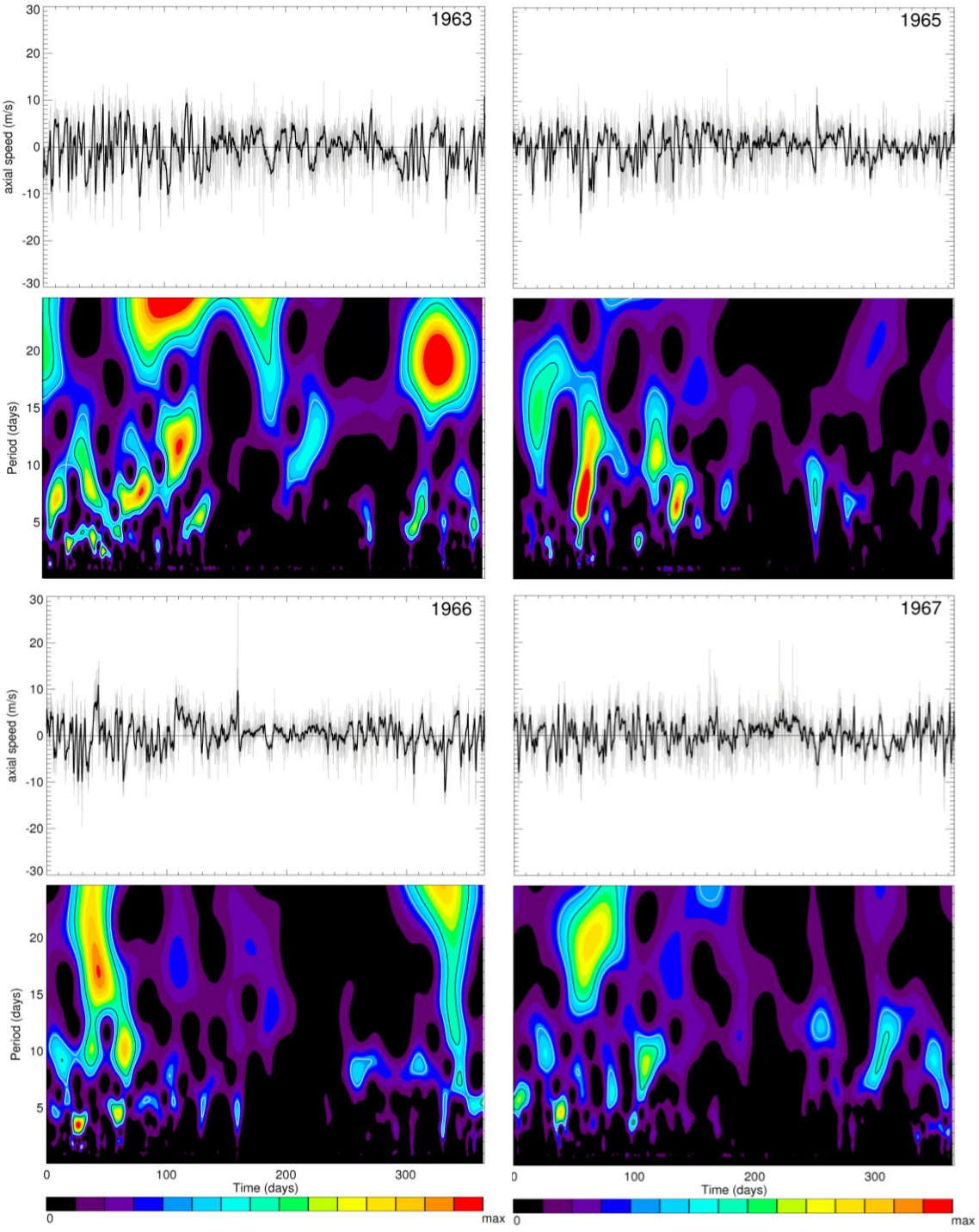

Figure A94. Same as figure A91, 1963, 1965, 1966, and 1967.

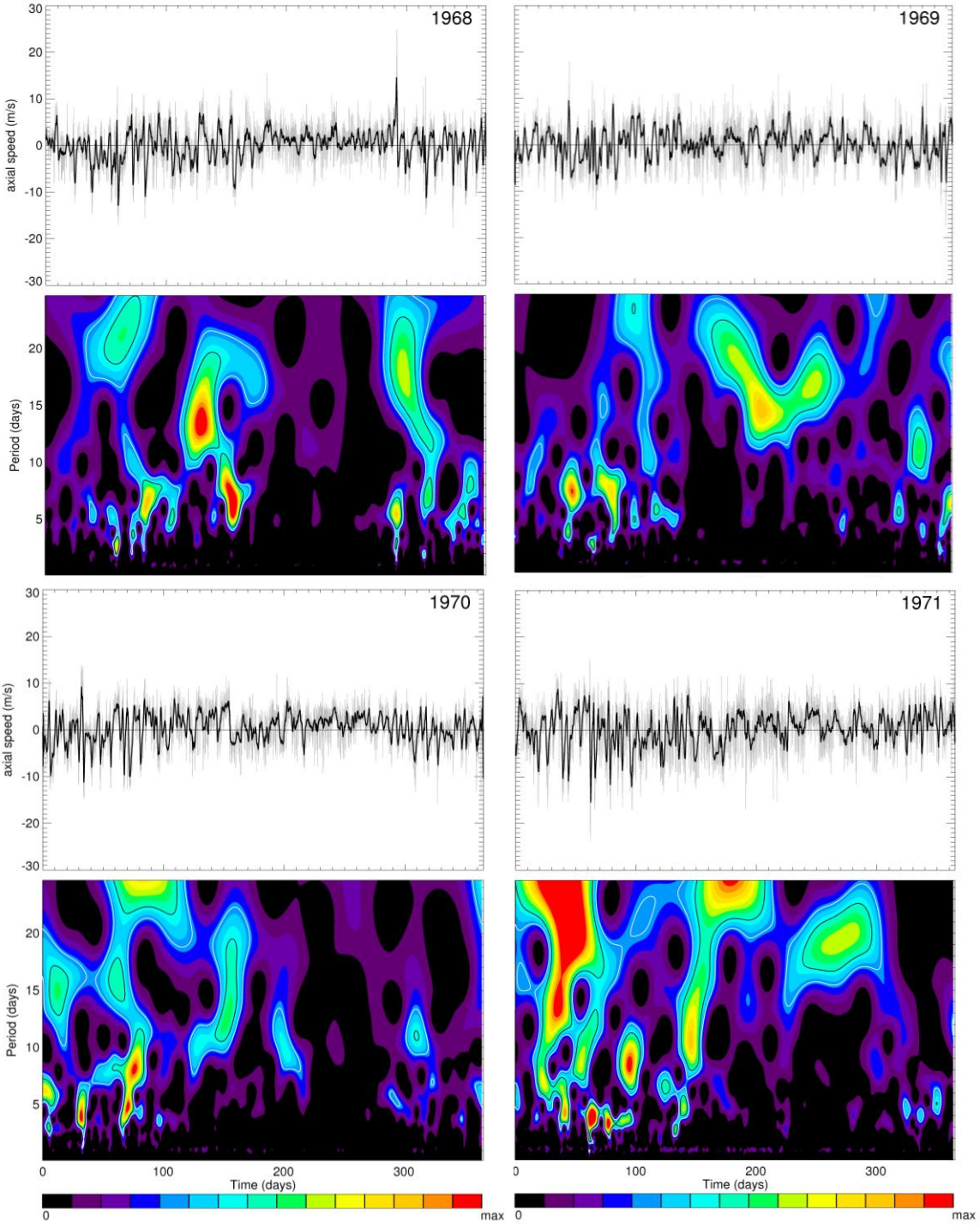

Figure A95. Same as figure A91, 1968-1971.

Appendix D (Continued)

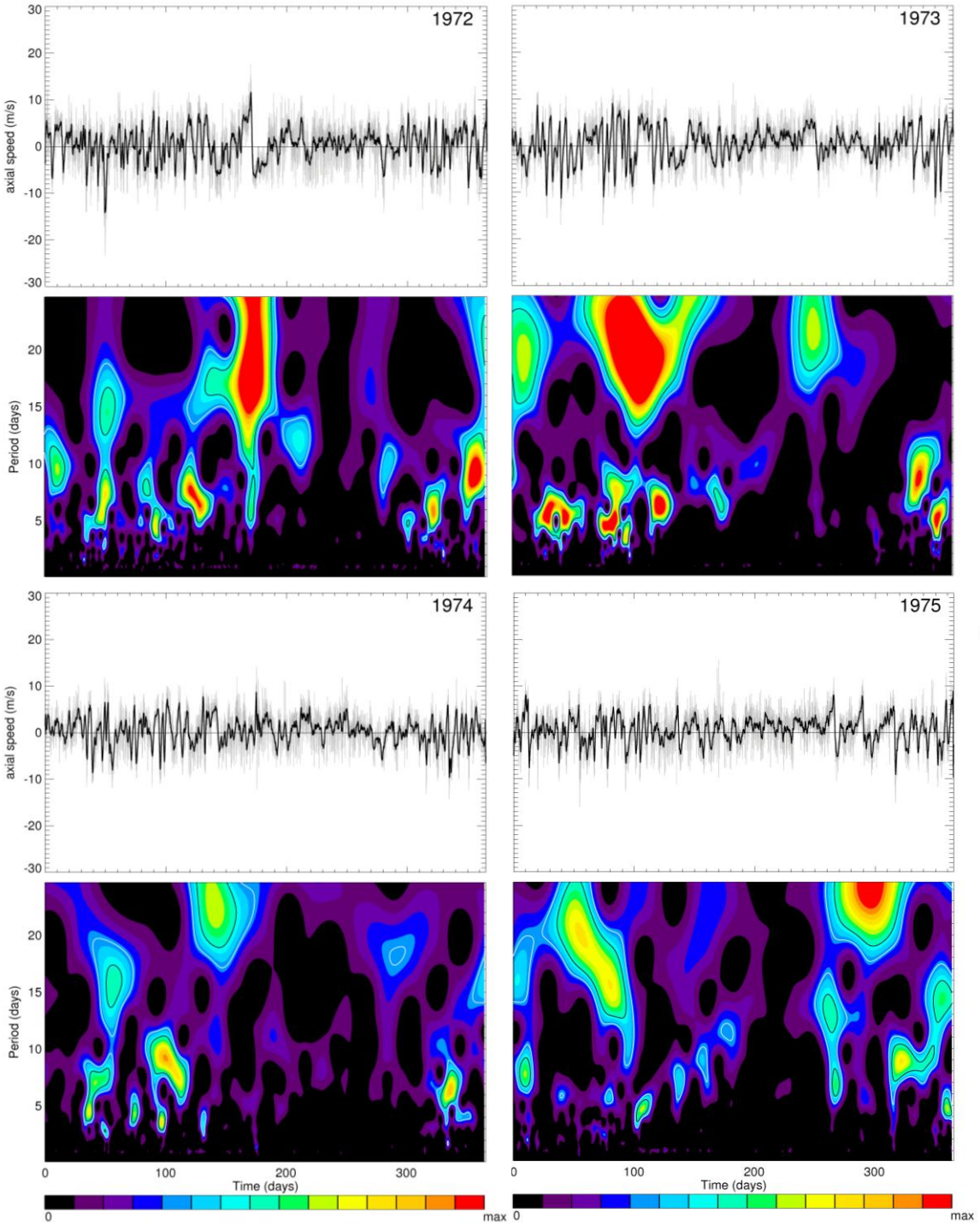

Figure A96. Same as figure A91, 1972-1975.

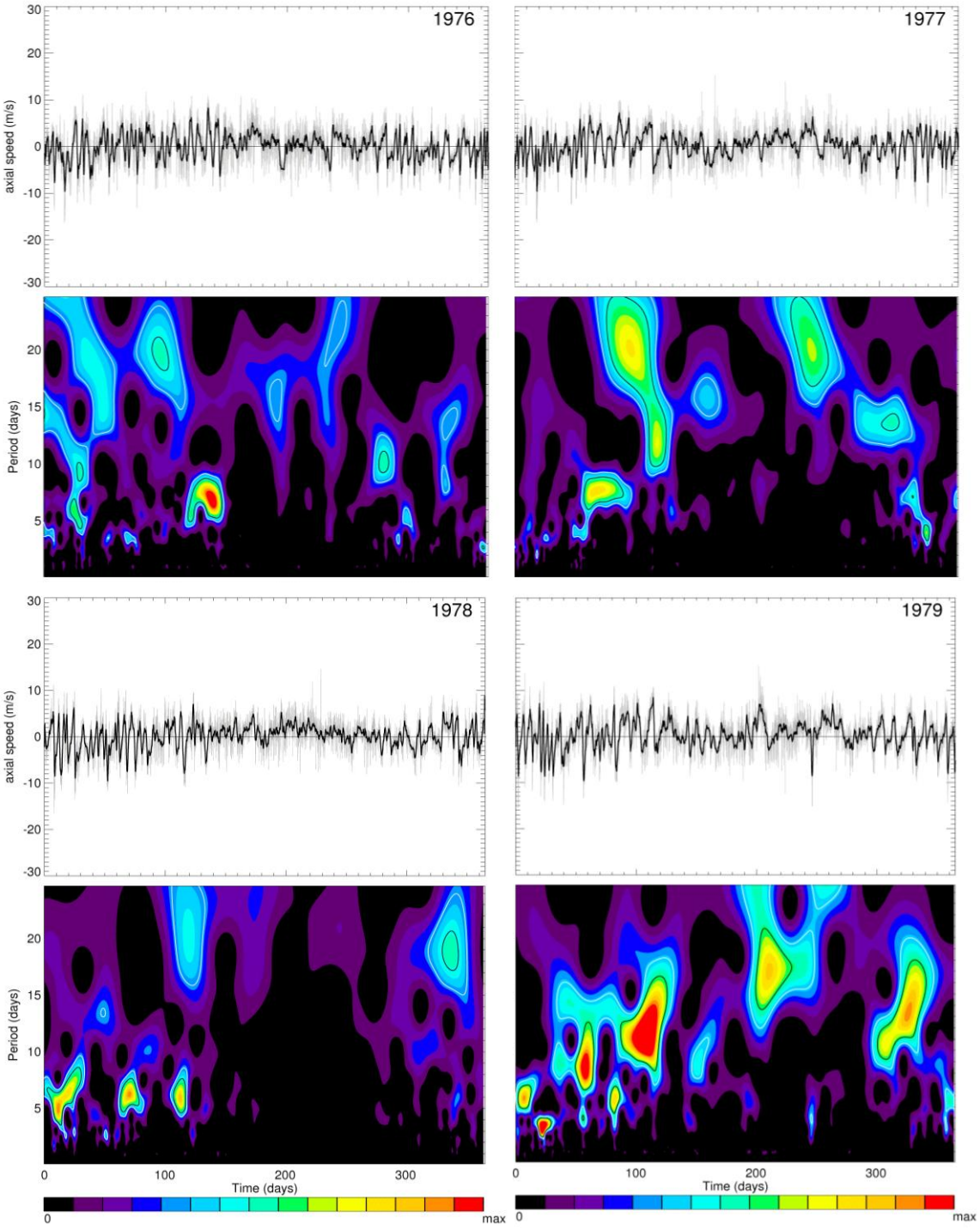

Figure A97. Same as figure A91, 1976-1979.

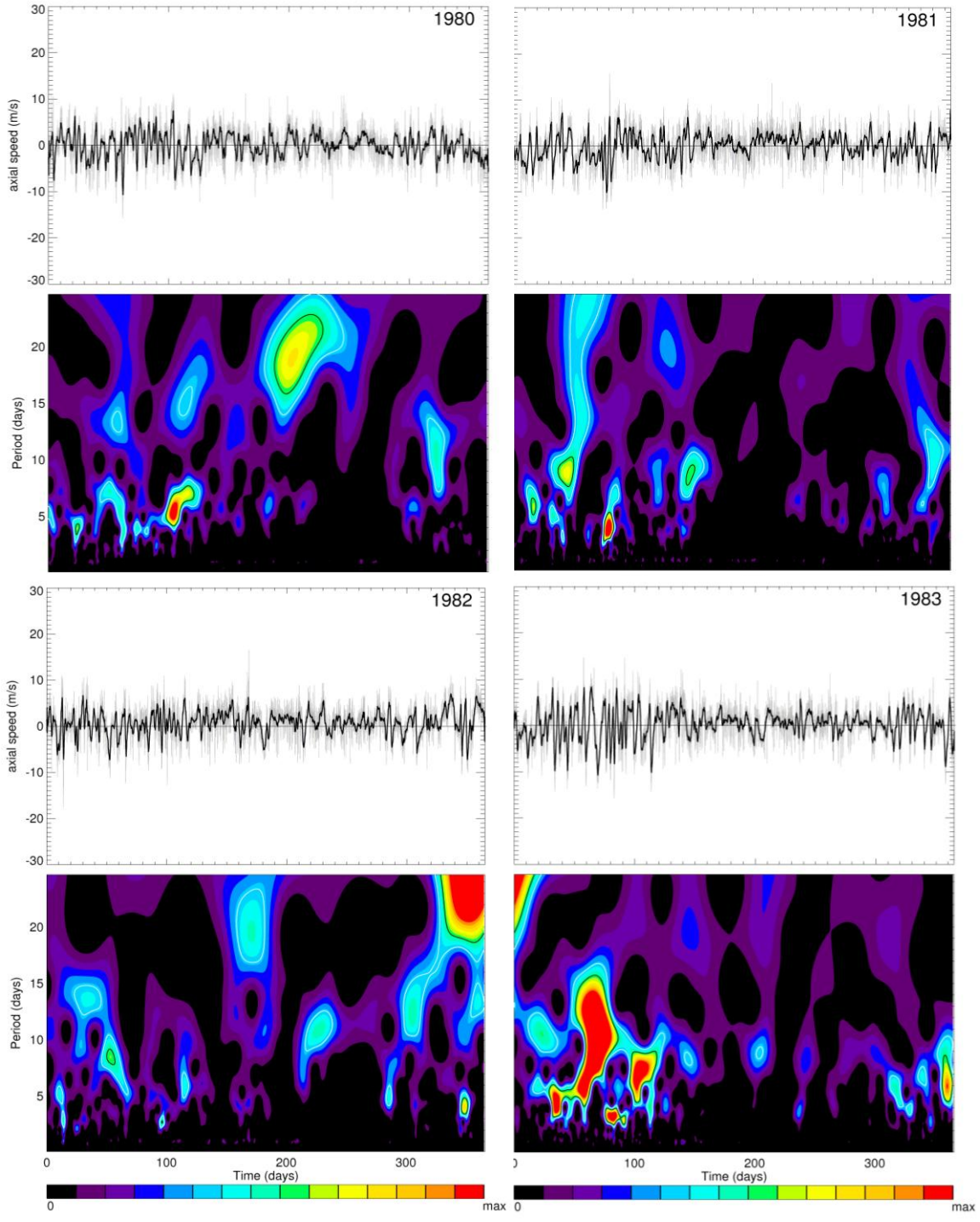

Figure A98. Same as figure A91, 1980-1983.

Appendix D (Continued)

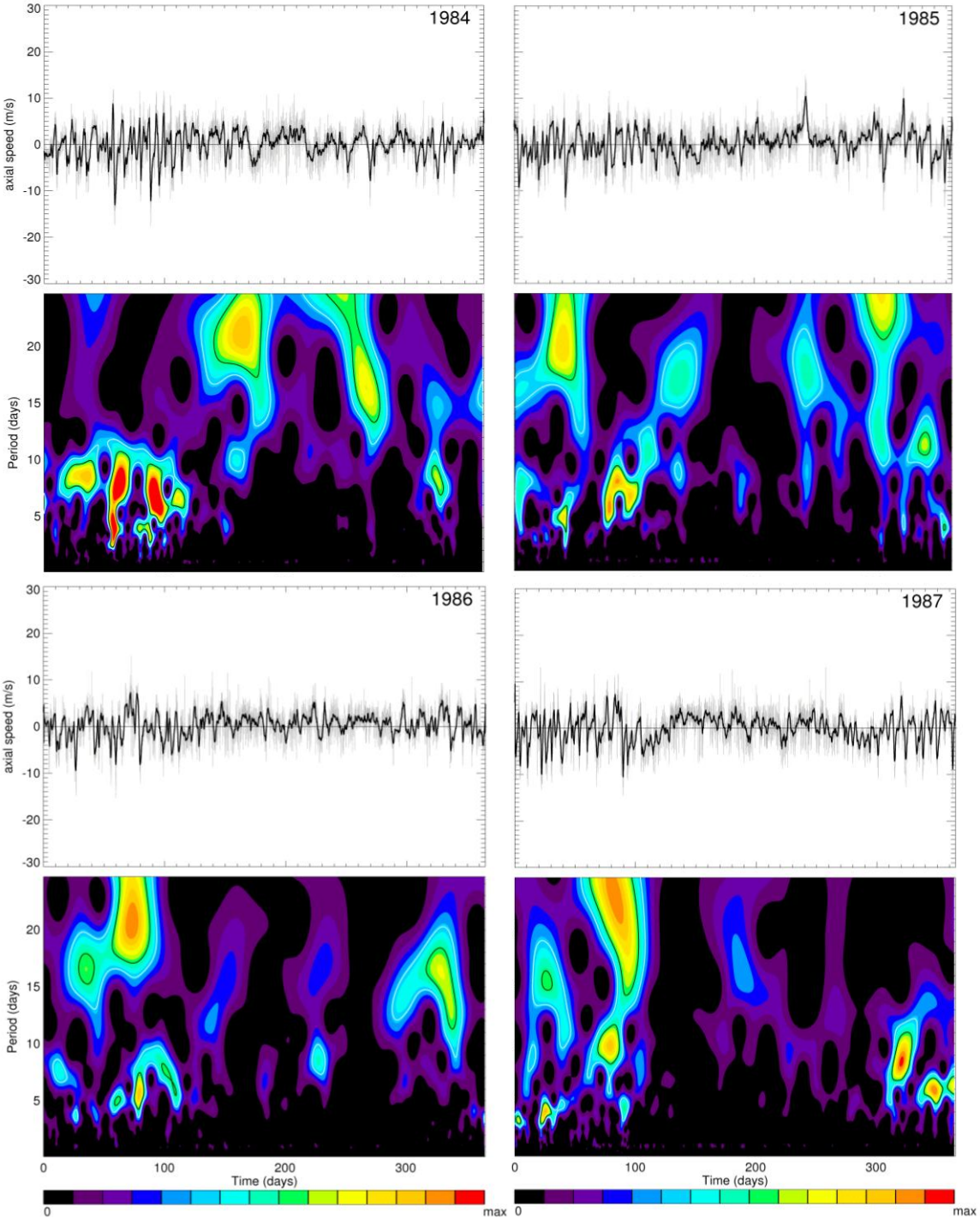

Figure A99. Same as figure A91, 1984-1987.

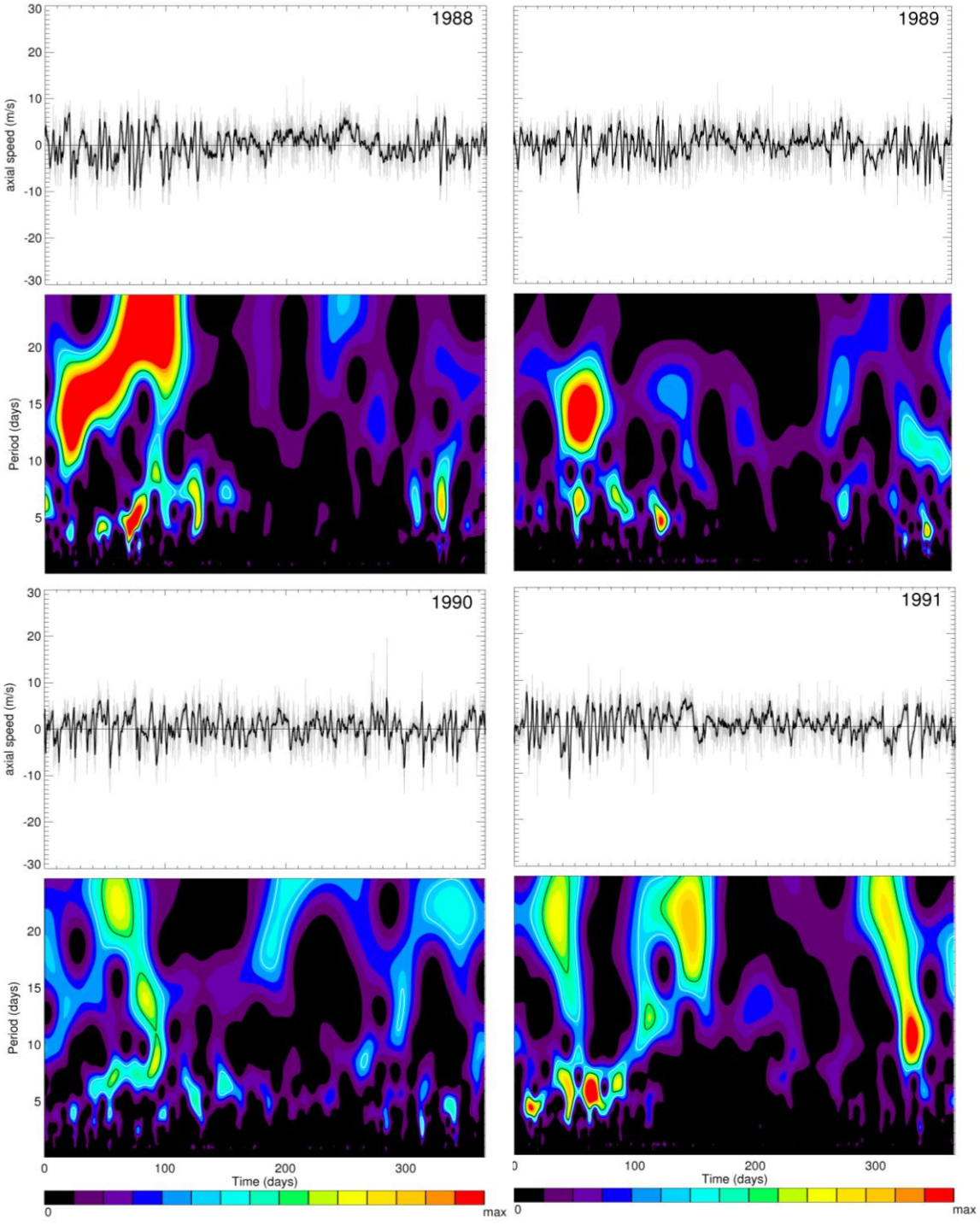

Figure A100. Same as figure A91, 1988-1991.

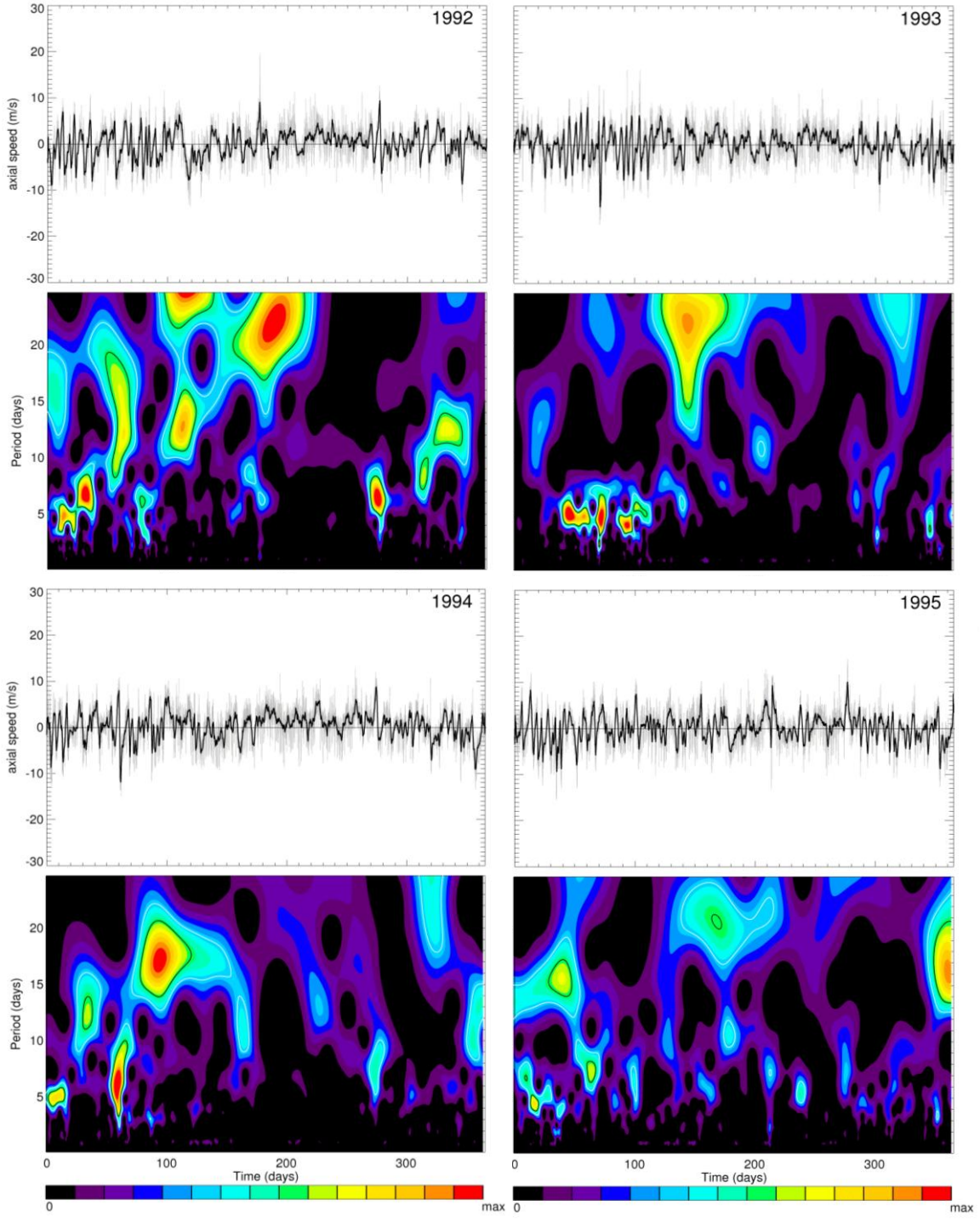

Figure A101. Same as figure A91, 1992-1995.

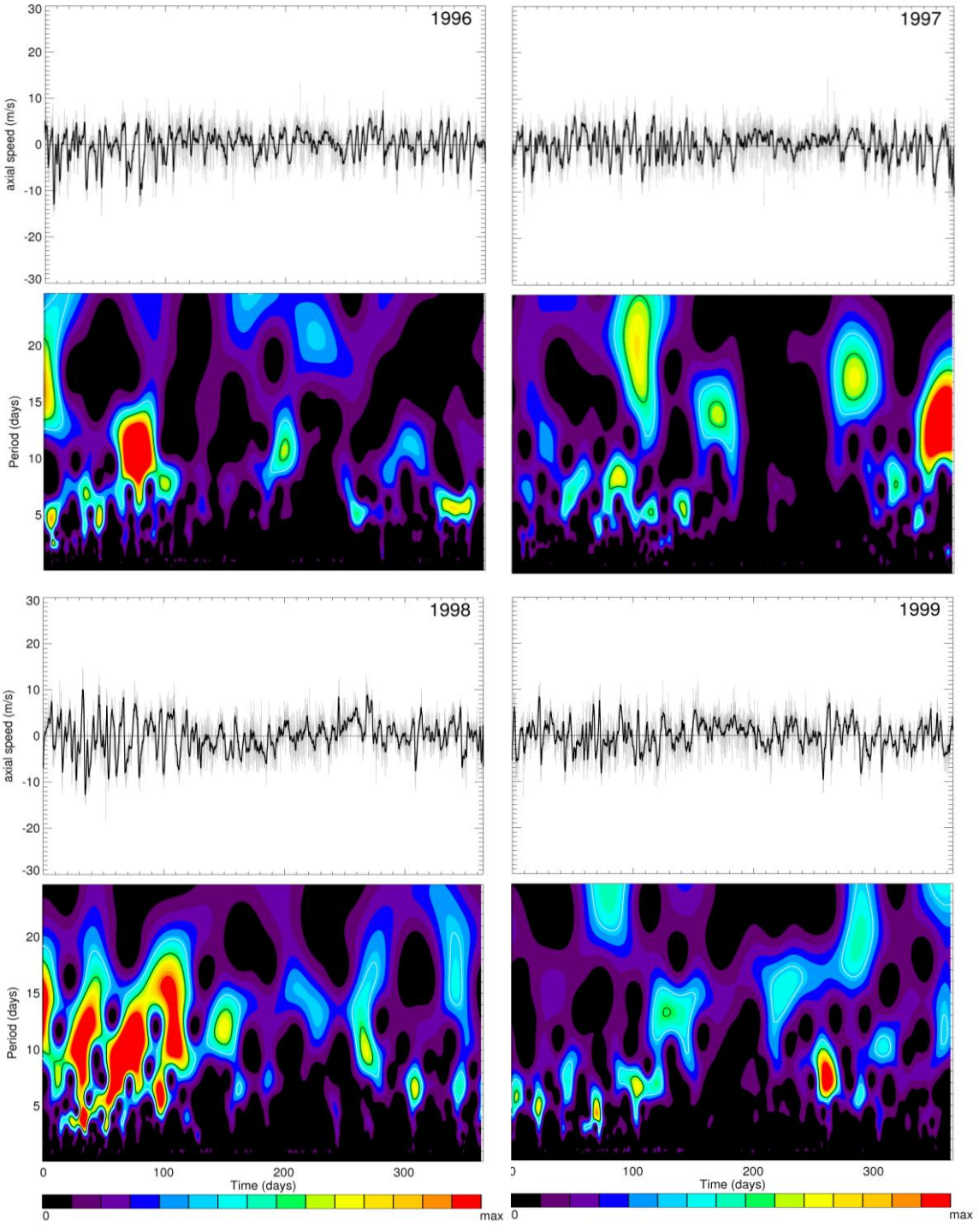

Figure A102. Same as figure A91, 1996-1999.

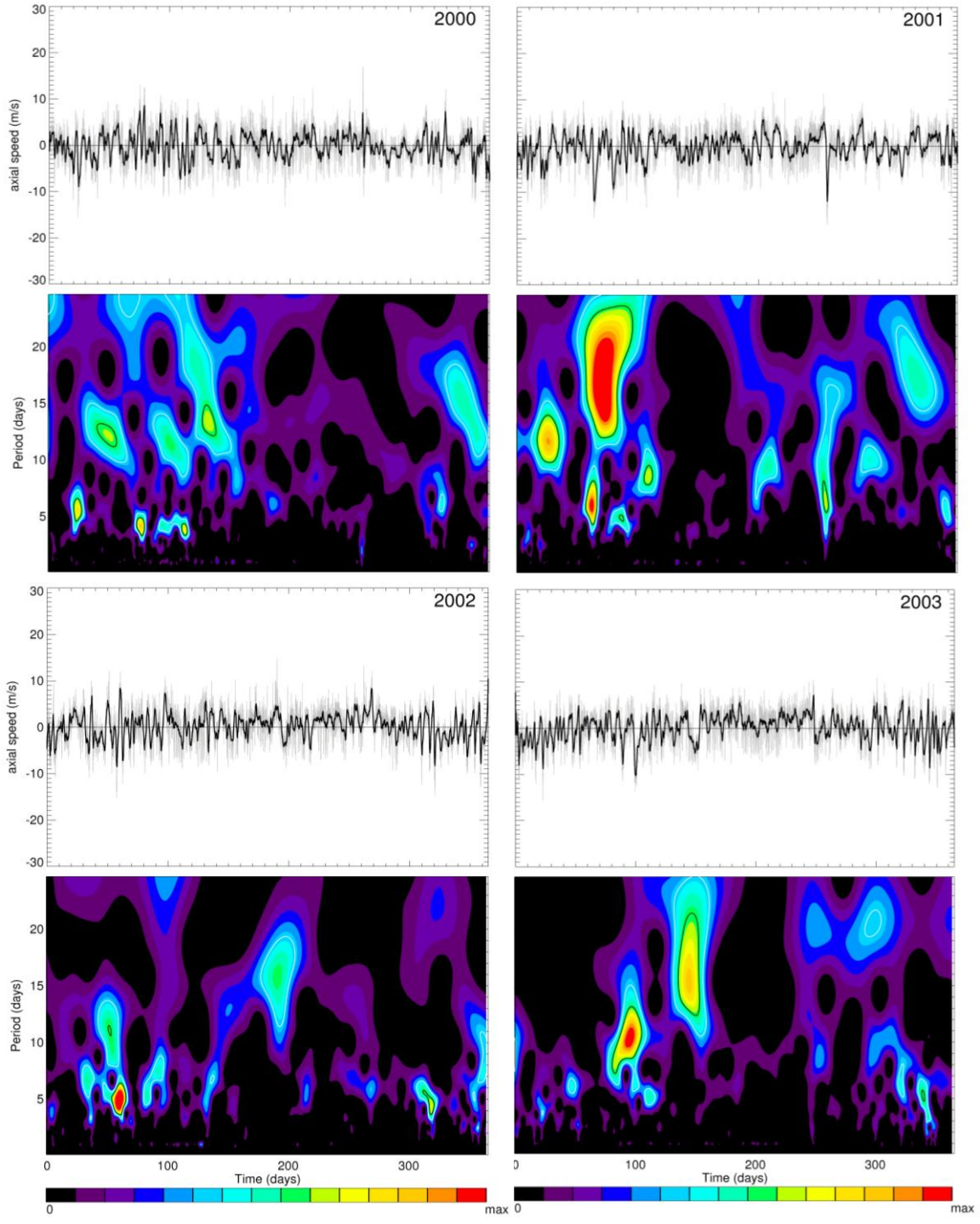

Figure A103. Same as figure A91, 2000-2003.

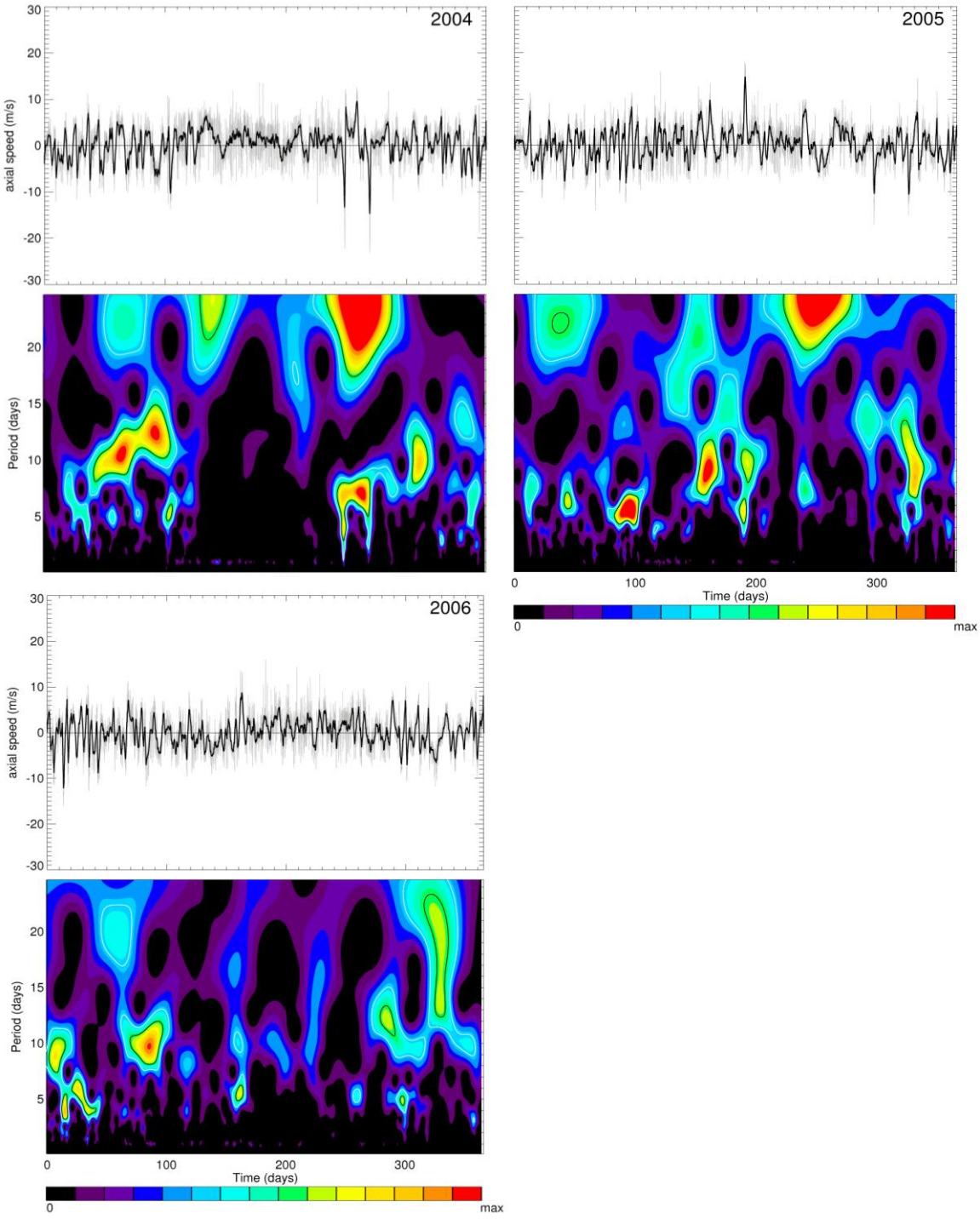

Figure A104. Same as figure A91, 2004-2006.

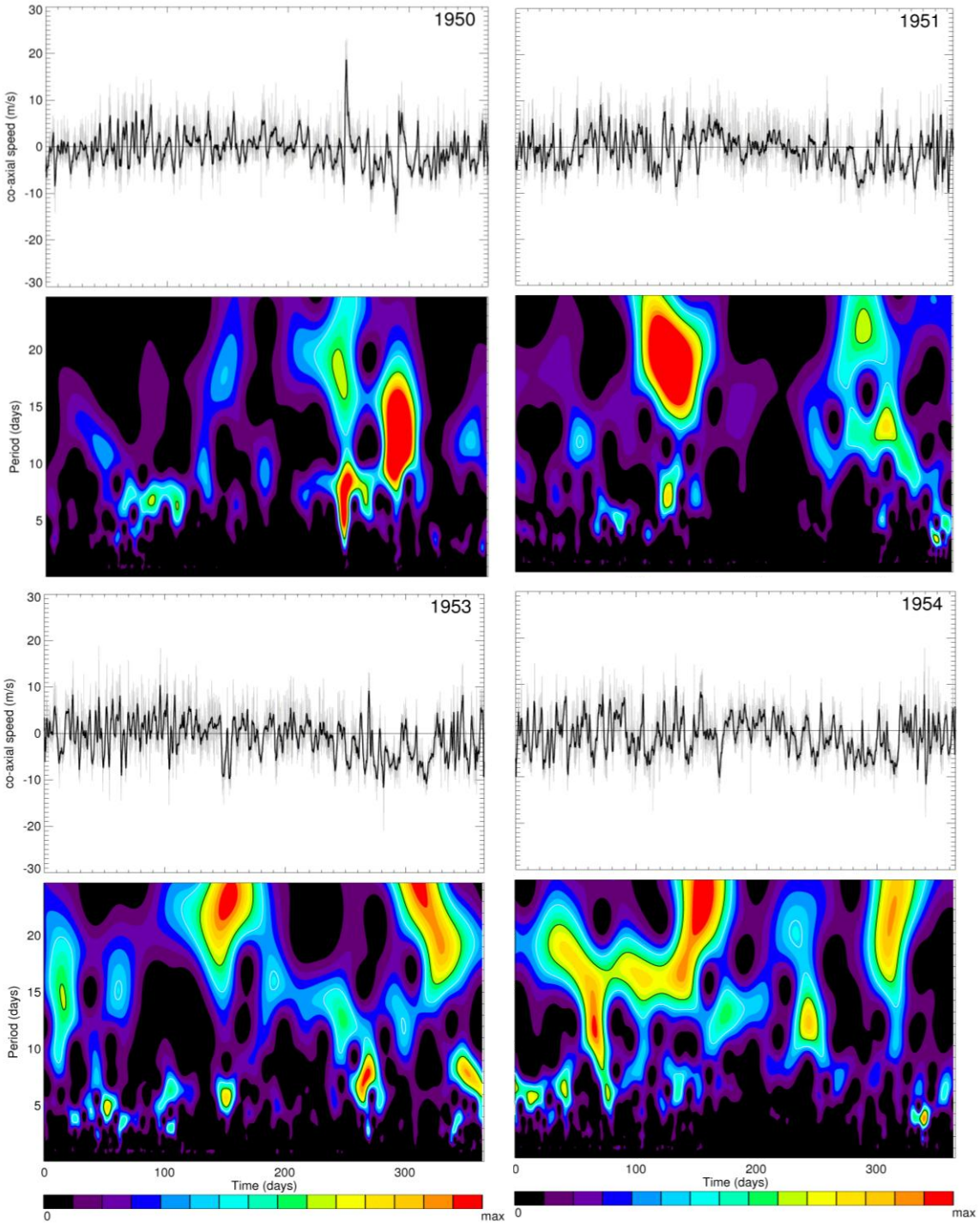

Figure A105. Instantaneous co-axial wind component (gray) and 25-hr smoothed co-axial wind component (thick black). Co-axial wind component wavelet transform for 1950, 1951, 1953, and 1954, with 95% significance levels (white lines) and 99% significance levels (black lines) shown.

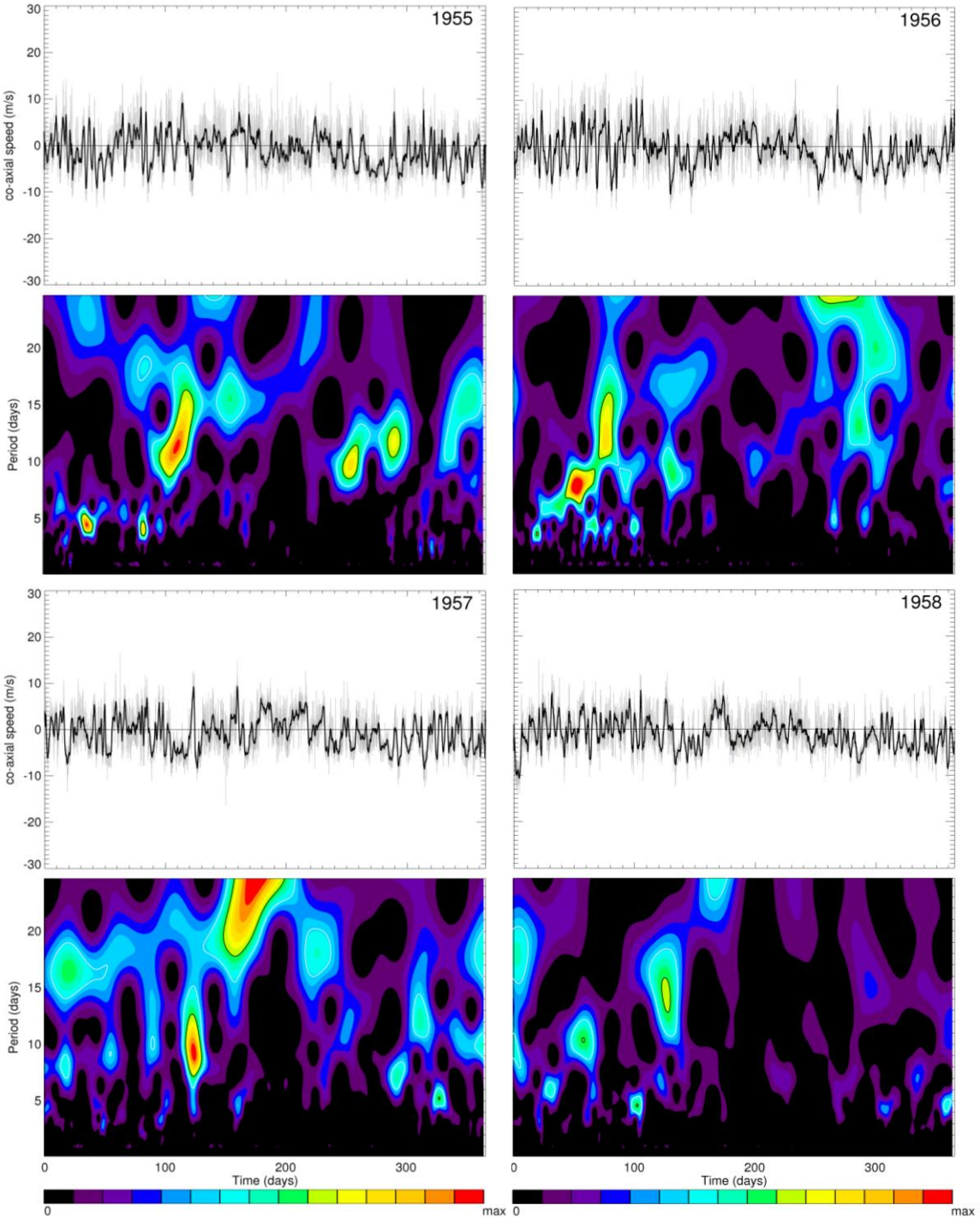

Figure A106. Same as figure A105, 1955-1958.

Appendix D (Continued)

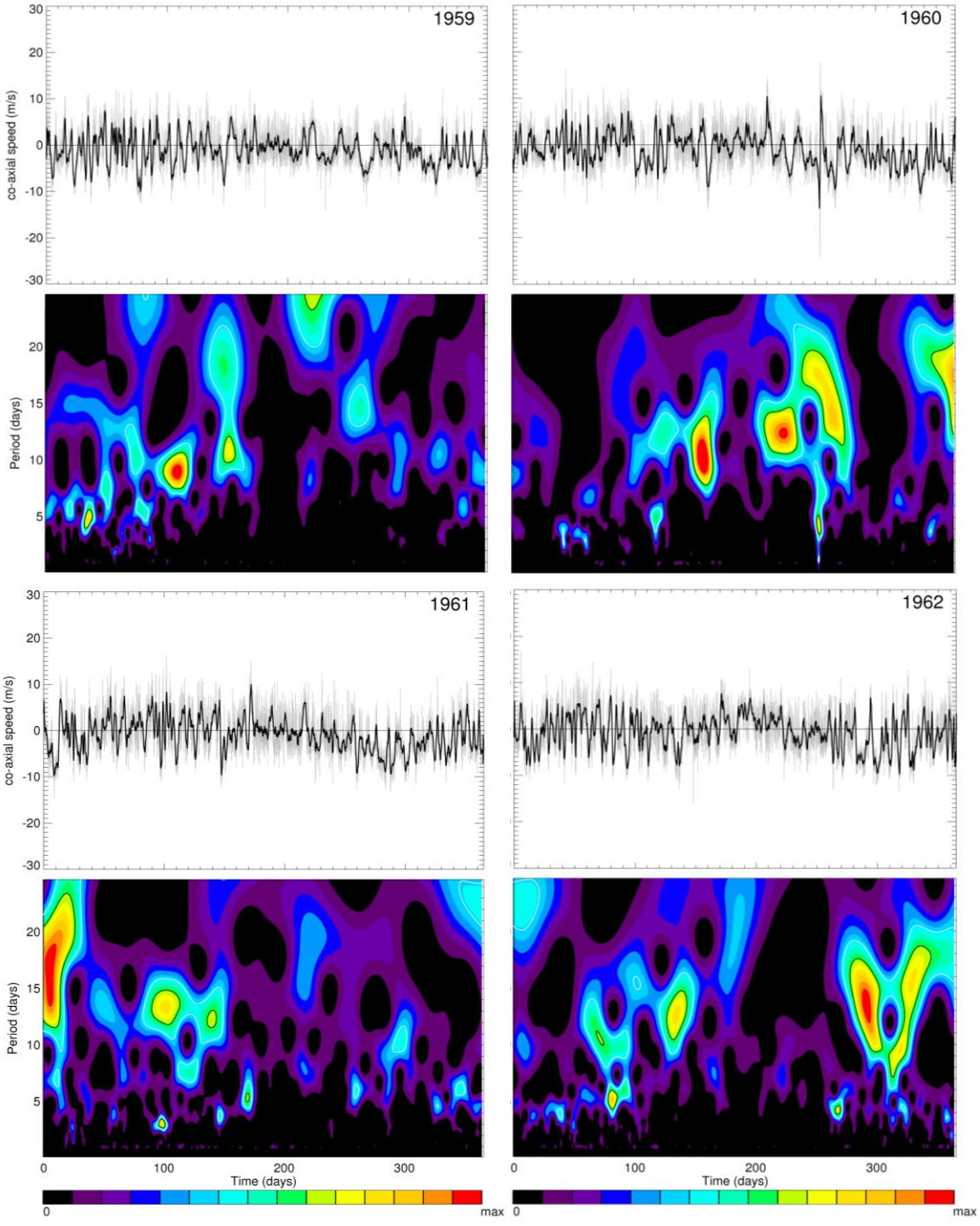

Figure A107. Same as figure A105, 1959-1962.

Appendix D (Continued)

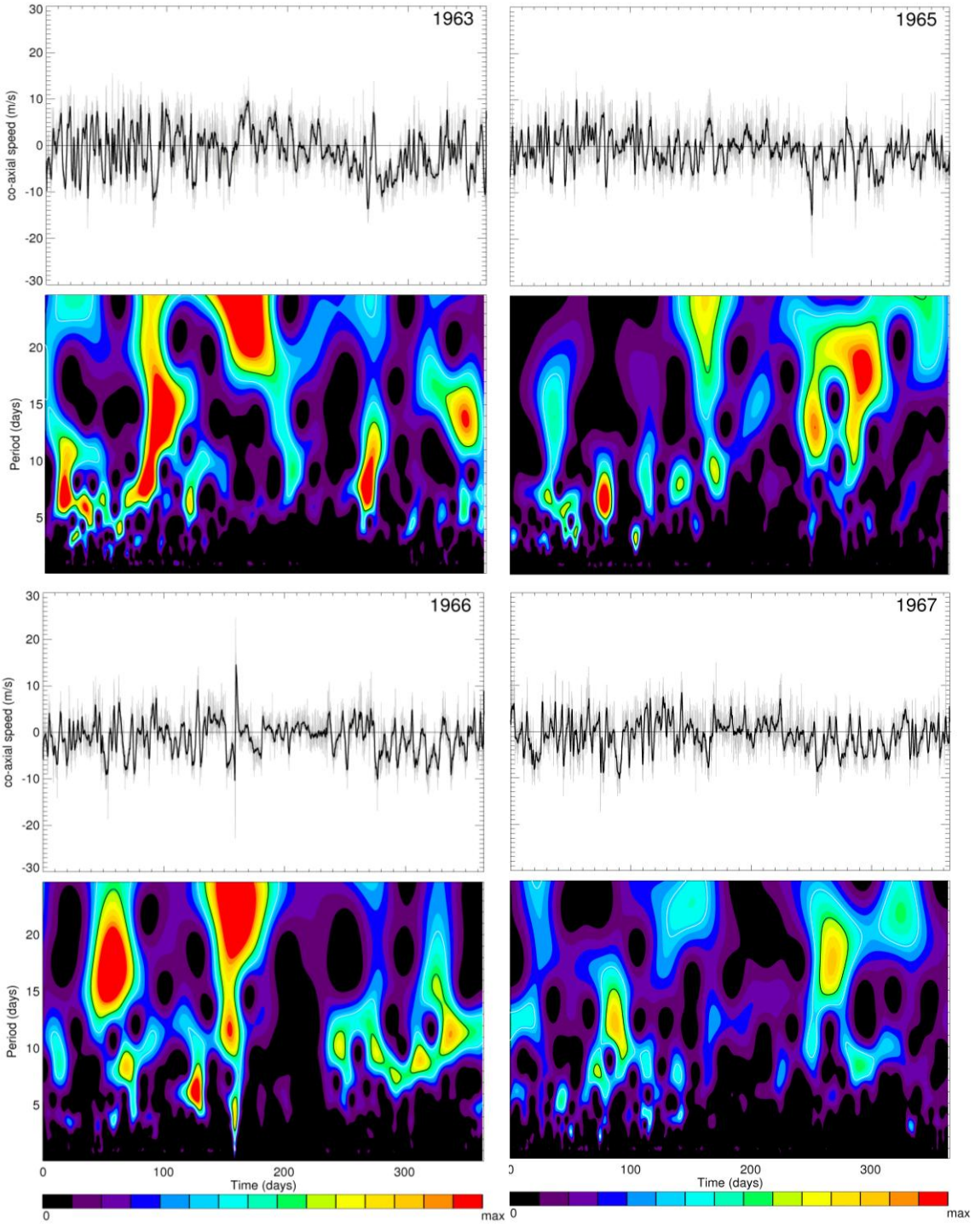

Figure A108. Same as figure A105, 1963, 1965, 1966, and 1967.

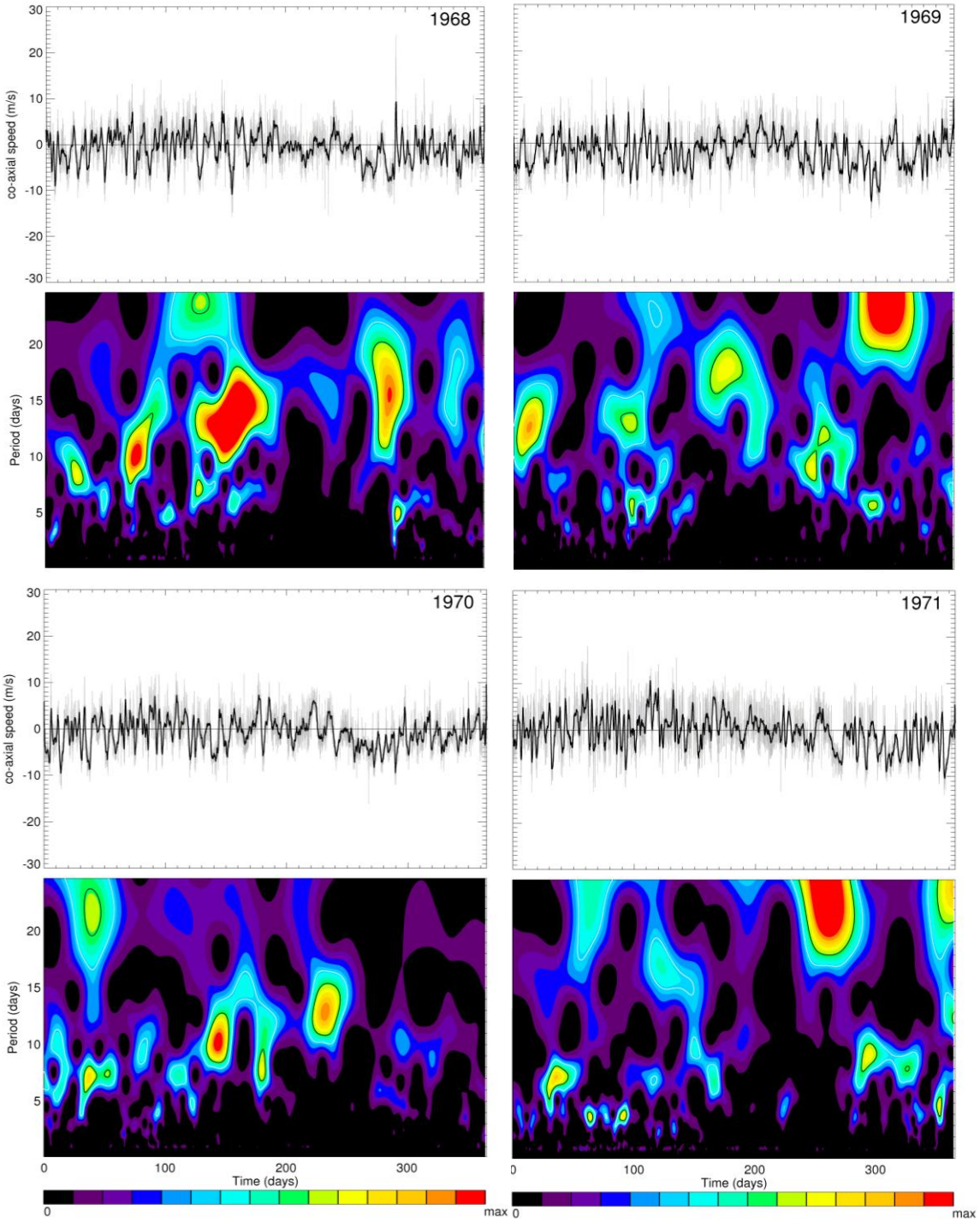

Figure A109. Same as figure A105, 1968-1971.

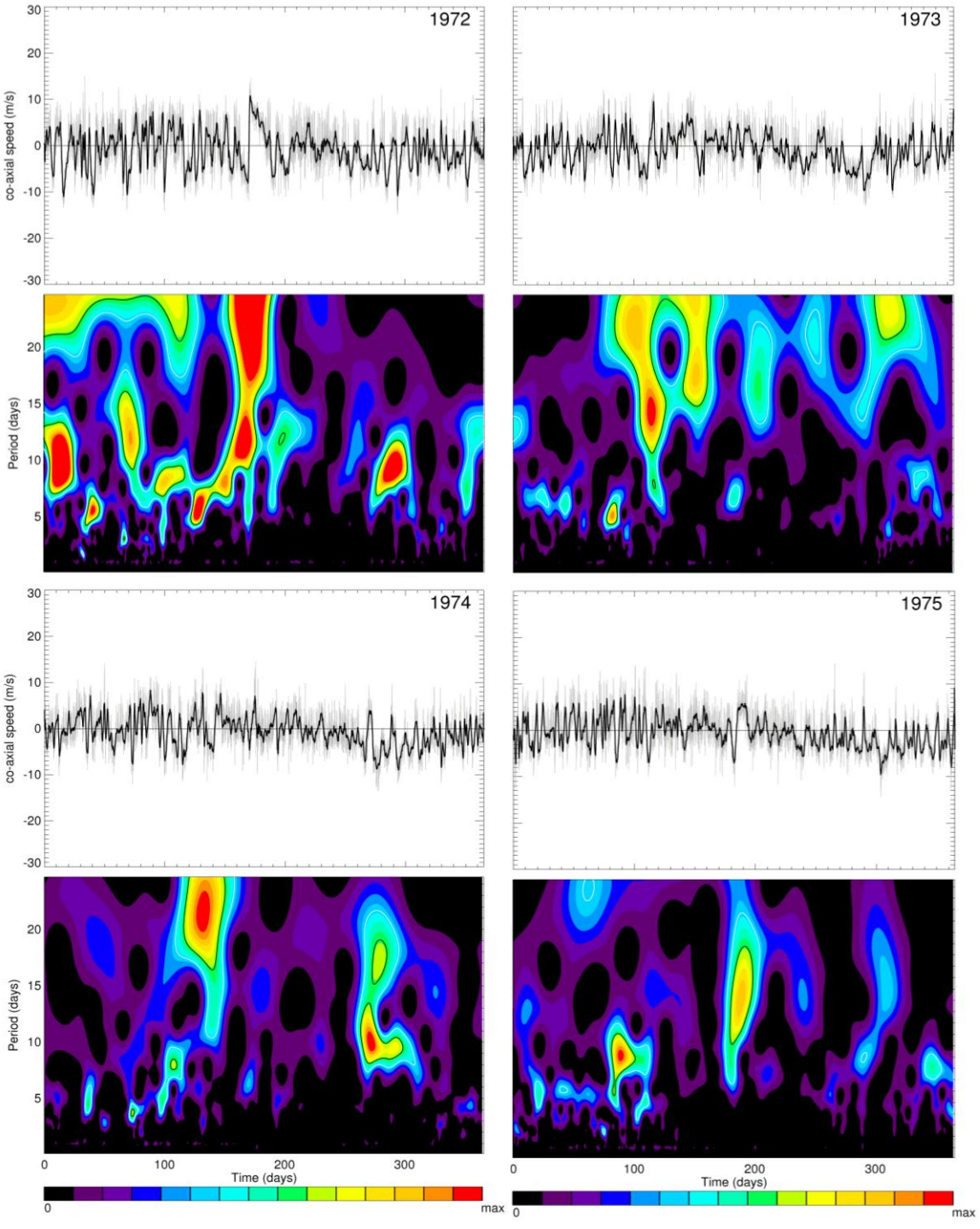

Figure A110. Same as figure A105, 1972-1975.

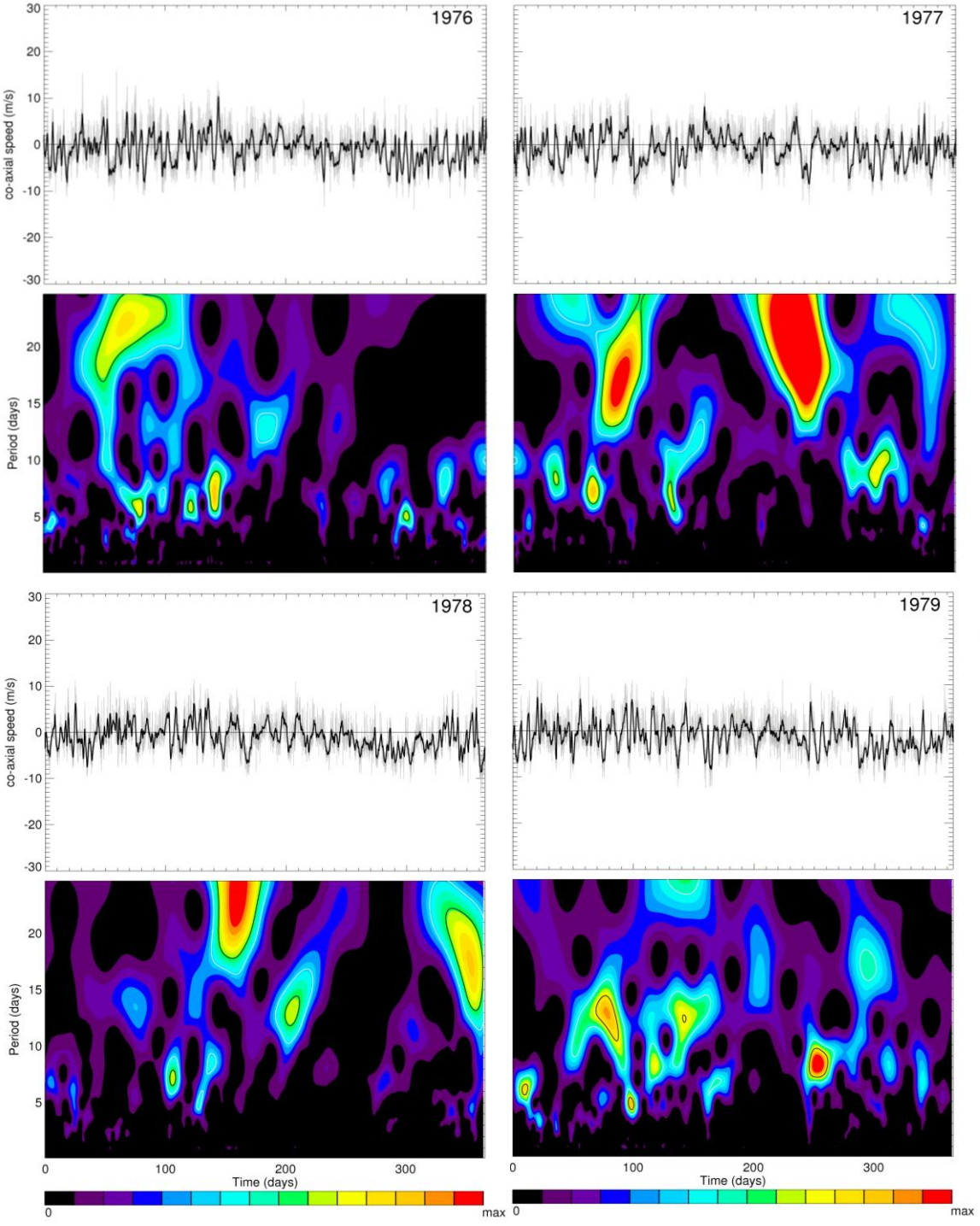

Figure A111. Same as figure A105, 1976-1979.

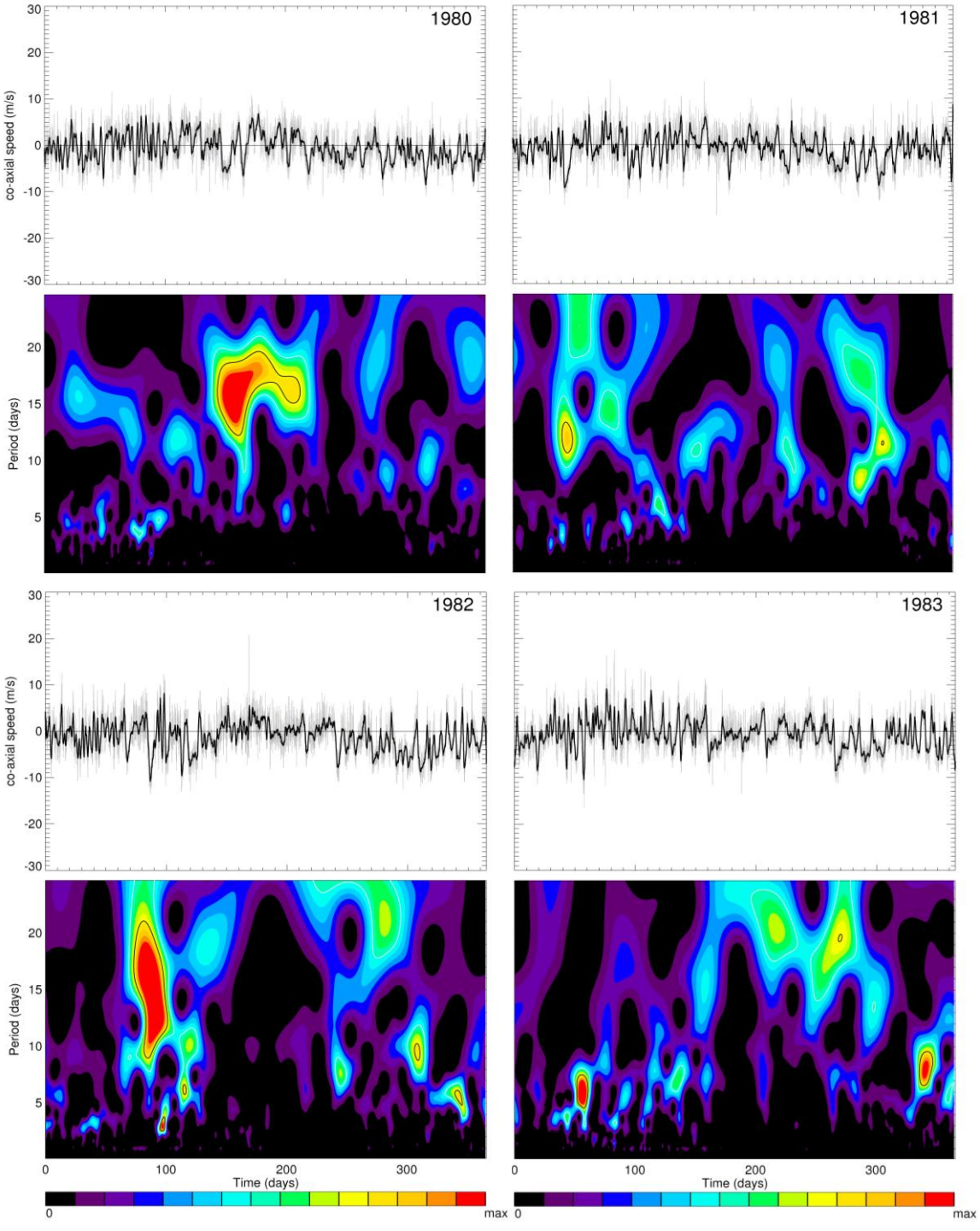

Figure A112. Same as figure A105, 1980-1983.

Appendix D (Continued)

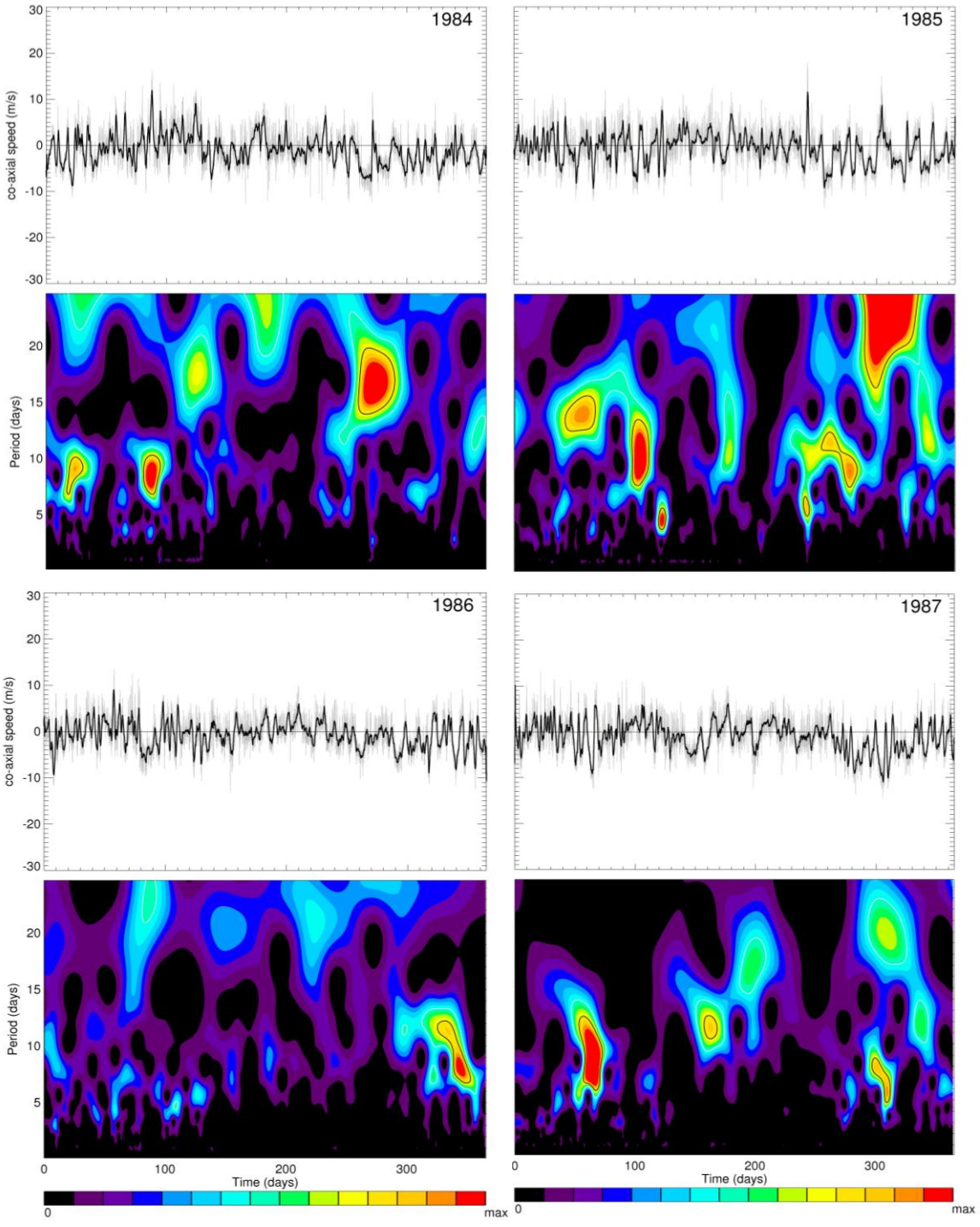

Figure A113. Same as figure A105, 1984-1987.

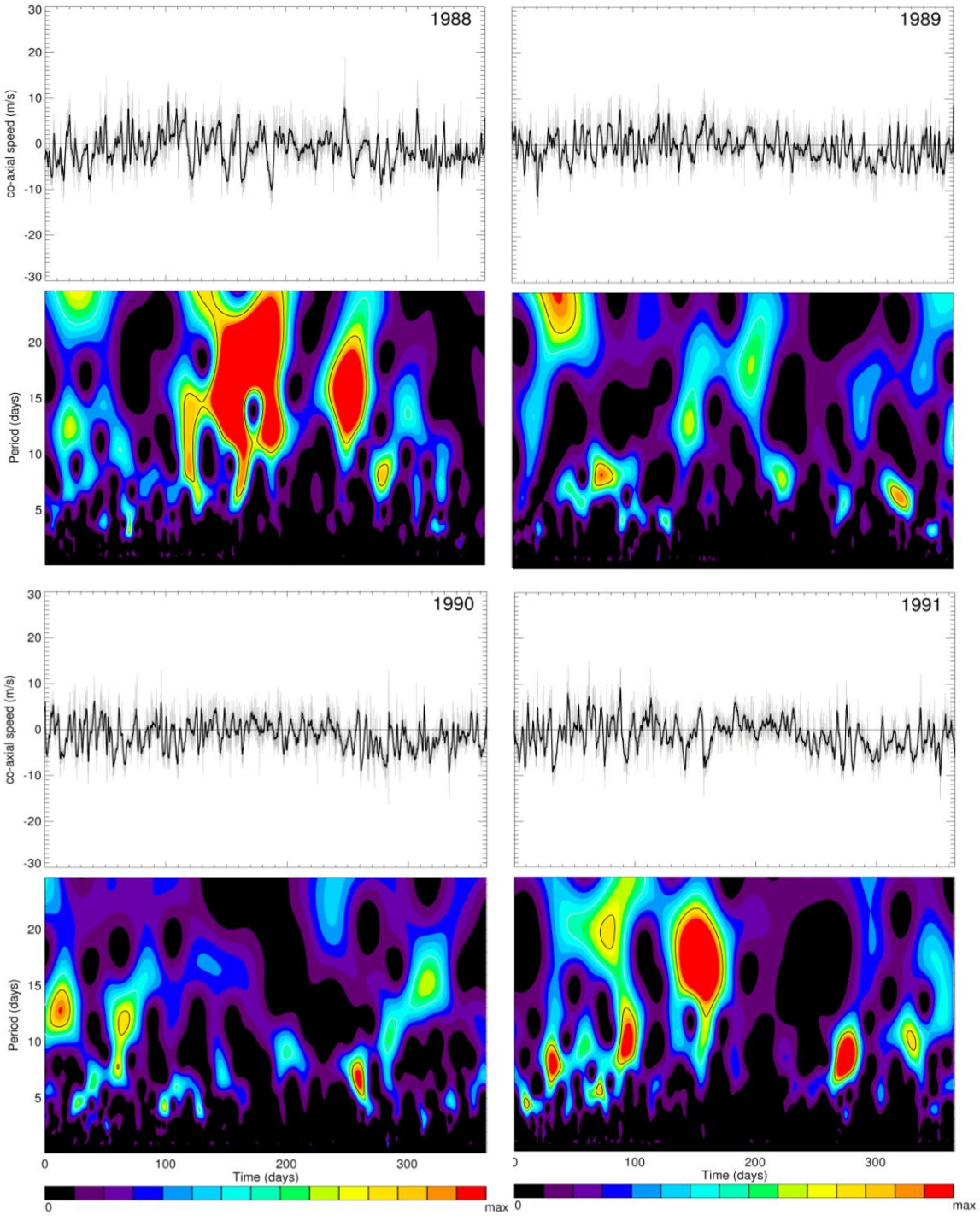

Figure A114. Same as figure A105, 1988-1991.

Appendix D (Continued)

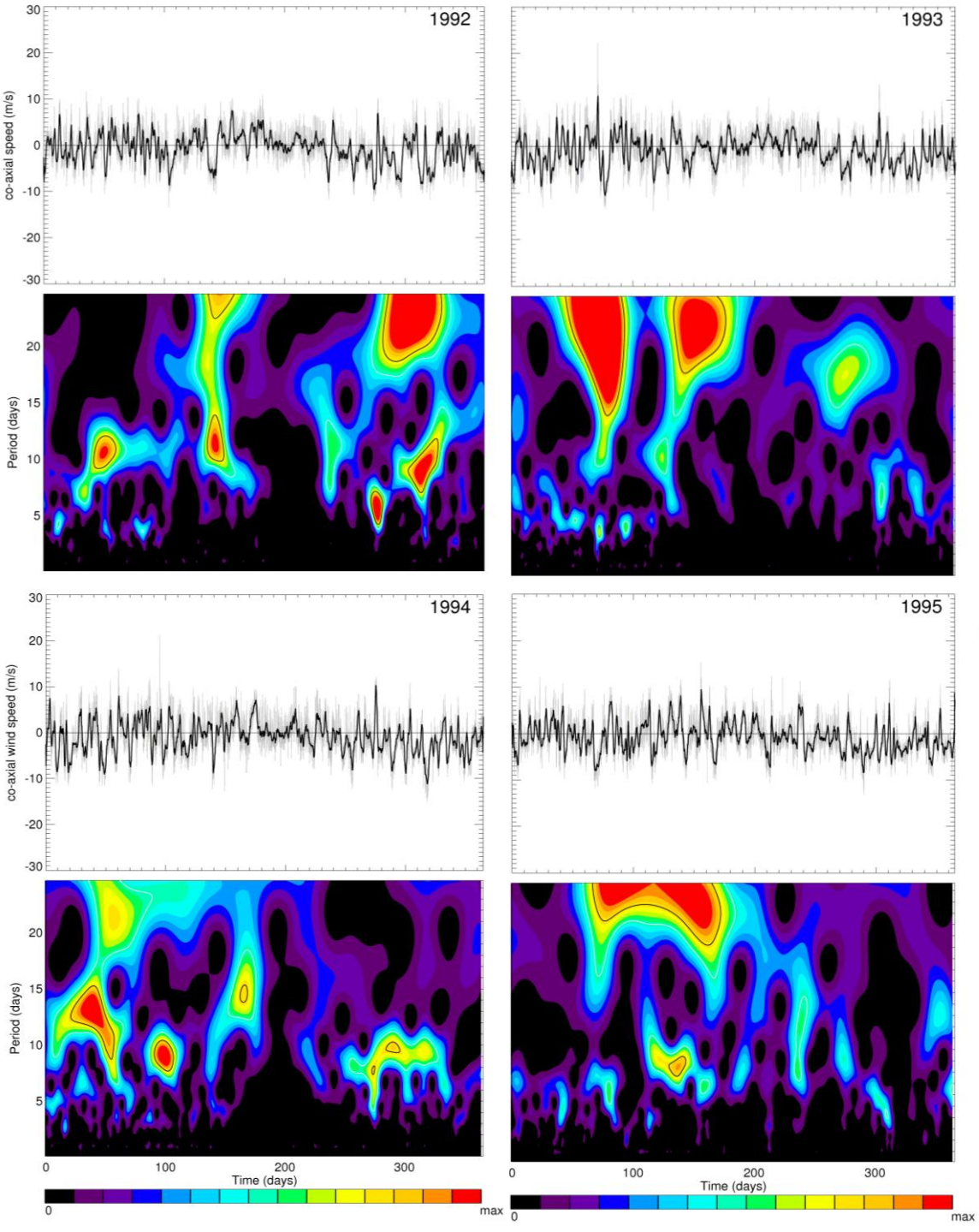

Figure A115. Same as figure A105, 1992-1995.

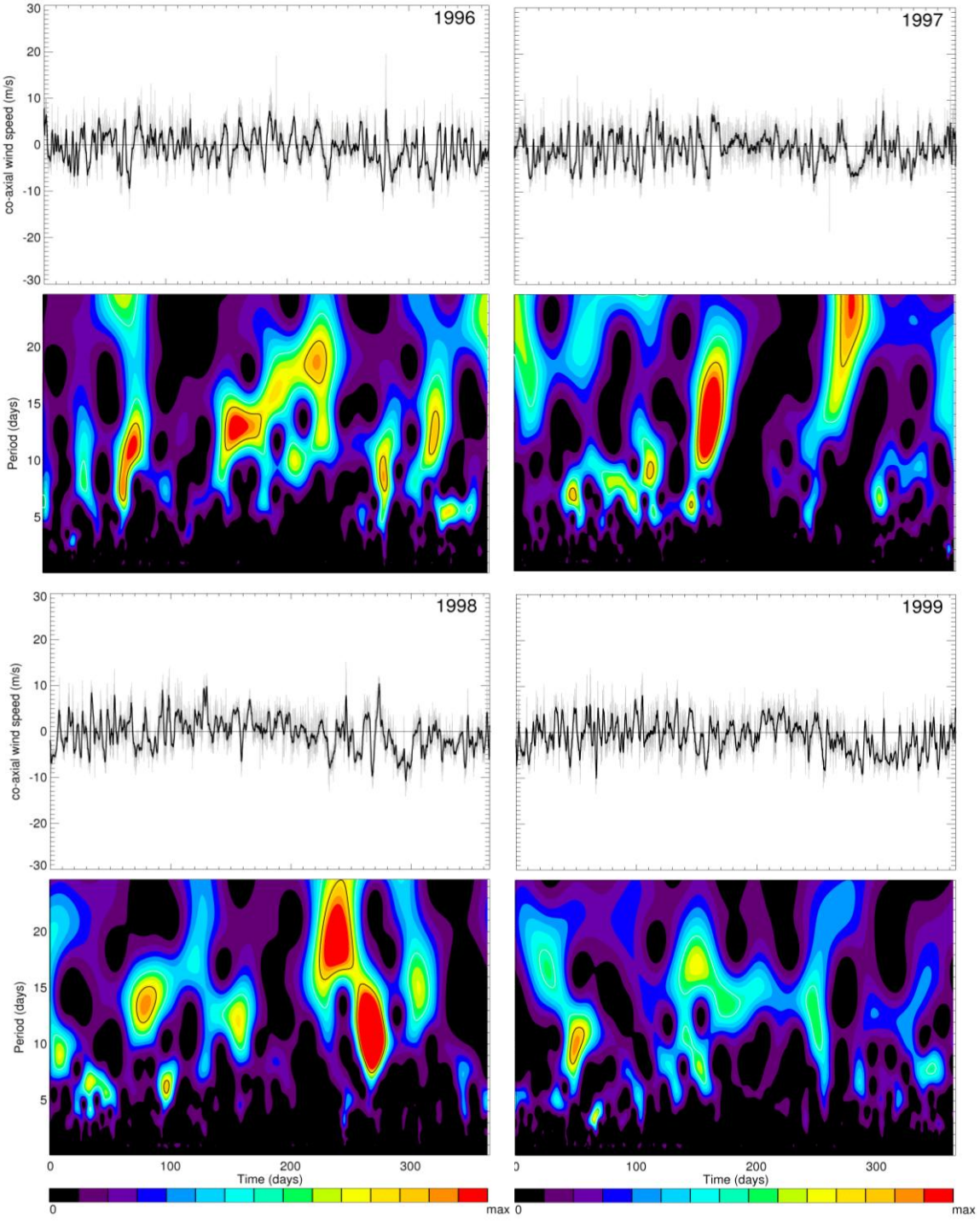

Figure A116. Same as figure A105, 1996-1999.

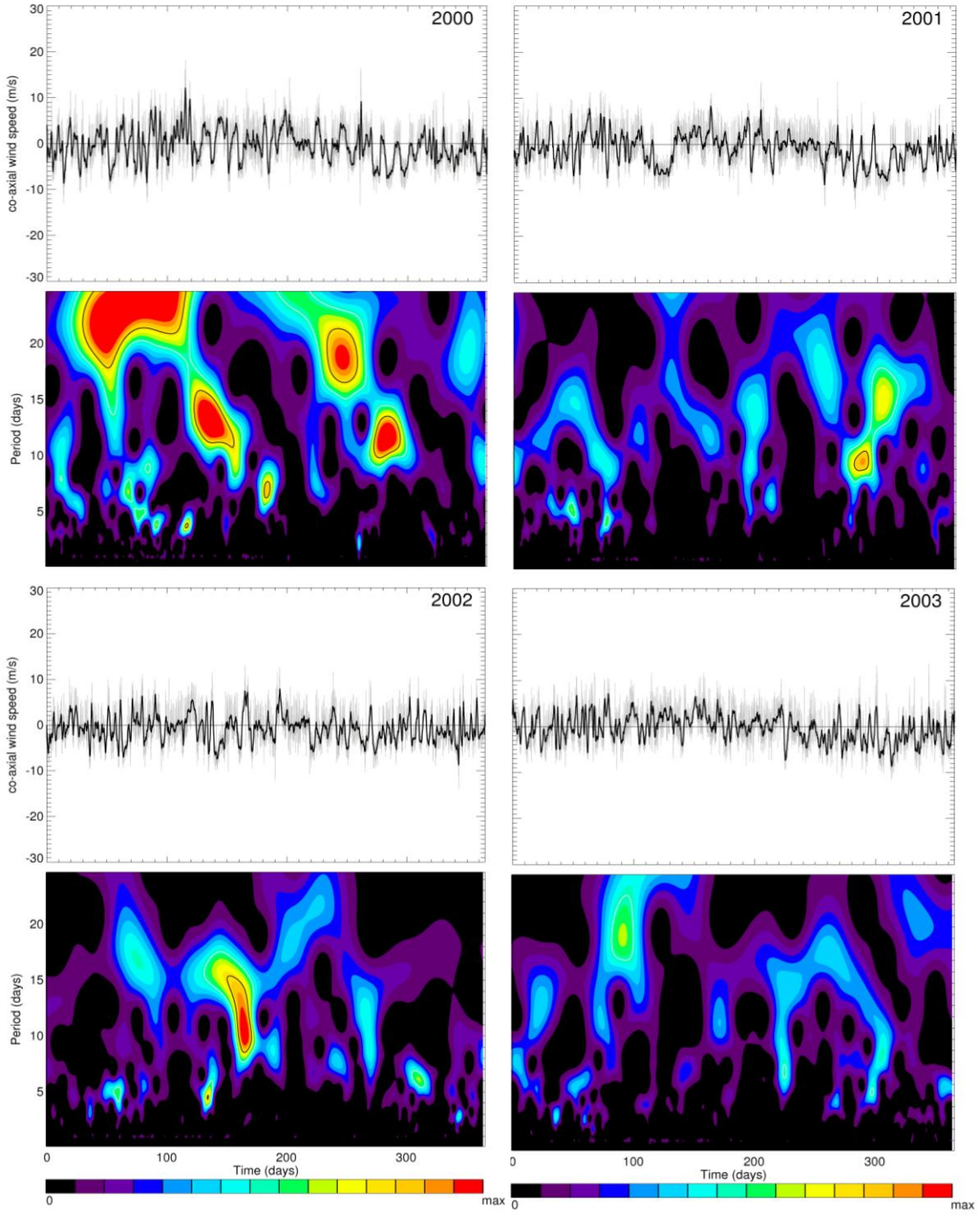

Figure A117. Same as figure A105, 2000-2003.

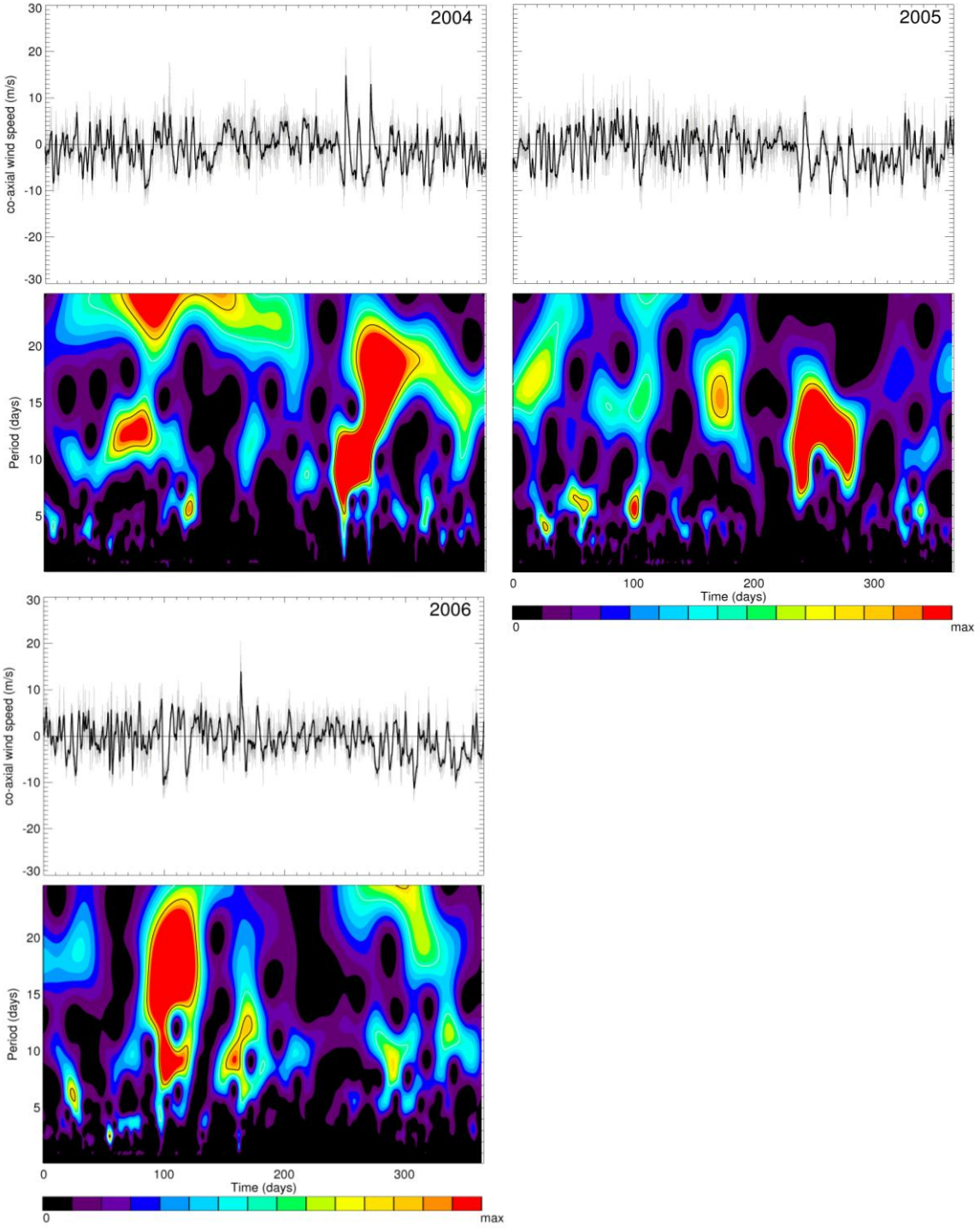

Figure A118. Same as figure A105, 2004-2006.

Appendix E: Yearly normalized bay volume anomalies

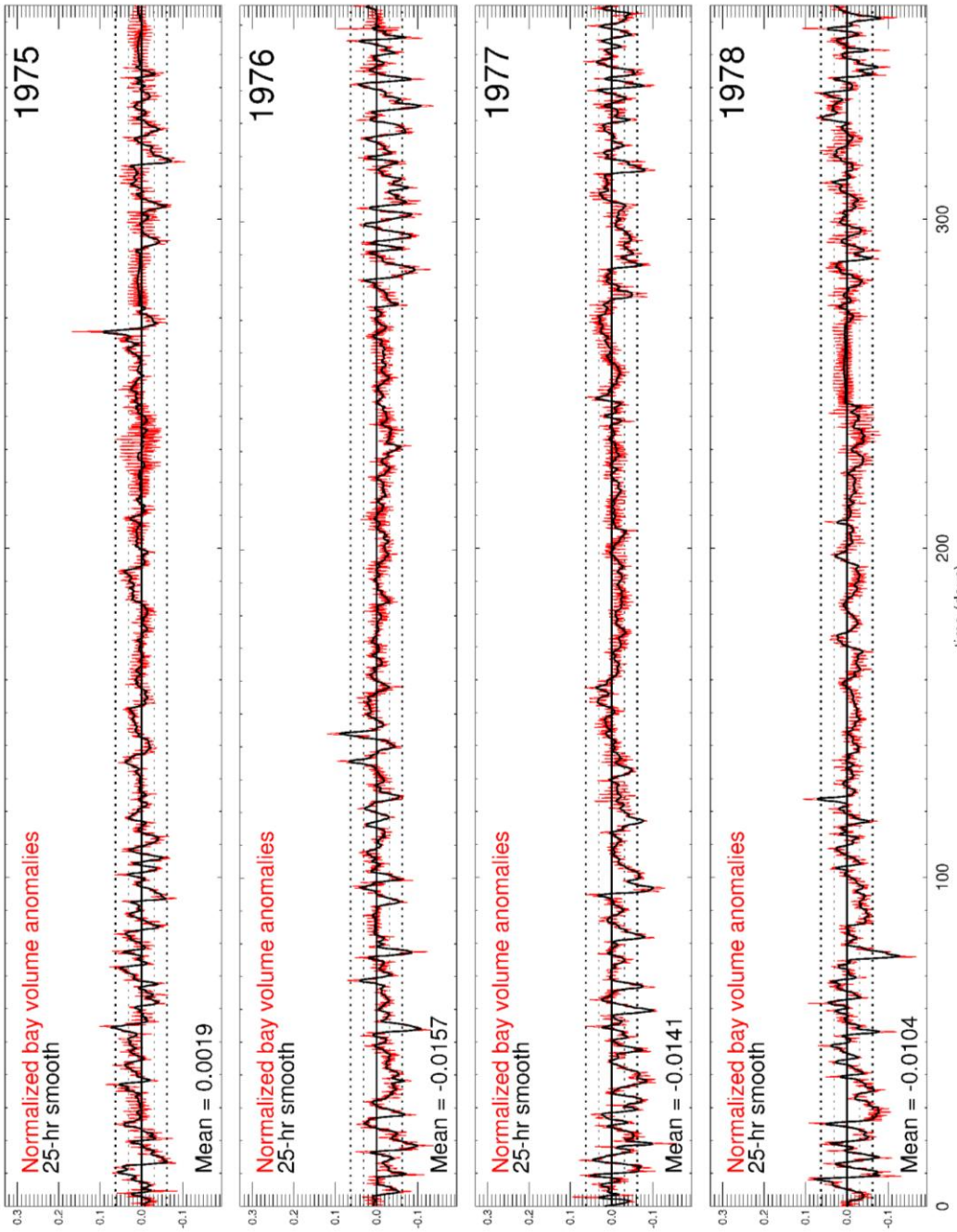

Figure A119. Normalized bay volume anomalies, 1975-1978.

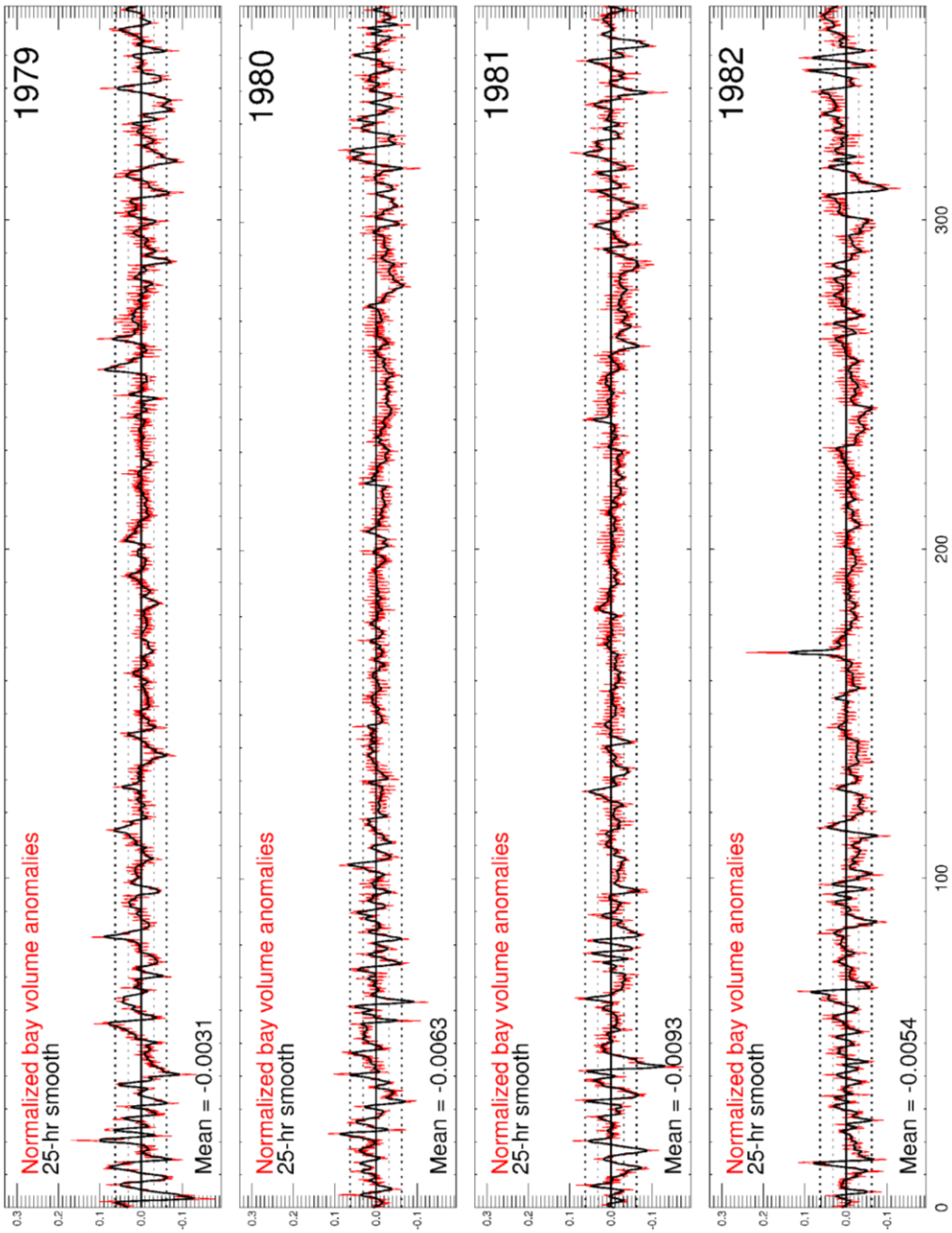

Figure A120. Same as figure A119, 1979-1982.

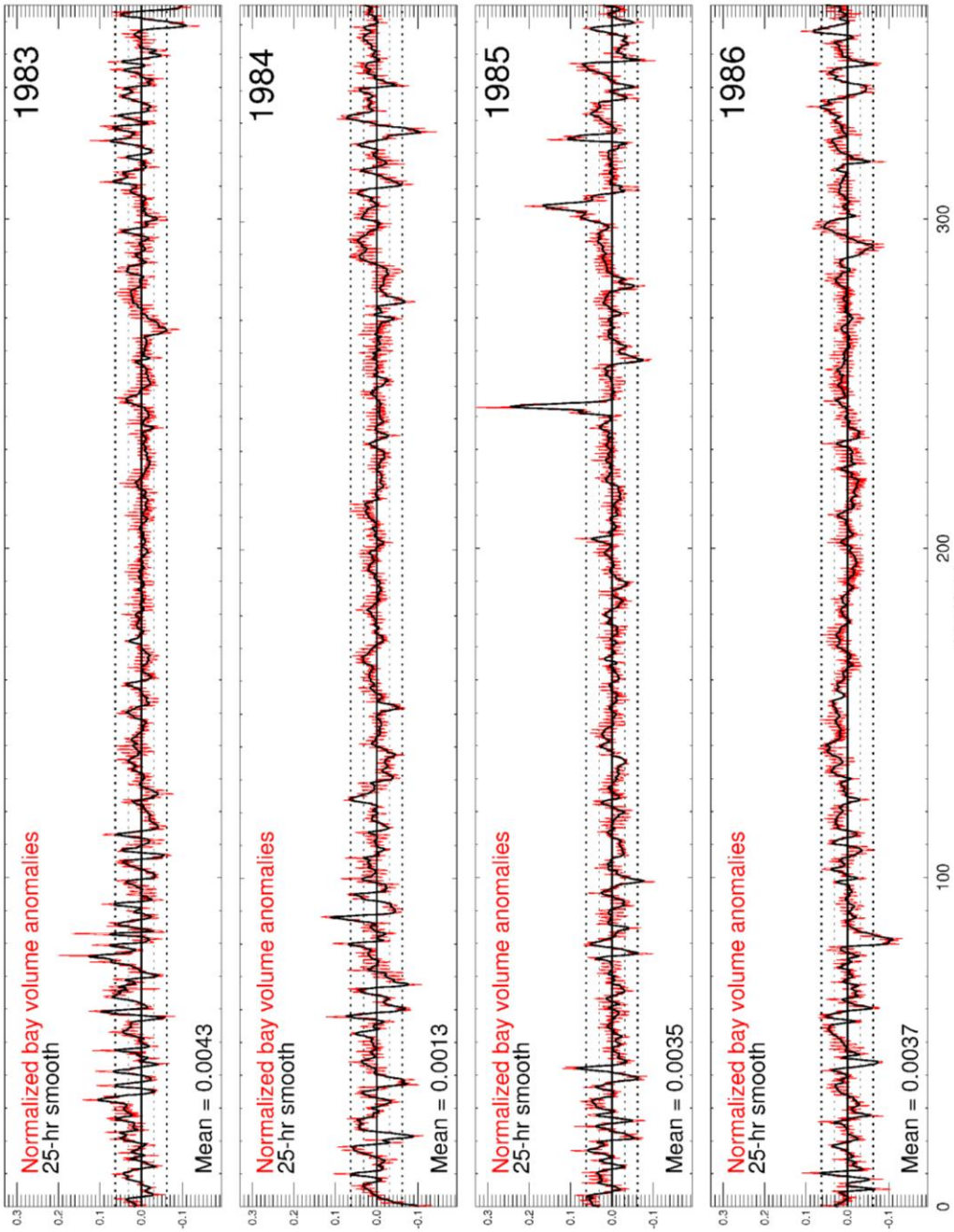

Figure A121. Same as figure A119, 1983-1986.

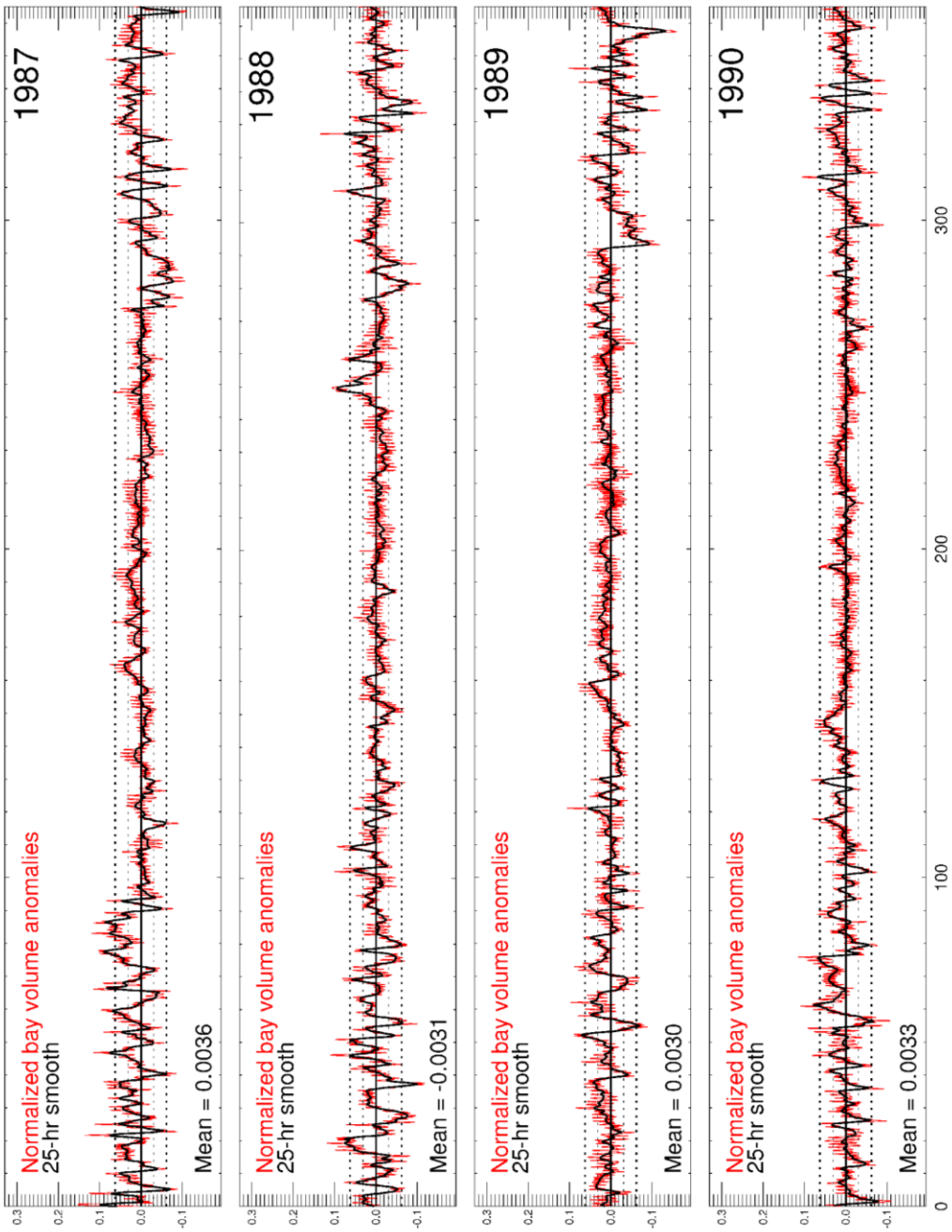

Figure A122. Same as figure A119, 1987-1990.

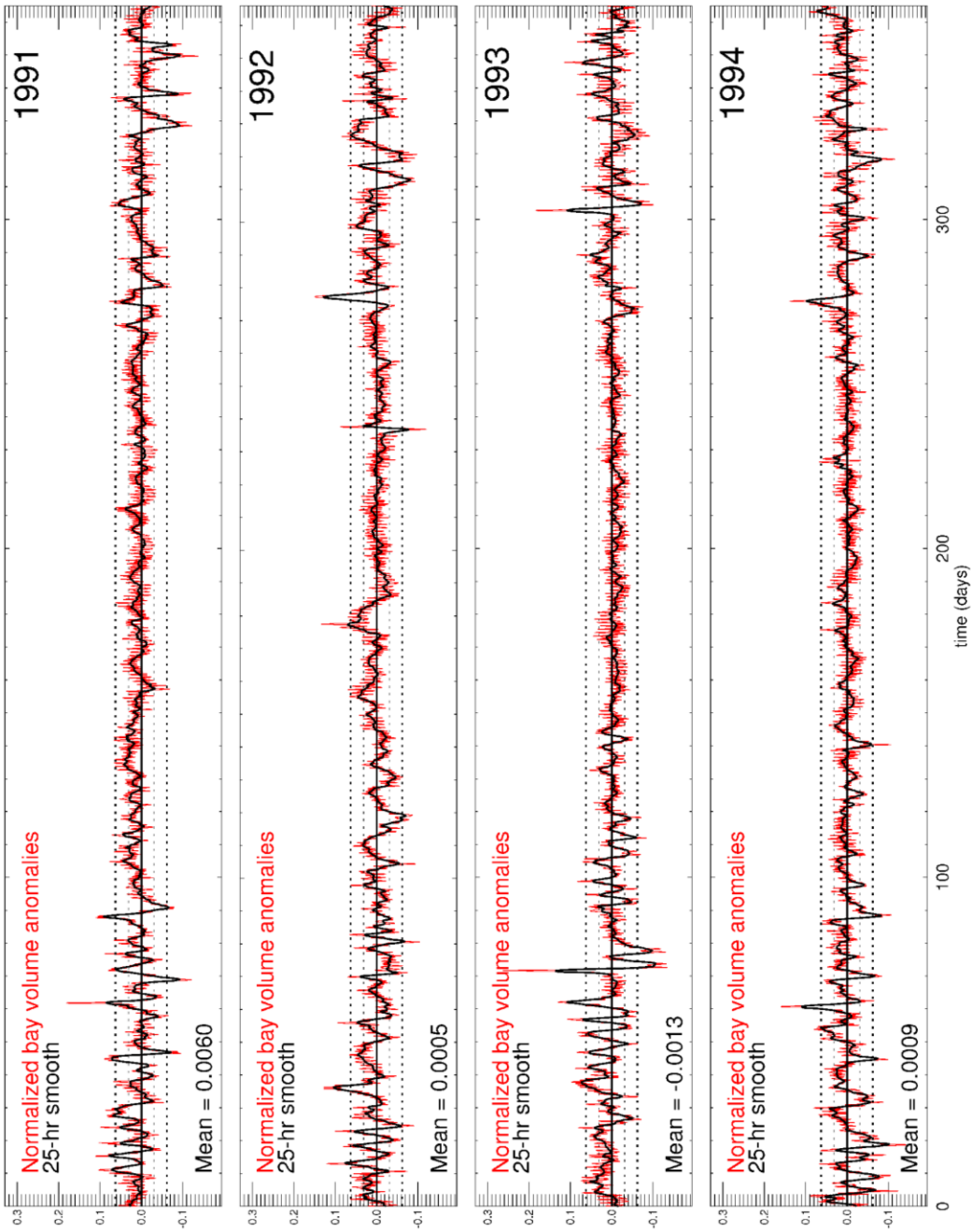

Figure A123. Same as figure A119, 1991-1994.

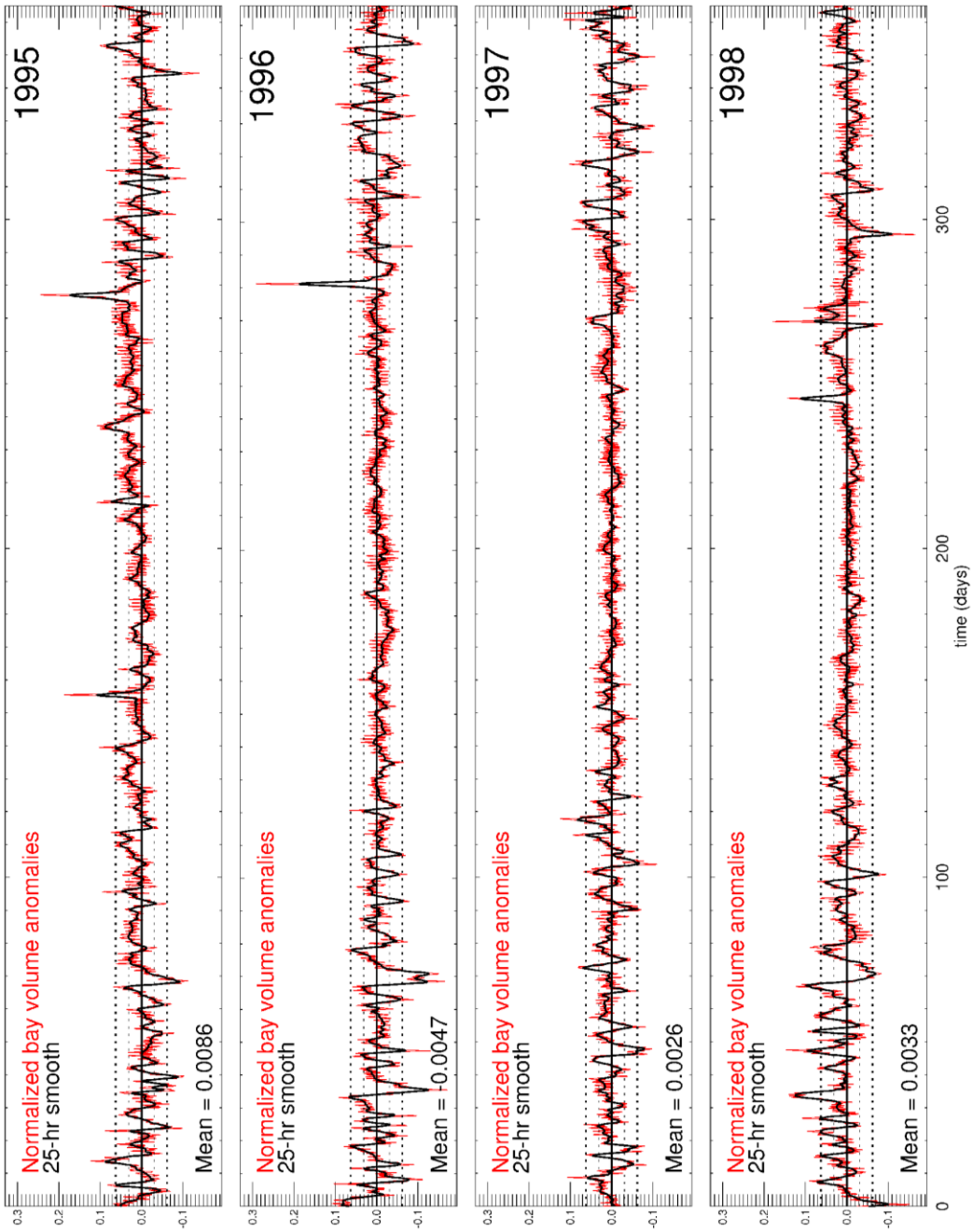

Figure A124. Same as figure A119, 1995-1998.

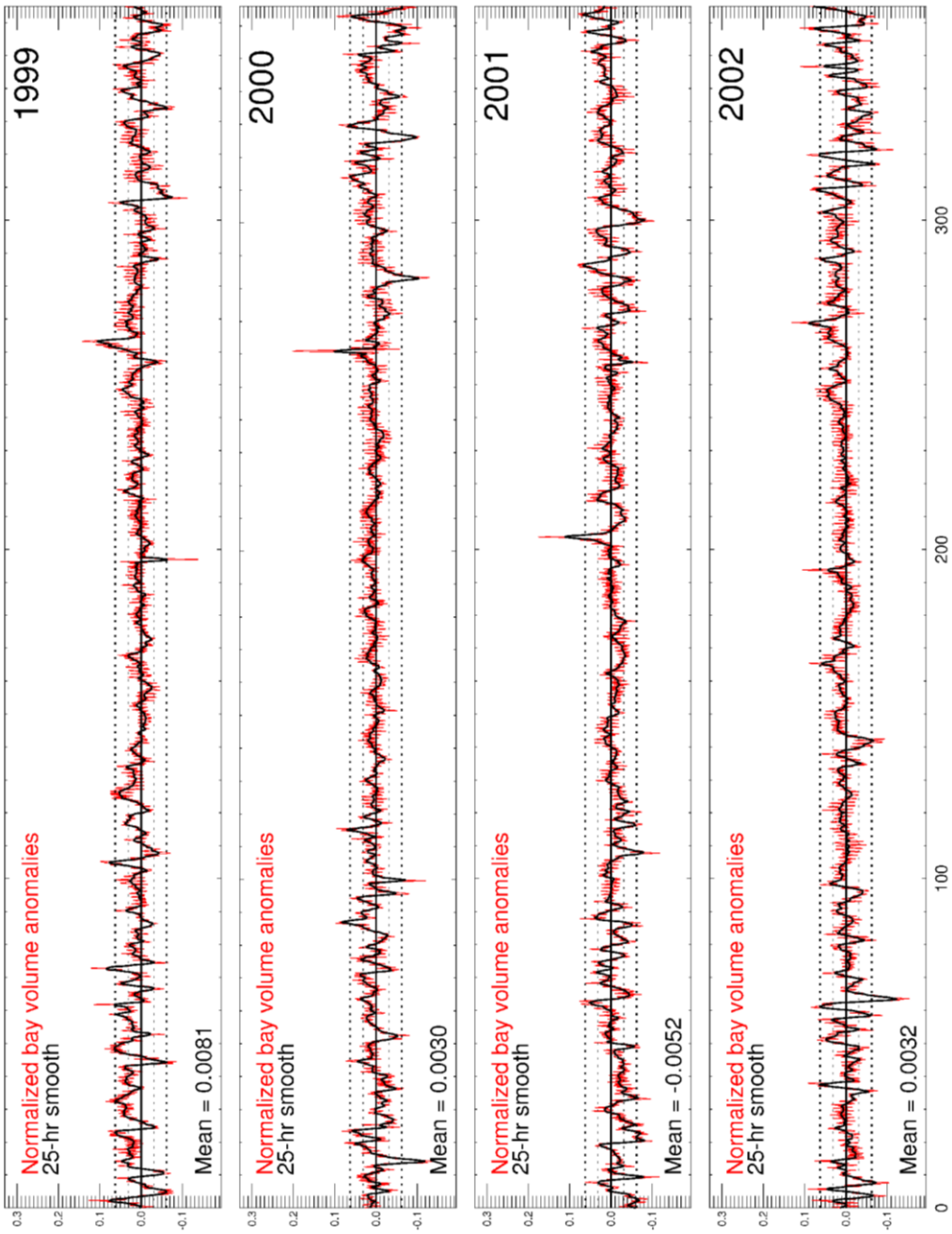

Figure A125. Same as figure A119, 1999-2002.

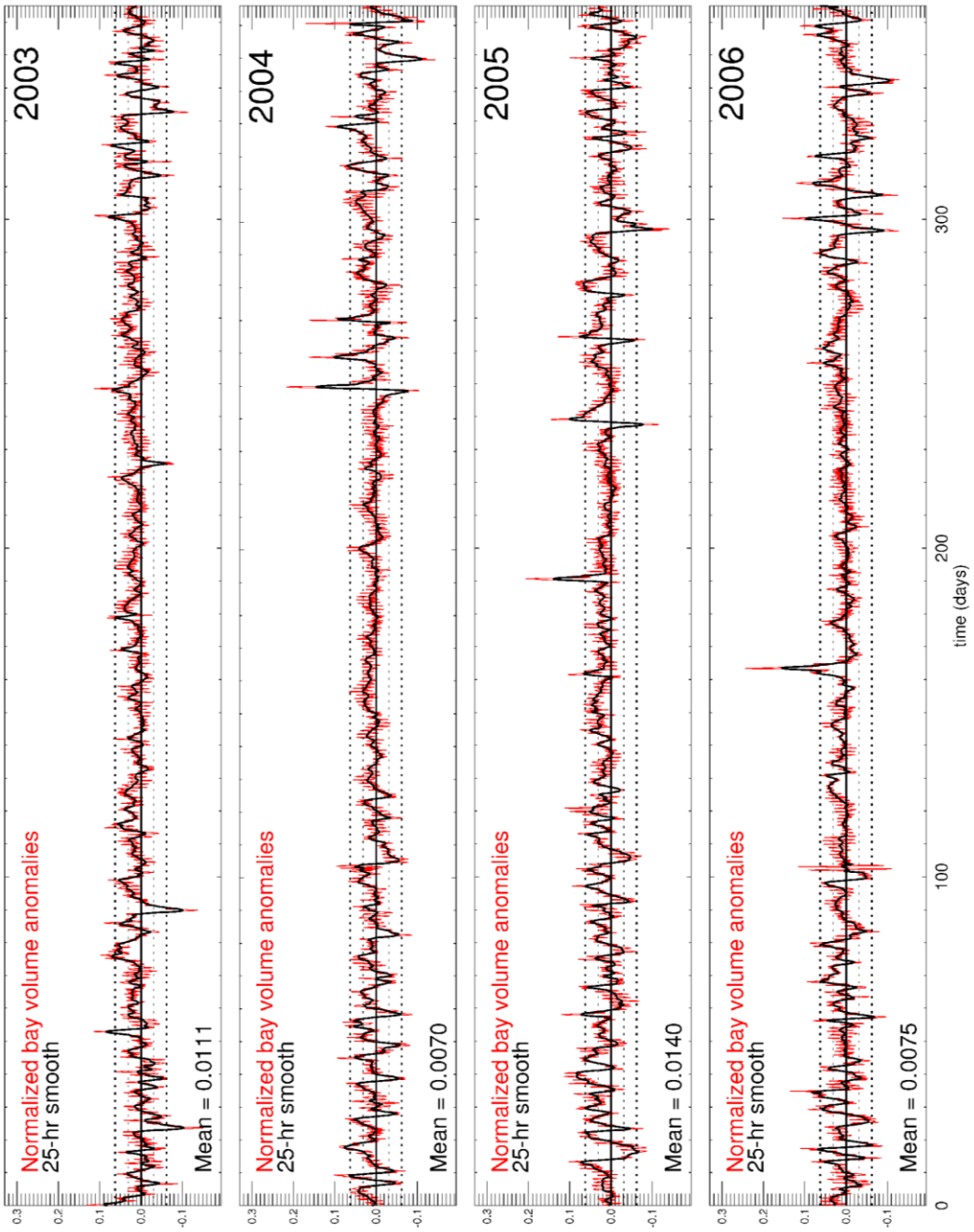

Figure A126. Same as figure A119, 2003-2006.

Appendix F: Yearly normalized flushing rates

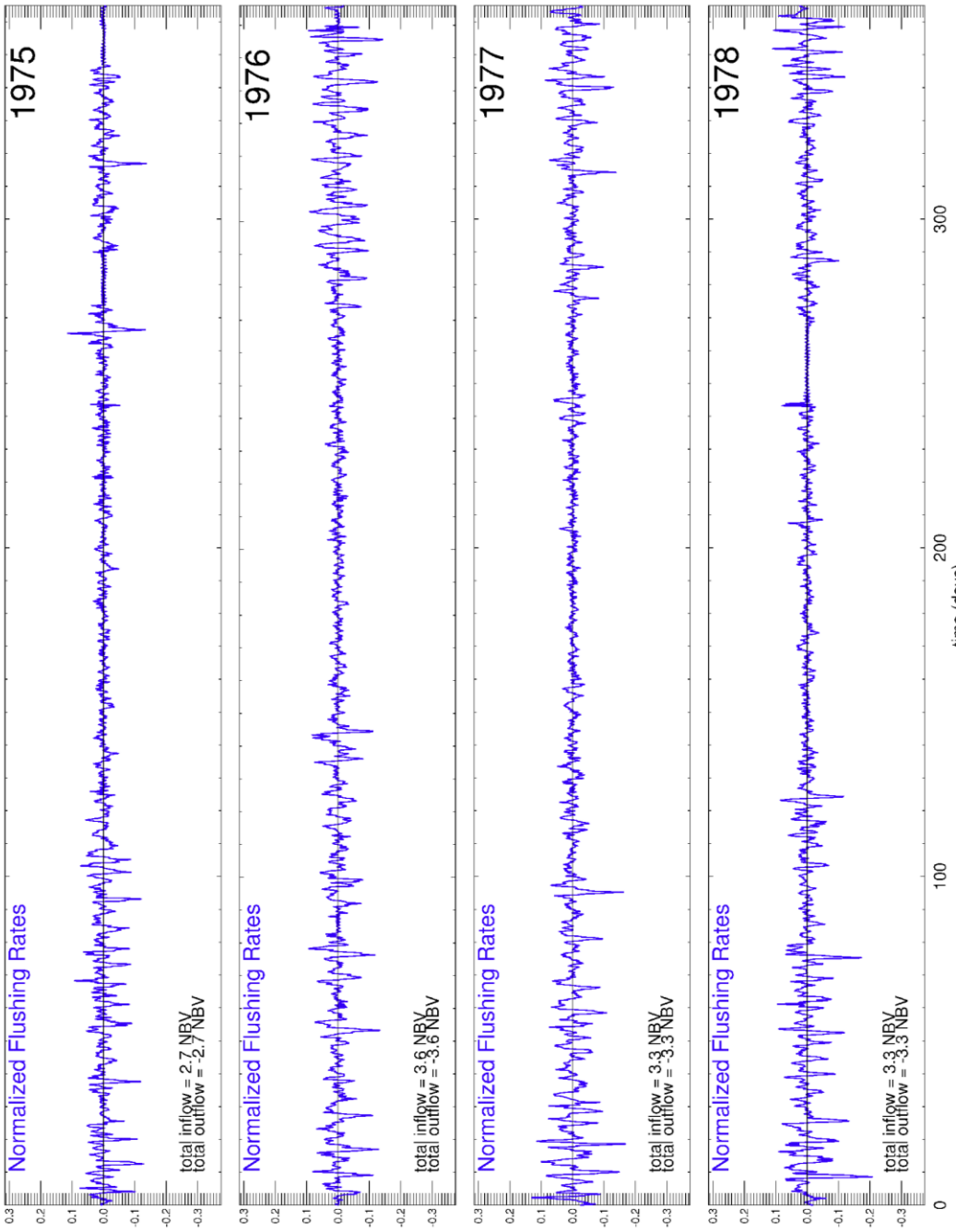

Figure A127. Normalized flushing rates, 1975-1978

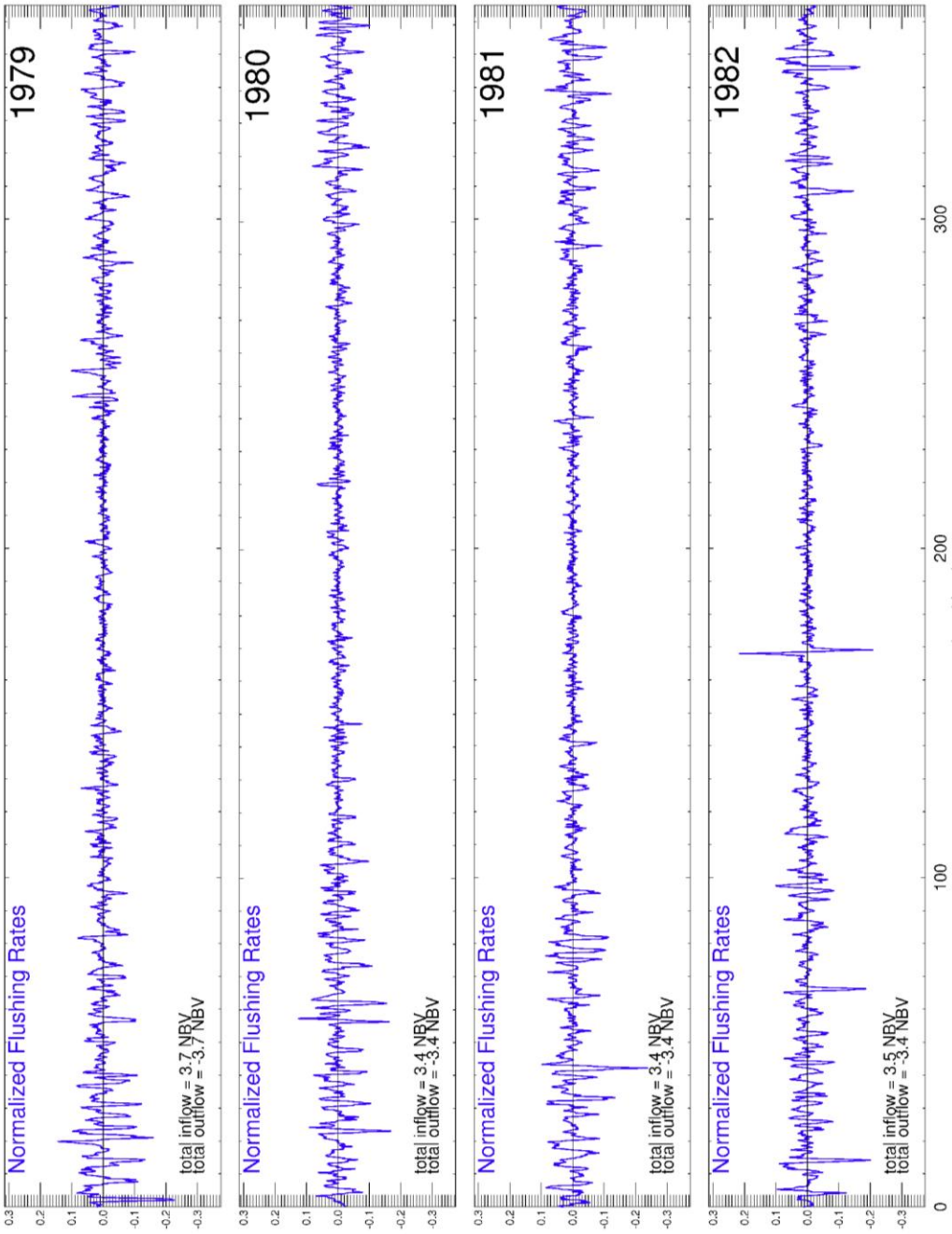

Figure A128. Same as figure A127, 1979-1982

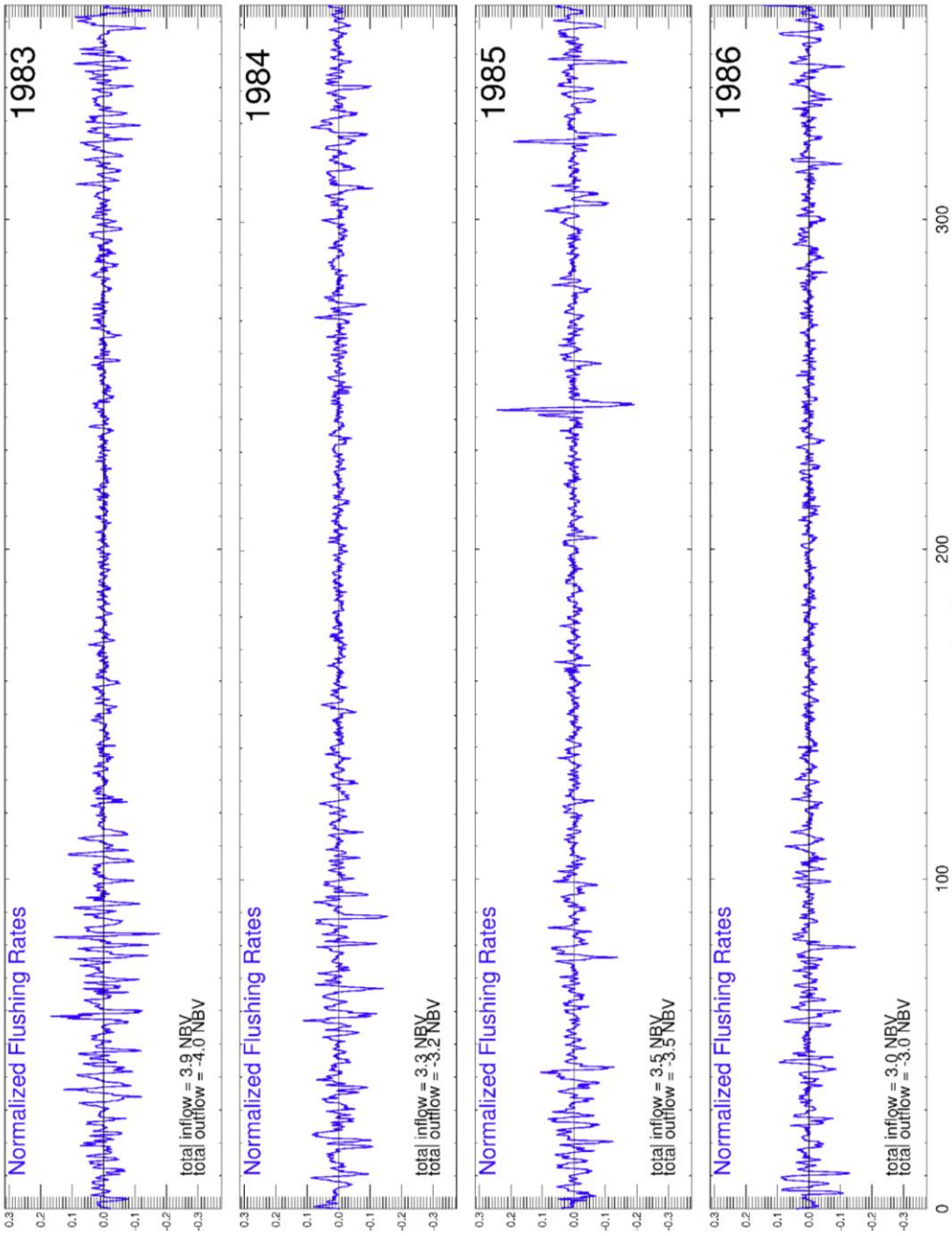

Figure A129. Same as figure A127, 1983-1986.

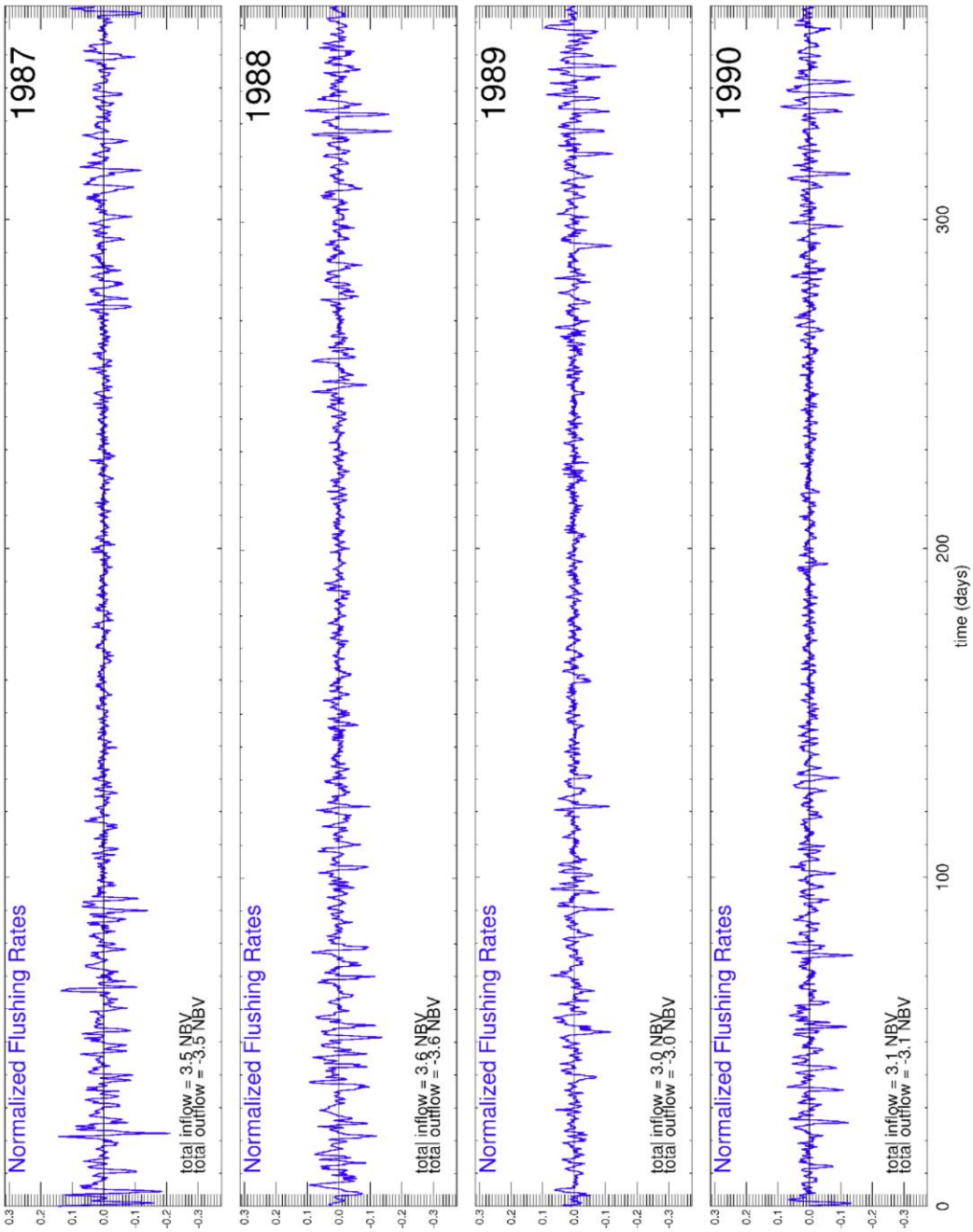

Figure A130. Same as figure A127, 1987-1990.

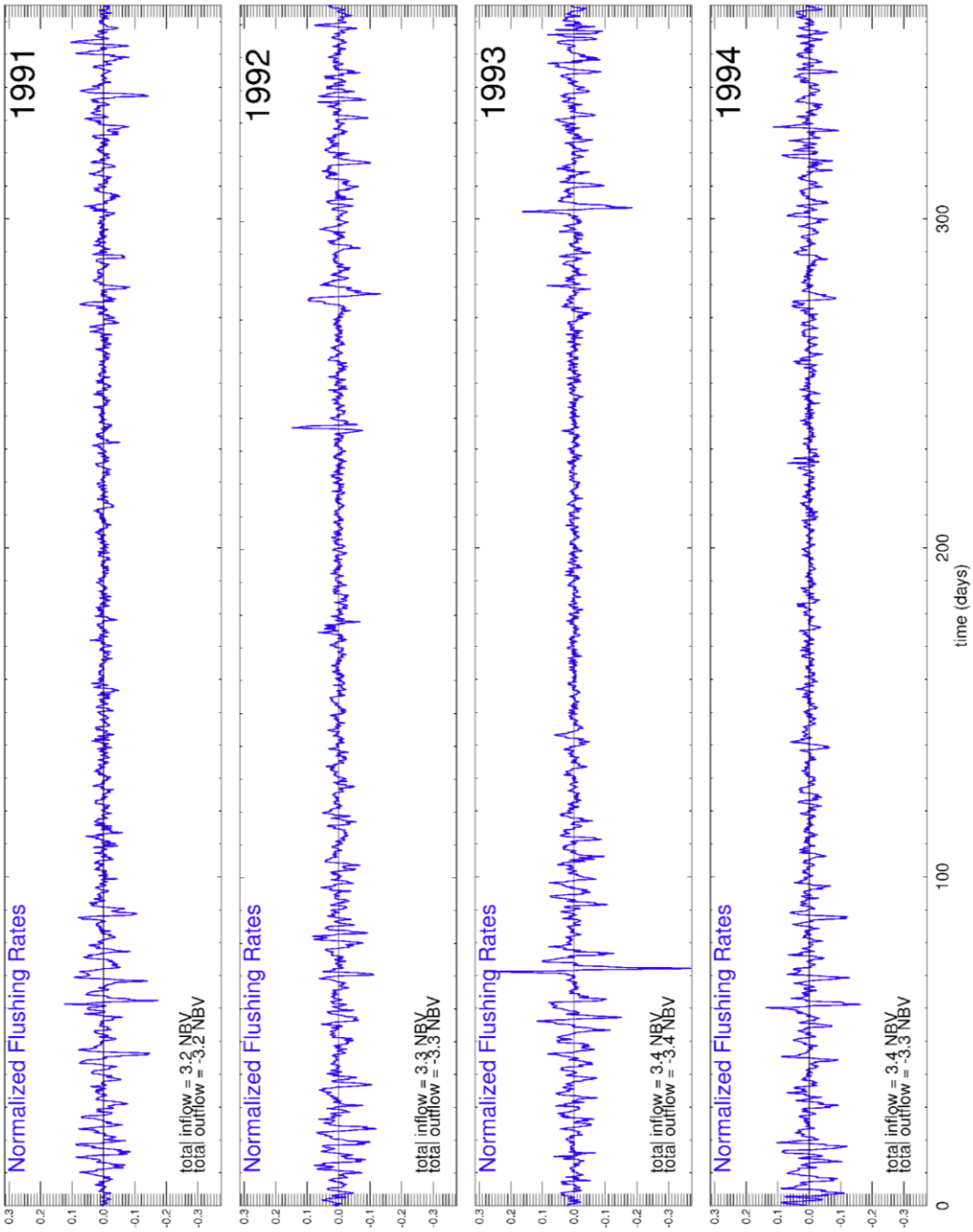

Figure A131. Same as figure A127, 1991-1994.

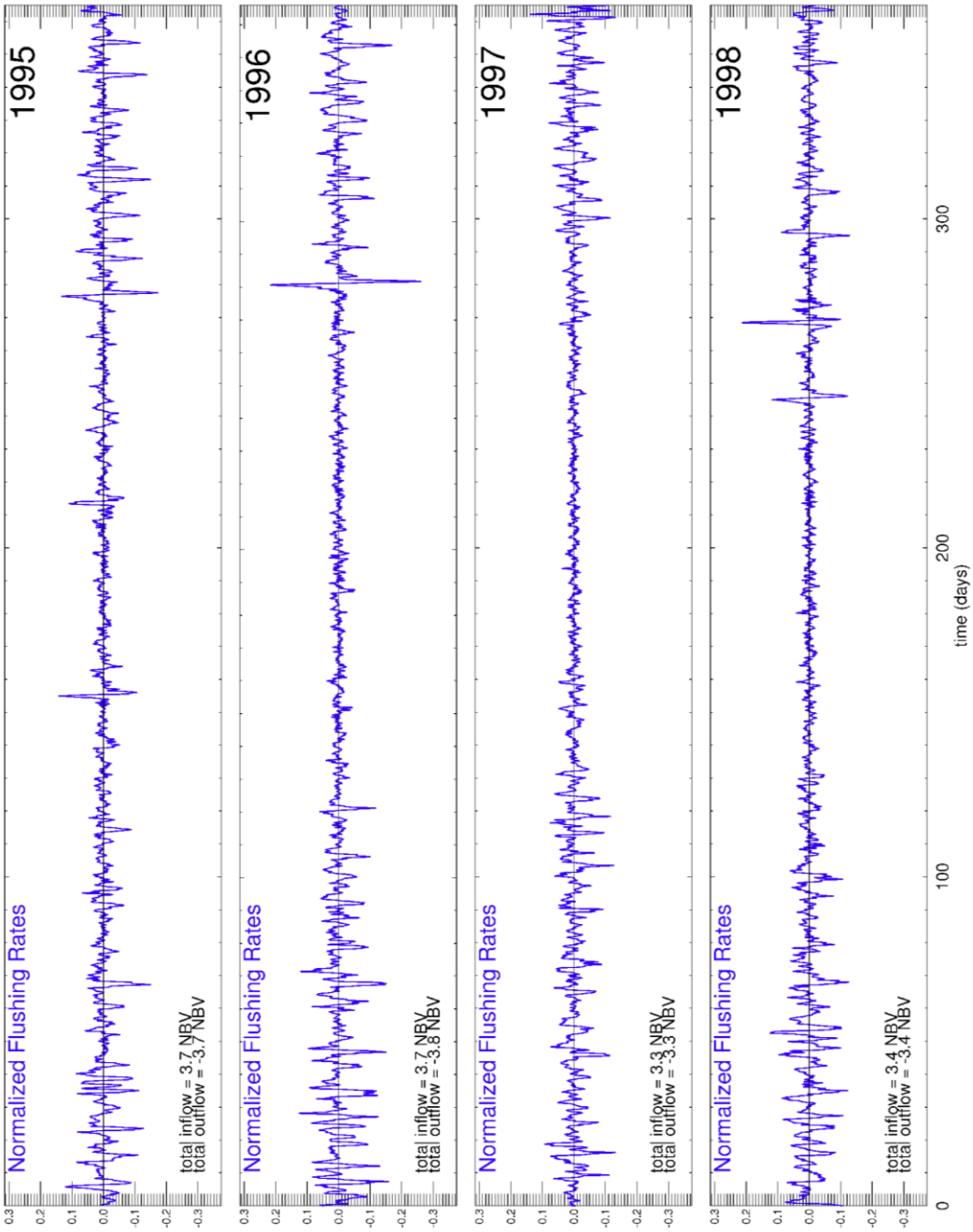

Figure A132. Same as figure A127, 1995-1998.

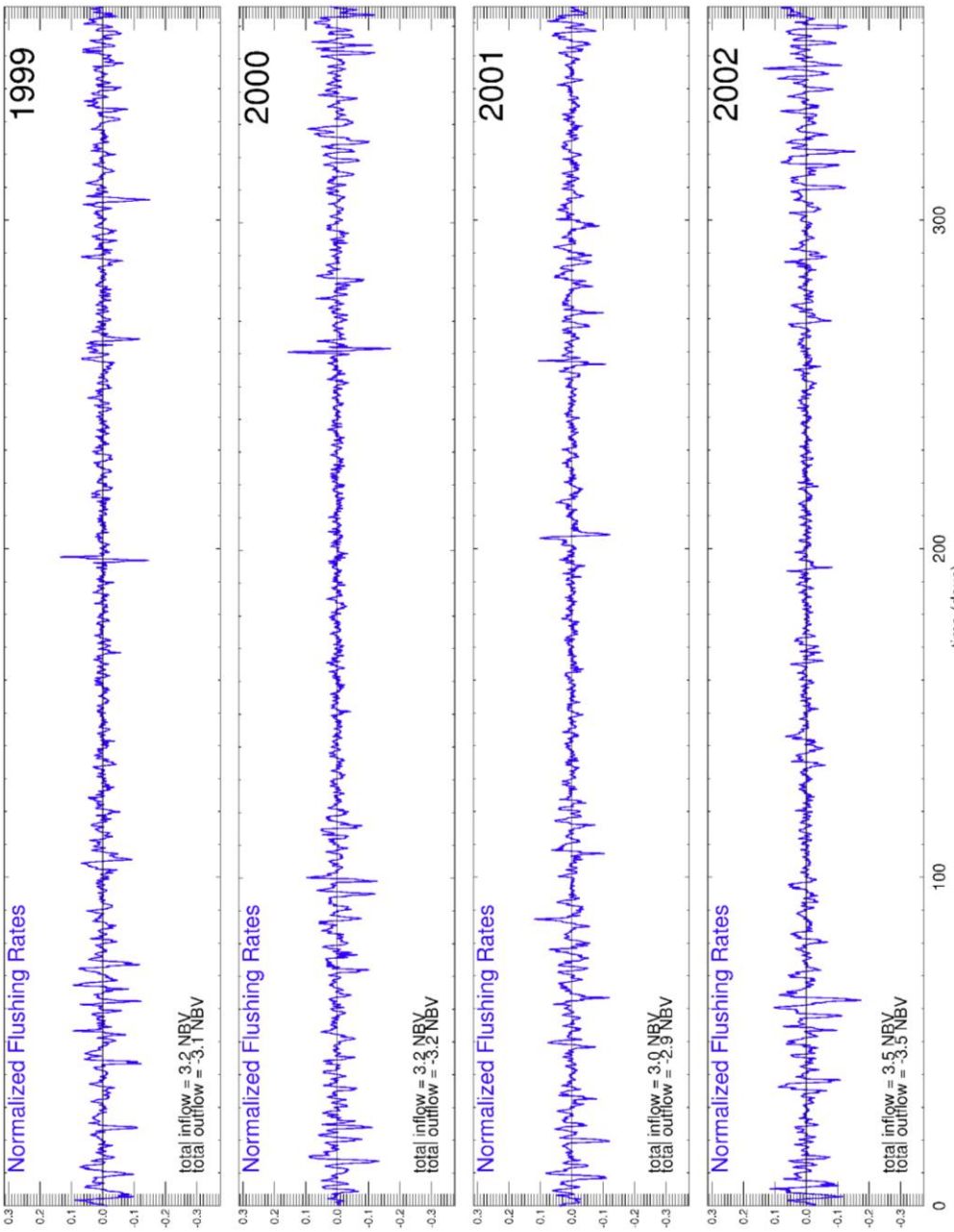

Figure A133. Same as figure A127, 1999-2002.

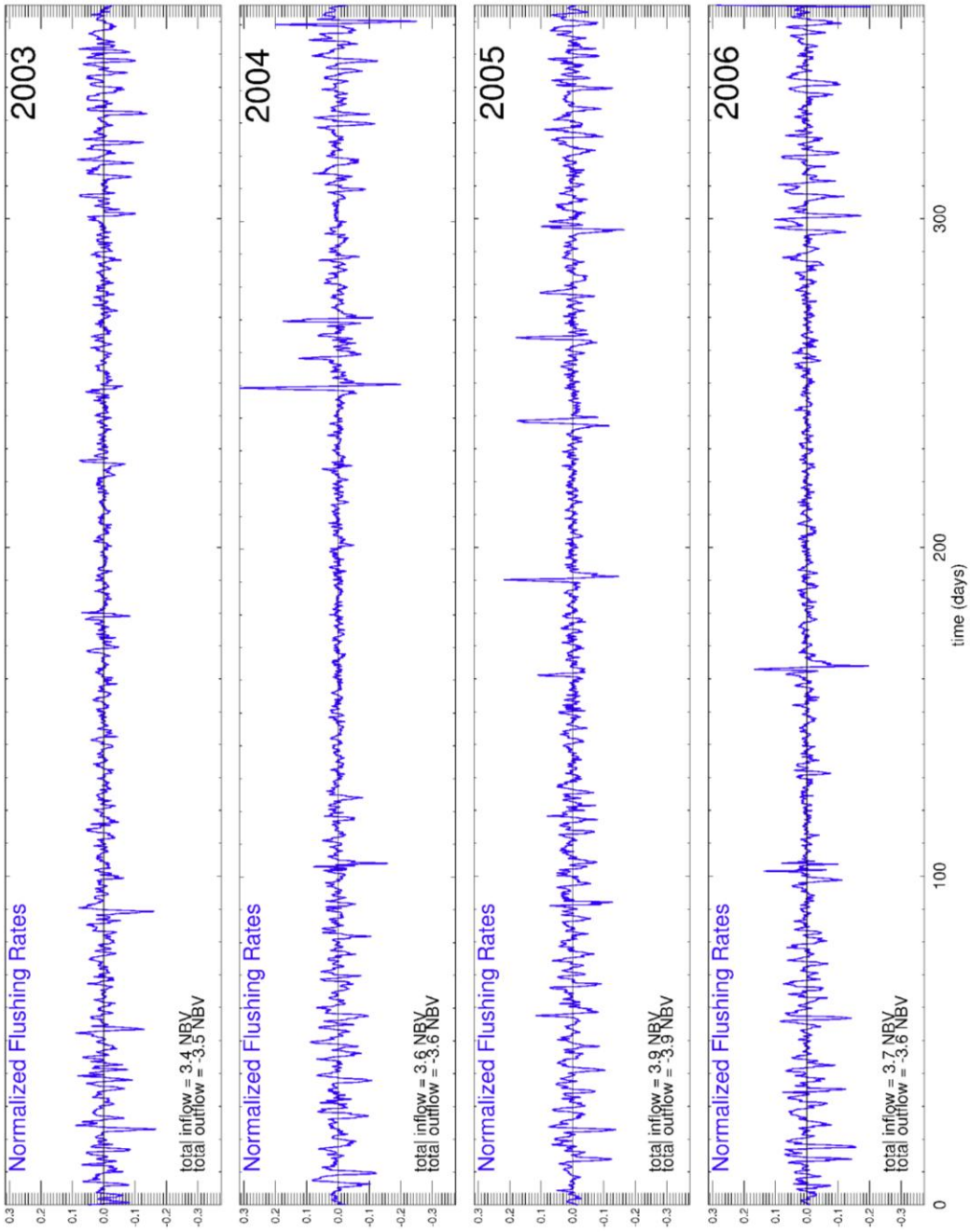

Figure A134. Same as figure A127, 2003-2006.

Appendix G: Scatter plots of normalized bay volume anomalies and flushing rates versus wind components

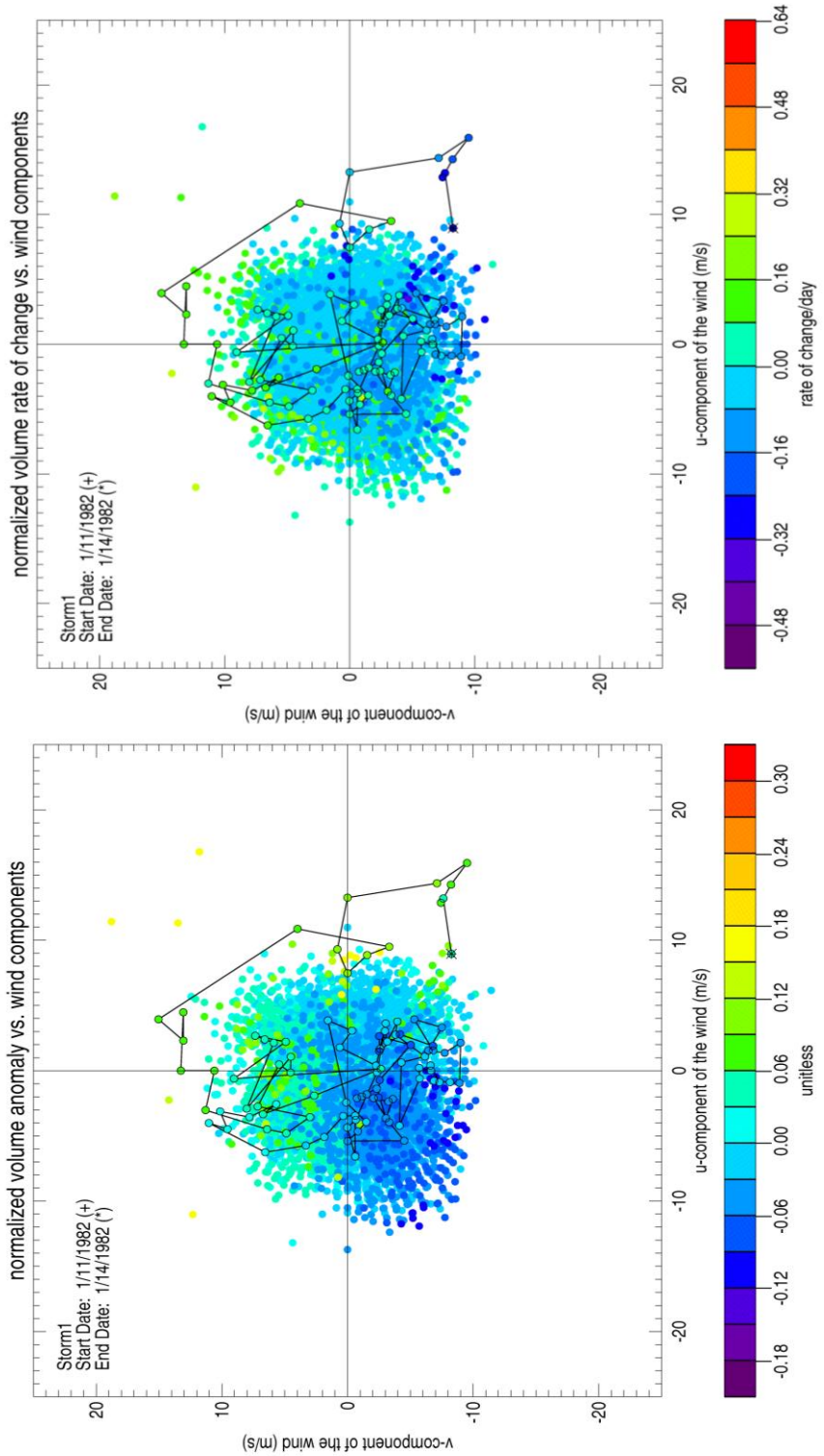

Figure A135. Scatter plot of normalized volume anomalies (left) and normalized volume rates of change (right) versus the zonal (v) and meridional (u) wind components for the year 1982. Outlined path represents the evolution of Storm 1 as it made its way through the Tampa Bay area. Colors represent normalized volume anomalies and rate of change per day.

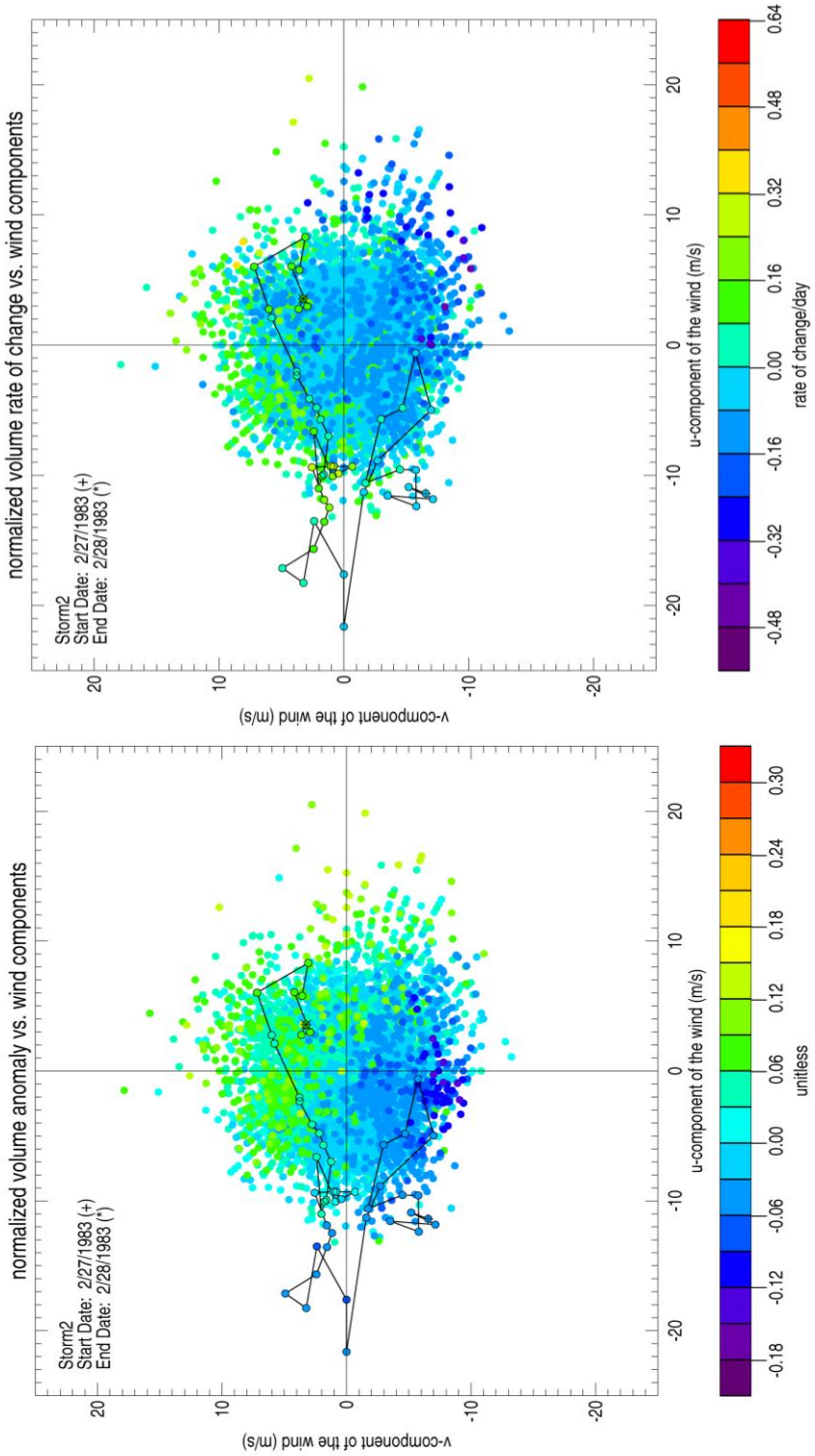

Figure A136. Same as figure A135 for Storm 2 in 1982.

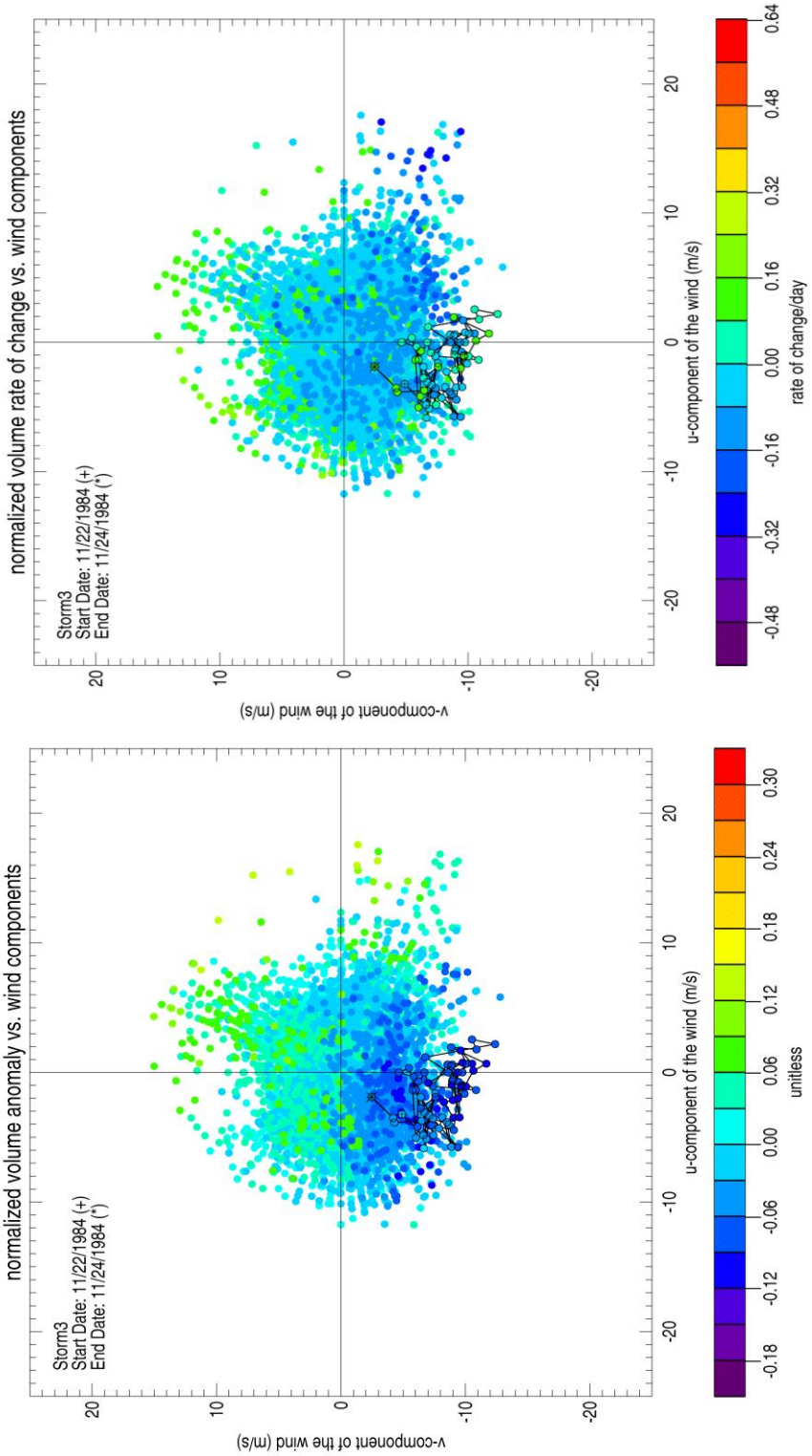

Figure A137. Same as figure A135 for Storm 3 in 1984.

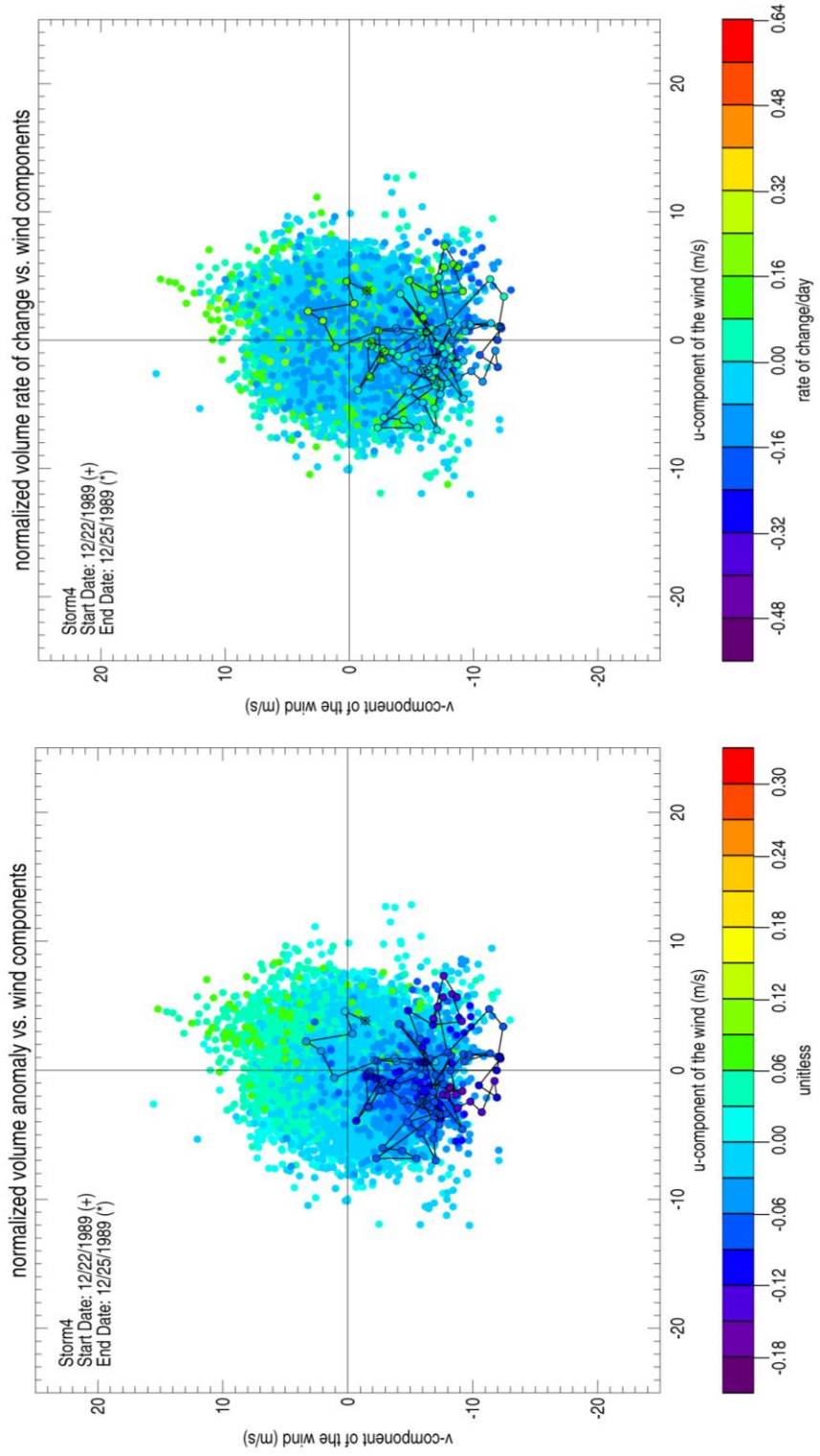

Figure A138. Same as figure A135 for Storm 4 in 1989.

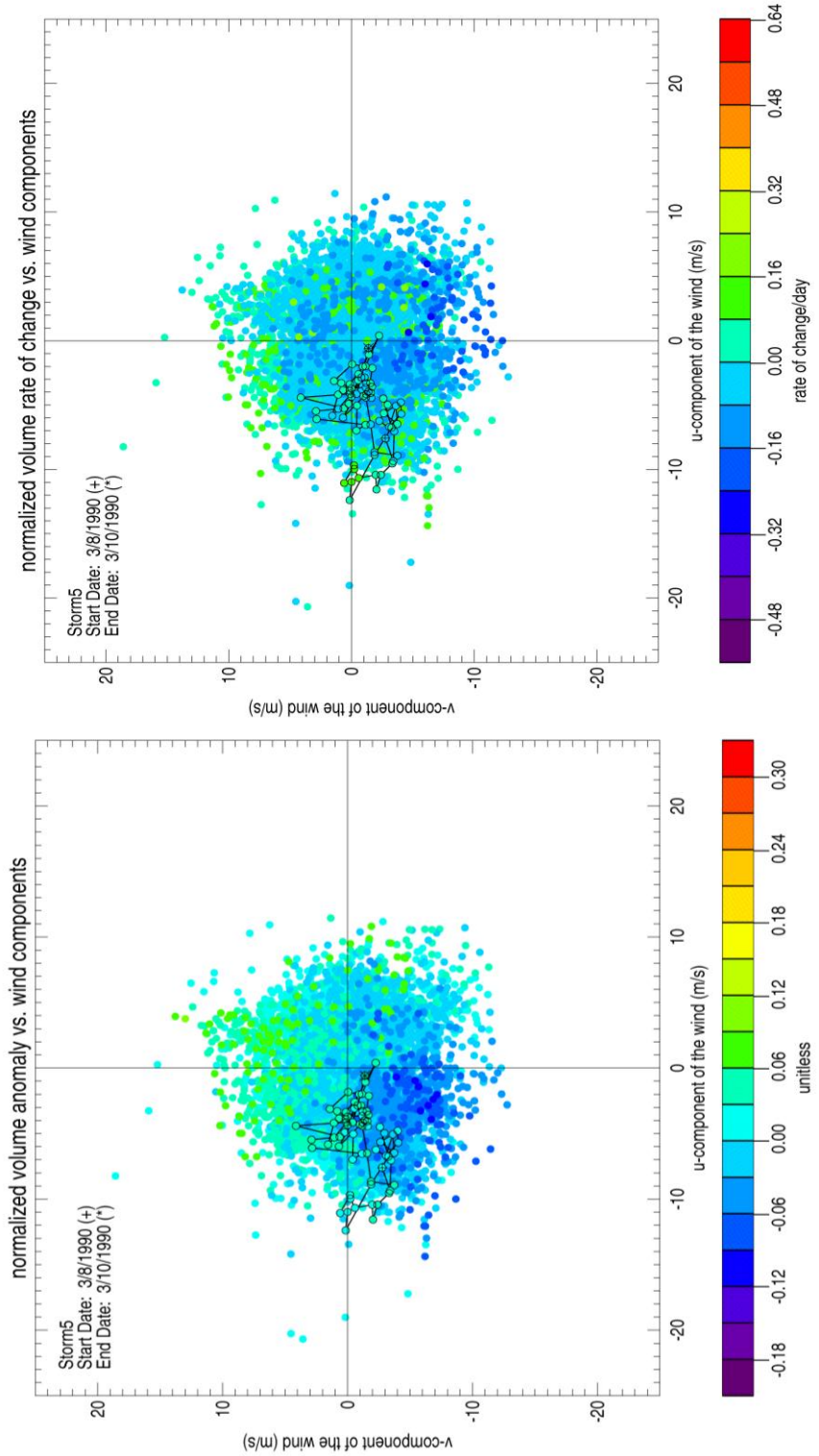

Figure A139. Same as figure A135 for Storm 5 in 1990.

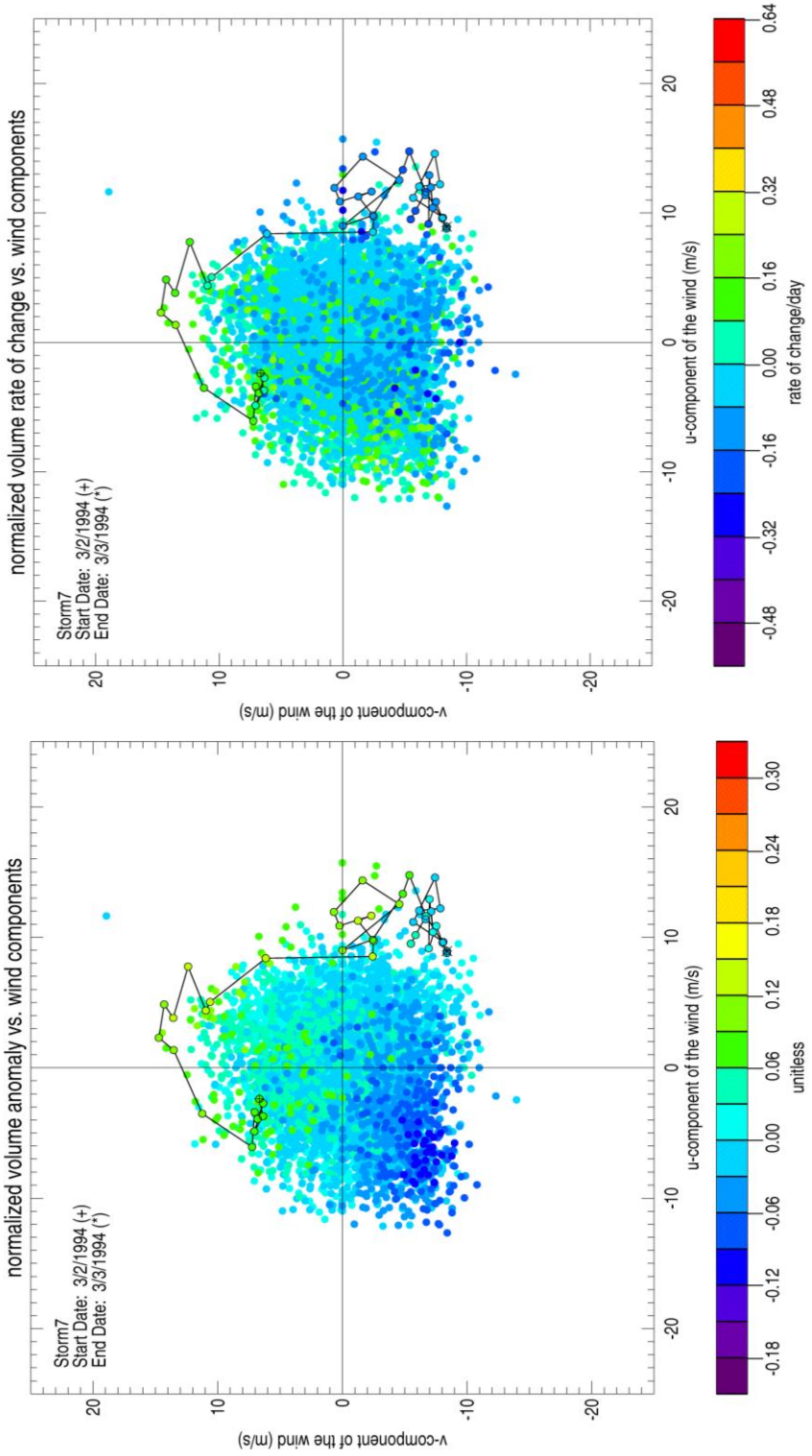

Figure A140. Same as figure A135 for Storm 7 in 1994.

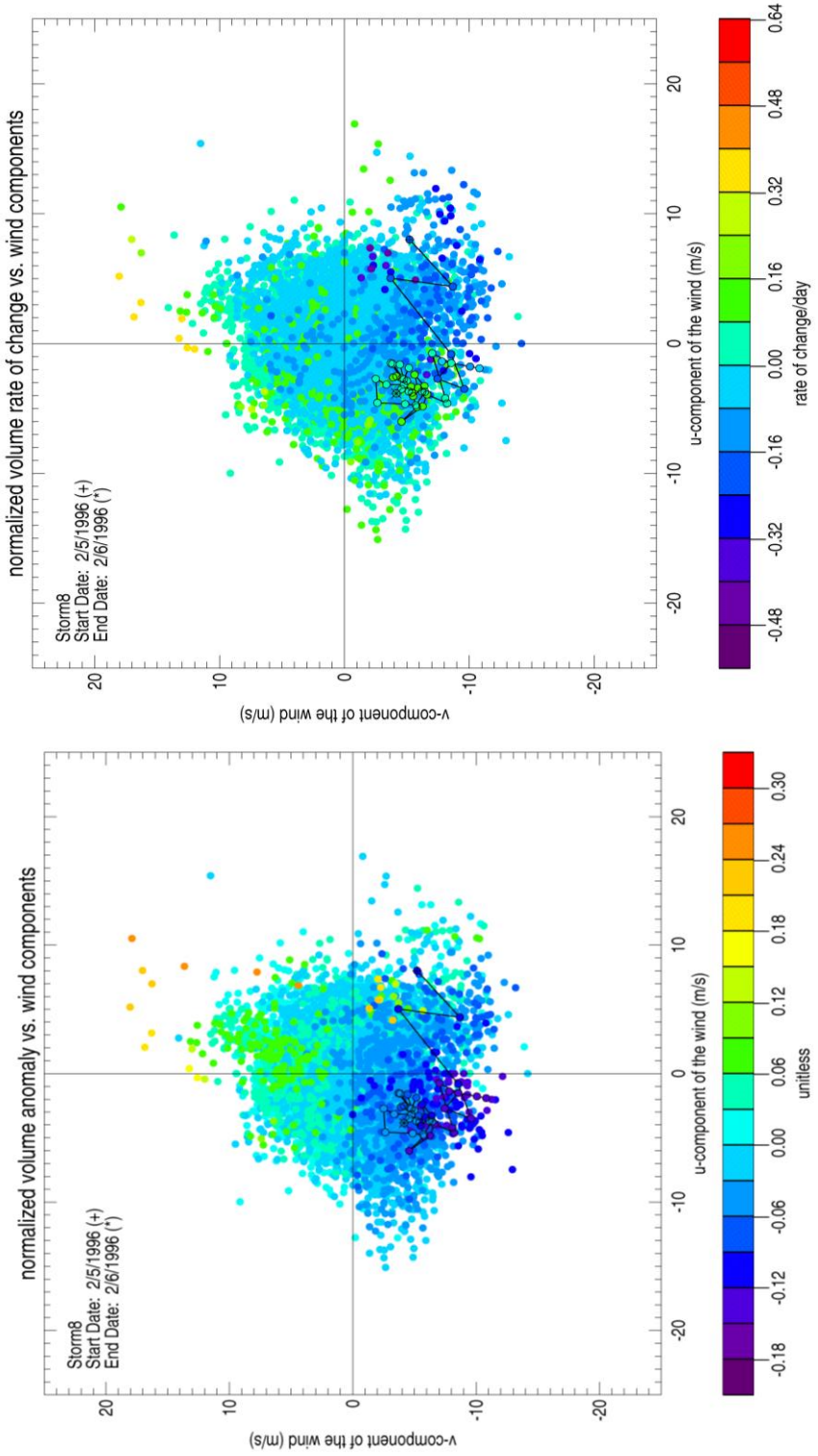

Figure A141. Same as figure A135 for Storm 8 in 1996.

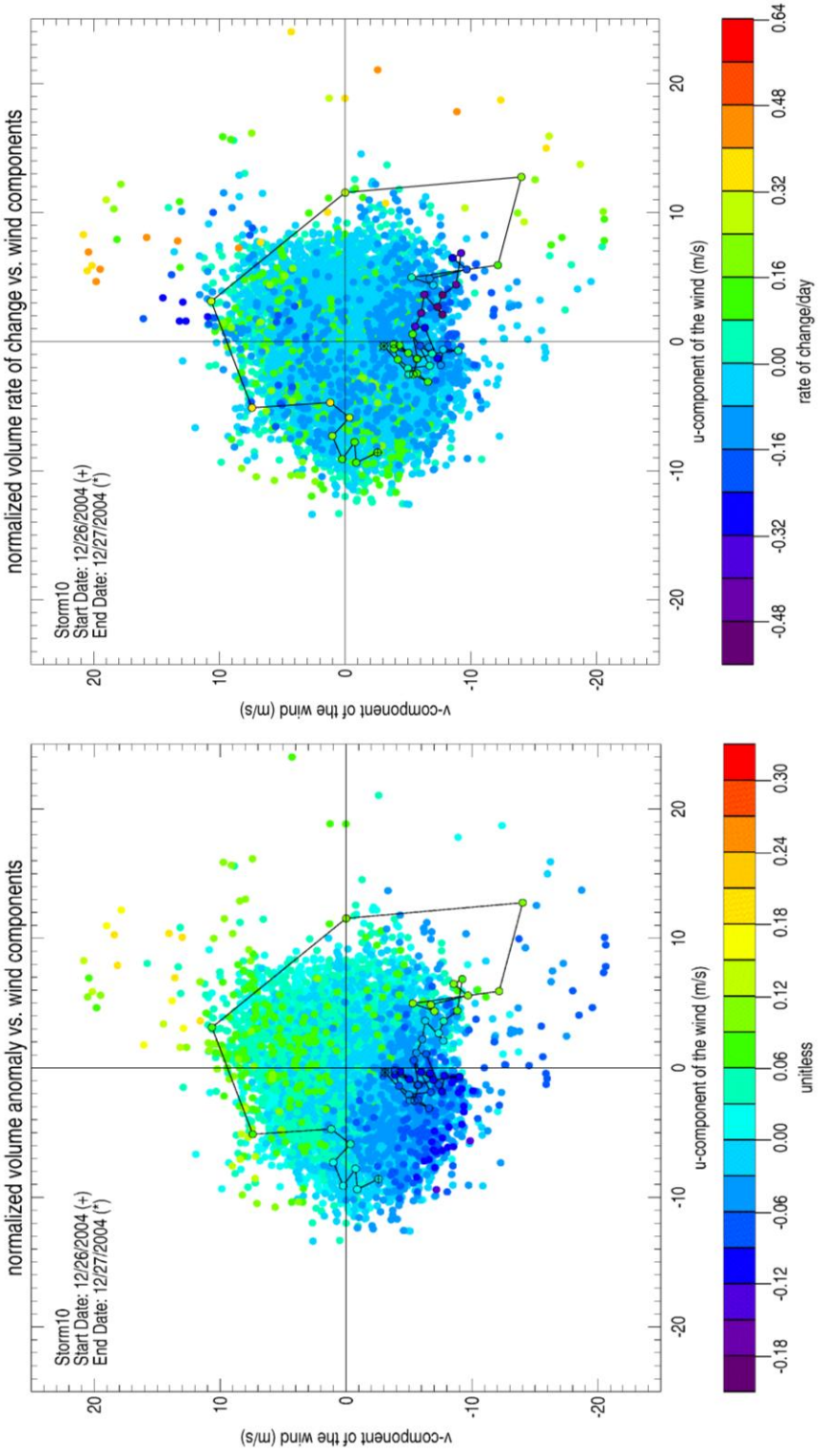

Figure A142. Same as figure A135 for Storm 10 in 2004.

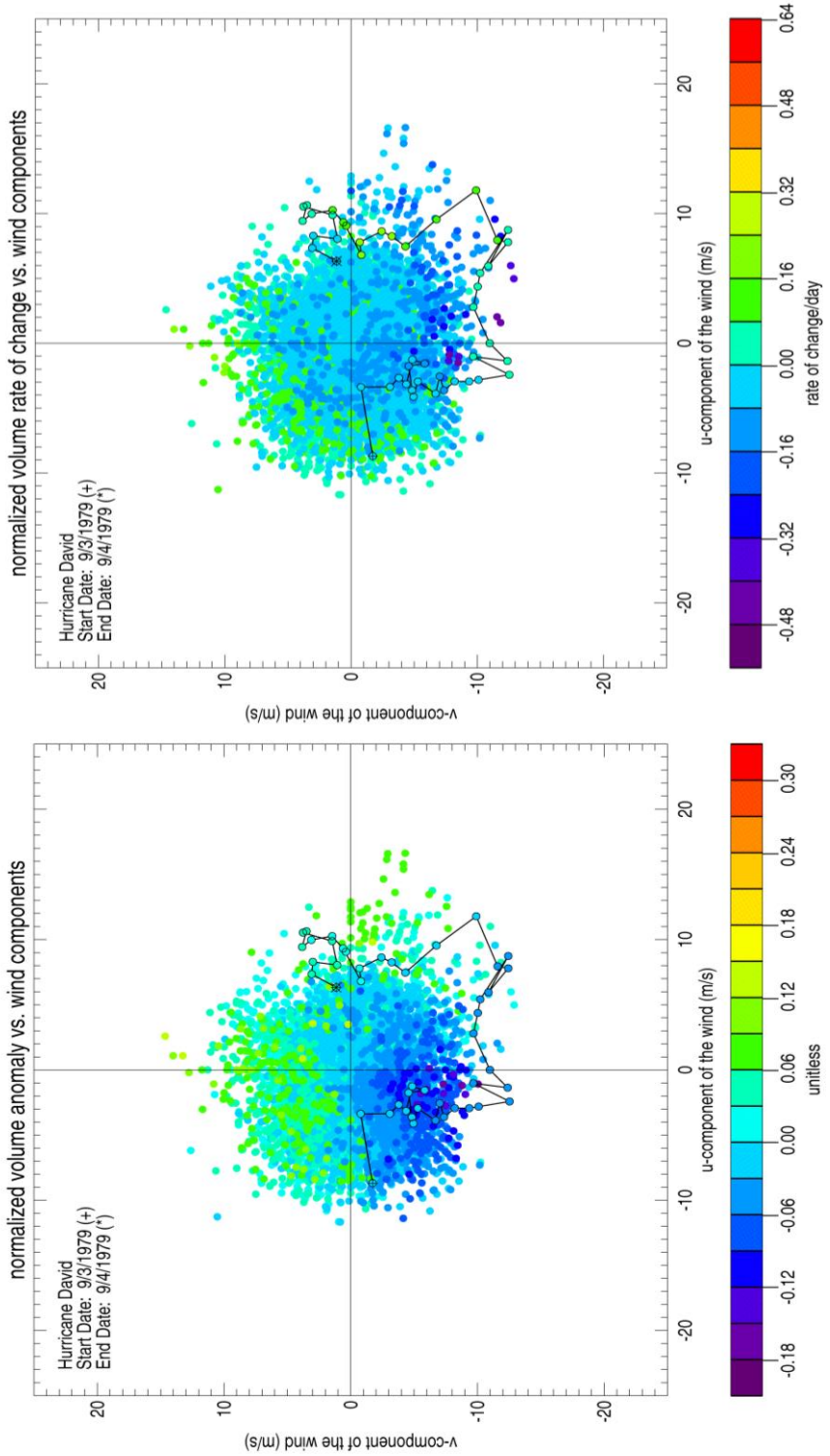

Figure A143. Same as figure A135 for Hurricane David.

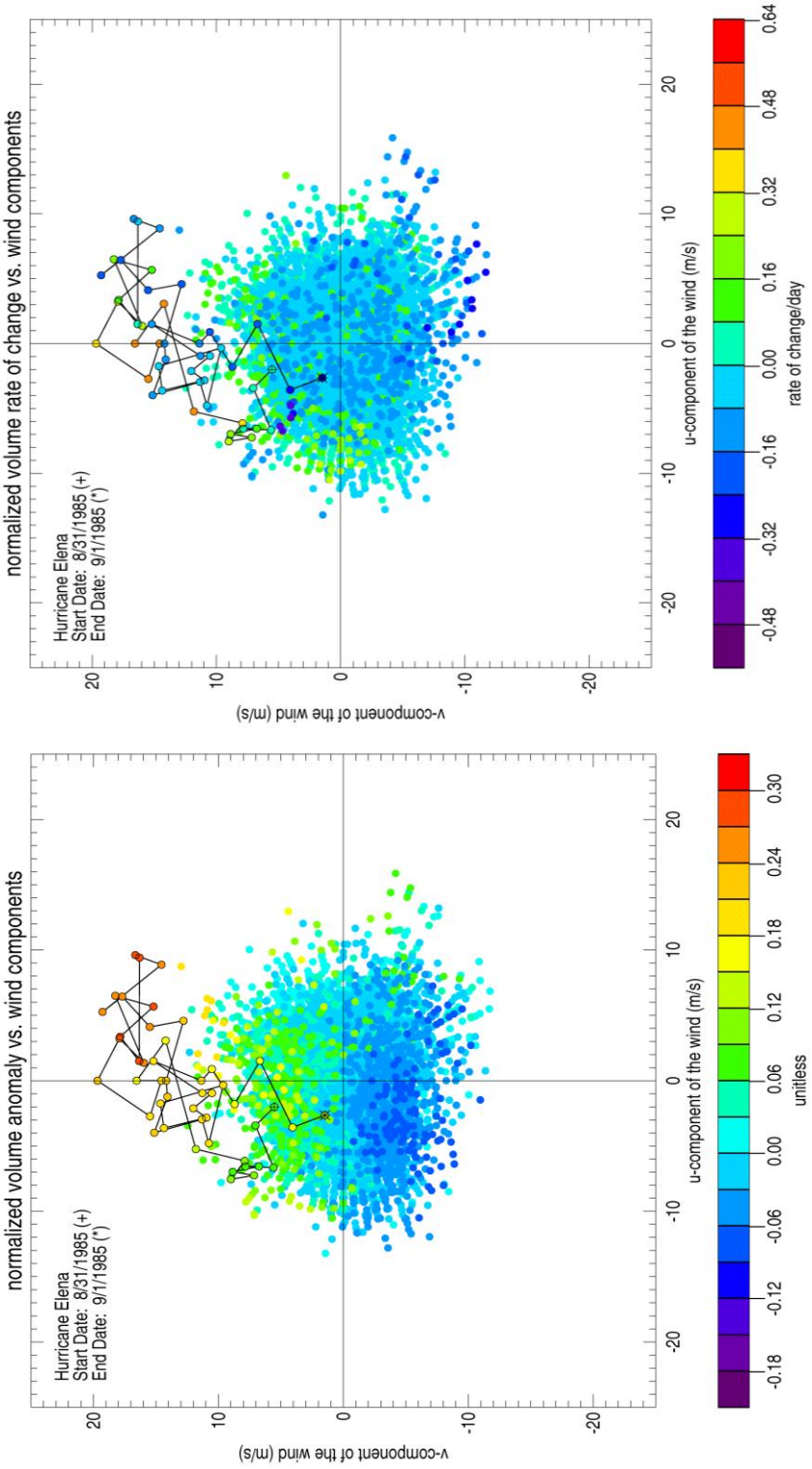

Figure A144. Same as figure A135 for Hurricane Elena.

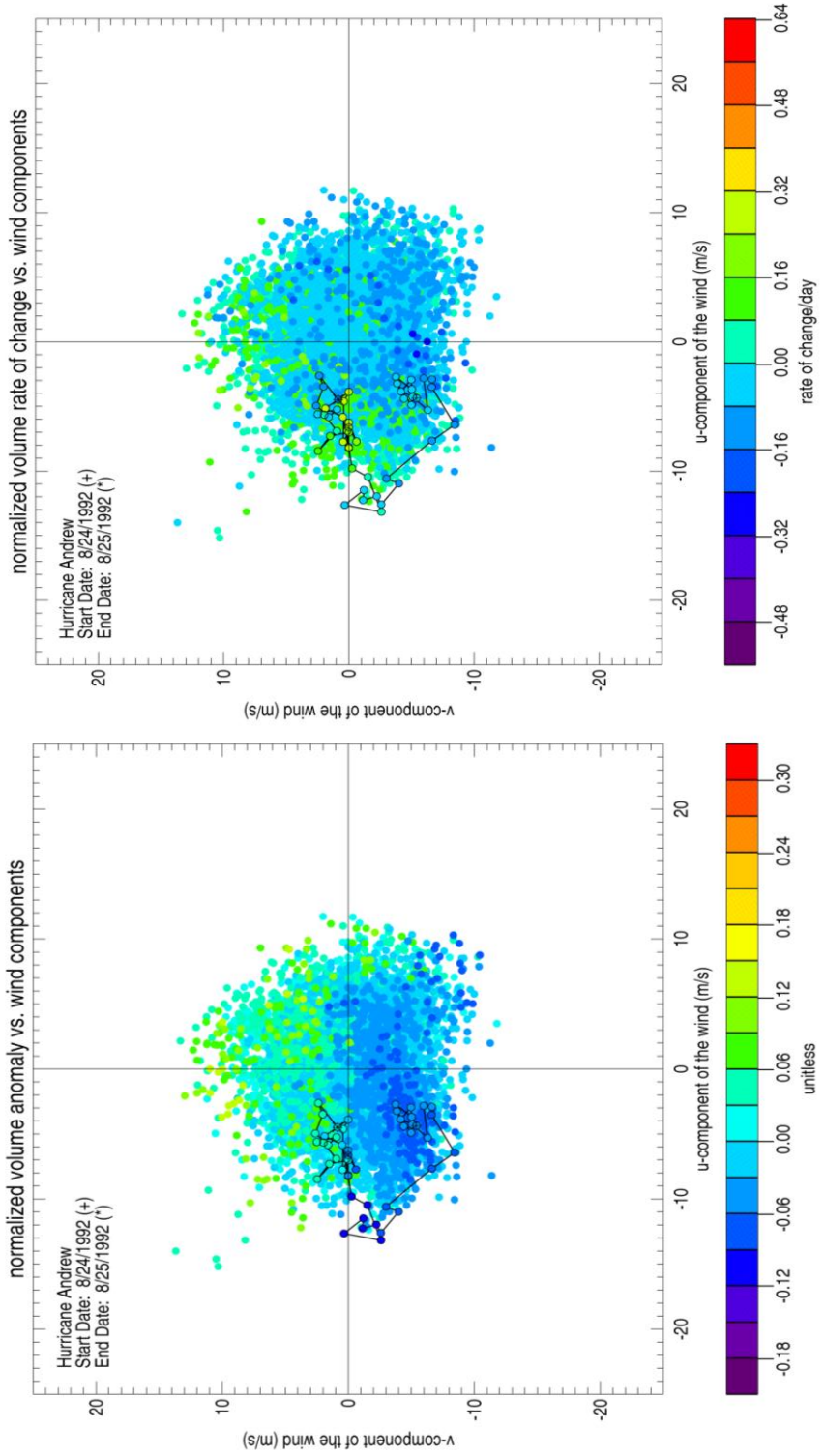

Figure A145. Same as figure A135 for Hurricane Andrew.

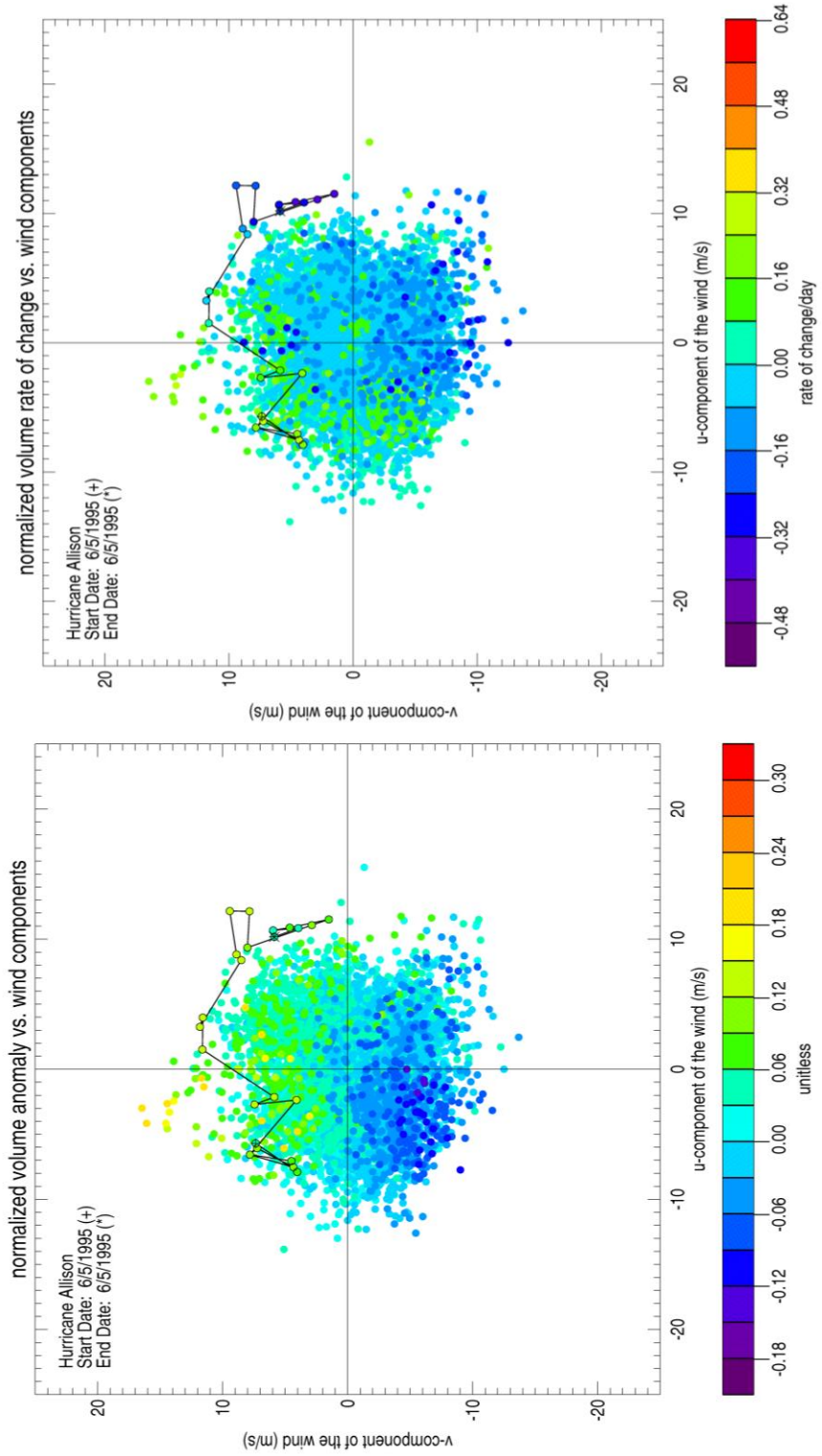

Figure A146. Same as figure A135 for Hurricane Allison.

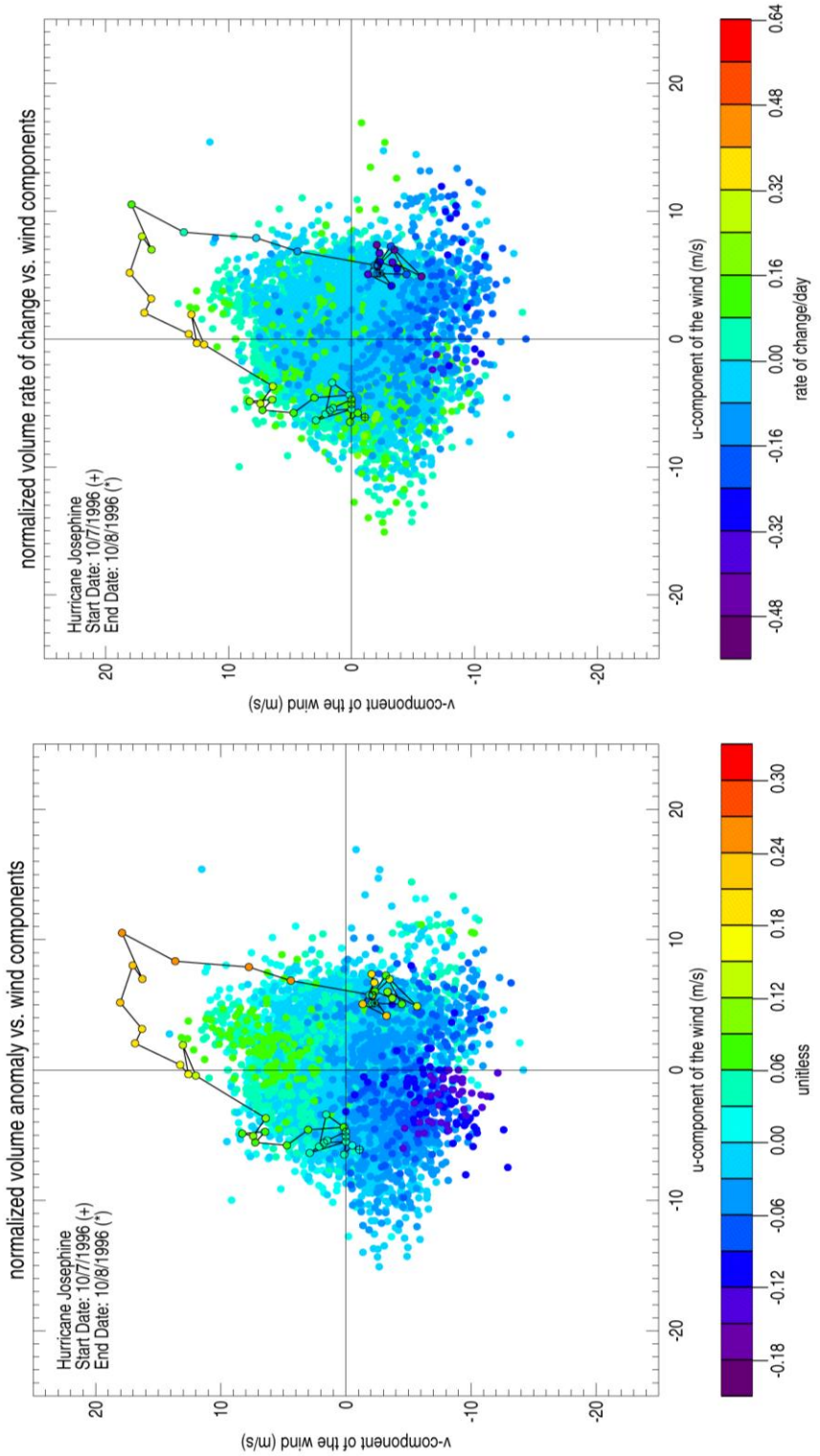

Figure A147. Same as figure A135 for Hurricane Josephine.

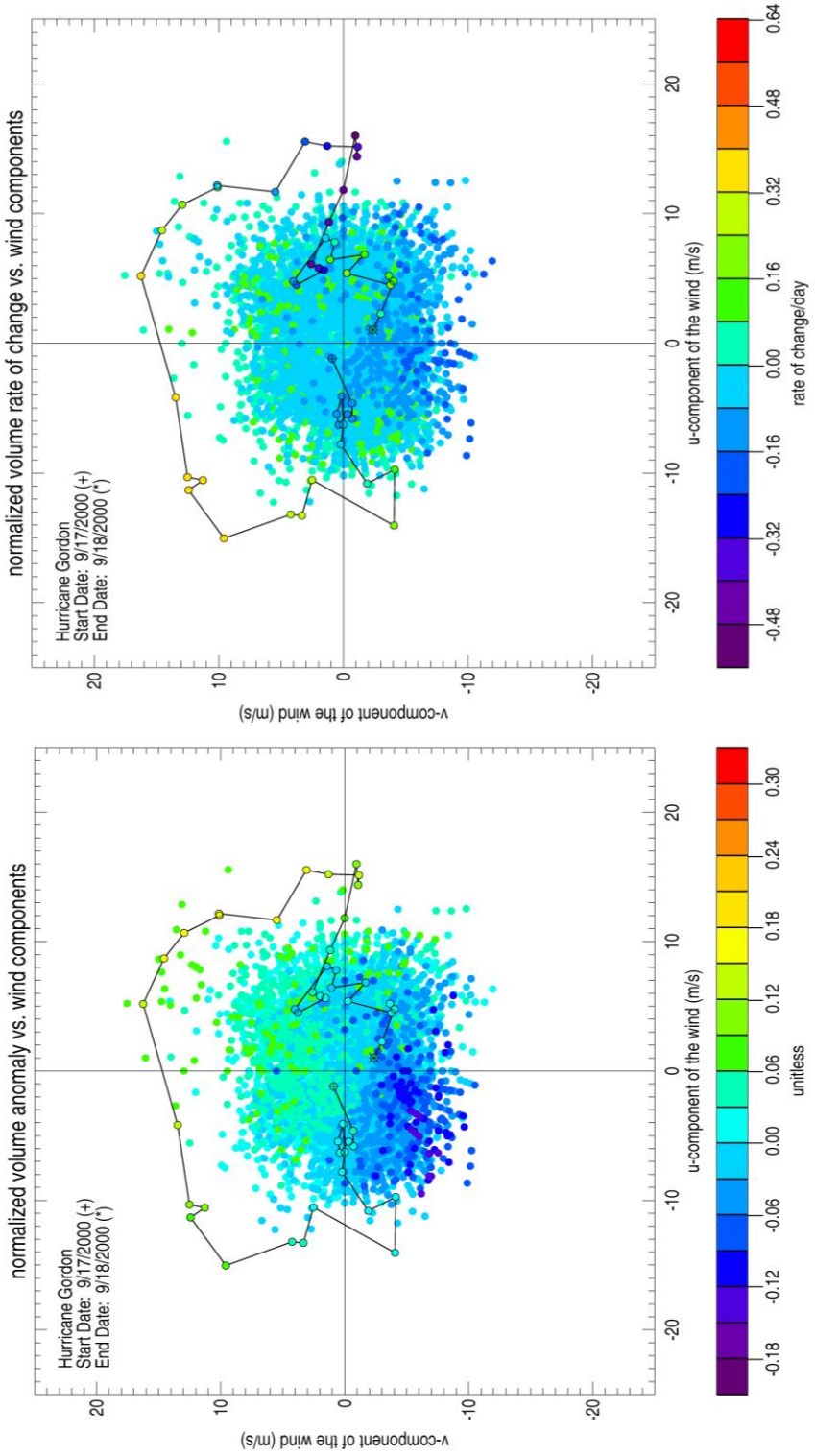

Figure A148. Same as figure A135 for Hurricane Gordon.

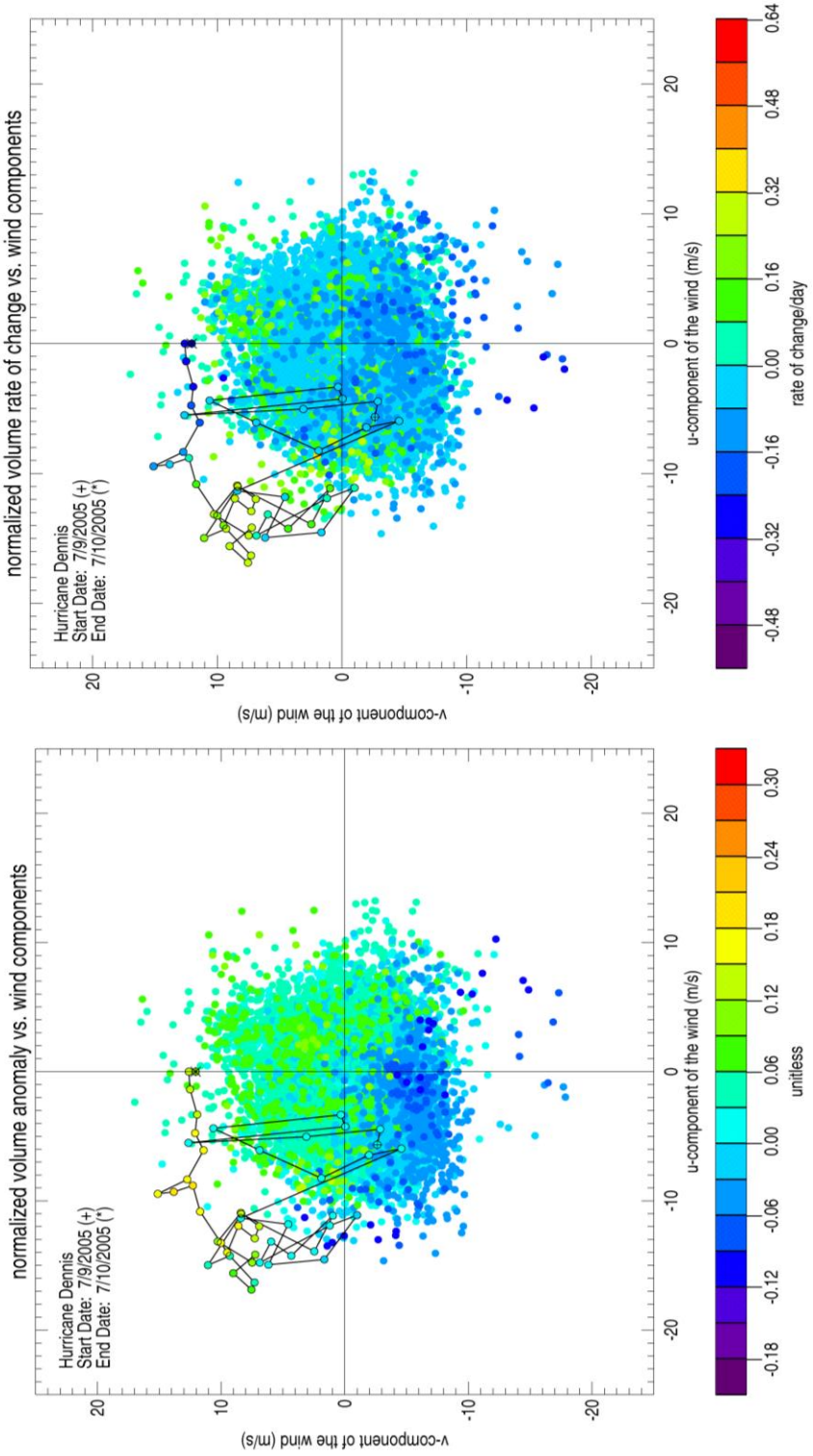

Figure A149. Same as figure A135 for Hurricane Dennis.

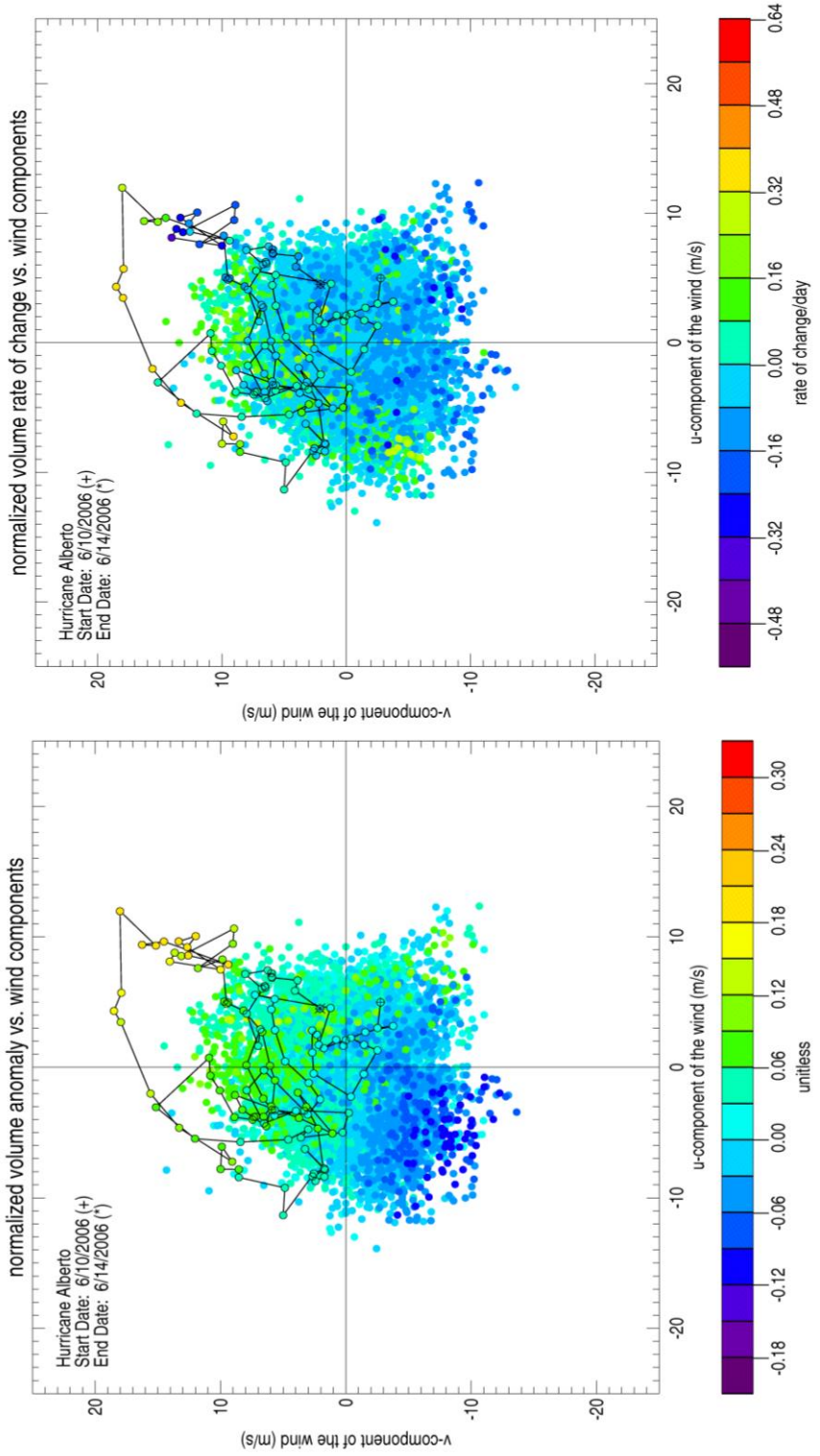

Figure A150. Same as figure A135 for Hurricane Alberto.

About the Author

Monica Wilson received a Bachelor of Arts degree in Marine Science and Computer Science from Eckerd College in 2003. While at Eckerd, she was part of the women's soccer team and spent her summers working for her major advisor, Dr. Gregg Brooks, as part of the geology crew. Her work included going out on day trips to the west coast of Florida to collect sediment cores and perform grain size analysis. She went on to receive her Master of Science degree in Marine Science from the University of South Florida in 2007. After obtaining her M.S., Monica continued at the University of South Florida and entered the Ph.D. program in the fall of 2007. While in the Ph.D. program, Monica spent three summers with the Oceanography Camp for Girls, an educational outreach program for girls entering into high school in Pinellas County. She spent some of her time out on the water helping assist in operations of the real time observing system located in Tampa Bay, FL and helped test and evaluate oceanographic sensors. She was also a volunteer assistant coach for the women's soccer team at Eckerd College and a soccer coach for her sons' soccer teams. Since her time at USF, Monica has been lead author on two publications and co-author on a couple of other publications . Under the advisement of Dr. Mark Luther her doctoral research focused on using observational data as well as a numerical model to investigate synoptic to interannual variability in volumetric flushing of Tampa Bay, FL.